TABLE OF CONTENTS

LIST OF TABLES

Page

LIST OF FIGURES

Page

XX

LIST OF ABREVIATIONS

A	Altin
AM	Alpine Meadow
AWS	Automatic Weather Station
BL	Burwash Landing
C	Carmacks
DEM	Digital Elevation Model
DOC	Dissolved Organic Carbon
GMWL	Global Meteoric Water Line
HBCM	Hydrochemical Basin Characterization Method
HJ	Haines Junction
ICP-OES	Inductively Coupled Plasma Optical Emission Spectrometry
IPCC	The Intergovernmental Panel on Climate Change
IQR	Interquartile Range
LMWL	Local Meteoric Water Line
MK	Mann-Kendall Test
PCA	Principal Component Analysis
PF	Proglacial Field
PW	Peak Water
SR	Spearman's Rho Test
SW	Southwestern
SWE	Snow Water Equivalent

SWBM	Simple Water Balance Model
T	Teslin
TLC	Time Lapse Camera
XRF	X-ray Fluorescence

LIST OF SYMBOLS AND UNITS OF MEASUREMENTS

%	percent
‰	per mile
°C	degree Celsius
h	hour
cm	centimeter
km	kilometer
m	meter
mL	milliliter
mm	millimeter
M	moll
µS	micro Siemens
ppm	part per million
s	second

INTRODUCTION

Under unprecedented climate change (IPCC, 2014; 2019), the cryosphere (frozen portion of Earth's water) is the fastest part of climate system to respond (Xiao, Wang, & Qin, 2015). In mountainous regions, the components of the cryosphere such as glaciers, snow cover, and permafrost regulate flow and thus affect both water quantity and quality for ecosystems and the population situated downstream (Barnett, Adam, & Lettenmaier, 2005; Immerzeel et al., 2019; Huss et al., 2017; Viviroli, Dürr, Messerli, Meybeck, & Weingartner, 2007). In addition to supply and regulation functions, the cryosphere provides habitat and cultural services (Huss et al., 2017; Wang, Liu, & Zhang, 2019; Xiao, Wang, & Qin, 2015). Understanding and mimicking a cryospheric response to climate change is thus crucial for water resources management, as well as for various ecosystem services.

The greatest warming during the upcoming century is projected to happen over northern latitudes (Meehl et al., 2007; Larsen et al., 2014). In these regions, the subarctic glacierized watersheds are among the most complex hydrological systems because they possess hydrological features of both cold and temperate regions (Brown, Ferrians, Heginbottom, & Melnikov, 2002) and often preserve legacy hydrological features from antecedent climates and glaciations such as rock glaciers, ice-cored moraines and buried ice formations (e.g., Johnson, 1986). In a context of extreme vulnerability of subarctic populations and ecosystems to climate change (Hinzman et al., 2005; Jacobsen, Milner, Brown, & Dangles, 2012; Larsen et al., 2014), improving the knowledge necessary to accurately project the impact of environmental changes on the subarctic glacierized watersheds is of primary importance.

The estimated impact of climate changes on glacierized watershed hydrology is commonly modelled under the assumption that the evolution of glacier extent is the dominating factor that should be accounted for (Hood et al., 2006). In numerical models, glacier- and snowmelt are often the only considered cryospheric components affecting a watershed outflow (e.g., Gascoin et al., 2011; Huss, 2011; Kaser, Grosshauser, & Marzeion, 2010). In addition, the hydrological systems from portions of watersheds not covered by glaciers are represented by groundwater

routing (e.g., Farinotti, Usselmann, Huss, Bauder, & Funk, 2012; Koboltschnig, Schöner, Zappa, & Holzmann, 2007; Naz, Frans, Clarke, Burns, & Lettenmaier, 2014; Ragettli, Cortés, McPhee, & Pellicciotti, 2014; Pomeroy et al., 2007), where groundwater component is often modelled based on calibration (Hood et al., 2006). However, glaciers are only one of the climate-sensitive hydrological features of the subarctic glacierized catchments. At a watershed scale, this underrepresentation of the non-glacierized part of alpine watersheds potentially leads to biases in runoff predictions, as changes affecting other water sources are neglected. The risk of biased predictions is even more pronounced in Nordic environments, where numerous cryospheric components play an important role in the hydrological balance.

Cold-region-specific hydrological components, such as small scale slope processes in permafrost underlain terrains have been intensively studied in the subarctic (Carey & Quinton, 2004; Carey & Woo, 1998, 2001a, 2001b; Quinton & Marsh, 1999) and their hydrological role is now well identified (Woo, 2012). Regrettably, this is not the case for the hydrological role of proglacial fields including their groundwater systems, buried ice, ice-cored moraines and icings. The relative importance of the hydrological processes associated with such feature in glacierized watersheds has not yet been estimated (Vincent, Violette, & Aðalgeirsdóttir, 2019).

Several conceptual models, which describe proglacial field hydrology, exist for glacierized watersheds in the tropical Andes (e.g., Baraer et al., 2014; Gordon et al., 2015; Somers et al., 2016), temperate glacierized watersheds in the Alps (e. g., Kobierska, Jonas, Kirchner, & Bernasconi, 2014; Penna, Engel, Bertoldi, & Comiti, 2017; Ward, Malard, Tockner, & Uehlinger, 1999), in the Rockies (e.g., Langston, Bentley, Hayashi, Mcclymont, & Pidlisecky, 2011; McClymont et al., 2011; Muir, Hayashi, & Mcclymont, 2011), and in the Himalayas (e.g., Ma et al., 2017). Those studies often focused either on one or several hydrological features, or on watershed groundwater component. The only examples of attempts to establish subarctic conceptual models are found in Iceland (e.g., Dochartaigh et al., 2019; Levy, Robinson, Krause, Waller, & Weatherill, 2015). Thus, most of the existing conceptual models of glacierized watershed describe in detail only one or several hydrological components such

as rock glaciers, talus slopes, and moraines (e.g. Langston, Bentley, Hayashi, Mcclymont, & Pidlisecky, 2011; McClymont et al., 2011; Muir, Hayashi, & Mcclymont, 2011; Williams, Knauf, Caine, Liu, & Verplanck, 2006). Subarctic glacierized watershed hydrological processes, related to the presence of such features as ice-cored moraines and buried ice, are not represented in these conceptual models. These features, however, are known to have high storage capacity and complex groundwater distribution systems (Langston et al., 2011; McClymont et al., 2011; Roy & Hayashi, 2009) and thus are known to affect significantly watershed hydrology. In addition, groundwater systems within proglacial fields are highly interconnected with surface water systems, and respond fast to changes in glacier geometry and water supply (Kobierska et al., 2014; Levy et al., 2015; Magnusson et al., 2014; Ward et al., 1999). Climate change projections on the watershed scale are limited by process understanding in mountainous glacierized catchments (Mimeau et al., 2019; Salzmann, Huggel, Rohrer, & Stoffel, 2014). To accurately project the response of these systems to environmental changes it is necessary to better understand and quantify the role of hydrological components other than glacier meltwater in runoff production.

Based on this contextual background, I hypothesize that subarctic proglacial areas play an important role in the hydrology of glacierized valleys, and that glacier retreat is not the only driver of their hydrological response to climate change. The main objective of this project is thus to improve the knowledge necessary to project the impacts of environmental changes on the hydrology of subarctic regions, and to achieve it I specify several research questions:

1. What is the role of shrinking glaciers in recent (last 3-7 decades) hydrological changes in the southwestern Yukon and what are future hydrological changes in the region?
2. Which hydrological components play an important role in summer runoff production in headwater of a subarctic watershed?
3. Which hydrological components are responsible for generation of winter baseflow in the headwaters of subarctic watersheds of different complexity?

In order to answer these research questions, St. Elias Mountains, situated in the Canadian subarctic, were chosen as a study region. This area is a remote region of the southwestern

Yukon, which can be seen as a natural laboratory for understanding the impact of environmental changes on the subarctic glacierized watersheds, yet it has only been studied occasionally so far. The study region is situated on the southern edge of the subarctic area, which is especially sensitive to changes in climatic forcing (Nilsson, Polvi, & Lind, 2015). Among the world's glacierized regions, this particular one has been the second after the Canadian Arctic in contribution to global sea level rise during the period 1961-2000 (Radić & Hock, 2010). The St. Elias Mountains are projected to lose 70±10% of glacier volume by the end of the century (Clarke, Jarosch, Anslow, Radić, & Menounos, 2015) which will lead to a substantial decrease in glacier melt contribution to runoff (Bliss, Hock, & Radić, 2014).

This project is based on 3 summer field campaigns in the glacierized watershed in the St. Elias Mountains, laboratory analysis, statistical analyses, and remote sensing techniques and products. A multi-technique approach is used to better understand the hydrological processes of the proglacial area. This choice is made due to the high hydrological complexity met in such environments. Among others, the high number of potential water sources, the limited length of the field campaigns, and the difficulties to equip the valley with long-lasting monitoring equipment have motivated this choice. Among the techniques used for the project, those based on natural tracers, hydro-meteorological monitoring and time lapse imagery are the most important.

Answering of the first research question provides new insights into hydrological changes in the southwestern Yukon and helps isolating and quantifying the role of glacier retreat in those changes. The role of glacier retreat in the region was previously estimated only qualitatively based on watersheds' hydrological regimes (Fleming, 2004) or their current glacier cover (Fleming & Clarke, 2003). In the present project I use two approaches in parallel - one based on statistical hydro-climatology, and another based on hydro-glaciological numerical modelling. The results of this part of the project allow linking the hydrological response of different watersheds to glacier retreat parameters, positioning of watersheds in terms of peak water, and providing estimates of the magnitude of change in discharge during/after peak water. The repercussions of that work are global: mountain glaciers are the core of the world's

"water towers" like the Himalayas, Andes, Alps, and Northern Rockies (Immerzeel et al., 2019).

Answering the second and the third research question results in a more comprehensive description of the hydrological role of different components within subarctic proglacial fields during both summer and winter seasons. Moreover, it helps quantifying the importance of the proglacial field in watershed hydrology in a context of environmental changes. By better characterizing the hydrological systems specific to the proglacial field, the present research will help the development of a new generation of hydrological models, which in turn can provide more objective projections for water resources management.

In addition, selecting proglacial fields as key areas of investigation has potential to impact the scientific community. Proglacial fields exhibit high dynamics and vulnerability under current climatic conditions (Johnson, 1971, 1992; Schomacker, 2008). They are expanding as glaciers are retreating, and subsequently evolve due to the presence of climate-sensitive hydrological features. In their recent paper, Heckmann, Mccoll, and Morche (2016) highlight the increasing interest in proglacial areas and the lack of knowledge in this field. In many contexts, such as hydrology, sediment transport and extreme outbursts, proglacial field investigation is important. In the context of water resources in glacierized watersheds under changing climatic conditions, the proglacial field can play an important role in water storage (Langston et al., 2011; McClymont et al., 2011; Roy & Hayashi, 2009).

CHAPTER 1

HYDROLOGY OF GLACIERIZED SUBARCTIC WATERSHEDS

This chapter is dedicated to presenting hydrological systems of subarctic glacierized watershed, their related hydrological processes and their evolution under changing climate based on the recent and still relevant literature. In order to avoid overlaps with Chapters 3, 4 and 5, I here prioritize descriptions that allow the understanding of those systems in an integrated way and provide fewer details on what the aforementioned three chapters are focusing on, namely regional hydrological changes, the contribution from non-glacierized parts of highly glacierized catchments, and icing formations and winter specific hydrological processes.

Subarctic glacierized watersheds are complex systems due to unique co-habitat of temperate-climate-specific hydrological components with cold-region-specific ones, which results in phenomena such as discontinuous permafrost, polythermal glaciers and the presence of both colluvial landforms and moraines containing buried ice. Therefore, one can say that the runoff from these hydrological systems arises from combined effects of energy exchanges, mass exchanges within and between hydrological components and their hydraulics. As a result, hydrological processes are described hereafter for different periods of the year, namely winter, snowmelt, and summer. The winter period is characterized by negative temperatures, solid precipitation and snow and ice accumulation. The snowmelt period starts when air temperature rises above 0°C during the day, and is characterized by the depletion of snow cover. The summer period is characterized by the absence of snowpack on slopes and valley floor, and positive mean daily temperatures.

Conceptually, I will divide subarctic glacierized watershed into three zones: main glacier, proglacial field (i.e. transitional landscape from glacierized to non-glacierized, Heckmann, Mccoll, & Morche, 2016) and alpine meadow (i.e. grassland in lower parts of the watershed, Hayashi, 2019). Even though those three parts interact with one another, for readability, they are presented separately hereunder. The first two sections describe hydrological processes

related to glaciers and the evolution of these processes under changing climate. Section 3 and 4 are dedicated to hydrological processes within the proglacial field and their response to increasing temperatures respectively. Finally, Sections 5 and 6 are focused on the lower part of the watershed that coincides with the alpine meadow and describe related hydrological processes and their projected changes.

1.1 Glaciers hydrology

Since there exists a large body of literature about glaciers hydrology in all regions, this section is mostly based on the reviews and "classic" works in glaciology and glacier hydrology. Also, as this project is based in a watershed where no debris-covered glaciers are observed, the review on their hydrology is not presented.

The runoff generated by glaciers is controlled by meltwater production resulting from ablation processes, water storage through accumulation, and routing of meltwater above and within the glacier system. Ablation processes, which provide water input into the system, take place at the glacier surface (supraglacial melting), within the glacier (englacial melting) and at the glacier bed (subglacial melting) (Walder & Fountain, 1998). In addition, water can be supplied to the system by external sources such as precipitation and snowmelt (Irvine-Fynn & Hodson, 2011). These different sources contribute to the total glacier runoff in different ways, supraglacial melting being a major source of water for most glacierized areas (Hock, 2005). Supraglacial melt occurs when the surface energy balance is positive and the surface is at melting point. Pronounced diurnal cyclicity of energy components, especially the radiative ones, imposes a marked diurnal variability in supraglacial melt (Jansson, Hock, & Schneider, 2003). Meltwater production reaches its peak during the day, following shortwave radiation and air temperature maxima. It reaches its minimum during the night when there is no or little energy available for melting (e.g., Klok, Nolan, & Van den Broeke, 2005). In the subarctic at the seasonal scale, most of the annual runoff is concentrated within the ablation season, when temperature and radiation are higher, and it is small during the accumulation season, when most of the precipitation is stored as snow (e.g., Huss, Bauder, & Funk, 2009; Moore &

Demuth, 2001). Water can also be stored during the ablation season and it depends on the spatial distribution of the seasonal snowpack and firn layers. By storing water, snow and firn layers delay water delivery to the englacial and subglacial conduits and cavities, and tend to smooth the diurnal variations in meltwater input (Walder & Fountain, 1998). Delay times can range between several days to weeks for the firn area, and are of the order of few hours for ice-covered areas (Jansson et al., 2003). Once released, water undergoes routing processes. The routing system of a clean-ice glacier can be divided into supraglacial, englacial and subglacial (Irvine-Fynn & Hodson, 2011) (Figure 1.1).

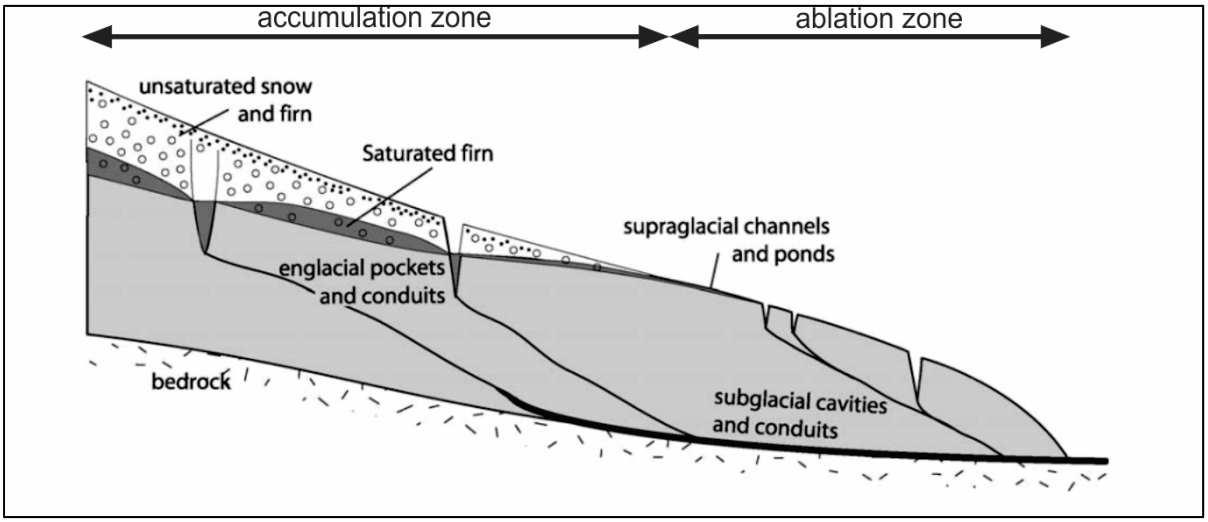

Figure 1.1 Hydrological system of a temperate glacier
Adapted from Jansson et al. (2003)

Supraglacial channels develop on the glacier surface and drain meltwater via crevasses and moulins into the englacial and subglacial drainage system (Nienow, Sharp, & Willis, 1998). In there, water can be transported by percolation through ice (distributed or "slow" drainage system) or more efficiently by means of englacial passages (channelized or "fast" drainage system). The increasing amount of water during the ablation season augments the water pressure within the glacier and leads to widening of channels, headward channel growth as snowline retreats up-glacier, and enhanced hydro-fracturing leading to the evolution of the drainage system in the course of the melt season (Nienow et al., 1998). As a result of water

routing, on a watershed scale glacier cover has a buffering effect on runoff (Fleming & Clarke, 2005; Fountain & Tangborn, 1985) with the lowest variability observed for watersheds where 40% of the area is glacierized (Walder & Fountain, 1998).

Based on the ice temperature distribution, glaciers can be classified as cold (ice temperature is below melting point), temperate (ice is at melting point) and polythermal (mixture of two). The thermal structure of a glacier depends on climate, meltwater refreezing, heat production associated with glacier dynamic processes, and geothermal heat sources (Irvine-Fynn & Hodson, 2011). The thermal structure has important implications on glacier hydrology since unlike for temperate ice, water cannot percolate though the cold ice (Irvine-Fynn & Hodson, 2011). As a result, the presence of cold ice will restrict water percolation to the en- and subglacial systems and thus water routing will be mainly performed via supraglacial channels (Hodgkins, Tranter, & Dowdeswell, 1997). However, for certain cold glaciers icing formation due to winter subglacial drainage was observed and explained by water stored in channels underneath the glacier (Bælum & Benn, 2011; Naegeli, Lovell, Zemp, & Benn, 2014; Wainstein, Moorman, & Whitehead, 2014), which sometimes extend to moraine complex (Moorman, 2003). In the study area glaciers are most likely polythermal (Flowers, Copland, & Schoof, 2014; Wilson, Flowers, & Mingo, 2013). Thermal regimes of two middle-size glaciers in the region were investigated and it was shown that temperate ice is located in most of the accumulation zone (Figure 1.1), and ice thickness decreases towards ablation zone (Wilson & Flowers, 2013). Temperate ice in the accumulation zone can be explained by heat production via meltwater percolation and refreezing in accumulation zones. The produced heat can eliminate cold wave close to the surface (Wilson et al., 2013). This hypothesis was supported by observations of supraglacial runoff in the ablation area (Wilson et al., 2013). Observations of subglacial streams discharging from glacier tongues suggested that glaciers are temperate in parts of the terminus area.

In cold permafrost-underlined regions, glaciers insulate the ground underneath, influencing the distribution of taliks (year-long unfrozen ground). During winter, taliks allow releasing of water stored in glaciers to the surface, which in turn can result in icing formations in an

immediate proglacial field (e.g., Sobota, 2016; Woo, 2012; Yde et al., 2012). Perfect conditions for icing formation imply that water flows for some distance before it freezes and, thus, these conditions are characterized either by slightly negative temperatures or by constant high rates of discharge during winter (Moorman & Michel, 2000). Icings are defined as a mass of surface ice formed during the winter by a successive freezing of sheets of water (Carey, 1973) and are generated when water floods onto existing ice (Moorman & Michel, 2000), snow surfaces (Hodgkins, Tranter, & Dowdeswell, 2004; Moorman & Michel, 2000; Stachnik, Yde, Kondracka, Ignatiuk, & Grzesik, 2016), or flows in between existing icing layers and freeze (Moorman & Michel, 2000). Thus, icing can grow both from the bottom due to ice accretion, and from the top due to water freezing and incorporation of snow (Stachnik et al., 2016). When water freezes quickly (i.e. flow rate is equal or smaller than freezing rate), a white bubbly ice layer is formed, and when the freezing is slow - it results in a clear ice layer (Moorman & Michel, 2000). When unfrozen water gets trapped between ice layers or when there is groundwater discharge underneath the existing ice layer, blister or icing mound can be formed due to increased hydrostatic pressure resulting from the freezing of trapped water (Carey, 1973; Michel, 1986).

1.2 Glacier response to climate change

In response to the current changing climate, glaciers are declining and retreating all over the world (Bliss, Hock, & Radić, 2014; Oerlemans, 2005; Zemp et al., 2015) with the exception of the Kunlun Shan region, where positive mass balances are reported, making the so-called "Karakoram anomaly" (Brun, Berthier, Wagnon, Kääb, & Treichler, 2017; Farinotti, Immerzeel, Kok, Quincey, & Dehecq, 2020; Hewitt, 2005; de Kok, Tuinenburg, Bonekamp, & Immerzeel, 2018). Otherwise, the primary response of glaciers to rising temperatures is the increase in glacier runoff as a result of higher melt rates. During this first stage, enhanced melt per unit area balances out the reduction in glacier volume. When the glacier volume decreases significantly and becomes too small to provide enough meltwater, runoff starts decreasing (Jansson et al., 2003). The turning point is commonly referred to as peak water (Carey et al., 2014; Huss & Hock, 2018; Mark, Mckenzie, & Gomez, 2005; Milner, Brown, & Hannah,

2009; Moore et al., 2009). Some studies have shown that the switch between increasing and decreasing streamflow coincides with a glacier cover decrease below 10% of the watershed area (Birsan, Molnar, Burlando, & Pfaundler, 2005; Fleming & Clarke, 2003; Hodgkins, 2009; Pellicciotti, Bauder, & Parola, 2010). In terms of runoff variability, meltwater routing becomes more efficient as glacier loses its thickness, which leads to increased diurnal amplitudes in runoff (Walder & Fountain, 1998; Hock, Jansson, & Braun, 2005). Seasonal and year-to-year runoff variability of a glacierized watershed also increases, as the glacier cover continues losing its buffering capacity (Fleming & Clarke, 2005; van Tiel, Kohn, Van Loon, & Stahl, 2019; Walder & Fountain, 1998). In addition, peak discharge timing shifts towards earlier in the season, closer to snowmelt peak (Beniston et al., 2018). A recent global study by Huss and Hock (2018) used the Global Glacier Evolution Model to calculate changes in glacier mass and subsequent changes in river runoff, and showed that most glacierized catchments south from the subarctic area, with an exception of Himalaya region, have passed peak water. The same study shows that, in the subarctic St. Elias Mountains (Yukon, Canada), large glacierized watersheds have not yet reached peak water, and that a continuous increase in glacier runoff contribution to main stream runoff during an ablation season (i.e. July – October) for the period 2000-2090 is projected (Huss & Hock, 2018). In the same region, Fleming and Clarke (2003) also report an increase in annual runoff volumes for all glacierized watersheds and detect no changes for non-glacierized watersheds, suggesting that glacier cover is a primary control over magnitude and direction of watershed's response to changes in climatic forcing. Brabets and Walvoord (2009) detected an increase in annual discharge for some glacier-fed streams in the Yukon River Basin, which they also attributed to increased glacier melt contribution. In neighbouring subarctic Alaska, an increased flow variability and intensive flow reduction is projected for the ablation season and during the recession period for the end of the century (Van Tiel et al., 2018).

Glacier retreat is known to affect the geomorphology of the immediate proglacial field and, as a result, will change the distribution of moraine-dammed lakes (Johnson, 1986), which in some cases can lead to river piracy and thus have implications for downstream runoff (Shugar et al., 2017). Another geomorphological consequence of glacier retreat is stagnant glacier ice

deposition within the immediate proglacial field. This ice gradually gets buried by glacier moraines and slope colluvial material, thus forming buried ice features (Everest & Bradwell, 2003; Johnson, 1986; Schomacker, 2008).

Climate change and consequent glacier shrinkage will also affect glaciers thermal regime. Simulations show that, under negative mass balance conditions, mid-sized glaciers in the study region exhibit general cooling and will become entirely cold before disappearing (Wilson & Flowers, 2013; Wilson et al., 2013). This can be explained by the thinning of firn layers and retreating accumulation zone (Wilson & Flowers, 2013). A potential decrease in icing extent next to glacier terminus can be expected due to changes in glacier thermal regimes from polythermal to cold (Sobota, 2016). However, a potential increase in icing extent can result from an increase in average winter temperatures, occurrence of melt events and increase in winter discharge (Sobota, 2016).

1.3 Proglacial field hydrology

Studies addressing hydrology within subarctic proglacial field are limited (e.g.,Vincent, Violette, & Aðalgeirsdóttir, 2019), and thus its conceptual hydrological model is summarized based on studies in tropical mountains (Peru and Chile), temperate mountains (Alps and Rockies), and a few studies from mountainous catchments in arctic and subarctic areas (Alaska and Iceland).

Proglacial fields are transitional landscapes “from glacial to non-glacial conditions” (Heckmann et al., 2016). They are characterized by the presence of features such as talus slopes, moraines, and they are regularly flooded by glacier meltwater (Cooper, Wadham, Tranter, Hodgkins, & Peters, 2002). In glacierized watersheds in temperate-climate mountains, the groundwater stored in moraines and talus buffers a watershed response to both melt and precipitation events (Cochand, Christe, Ornstein, & Hunkeler, 2019; Langston, Bentley, Hayashi, Mcclymont, & Pidlisecky, 2011; McClymont et al., 2011) and maintains summer baseflow (Muir et al., 2011). The mechanism by which they contribute to the runoff is similar

to fill-and-spill mechanism where water accumulates in small bedrock depressions at the bottom of the moraine/talus (Langston et al., 2011; Muir et al., 2011). The runoff from these colluvial features is also important during winter season, in particular during years with reduced snowmelt (Stoelzle, Schuetz, Weiler, Stahl, & Tallaksen, 2019). In some regions groundwater discharge from a talus can be the dominant component of the winter baseflow (Cochand et al., 2019; Clow et al., 2003; Muir et al., 2011).

As a result of glacier dynamics (glacier advance, surging, and retreat), specific features, such as buried ice and ice-cored moraines, form in the subarctic proglacial field (Johnson, 1971). A debris cover above buried ice or ice core shields it from direct radiation, and thus the energy for melting is delivered to the ice surface by means of heat transfer through the debris cover. Ice-cored moraine ablation can be enhanced by the removal of the debris and bare ice exposure. The removal of the debris layer can happen as a result of its saturation by meteoric water and consequent sliding due to gravitational processes. Moreover, glacier meltwater can erode moraine sediments and, in addition to producing thermal erosion of the ice, it can destabilize the debris layer and trigger its further removal (Johnson, 1971).

Within proglacial areas, two groundwater systems are often distinguished: the shallow (or fast) and the deep (or slow) groundwater (Crossman, Bradley, Boomer, & Milner, 2011; Hood, Roy, & Hayashi, 2006; McClymont et al., 2011; Roy & Hayashi, 2009). A shallow system comprises upper layers of glacier sediments, where the infiltration into deeper layers can be abstracted by impermeable boundaries such as buried ice (Langston et al., 2011; McClymont et al., 2011; Roy & Hayashi, 2009) or shallow bedrock (Roy & Hayashi, 2009). In deep groundwater systems, water either flows through the network of fractures within the bedrock (Ajami, Troch, Maddock, Meixner, & Eastoe, 2011) or on the top of the bedrock (McClymont et al., 2011). In permafrost underlined regions, these systems evolve as the thaw season progresses and thawed layer thickness changes (Cooper et al., 2002).

Proglacial field groundwater aquifers are recharged by glacier melt (Liljedahl, Gaedeke, O'Neel, Gatesman., & Douglas, 2016; Roy & Hayashi, 2009), snowmelt (Brown et al., 2006;

Cochand et al., 2019; Muir et al., 2011; Penna et al., 2014; Roy & Hayashi, 2009), rain (Dochartaigh et al., 2019; Roy & Hayashi, 2009), possibly buried (or stagnant) ice melt (Cooper et al., 2002; Levy, Robinson, Krause, Waller, & Weatherill, 2015; Roy & Hayashi, 2009) as well as water discharging from moraines and taluses (Dochartaigh et al., 2019). In general, at the beginning of the ablation season, snowmelt is the principal source of groundwater recharge and, as the season progresses, its role diminishes and the recharge from both ice melt and rain increases (Crossman et al., 2011). Due to its limited storage capacity, at the beginning of the ablation season, an aquifer within the proglacial field is mostly recharged. Later in the ablation season, when the level in the stream subsides following the melt rates decrease, the groundwater stored in this aquifer is discharged into the stream (Cooper et al., 2002). As stored water discharges, the water table gradually lowers (Cochand et al., 2019; Dochartaigh et al., 2019).

The contribution of these different hydrological components to the subsurface flow is complex and it both depends on the season and varies in space: within the parts that are closer to the glacier and the main stream, the groundwater aquifer is mostly recharged by glacier meltwater (Dochartaigh et al., 2019; Levy et al., 2015), whereas further from the stream its recharge is dominated by precipitation and/or water from moraines and taluses (Dochartaigh et al., 2019). Moreover, when moving downstream from the glacier outlet, groundwater discharge into main stream is observed, whereas at the upper reaches the groundwater aquifer is mainly recharged by the stream (Dochartaigh et al., 2019).

1.4 Proglacial field evolution under changing climate

There are not many observations yet about the evolution of subarctic proglacial field hydrology in a context of climate change, and most of the relevant studies focus on the evolution of groundwater systems within the non-glacierized part of the watershed. Thus, this sub-section will describe the hydrogeological changes within a proglacial field in response to climatic-change-driven hydrological changes.

In response to climate change, a decline of groundwater levels was observed in glacierized watersheds in British Columbia, Canada (Moore, Allen, & Stahl, 2007) and in Skeidararsandur, Iceland (Levy et al., 2015). The most pronounced changes are observed close to glacier margins, and the less pronounced are in the area of groundwater seeps (i.e. slow groundwater discharge through the voids and cracks in unconsolidated materials,Woo, 2012) (Levy et al., 2015). A pronounced lowering of water table next to glacier terminus is possibly a consequence of a decrease in aquifer recharge by glacier meltwater as glacier retreats (Levy et al., 2015). This hypothesis is confirmed by previous observations of a decline in groundwater levels in autumn and early spring when glacier ablation seizes (Robinson, Fairchild, & Russell, 2008), and by an observed direct link between meltwater production and groundwater levels close to glacier terminus (e. g. Cooper et al., 2002; Magnusson et al., 2014). In addition, glacier retreat will lead to a decrease in overburden pressure, which in turn will lower the hydraulic gradient within the proglacial field aquifer (Levy et al., 2015). In response to climate change, meltwater channels within the proglacial field will likely alter their positions following the change in glacier tongue position and its geometry, and due to ice-cored features formation (Johnson, 1986). This meltwater channles adjustement will affect surface-groundwater exchange. In addition, the hydrogeological system within the proglacial field is affected by changes in moraine lakes: in Skeidararsandur, groundwater levels measured close to moraine lakes declined following the decrease of lake area (Levy et al., 2015). Here, buried ice ablation can enhance the evolution and disappearance of moraine lakes (Levy et al., 2015).

Changes in water balance components such as precipitation and evaporation can affect shallow groundwater systems either directly, by changing water input to the system, or indirectly, by affecting meltwater production (Levy et al., 2015). In particular, precipitation events can enhance the melt of glaciers (Oltmanns, Straneo, & Tedesco, 2019) or that of buried ice by eroding the debris cover (Johnson, 1971; Levy et al., 2015). Indeed, buried ice degradation by backwasting seems to be more efficient in temperate humid climatic conditions, and minimal in cold dry climates (Schomacker, 2008).

On a larger scale, several modelling-based studies have attempted to predict groundwater/baseflow evolution in upper glacierized watersheds over the next century. In the Nepalese Himalaya, the baseflow is projected to increase, and together with increasing precipitation, it will maintain an increase in total runoff regardless the decreasing glacier runoff (Immerzeel, van Beek, Konz, Shrestha, & Bierkens, 2012). In the Peruvian Andes, relatively constant projected groundwater discharge will also buffer decreasing glacier runoff (Somers et al., 2019). In this region, glacier meltwater does not contribute significantly to groundwater storage, and an eventual decrease in groundwater discharge is attributed to increasing evaporation (Somers et al., 2019). Finally, in the Canadian Rockies modelling results for glacierized watershed show an increase in groundwater contribution to the total runoff throughout the year apart from July and August, when it is projected to decrease (Loukas, Vasiliades, & Dalezios, 2002). The groundwater input is projected to become more uniformly distributed throughout the year as a result of its increase during spring, summer and autumn, and its decrease during winter (Loukas et al., 2002).

1.5 Subarctic alpine meadow hydrology

In the alpine meadows of subarctic glacierized watersheds, hydrology is characterized by the presence of permafrost and seasonally frozen ground. Thus, to illustrate potential effects of permafrost on watershed hydrology, this section is based on studies from areas underlined by discontinuous permafrost.

The frozen ground is usually considered impermeable to groundwater flow (Woo, 2012). Groundwater circulation within permafrost underlain slopes can be suprapermafrost (above permafrost), intrapermafrost (in taliks, faults, and conduits within permafrost) and subpermafrost (below permafrost) (Woo, 2012). Because of the low hydraulic conductivity of frozen soil, the infiltration and storage capacity of subarctic aquifers are in general temperature-dependent (Hayashi, 2013; Woo, 1986). As a result, there is a spatial dependence of soils' hydrological properties. For example, processes on South-facing (S-slope) and North-facing (N-slope) slopes of watershed differ due to differences in the incoming solar radiations.

Conceptually, the common effects of these differentiations are higher snow water equivalent (SWE) for N-slopes prior to melt, presence of permafrost and of an organic top layer (Carey & Woo, 1998; 2001b). It is important to note, that the subdivision into S- and N-facing slopes is mainly conceptual and that the hydrological systems of the watershed can be more complex.

With lower SWE, S-slope becomes snow free earlier in the snowmelt season. In the absence of permafrost, as the seasonal frost table lowers, water produced by snowmelt infiltrates into the mineral soil layer, thus, producing limited surface runoff and supplying the unfrozen groundwater reservoir. Once snow free, liquid precipitation infiltrates the S-slope and delays their contribution to the main stream (Carey & Quinton, 2004).

On N-facing slopes, infiltration is restricted due to underlying permafrost and, therefore, surface runoff plays a greater role in the contribution to main streams. At the beginning of the thawing season, the surface runoff from the N-facing slope is delayed because water produced by snowmelt can be stored in a thicker snowpack (Carey & Woo, 1998), and because infiltrated water is used for organic layer pre-wetting (Carey & Woo, 2001a). Once the snowpack has melted, the runoff production and the response time to liquid precipitation events from the N-facing slope will depend on the unfrozen layer thickness. Only once the upper organic layer has thawed, the flow can be enhanced by the presence of preferential paths within the organic layer (Woo, 2012). Once the flow is shifted to the mineral soil layers that start thawing, runoff rate decreases due to the lower permeability of mineral soils. The switch between these two horizons can also happen due to water table rise as a result of precipitation events. N-facing slopes are conceptually divided into two zones: the slope base with a thicker organic layer and the upslope area with a thinner organic layer (Quinton & Marsh, 1999). When water table rises, both zones deliver water through the saturated organic layer to the main stream (Carey & Woo, 2001a). Once the water table lowers, the upslope area becomes hydrologically disconnected from the stream, and only the slope base keeps on contributing to the stream (Quinton & Marsh, 1999).

Taliks in areas underlain by permafrost can affect hillslope hydrology. Their spatial distribution will affect the recharge of the groundwater system, the contribution to streams, and the occurrence of springs. Large icings (aufeis) are common features of permafrost underlined terrains (Yoshikawa, Hinzman, & Kane, 2007). In some regions, icings can represent the second-largest surface water storage after snow, and can store up to 40% of winter outflow (Yoshikawa et al., 2007). The sources for icing formations can be supra- (Clark & Lauriol, 1997; French & Heginbottom, 1983; Pollard, 2005), intra- and/or subpermafrost water (Hu & Pollard, 1997; Kane & Slaughter, 1973; Kane, 1981; Pollard, 2005; Yoshikawa et al., 2007). Icings that are fed by intra- or subpermafrost water continue to grow throughout the winter (Kane, 1981; Pollard, 2005; Yoshikawa et al., 2007), whereas icings that are only fed by suprapermafrost water cease to grow before the end of the winter when water storage within suprapermafrost aquifer is exhausted or when conduits, which deliver water to the surface, freeze (Pollard, 2005). In addition, icings in these regions can be formed from river ice itself when an accumulation of frazil ice crystals occurs in stream's super cooled water (Hu & Pollard, 1997). The ice cover then grows and eventually reduces the cross-section of the stream, thus, damming the water upstream of the icing. This damming effect provokes icing growth upstream as well as flooding of the original ice cover until the flow decreases substantially to reach the conduit capacity (Hu & Pollard, 1997).

1.6 Subarctic alpine meadow evolution under changing climate

Modelling results (Zhang et al., 2013; Zhang, Chen, & Riseborough, 2008a, 2008b) and both direct and indirect observations (Hinzman et al., 2005; James, Lewkowicz, Smith, & Miceli, 2013; O'Donnell, Aiken, Walvoord, & Butler, 2012; Smith, Burgess, Riseborough, & Nixon, 2005; Tarnocai, Nixon, & Kutny, 2004) show that the increase of air temperatures is warming permafrost and increasing the thickness of the active layer, creating new groundwater pathways as well as keeping groundwater flow active for a longer period during the freezing season. This leads to an increased hydraulic connectivity and enhanced groundwater flow. As a result, groundwater reservoir storage capacity increases (Walvoord & Kurylyk, 2016; Velicogna, Tong, Zhang, & Kimball, 2012). However, the deepening of the active layer leads to the

lowering of the water table and thus potentially decreases the hydraulic gradient which, in some cases, can counteract the effect of the increased connectivity on groundwater flow (Walvoord & Kurylyk, 2016). Moreover, as the thickness of the active layer increases, the water is routed though deeper and less conductive mineral soil layers, which decreases its flow rate (Quinton & Baltzer, 2013).

According to modelling results, the deepening of the active layer and the increase of groundwater storage can provoke changes in regional connectivity between catchments and eventually lead to a decrease in groundwater contribution to the runoff in the headwaters and upstream reaches, and an increase in the downstream sections of continuous permafrost watersheds (Bense, Kooi, Ferguson, & Read, 2012; Lamontagne-Hallé, McKenzie, Kurylyk, & Zipper, 2018). Other modelling works suggest that, due to permafrost thaw, the magnitude and spatial extent of groundwater contribution to stream will increase (Ge, McKenzie, Voss, & Wu, 2011; Bense et al., 2012; Evans & Ge, 2017). This increase will be accompanied by a concurrent enhanced formation of taliks (Lamontagne-Hallé et al., 2018; McKenzie & Voss, 2013; Zhang et al., 2008a, 2008b), a decrease in proportion of suprapermafrost water to baseflow, and its shift towards deeper sources (Walvoord, Voss, & Wellman, 2012). For example, in the Yukon River headwaters, the rate of permafrost-thaw-induced increase in groundwater contribution to the runoff is estimated to range between 0.7 and 0.9% per year (Walvoord & Striegl, 2007).

Another potential impact of warming air temperatures is the direct contribution of water from a porewater phase change due to thawed permafrost, but it is expected to influence the runoff to a much lesser extent in comparison with projected hydrogeological changes (Walvoord & Kurylyk, 2016).

Areas with seasonally frozen ground are also projected to undergo an increase in groundwater discharge, but with a much smaller magnitude (Evans & Ge, 2017). In particular, for hillslopes where groundwater reservoir is mostly recharged by snowmelt, modelling results predict an

increase in spring and a decrease in summer groundwater discharge (Evans, Ge, Voss, & Molotch, 2018).

Currently, no concurrent trends in volume of icings (aufeis) and their special distribution are observed in permafrost-underlined terrains (Morse & Wolfe, 2016; Yoshikawa et al., 2007). This can be explained by the fact that an increase in the winter baseflow due to permafrost thaw is balanced out by an increased occurrence of warmer winter temperatures (Walvoord & Kurylyk, 2016).

CHAPTER 2

CONCEPTUAL METHODOLOGY AND THESIS ORGANIZATION

The lack of knowledge about the hydrological processes in glacierized catchments, other than those directly related to glaciers, is starting to be recognized (e.g., Hood et al., 2006). Closing the existing gap becomes more timely as temperatures continue to rise and glaciers continue to retreat (Immerzeel et al., 2019). Climatic changes also urges us to adjust the research procedure since the system behavior that we currently try to project is most likely "beyond the range of previously observed variability" (Wagener et al., 2010). Taking those statements into account, I decided at the early stage of this research project that i) the project would focus on understanding integrated hydrological processes in glacierized catchments, and ii) *in situ* data collection would be necessary accepting the challenge such field activity represents. Indeed, field expeditions in remote areas generate high costs and increase risks, such as inevitable instrument failures in such environments, bad weather, and potential difficulties to publish resulting "case studies" in international journals (Blume, van Meerveld, & Weiler, 2017; Burt & McDonnell, 2015).

The first phase in the Baconian (scientific) method consists of iterations between the research question and background check (Figure 2.1) (Bacon, 1960). This phase is presented in the Introduction and Literature review sections of the present thesis (Chapters 1 and 2). The next phase is dedicated to constructing the initial hypothesis and setting up a research objective and research questions, and it is also addressed in the Introduction. The third phase of the project, which is described in the upcoming section, consists of defining the experimental setup and designing data acquisition, and it is followed by data analysis and hypothesis confirmation or rejection (Figure 2.1).

2.1 Experiment design and data acquisition

The first step in the field-based research project is choosing an appropriate location for the field site. Motivated by the rapidly changing Polar Regions (Meehl et al., 2007; Larsen et al.,

2014) and the concurrent lack of hydrological studies in those regions in comparison with temperate climates (Burt & McDonnell, 2015; Vincent, Violette, & Aðalgeirsdóttir, 2019), I decided that the study site should be located in the Canadian subarctic.

When choosing a field site it is important to consider several logistical aspects in addition to scientific rationale. For instance, a research station where the team can be based and where equipment can be stored between field seasons can facilitate the work significantly. The site accessibility should also be taken into account as well as potential restrictions for research conduction (necessary permits, licences, allowed methods etc.). Finally, the infrastructure in the area should be developed enough to permit organizational steps such as equipment shipping and food supply. After considering those aspects, the Duke River watershed in the St. Elias Mountains, Yukon, was chosen as a field site (Figure 2.2). This watershed is part of the Water Survey of Canada network (Environment and Climate Change Canada, https://wateroffice.ec.gc.ca/), and has a gauging station at the river outlet.

This last point is important. Because of this existing Water Survey of Canada network, in the interim of the first field work preparations, it was possible to start an analysis of available historical hydro-meteorological time series. The goal of this analysis was to obtain the evidence of both meteorological and hydrological changes in the region based on observations. Coupled with analysis of hydrological regimes and peak water analysis (see Chapter 3), it allowed understanding of the role of glacier retreat in recent hydrological changes in the region, and therefore made the first step of the initial hypothesis confirmation or rejection.

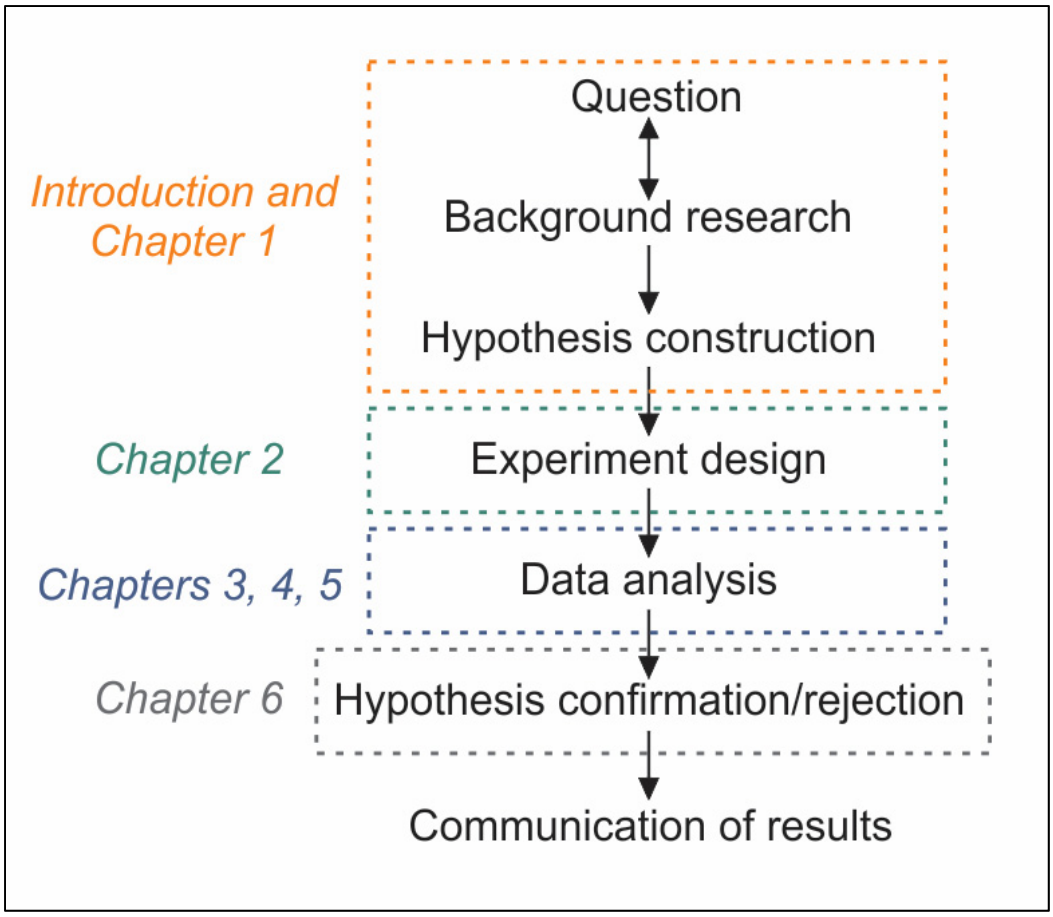

Figure 2.1 Scientific method application in the project and thesis organization

Two other research questions (see research questions 2 and 3 in the Introduction) required field work data collection. Prior to the first field campaign, one has to obtain a permit to conduct field work in the chosen field site. For the Kluane region, those include a permit from Parks Canada and Kluane First nation, a backcountry permit, a landing permit and a Scientists and Explorers License. According to the agreement with Parks Canada, only 4 field campaigns were allowed with a maximum participants number of 3 and with a duration of no longer than 15 days. Due to these restrictions and the remoteness and difficulty to access, a multi-technique approach was chosen in the field. Conceptually, this approach aims to measure and observe hydrological processes in the studied watershed from different perspectives addressing the mitigation of risks related to potential equipment failure. Field techniques included hydro-meteorological monitoring, time lapse imagery, and natural tracers. The project included four

field campaigns: 26 June-12 July 2015, 10-24 June 2016, 30 July-15 August, and 11-28 June 2018. The main motivation to conduct field campaigns in these periods was to be able to capture hydrological systems during different parts of the ablation season.

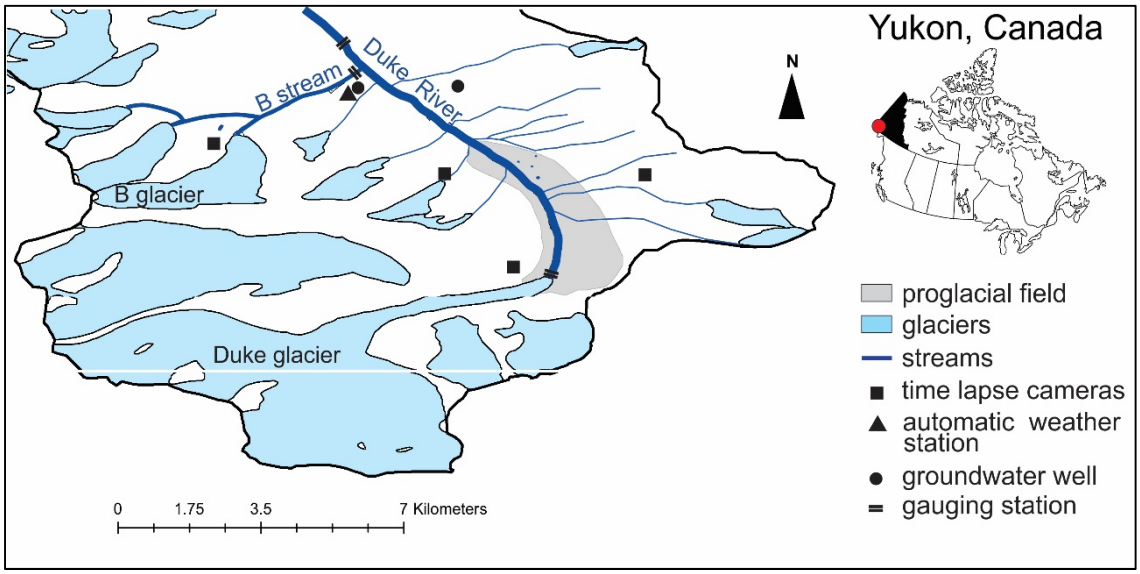

Figure 2.2 Upper Duke River valley with location of main monitoring equipment

The first field campaign took place during the period of 26 June – 12 July 2015 in the upper Duke River valley and served mostly as a reconnaissance and preliminary exploration. The scientific program of this campaign focused on installing long-term monitoring equipment in the main valley and in one of the smaller sub-watersheds (called watershed B hereafter), and collecting samples for hydrochemical analysis. Among monitoring equipment, three gauging stations were installed at outlet of the Duke Glacier, downstream in the Duke River and in a B stream prior to the junction with the Duke River (Figure 2.2). The goal was to obtain hourly time series of discharge that would eventually help to quantify the contribution of different water sources into those streams. Both the Upper Duke River valley and the B watershed were equipped with a total of four time-lapse cameras (featuring the Duke Glacier and its proglacial field, the upper part of the Duke River valley, and the main glacier of the B watershed) (Figure 2.2). Each of those cameras was coupled with temperature and relative humidity sensors as well as with a snow-scale. Together with pressure transducers, temperature probes were

inserted into soil boreholes to monitor groundwater level and temperature evolution throughout the year. Finally, an automatic weather station (AWS) was mounted in the Duke Valley bottom close to the junction with B stream. It measured air temperature, relative humidity, atmospheric pressure, wind speed and direction, total radiation and liquid precipitation.

During the first field campaign, water samples from different water sources were collected in the B watershed to be analyzed for stable isotopes, major ions and organic carbon concentration. Waters originating from different sources (end-members) can present unique hydrochemical and isotopic signatures as a result of the specific hydrological, geological, and biological processes to which they have been exposed (Drever, 1997). Therefore, those natural tracers can be used (i) to get insights into hydrological, geological, and biological processes acting on the end-member, and (ii) to quantify the end-member's contribution to the runoff based on relative concentrations of natural tracers in the end-member and in the runoff. The original plan included hydrochemical sampling of the entire Upper Duke River Valley. However, after not being able to cross the Duke River (not even next to the glacier tongue, nor at 3 a. m.) with the equipment that was available that year, this plan had to be cancelled that year.

Several lessons were learned during the first field campaign. First, as the size of the watershed was too large for the project objectives, the targeted research area had to be decreased. Also, a system to cross the main river in safe conditions had to be designed and mounted for the next campaigns. Finally, it was observed that the wildlife contributed to the damage of monitoring instruments. That possibility had been anticipated for bears but not for marmots and sheep.

During the field campaign of 2016, the maintenance of existing monitoring equipment was carried out and new devices were installed. During this field campaign both sides of the valley were accessible and thus additional time lapse cameras and groundwater wells were placed on the other side of the valley (Figure 2.2). Also, a sampling of water for hydrochemical analysis was collected within the entire Upper Duke River watershed and was repeated in the B watershed. The gauging station next to the Duke Glacier tongue was no longer in place. The

one downstream from the confluence with the B watershed was in place, but no longer under water as the stream shifted due to an accumulation of sediments.

The field campaign of 2017 consisted of the maintenance and removal of existing monitoring equipment, geophysical measurements in the proglacial field with ground-penetrating radar and electromagnetic induction, and hydrochemical sampling along the geophysical lines in the Upper Duke River and also repeating sampling in the B watershed.

Finally, the last 2018 field campaign was about removing equipment from the study area following the agreement with Parks Canada.

2.2 Data analysis and hypothesis confirmation

The subsequent phases of the scientific research are presented in the following chapters. Chapters 3, 4, and 5 are dedicated to the data analysis for each of the three research questions presented at the Introduction. Chapter 3 presents the paper "Linking Mountain Glacier Retreat and Hydrological Changes in Southwestern Yukon" published in Water Resources Research. The main objective of this article was to isolate and quantify the role of shrinking glaciers in recent hydrological changes in southwestern Yukon by using an enhanced dual approach which is based on trend analysis of discharge time series and model-based peak water analysis. The specific objectives were to: 1) disentangle glacier-related regional hydrological changes from those that are not driven by glacier retreat, 2) position glacierized watersheds in relation to the peak water and 3) identify those glacier characteristics that drive hydrological changes. The results of this paper answered the first research question of this project and allowed exploring hydrological processes in the region.

Chapter 4 is based on the article "How significant are water sources other than glacier in arid highly glacierized subarctic watershed?" submitted to the Journal of Hydrology. Based on data collected over the first, second and third field campaigns, the paper disentangles the importance of all hydrological components (e.g., glacier meltwater, ice-cored moraines and buried ice,

talus, alpine meadow) to the total runoff of the so called B watershed, under different meteorological conditions. It aimed to answer the following research questions: 1) in highly glacierized subarctic watersheds, is there any significant contribution from sources other than glaciers? 2) Is it possible to identify specific contributing sources and to quantify their contributions to the watershed runoff? 3) How does the runoff components contribution change under different meteorological conditions? By answering those research questions the paper puts into light the complexity of the hydrological system in glacierized subarctic watersheds during the ablation season.

The paper “Proglacial icings as records of winter hydrological processes”, submitted to the Cryosphere Journal, makes the Chapter 5. It is based on the results of the second and third field campaigns. The main objective of this study was to better understand the genesis of icings in the Upper Duke River valley to obtain new insights into the generation of winter baseflow. The following research questions were specified: 1) is glacier runoff the most important water contributor to winter baseflow and to icings formation? 2) Does the water from the suprapermafrost layer contribute to icing formation and hence to winter baseflow? And 3) are there other hydrological sources that contribute substantially to icings formation? The results of this study shed a light on winter hydrological processes in glacierized subarctic watersheds.

Chapter 6 is dedicated to the thesis discussion which will put together the objective, hypothesis and the results summarized in three papers. As a result, the initial will be either confirmed or rejected. In particular, the first part of the hypothesis - the subarctic proglacial areas play an important role in the hydrology of glacierized valleys - will be confirmed if our results show that water sources within proglacial field contribute to runoff throughout the ablation (Chapter 4) and winter season (Chapter 5). These results together with the results of trend attribution (Chapter 3), will help to confirm the second part of the initial hypothesis - glacier retreat does not entirely define their hydrological response to climate change – in case substantial changes are observed in different hydrological regimes. Moreover, in this chapter project implication will be discussed as well as potential ways forward.

CHAPTER 3

LINKING MOUNTAIN GLACIER RETREAT AND HYDROLOGICAL CHANGES IN SOUTHWESTERN YUKON

A. Chesnokova,[1] M. Baraër,[1] T. Laperrière-Robillard,[1] and K. Huh[2]

[1]Department of Construction Engineering, École de technologie supérieure,
1100 Notre-Dame West, Montreal, Quebec, Canada H3C 1K3
[2]Department of Geography and Anthropology, California State Polytechnic University,
3801 West Temple Avenue, Pomona, California, USA 91768

Paper published in the *Water Resources Research Journal*, January 2020

Abstract

This study aims to isolate and quantify the role of shrinking glaciers in recent hydrological changes in eight watersheds in the southwestern Yukon (Canada) by using an original dual approach that consists of (i) watershed hydrological regime identification, followed by a trend analysis of discharge time series, and (ii) a model-based peak water (PW) analysis using glacier cover change measurements. A distinction between hydrological regimes is a necessary add-up to commonly used trend attribution methods as the lake-runoff regime shares common characteristics with the glacier regime. Results show a link between shrinking glaciers and hydrological changes in the region, but the link is complex, and glacier retreat does not explain all the observed changes. Model outputs show that the two watersheds with a glacierized area exceeding 30% and one watershed with 2.9% glacierized area have not reached PW, whereas a 9.2% glacierized watershed and another watershed with 2.1% glacierized area have already passed it. These results suggest that glacierized area alone cannot explain short-term changes related to watershed current position in terms of PW, and the rate of glacier retreat must be considered. By contrast, the actual rate of glacier retreat does not influence long-term changes, such as the magnitude of PW and of the consequent drop in discharge. Once glaciers will have retreated to a point close to extinction, declines in summer discharge from 10% to 70% and proportional to the actual glacier cover are anticipated at watersheds that are currently more than 9% glacierized.

Key Points

1. Noticeable acceleration of glacier retreat occurred in southwestern Yukon since 1999 with measured consequences for the regional hydrology.
2. Various hydrological changes have been detected at the study watersheds. Glacier retreat explains many but not all of those changes.
3. Long-term hydrological changes are glacier cover dependent while decadal-scale changes are driven by glacier retreat rate.

Keywords: peak water, trend analysis, glacierized catchments, southwestern Yukon

3.1 Introduction

The decay of such cryosphere components as snow, ice, or permafrost is one of the most conspicuous environmental changes that affect mountains around the globe (e.g., Beniston et al., 2018; Marzeion, Jarosch, & Hofer, 2012). The cryosphere is an important source of water in mountainous regions (Huss et al., 2017), and losing portions of it is predicted to lead to adverse societal, ecological, and economic impacts far downstream (Beniston et al., 2018; Kistin, Fogarty, Pokrasso, McCally, & McCornick, 2010; Mark et al., 2017; Vuille et al., 2018). Shrinking cryosphere impacts on water resources were and continue to be the object of intense research on a local (e.g., Finger, Heinrich, Gobiet, & Bauder, 2012; Hirose & Marshall, 2013; Jost, Moore, Menounos, & Wheate, 2012; Ragettli et al., 2015), regional (e.g., Condom et al., 2012; Frans, Istanbulluoglu, Lettenmaier, Fountain, & Riedel, 2018; Kang, Liu, Xie, Xin, & Shen, 2009; Koboltschnig & Schöner, 2011), and global scale (e.g., Fountain & Tangborn, 1985; Kaser, Grosshauser, & Marzeion, 2010; Huss & Hock, 2018). Despite major advances, identifying direct causal links between measured hydrological changes and a particular cryospheric phenomenon remains challenging at a watershed scale (D. H. Burn & Hag Elnur, 2002). Hydrological implications of a shrinking cryosphere frequently result from several of its terrestrial components operating synergistically or antagonistically with other hydrological components (Prowse, 2009). In the case of glacierized catchments, such

components as glaciers, seasonal snow cover, buried ice, and icings (a mass of surface ice formed during the winter by successive freezing of sheets of water; Carey, 1973) can contribute to the supply of meltwater to the watershed outflow, adding to the surface runoff and groundwater (Brown et al., 2006; Clow et al., 2003; Yoshikawa et al., 2007). The resulting difficulty in differentiating glacier retreat from other causes of discharge variations makes hydrological trend attribution in such systems a complex exercise (Duethmann et al., 2015).

Two different approaches are traditionally used in trend attribution in glacierized catchments: historical data analysis and modeling (Kormann, Bronstert, Francke, Recknagel, & Graeff, 2016). Data analysis commonly uses statistical methods for trend detection, either on existing hydrological data only (Dery et al., 2009; Fleming & Clarke, 2003) or on both hydrological and meteorological data (Birsan et al., 2005; Pellicciotti et al., 2010). The influence of glaciers can be then estimated either by comparing the results among watersheds with different glacier cover (e.g., Birsan et al., 2005; Fleming & Clarke, 2003) or by performing additional trend detection on glacier mass balance time series where available (e.g., Li, Wang, Zhang, Wang, & Li, 2010; Pellicciotti et al., 2010). The main advantage of the historical data analysis approach is that it provides a reliable estimate of recent changes in real discharge variables (Shahgedanova et al., 2018; Stahl et al., 2010). However, while the attribution of statistically identified historical trends to specific drivers of change can be accomplished with some confidence using paired catchment experiments (e.g., Dahlke, Lyon, Stedinger, Rosqvist, & Jansson, 2012; Fleming & Dahlke, 2014a, b) or a two-step process involving river-by-river trend detection followed by statistical tests to establish relationships with specific watershed properties such as the extent of glacier cover (Fleming & Clarke, 2003; Stahl & Moore, 2006), studies based on trend detection are sometimes limited by being based solely on qualitative reasoning.

Modeling approaches make it possible to generate synthetic discharge time series in response to different climate scenarios at the watershed scale and to study the main drivers of modeled hydrological changes. Different types of glacio-hydrological models, ranging from complex distributed process-based to simple conceptual models, are commonly used for investigating

climate change impacts on glacierized catchment outflows (Farinotti et al., 2012; Frans et al., 2018; Horton, Schaefli, Mezghani, Hingray, & Musy, 2006; Jeelani, Feddema, Van Der Veen, & Stearns, 2012; Jost et al., 2012; Naz et al., 2014; Nolin, Phillippe, Jefferson, & Lewis, 2010; Ragettli, Immerzeel, & Pellicciotti, 2016; Stahl, Moore, Shea, Hutchinson, & Cannon, 2008; Van Tiel et al., 2018). However, a distributed physically based glacio-hydrological model (e.g., Naz et al., 2014) can only be applied in regions that possess extensive data sets that include glacier mass balance records, complete meteorological data, and occasional estimates of different hydrological variables (e.g., evapotranspiration, infiltration, snowmelt). For remote regions, however, where only temperature and precipitation measurements at low elevations are available, a conceptual model (e.g., Horton et al., 2006; Jeelani et al., 2012) often represents the only option. In addition, the modeling approach requires reliable regional climate change projections of high spatial resolution that do not always exist. Finally, in areas with limited instrumentation, model parameters, including those describing glacier melt and snowmelt, are often calibrated against discharge measurements (Saelthun et al., 1998), which affects the models' physical representation of processes (Franz & Karsten, 2013) and potentially leads to equifinality (Beven, 2006).

Thus, in studies of complex open environmental systems, the greatest confidence resides with outcomes that are consistent across multiple independent methodologies, including both process simulation and historical data analysis (Fleming, 2018). The explicit representation of process physics in a glacio-hydrologic simulation model, for example, can provide additional valuable insights in trend attribution (Merz, Vorogushyn, Uhlemann, Delgado, & Hundecha, 2012; Unger-Shayesteh et al., 2013).

To our knowledge, a limited number of studies have combined both historical data analysis and modeling in a dual approach for trend attribution in glacierized catchment. The dual approach has been applied in the Western United States by Hamlet, Mote, Clark, & Lettenmaier (2005, 2007) to identify the main drivers of trends in measured snow water equivalent, soil moisture, and evapotranspiration. In the same region, Hidalgo et al. (2009) used both global climate and hydrological models to assess the main drivers of earlier

snowmelt peak. Jeelani et al. (2012) in Western Himalaya, India, complemented the results of a water budget model with a trend analysis of temperature and precipitation time series. In Norway, Engelhardt, Schuler, & Andreassen (2014) applied a conceptual glacio-hydrological model to perform discharge time series trend attribution. Duethmann et al. (2015) used multiple linear regressions and a conceptual hydrological model with a process-oriented approach to link measured increases in stream discharge to glacier melt and climatic conditions in different catchments of Central Asia. Baraer et al. (2012) used a simple water balance hydrological model to allow for pattern recognition in stream discharge time series in Peruvian Cordillera Blanca. That study situates different watersheds against the peak water (PW), a conceptual break point that is regularly used to characterize glacier retreat influence on the long-term evolution of discharge parameters (Carey et al., 2014; Huss & Hock, 2018; Jansson et al., 2003; Mark et al., 2005; Milner et al., 2009; Moore et al., 2009). In conditions of continuous retreat, glaciers produce an initial increase in runoff as they lose mass. The discharge then reaches a turning point, a plateau called PW, and subsequently declines as the volume of glacial ice continues to decrease. This post-PW phase of water decline is characterized by decreases in the annual and ablation season discharges and an increase in flow variability.

In the present study, we apply the dual approach proposed by Baraer et al. (2012) to eight watersheds with different glacierized covers in the southwestern (SW) Yukon, in northern Canada. A recent increase in air temperatures in the SW Yukon is consistently reported in the literature (Arendt, Walsh, & Harrison, 2009; Arndt et al., 2010; Bunbury & Gajewski, 2012; Janowicz, 2010; Vincent et al., 2015; Whitfield & Cannon, 2000), while changes in precipitation remain uncertain. Arendt et al. (2009) detected an increase in total annual precipitation but at a limited number of the studied stations. According to their study, two stations situated in the SW Yukon show significant increases (between 0 and 375 mm) for the period 1950–2000. Janowicz (2008) also notes a possible 5%–15% increase in precipitation in the SW Yukon over the past 3 decades but stresses a disparate situation among the 10 weather stations he studied, with a negative trend in summer precipitation at one site (Janowicz, 2010). Barrand and Sharp (2010) report a reduction in winter precipitation. Vincent et al. (2015) observed a 10–20% increase for the period 1948–2012 in total annual precipitation in the area

as well as a 30–40% increase in winter precipitation and a 10–20% increase in some areas during summer and fall.

Concurrent changes in the study area touch different components of the cryosphere, namely, snow, permafrost, and glaciers. The SW Yukon exhibits a decline in spring snow cover duration of approximately 6 to 8 days per decade for the period 1945–2005 (Brown & Braaten, 1998; Williamson et al., 2018). Permafrost in the Yukon River Basin is actively warming and thawing throughout the basin (O'Donnell et al., 2012) and along the Alaska Highway (Derksen et al., 2012; Smith, Roy, Lewkowicz, & Chartrand, 2017). Extensive glacier shrinkage in the Yukon has been occurring since at least 1958 (Derksen et al., 2012), with an acceleration of mass loss after the 1990s (Arendt et al., 2009). The St. Elias Mountains, situated in the SW Yukon, are characterized by the rapidity of glacier retreat (Radić & Hock, 2010) and are projected to lose 70±10% of glacier volume by 2100 (G. K. C. Clarke et al., 2015), which should lead to a decrease in glacier melt contribution to runoff (Bliss et al., 2014). For the period 1958–2008, Barrand and Sharp (2010) report a 22% loss of glacier area in the St. Elias Mountains, where glaciers of all sizes underwent changes. In general, the St. Elias Mountains exhibit the largest negative mass balance in the Gulf of Alaska (Luthcke, Arendt, Rowlands, McCarthy, & Larsen, 2008), having lost nearly a 0.5 m/year water equivalent during the period 1962–2006 (Berthier, Schiefer, Clarke, Menounos, & Rémy, 2010). However, isolating glacier retreat influence on measured stream discharge in the SW Yukon is problematic because the region is characterized by strong seasonal contrasts in temperatures and a variety of cryospheric elements—such as glaciers, snow, and permafrost—that play a significant hydrological role (Prowse, 2009).

Several studies have described resulting hydrological changes in the SW Yukon. In the early 2000s, Whitfield (2001) reported increases in streamflow throughout most of the year, particularly during the winter months. This tendency has been confirmed by Yue, Pilon, and Phinney (2003) and Janowicz (2008, 2011). Fleming and Clarke (2003) detected that glacierized catchments showed an increase in annual discharge, while the non-glacierized ones showed a decrease. Zhang, Harvey, Hogg, and Yuzyk (2001), followed by Stewart, Cayan, and

Dettinger (2005), reported snowmelt-related changes in freshet timing. The sensitivity of SW Yukon hydrology to climate-related changes in snow cover was later confirmed by Rasouli, Pomeroy, Janowicz, Carey, and Williams (2014).

Different studies related to glacial retreat impacts on river discharge share the conclusion that, unlike glacierized watersheds in Central BC (Stahl & Moore, 2006), PW has not yet been reached in the studied region (Huss & Hock, 2018; Moore et al., 2009), around the Gulf of Alaska (Beamer, Hill, McGrath, Arendt, & Kienholz, 2017; Valentin, Hogue, & Hay, 2018), or across the entire Yukon River Basin (Brabets & Walvoord, 2009a).

These ongoing hydrological changes are predicted to have numerous adverse impacts in the region. Glacier retreat and associated streamflow changes may affect water quality by reducing the dilution of solutes, decreasing sediment load, and increasing stream temperature during the warm months of the year (Fleming & Clarke, 2003; Hood & Berner, 2009; Moore et al., 2009). These impacts are expected to affect the floral and faunal composition of rivers (Dorava & Milner, 2000; Fleming, 2005; Milner et al., 2009; O'Neel et al., 2015) and to cause cascading impacts on the livelihood security of local communities in the Yukon Basin (Wilson, Walter, & Waterhouse, 2015). Anticipating these impacts requires that progress be made in associating hydrological changes with specific cryospheric changes, among other factors.

In light of the above, the objective of this study is to isolate and quantify the role of shrinking glaciers in recent hydrological changes in the SW Yukon by using an enhanced dual approach. More specifically, this study aims to (1) disentangle glacier-related regional hydrological changes from those that are not driven by glacier retreat, (2) position glacierized watersheds in relation to the PW, and (3) identify those glacier characteristics that drive hydrological changes.

3.2 Study area

The study area consists of eight watersheds in the SW Yukon, Canada, selected based on their location, data availability, quality, and representativeness of regional variety of sizes and glacier covers. They are identified throughout the text by their river name (Figure 3.1 and Table 3.1). The examined watersheds are situated on the eastern slope of the St. Elias Mountains and on the Northeastern Coastal Mountains, and their elevation ranges span from 1,250 to 4,300 m. The spatial extent and glacierized area of watersheds vary from 375 to 7,750 km^2 and from 0% to 30.4%, respectively. Watersheds with a glacierized area higher than 30% are characterized by the highest annual and ablation season discharges, and watersheds with no glacier cover have the lowest ones (Table 3.1).

The study area is on the zone of discontinuous and sporadic permafrost (Brown & Braaten, 1998) and includes many surge-type and debris-covered glaciers (Crompton & Flowers, 2015; Kienholz et al., 2015; Sevestre & Benn, 2015). The climate in the SW Yukon is continental, with a mean annual air temperature between −2 and −6°C and a mean annual total precipitation between 250 and 400 mm (Wahl, Fraser, Harvey, & Maxwell, 1987). The highly glacierized St. Elias Mountains (Kienholz et al., 2015) create a strong precipitation shadow effect over most of the study area (Anderson, Abbott, Finney, & Burns, 2005), limiting precipitation events to mainly convective precipitation and storms (Burn, 1994).

Table 3.1 Description of studied watersheds

River	Water Survey of Canada ID	Outlet coordinates		Discharge data		Areas		Average discharge		Elevation	
		Lat. N.	Lon. W.	First year[a]	Length (years)	Tot. (km^2)	Glac. (%)	Annual (m^3/s)	Jul.–Aug. (m^3/s)	Average (m)	Range (m)
White	09CB001	61°59'	140°33'	1974	34	6,230	30.4	116.9	377.9	1,825	701–5,000
Alsek*	08AB001*	60°07'	137°58'	1981	27	7,750	30.2	188.5	617.6	1,436	446–4,410
Duke	09CA004	61°20'	139°10'	1981	29	654	9.2	8.4	27.3	1,767	894–3,042
Tatshen-shini	08AC002	60°07'	137°05'	1989	26	1,750	2.9	29.5	56.5	1,295	587–2,238
Wheaton	09AA012	60°07'	134°53'	1956	45	684	0.5	8.0	17.5	1,410	667–2,418
Tak-hanne	08AC001	60°06'	136°55'	1984	30	375	0	4.3	6.9	1,352	712–2,141
Takhini	09AC001	60°51'	135°44'	1948	65	7,050	2.1	63.0	168.2	1,291	657–2,533
Sekul-mun	08AA008	61°33'	137°32'	1981	32	1,240	0	5.7	13.7	1,400	939–2,196

[a] - The last year for discharge time series for all watersheds is 2015

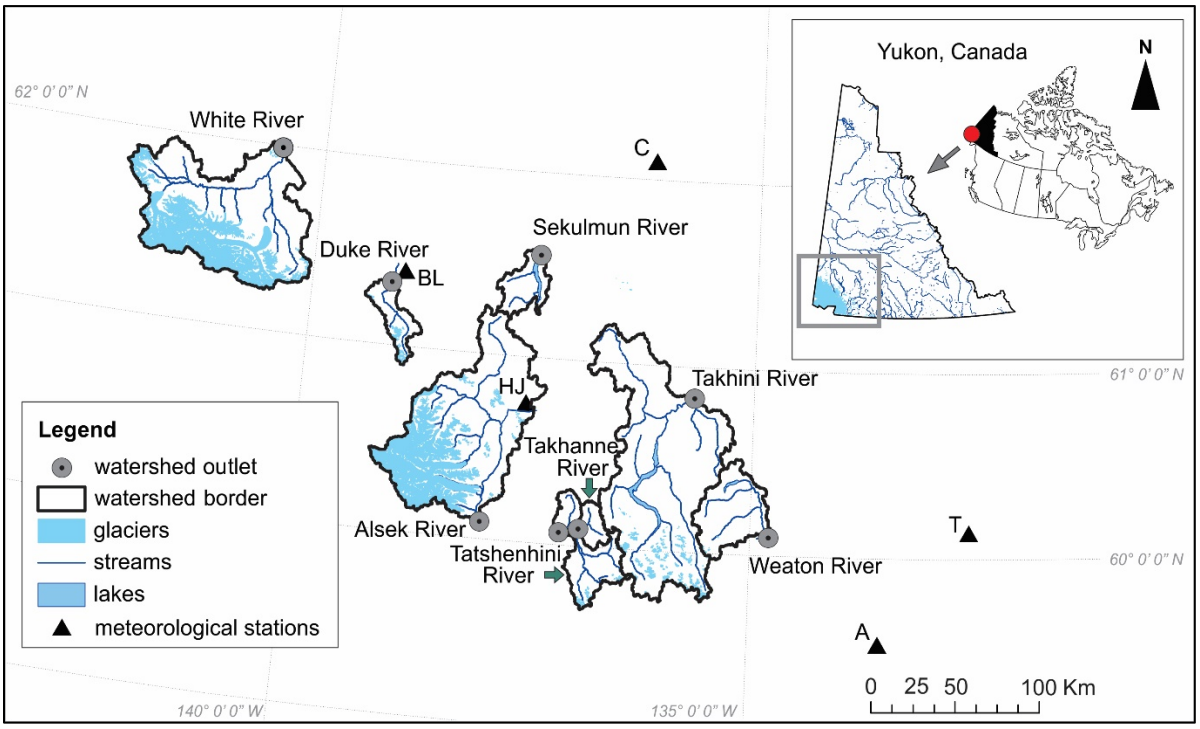

Figure 3.1 Study area and the selected watersheds in the southwestern Yukon, Canada. Gray circles with black points correspond to the outlets of the watersheds. Triangles highlight the position of the meteorological stations, corresponding to Burwash Landing (BL), Haines Junction (HJ), Altin (A), Carmacks (C), and Teslin (T)

3.3 Data and methods

3.3.1 Overview of methods

The enhanced dual approach that was used to investigate the role of shrinking glaciers in the hydrological regimes of the eight watersheds in the study area consists of trend detection in historical discharge variables and a model-based PW analysis. The first step in the trend detection was the preprocessing of the discharge time series. This preprocessing included treating time series for missing data and deriving 11 discharge variables. The watersheds were then clustered based on their hydrological regimes to isolate catchments under glacier influence. Trend detection was performed on the 11 variables using three different statistical techniques to limit the possibilities of trend misidentification.

We quantified glacier cover changes by means of a glacier inventory. The inventory uses existing inventory as a starting point and consists of refining glaciers outline for each study watershed. This exercise is conducted for 3 years over a period of 28 years. The resulting glacier retreat characteristics performed for each watershed covered three decades and were used as input to the Simple Water Balance Model (SWBM) (M. Baraer et al., 2012). The model is parametrized mainly based on published values and generates synthetic discharge time series in response to 15 different scenarios that account for major uncertainties in glacier area and volume estimations. Model outputs comprise a PW diagnostic and allow placing detected trends in discharge time series into a glacier retreat perspective. We also carried out additional model simulations to tentatively answer two questions: (a) how likely trends in discharge might be reversed in case of a change of glacier retreat pace and (b) whether the PW analysis has been influenced by a possible increase in precipitation. The results of this last simulation were compared with actual trends detected in precipitation time series. Finally, trend attribution consisted of a comparison of trend detection, hydrological regime identification, and model outputs.

3.3.2 Observations and preprocessing

3.3.2.1 River discharge data

Daily discharge time series from eight stations from the Water Survey of Canada (Environment and Climate Change Canada, https://wateroffice.ec.gc.ca/), located at the outlets of the watersheds, were analyzed in this study (Figure 3.1). Table 3.1 summarizes the characteristics of the watersheds and the time series lengths and reports the stations' IDs. A reservoir that is controlled for hydroelectricity production purposes within the Dezadeash sub-watershed (08AA003, not shown on the map) is part of the Alsek watershed. Reservoirs are known to impact hydrological regimes by reducing the peak flows and altering the low flows' magnitudes as well as changing the peak flows and the low flows' frequencies (Grill et al., 2015; Mailhot, Talbot, Ricard, Turcotte, & Guinard, 2018). Thus, we used a hypothetical Alsek* catchment that excludes the Dezadeash sub-watershed. Its characteristics were

calculated by subtracting 08AA003's total and glacierized areas from those of the Alsek River catchment, and its daily discharge time series were obtained by subtracting station 08AA003's daily discharge from that of station 08AB001. The propagation time between both stations was not accounted for in this calculation given the time scales used in this study.

Hydrological changes were examined by analyzing the hydrographs of the eight watersheds and by specifically focusing on flow magnitude, timing, and variability. To characterize changes in flow magnitude, we extracted the following variables from daily discharge time series: mean annual discharge (Q_{yr} [m^3/s] calculated during the hydrological year, namely, October–September), mean discharge for the ablation period July–August (Q_{abl1} [m^3/s]), mean discharge for the ablation period May–August (Q_{abl2} [m^3/s]), mean five-day maximum and minimum discharge (Q_{max5d} [m^3/s] and Q_{min5d} [m^3/s], respectively), and mean winter (November–March) discharge (Q_w [m^3/s]). To characterize changes in the timing of hydrological flows, the day of the year with Q_{max5d} and Q_{min5d} (D_{Qmax5d} and D_{Qmin5d}, respectively) and the start of the ablation season (D_{abl}; or the first day of the year with a daily discharge increase greater than a threshold value) were used. The threshold values were fixed based on a visual inspection of the discharge time series. The objective was to target standardization as much as possible while accounting for watershed specificities. We applied a 0.1 m^3/s threshold to all the watersheds apart from White and Alsek*, which exhibit much higher discharge than the others. The threshold was fixed at 2 m^3/s for the White River and 1 m^3/s for the Alsek* River. Finally, the coefficients of variation of Q_{yr} (CV_{yr} [unitless]) and Q_{abl1} (CV_{abl1} [unitless]) were used to quantify changes in flow variability.

Although discharge time series have undergone quality checks from the Water Survey of Canada, they might contain missing values that may affect the derived variables used to characterize the hydrographs. A visual inspection of the discharge time series was performed for Q_{yr}, Q_{abl1}, Q_{abl2}, CV_{yr}, CV_{abl1}, Q_w, and D_{abl}, and years with more than one consecutive week missing were discarded. This rule allowed us to keep as many years as possible without jeopardizing data quality. To be able to calculate Q_{max5d}, Q_{min5d}, D_{Qmax5d}, and D_{Qmin5d}, we

decreased the range and discarded the year if more than five consecutive days were missing. The gaps in the data were not filled.

Each watershed lost at least one year of data due to this data screening. The maximum number of removed years was 15 for the Wheaton watershed. Otherwise, the number of rejected years varied between 1 (Tatshenshini watershed) and 8 (White and Alsek* watersheds). The length of discharge time series after preprocessing ranges from 25 to 64 years (Table 3.1).

3.3.2.2 Air temperature and precipitation data

To examine regional changes in air temperature and precipitation, we extracted such variables as mean annual and ablation season air temperature, mean annual snow, rain, and total precipitation from the Adjusted and Homogenized Canadian Climate Data (Mekis & Vincent, 2011; Vincent et al., 2012). The positions of meteorological stations are shown in Figure 3.1. Because of data scarcity, the Burwash Landing station (BL, 806.2 m above sea level [a. s. l.]; precipitation data are available for the period 1967–2008, and air temperature data are available for 1967–2018) was used as a reference station for the Duke and White River watersheds; the Haines Junction station (HJ, 595.3 m a. s. l., 1945–2007, 1945–2018) was used as a reference station for the Alsek*, Takhanne, and Tatshenshini River watersheds as they are all situated in the Shakwak Trench. The Carmacks station (C, 524.9 m a. s. l., 1943–2011, 1943–2018) was used to represent the Sekulmun and Takhini watersheds, both being situated in Whitehorse Valley. Finally, the Wheaton watershed was represented by two stations: Altin (A, 673.6 m a. s. l., 1967–2017, 1967–2018) and Teslin (T, 705.0 m a. s. l., 1944–1994, 1944–2018).

3.3.2.3 Glacier inventory

To perform model-based PW analysis, we needed data on glacier changes in the area. Glacier cover changes for each watershed were obtained by delineating glacier outlines for different years using freely available Landsat satellite images (Landsat Thematic Mapper 5, 7, and 8). Only August–September images with minimal snow and cloud cover were chosen. Based on

the temporal range of best available images suitable for the delineation, we chose the years 1989, 1998 (1999 for the White River watershed), and 2017, resulting in a time window of 28 years for the quantification of glacier cover changes.

Over the years, numerous methods have been developed to delineate clean glacier ice in a semi-automatic way (Hall, Ormsby, Bindschadler, & Siddalingaiah, 1987; Hanshaw & Bookhagen, 2014; Paul, 2002a, 2002b; Racoviteanu, Williams, & Barry, 2008; Smith, Bookhagen, & Cannon, 2015). Despite the interest these methods represent, we chose manual delineation for conducting the glacier inventory (Kienholz et al., 2015). At the scale at which delineation is performed, semi-automatic methods would still require manual correction for clouds, snow, fog, and bright rock surfaces (Howarth & Ommanney, 1986; Racoviteanu, Paul, Raup, Khalsa, & Armstrong, 2009) and therefore would become time-consuming compared with manual delineation. Moreover, some of the images used for the analysis contain defects (e.g., strips from Landsat 7 sensor failure in 2003) that are not compatible with semi-automatic methods.

Initial glacier delineation was performed using the Global Land Ice Measurements from Space (Kargel, Leonard, Bishop, Kaab, & Raup, 2014; available at https://www.glims.org/RGI/) shapefiles as a base. They were first modified in a way that each glacier was represented by an individual polygon instead of being merged with others. Delineating each individual glacier was required because glacier areas were used for glacier volume estimation in the SWBM. Glacier outlines were then modified according to the changes observed on satellite images for 1989, 1998, and 2017. Individual glacier area was subsequently calculated for the three years using ArcGIS®.

The uncertainty associated with individual glacier delineation was estimated by the error model proposed by Pfeffer et al. (2014):

$$e(s) = ke_1 s^p, \tag{3.1}$$

where p, e_1, and k are empirically derived coefficients equal to 0.7, 0.039, and 1, respectively (Pfeffer et al., 2014), and $e(s)$ and s correspond to the error and glacier area (both in km^2). The standard error for the entire region was then calculated by dividing the sum of individual glacier errors by the total glacier area.

The St. Elias Mountains are characterized by the presence of debris-covered glaciers (Kienholz et al., 2015), and several of them are situated within the borders of the White and Alsek* River watersheds. However, detecting the changes in debris-covered glaciers was out of the scope of this paper. Therefore, we assumed that the position of debris-covered tongues did not change significantly for the study period. This assumption was shown to be reasonable in other regions like Himalaya (Benn et al., 2012) and northern Pakistan (Herreid et al., 2015) for the periods of several decades.

The studied region is known for the presence of surging glaciers (Crompton & Flowers, 2015; Johnson, 1986; Sevestre & Benn, 2015). Therefore, particular attention was given to surging event detection when measuring positions of glacier tongues for different images. As no glacier tongue advance was detected, it was assumed that no surging event had a significant impact on glacier area changes estimation over the studied period in the studied watersheds.

3.3.3 Hydrological regimes

Hydrological regimes represent the integrated watershed responses to various climatic inputs, with precipitation and temperature being the most important ones (Zhang et al., 2001). These responses differ in terms of magnitude and timing of the peak discharge as well as its variability. In the study region, snowmelt contributions to the spring–summer freshet tend to peak in June (Brabets, Wang, & Meade, 2000). The presence of glaciers alters the watersheds' response in both the timing and magnitude of the peak discharge because glaciers act as natural water reservoirs at the watershed scale and because summer precipitation has to be routed through the glacier before reaching the stream. Hence, the hydrograph of a glacierized watershed is expected to exhibit less variability than that of a non-glacierized one (Fleming &

Clarke, 2005; Fountain & Tangborn, 1985; Jansson et al., 2003; Van Tiel et al., 2019; Walder & Fountain, 1998). Similarly, lakes accumulate snowmelt, rainfall, and glacier melt during the ablation season and release water when sufficiently filled. As a result, where the presence of glaciers or lakes dominates watershed response, the hydrograph will have its peak discharge later in the summer, possibly masking snow-induced June freshet, the so-called hybrid hydrological regime (Eaton & Moore, 2010). These three regimes are commonly observed in the study area. We will further refer to them as snowmelt runoff, glacier runoff, and lake runoff to highlight the main drivers following the classification of Brabets et al. (2000) for the Yukon River.

Hydrological regimes were characterized with the monthly fraction of annual runoff for each watershed (i.e., mean discharge for each month divided by mean annual discharge) (Fountain & Tangborn, 1985). Comparing hydrological regimes to one another required the monthly fraction of annual runoff of each watershed to be calculated over a common recording period. For the eight watersheds, the common recording period is 15 years long and covers the years 1990, 1995, 1996, 1999, 2001–2012, and 2015.

3.3.4 Trend detection

Four different methodologies were applied for detecting and quantifying hydrological changes, namely the nonparametric Mann-Kendall test (MK), the modified Mann-Kendall test, Spearman's rho test (SR) and the Sen's slop. This allowed us to account for possible uncertainties associated with specific methodologies for trend detection (Cox & Stuart, 1955; Clarke, 2010). All the applied methods are nonparametric. Unlike parametric tests, which are based on the assumption that the analyzed data are normally distributed, nonparametric tests do not make an assumption about the data distribution and thus are more suitable for hydrological time series with unknown distribution, missing data, and possible outliers (Kundzewicz & Robson, 2000). The MK test detects monotonic changes in time series by pairwise comparing an observation with previous observations and counting the number of decreases/increases (Mann, 1945; Kendall, 1975). Based on calculated test statistics and its

variance, the null hypothesis, which assumes randomness in time series, is either rejected or not. The alternative hypothesis assumes the existence of a monotonic trend. Positive serial correlation in time series increases the Type I error (i.e., the rejection of a true null hypothesis) because the variance of the MK test statistic increases with the magnitude of serial correlation (Cox & Stuart, 1955). To account for the possible presence of positive serial correlation and thereby minimize false trend detection, we used the modified MK (Hamed & Rao, 1998; Hamed, 2009), where serial correlation is evaluated from the time series, and then autocorrelation coefficients are used to modify the variance. Finally, SR, also a nonparametric rank-based technique, was applied. This test is based on a correlation between ranks in time and in magnitude for a pair of observations (Dahmen & Hall, 1990) and is slightly more sensitive to the outliers in comparison with MK (Croux & Dehon, 2010). We used a p-value of 0.05 as a significance level to reject the null hypothesis. Magnitudes of detected trends were estimated using Sen's slop, which calculates the slope for a given time series as a median value of slopes between among pairs of observations (Sen, 1968).

3.3.5 Hydrological modeling

3.3.5.1 Model description

The SWBM was adapted from the model used by Baraer et al. (2012) to support the interpretation of trends in measured discharge in the Cordillera Blanca, Peru. As in the original version, based on water budget, the model generates synthetic hydrographs using the watershed area, the initial glacierized surface, and the annual ice loss rate as input. The SWBM allows for studying the direct impact of glaciers' retreat on discharge, thereby eliminating the uncertainties stemming from modeling the response of the glacier to changes in climatic forcing. In the present case, components of the energy balance as well as physical characteristics of glacierized parts of the watersheds (glacier elevation range, slope orientation, ice flow, etc.) that influence meltwater production are integrated into the ice loss rate parameter. Moreover, most of the model parameters are taken from the literature, so if losses

to evapotranspiration and deep infiltration can be estimated, the SWBM can even be used for ungauged watersheds.

Modifications included the rationalization of internal parameters, the adjustment of the watershed glaciers' volume, and glacier annual retreat calculation methods, taking into account extra processes such as the seasonality in groundwater and evapotranspiration fluxes.

The annual water budget at a watershed scale can be expressed as follows (Baraer et al., 2012):

$$Q_{yr} = Q_{melt\,y} + Q_{slow\,y} + Q_{fast\,y} - EV_{ly}A_l, \tag{3.2}$$

where Q_{yr} is the stream discharge at the watershed outlet; $Q_{melt\,y}$, $Q_{slow\,y}$, and $Q_{fast\,y}$ are the glacier melt, slow-flow, and fast-flow components of the yearly average discharge, respectively; $EV_{l\,y}$ is the evaporation rate from lakes; and A_l represents the lake surface area. Fast flow represents the portion of precipitation that reaches the watershed outlet within a few days after rainfall and assumes no evapotranspiration loss. Slow flow represents water released from the watershed over a timespan longer than a few days and is assumed to be mainly groundwater based (Baraer et al., 2012). $EV_{l\,y}$ is assumed to have a substantial influence in a given watershed where lakes larger than 0.5 km^2 are present.

The yearly glacier melt discharge component is defined as the sum of a steady state component and a mass balance component minus the fraction of glacier ablation lost by sublimation:

$$Q_{melt\,y} = \left(P_y A_{gl} + 0.85\frac{\Delta V_{gl}}{\Delta t}\right)\left(1 - SUB_y\right), \tag{3.3}$$

where P_y corresponds to the annual total precipitation; A_{gl} is the watershed glacierized area; ΔV_{gl} is the annual change in the watershed glacier volume; Δt is the length of the study period (one year); SUB_y is the sublimation rate from ice surfaces, expressed as the portion of the yearly ablation volume; and 0.85 accounts for the relative density of glacier ice (Huss, 2013).

The yearly slow-flow discharge component corresponds mainly to groundwater contribution and is calculated as follows:

$$Q_{slow\,y} = \left(P_y - ETI_{ngl\,y}\right) A_{ngl} q_{ngl}, \tag{3.4}$$

where $ETI_{ngl\,y}$ is the yearly rate of losses to evapotranspiration and deep infiltration from non-glacierized areas, A_{ngl} is the non-glacierized portion of the watershed, and q_{ngl} is the percentage of annual precipitation excess that represents the annual base flow. The non-glacierized area of the watershed A_{ngl} corresponds to the difference between the total area and the glacierized area A_{gl} of the watershed.

The yearly fast-flow discharge component corresponds to surface runoff and the portion of vadose zone flows that contributes to stream discharge directly:

$$Q_{fast\,y} = \left(P_y - ETI_{ngl\,y}\right) A_{ngl} \left(1 - q_{ngl}\right), \tag{3.5}$$

The ablation season discharge is calculated using the same structure as in equation (2):

$$Q_{ab} = Q_{melt\,ab} + Q_{slow\,ab} + Q_{fast\,ab} - EV_{l\,y} A_l ev_{l\,ab}, \tag{3.6}$$

where $Q_{melt\,ab}$, $Q_{slow\,ab}$, and $Q_{fast\,ab}$ are the glacier melt, slow-flow, and fast-flow components of the ablation season average discharge, respectively; and $ev_{l\,ab}$ is part of the yearly evaporation from lakes occurring in July and August.

The glacier melt discharge component during the ablation season is calculated using a modified equation (3.3):

$$Q_{melt\,ab} = \alpha_{ab} \left(P_y A_{gl} + 0.85 \frac{\Delta V_{gl}}{\Delta t}\right) \left(1 - SUB_y sub_{ab}\right), \tag{3.7}$$

where α_{ab} is the fraction of annual ablation and sub_{ab} is the fraction of annual sublimation occurring in July and August.

The slow-flow discharge component of ablation season discharge is computed as follows:

$$Q_{slow\,ab} = \left(P_{ab} - ETI_{ngl\,y} eti_{ngl\,ab}\right) A_{ngl} q_{ngl}, \tag{3.8}$$

where P_{ab} corresponds to precipitation occurring in July and August and $eti_{ngl\,ab}$ represents the part of yearly loss rate to evapotranspiration and deep infiltration (in %) occurring in July and August.

Finally, **the fast-flow discharge component** is calculated using the following:

$$Q_{fast\,ab} = \left(P_{ab} - ETI_{ngl\,y} eti_{ngl\,ab}\right) A_{ngl} \left(1 - q_{ngl}\right), \tag{3.9}$$

The model also computes the **yearly coefficient of variation of discharge** Cv_{yr}:

$$Cv_{yr} = \frac{\sqrt{\left(Cv_{melt} * Q_{melt\,y}\right)^2 + \left(Cv_{slow} * Q_{slow\,y}\right)^2 + \left(Cv_{fast} * Q_{fast\,y}\right)^2 + \sum cov}}{Q}, \tag{3.10}$$

where Cv_{melt}, Cv_{slow}, and $Cv_{fast,}$ are the melt, slow-flow, and fast-flow coefficients of variations, respectively; and Σ_{cov} describes the sum of the flow types' pair covariance.

The ablation season coefficient of variation of discharge Cv_{ab} is computed by replacing the yearly discharge components with the ablation season ones in equation (10).

Table 3.2 Regional- (a) and watershed-specific (b) parameters used in the Simple Water Balance Model

a) Regional parameters:

Name	Units	Value	Description	Sources
$eti_{ngl\ ab}$	%	35	% of ETI_{ngl} occurring in July and August	Farnsworth and Thompson (1982)
$ev_{l\ ab}$	%	35	% of EV_l occurring in July and August	
SUB_y	%	1.4	Yearly glacier ablation from sublimation (in % of yearly ablation)	Wheler and Flowers (2011)
sub_{ab}	%	53	% of SUB_y occurring in July and August	Box and Steffen (2001)
$EV_{l\ y}$	mm/y	300	Yearly evaporation rate from lakes	Canadian National Committee for the International Hydrological Decade (1978)
β	-	1.182	Watershed volume–glacierized area scaling factor	Glacier inventory
α_{ab}	%	62.5	% of annual ablation occurring in July and August	Herdes (2014)
q_{ngl}	%	17.5	% of annual precipitation making the annual base flow	Walvoord and Striegl (2007)
$\sum cov$	-	0	Sum of covariance	Baraer et al. (2012)
CV_{fast}	-	1.3	Fast-flow coefficient of variation	
CV_{melt}	-	0.4	Meltwater coefficient of variation	
CV_{slow}	-	0.5	Slow-flow coefficient of variation	

b) Watershed-specific parameters:

Name	Units	Description	Source
$A_{gl(0)}$	%	Initial watershed glacierized area	Glacier inventory
A_t	km^2	Watershed area	Aster DEM
A_l	km^2	Lake area	Canvec data set (Natural Resources Canada, 2016)
Γ_0	-	Initial rate of glacier area loss	Glaciers inventory
Γ_{follow}	-	Glacier area loss rate evolution factor	
Name	**Units**	**Description**	**Source**
P_y	mm/y	Annual precipitation change rate	Worldclim database (Hijmans, Cameron, Parra,
P_{ab}	mm/y	July and August precipitation change rate	

			Jones, & Jarvis, 2005)
$ETI_{ngl\ y}$	mm/y	Yearly loss rate to evapotranspiration and deep infiltration	Adjusted
B	$m^{3-2\gamma}$	Watershed volume–glacierized area scaling factor	Glacier inventory

3.3.5.2 Model setup and verification

Running the SWBM required fixing 21 parameters that can be split into two categories: (1) 12 regional parameters that were kept unchanged for all watersheds; and (2) 9 watershed-specific parameters (Baraer et al., 2012). All of the regional parameters, apart from volume–glacierized area scaling factor β, were fixed based on relevant literature (Table 3.2).

Parameter β as well as 4 out of 9 watershed-specific parameters—namely, initial glacierized area A_{gl}, initial rate of glacier loss Γ_0, glacier area loss evolution factor Γ_{follow}, and watershed volume–glacierized area scaling factor B (Table 3.3)—were calculated using the glacier inventory outputs. β was estimated with a nonlinear regression applied to 18 (V_{gl}, A_{gl}) data points resulting from three years of inventory for the six glacierized watersheds. Watershed glacier volume V_{gl} was calculated as follows:

$$V_{gl} = \sum_{i=1}^{m} V_i = BA_{gl}^{\beta}, \tag{3.11}$$

where V_i is the volume of a given glacier i out of m inventoried in the watershed and B is the watershed volume–glacierized area scaling factor. This is calculated by applying a nonlinear regression to four data points: three years of (V_{gl}, A_{gl}) and the point (0,0). The volumes of individual glaciers V_i used to calculate V_{gl} were estimated based on the following volume–area power relationship (Bahr, Meier, & Peckham, 1997; Chen & Ohmura, 1990):

$$V_i = cA_i^{\gamma}, \tag{3.12}$$

where c and γ are empirical scaling parameters. Different values for scaling parameters have been proposed in the literature for global applications (Chen & Ohmura, 1990; Grinsted, 2013; Radić & Hock, 2010; Van de Wal & Wild, 2001) and for the northwestern North America (Arendt et al., 2006). In the present study, γ was kept constant at the theoretical value of 1.375 (Bahr et al., 1997), while we used three different values for c. Glacier volume estimates are very sensitive to the choice of scaling parameters (Barrand & Sharp, 2010), and considering three values helps capture the uncertainty associated with it. We chose the three values for c that represent the range found in the literature: 0.12 $m^{3-2\gamma}$ corresponded to a low estimate (e.g., Van de Wal & Wild, 2001); 0.28 $m^{3-2\gamma}$ to a high estimate (e.g., Arendt et al., 2006), and c = 0.2 $m^{3-2\gamma}$ to a medium estimate (e.g., Radić & Hock, 2010).

The evolution of the glacier area A_{gl} in time was computed using the following autoregressive model:

$$A_{gl(n+1)} = A_{gl(n)}\left(1 - \Gamma_{(n)}\right), \tag{3.13}$$

where $A_{gl(n)}$ and $A_{gl(n+1)}$ are glacier areas for years n and $n+1$, respectively; and $\Gamma_{(n)}$ is the rate of glacier area change for the year n. $\Gamma_{(n)}$ was estimated as follows:

$$\Gamma_{(n)} = \Gamma_0 + n\Gamma_{follow}\,, \tag{3.14}$$

where Γ_0 is the initial rate of glacier area loss and Γ_{follow} is the glacier area loss acceleration (or deceleration, if negative) factor. Both Γ_0 and Γ_{follow} were estimated from the best fit to equation (13), in which glacier areas from the inventory were normalized in relation to the first-year value. We used five different sets of values for Γ_0 and Γ_{follow} in model simulations to account for uncertainties in the glacier area delineation: a base set was obtained using normalized watershed glacier areas from the inventory (with area = 1 for the first year); and four other sets of factors were obtained by adding and subtracting half of the standard error (see Section 3.2.3) from normalized measured glacier areas (Table 3.3).

Other watershed-specific parameters, except ETI_{ngl}, were estimated using geographic information systems. The total watershed area A_t, was obtained from watershed delineation on Aster digital elevation model (DEM). The lake surface area A_l, was extracted from the CanVec data set (Natural Resources Canada, 2016). The annual precipitation P_y, necessary to calculate the glacier melt discharge component was taken from the spatial Worldclim database (Hijmans et al., 2005). The monthly precipitation for each watershed was obtained by averaging the spatial data within the watershed's borders in ArcGIS®. In the absence of a clear tendency arising from regional studies on precipitation changes (see Introduction), precipitation was kept invariant throughout the PW analysis, and the influence of a potential increase in precipitation on hydrological trends was evaluated through a supplemental round of simulations (see Section 3.5.5). ETI_{ngl} is the only parameter that was adjusted during simulations. It was obtained for each watershed by finding the best fit between simulated and observed Q_y and Q_{ab} for 15 scenarios arising from a combination of 5 glacier retreat sets of parameters with 3 volume–area scaling factor alternatives (Table 3.3). Its values were limited to a 20–500 mm/y range based on the values found in the literature (Ruairuen et al., 2015; Yuan et al., 2012).

Model verification was carried out by comparing modeled yearly and ablation season discharges with measured ones for the period 1989–2017 for all the studied watersheds. The Nash Sutcliffe efficiency, the normalized root mean square error, and the determination coefficient R^2 were the three objective functions used for model performance evaluation.

Table 3.3 Parameter adjustments leading to the 15 tested scenarios: (a) 5 adjustments of the base glacier cover values used to compute Γ_0 and Γ_{follow}, where e(s) represents the standard error computed based on measured glacier areas and "-" stands for no changes; (b) 3

alternatives of the glacierized area–volume scaling factor. Combining the 5 sets of Γ_0 and Γ_{follow} values with the 3 possible scaling factors leads to 15 scenarios

Period 1 (1989)	Period 2 (1998)	Period 3 (2017)
a) glacier cover adjustments:		
-	-	-
-	−0.5 e(s)	−0.5 e(s)
-	−0.5 e(s)	+0.5 e(s)
-	+0.5 e(s)	+0.5 e(s)
-	+0.5 e(s)	−0.5 e(s)
b) glacierized area–volume scaling factors:		
0.12 $m^{3-2\gamma}$		
0.20 $m^{3-2\gamma}$		
0.28 $m^{3-2\gamma}$		

3.3.5.3 Model outputs

Simulations covered the period 1989–2390. Selecting a multi-century simulation time allows for better situation of actual hydrological changes into a long-term perspective. However, model projections after 2017 should be taken with caution because they are based on the unverified assumption that the glacier retreat will keep accelerating at the same pace as over the period 1989–2017. Therefore, the time scale in projections can be seen as indicative only.

Primary outputs of the model are time series of the annual discharge Q_{yr} and annual coefficient of variation CV_{yr} as well as the July–August discharge Q_{abl1} and July–August coefficient of variation CV_{abl1} and the glacier area A_{gl} (Figure 3.4a). The model further calculates variables based on those time series for the PW analysis: a PW phase number for the year 2017, the PW discharge relative to the original discharge Q_{peak}/Q_0 for cases where PW is predicted as still to come, and the relative final discharge Q_{end}/Q_0 (M. Baraer et al., 2012). The last two variables were calculated for the period July–August, hydrologically the most sensible to glacier retreat.

3.3.5.4 Peak water analysis

The PW phases follow the definition proposed by Baraer et al. (2012), as illustrated in Figure 3.4a. The pre-PW phases are P1 and P2. P1 corresponds to the early stage of glacier retreat and is characterized by an increase in $Q_{ab/yr}$ and a decrease in $CV_{ab/yr}$. P2 situates between P1 and PW and is characterized by an increase in both $Q_{ab/yr}$ and $CV_{ab/yr}$. At PW, Q_{yr} reaches its maximum. The post-PW phase P3 starts with PW and covers the pronounced decline in discharges and the corresponding increase in the coefficients of variation. Phase P4 represents the end of the glacier's influence on outflows, when changes in discharges are progressively less pronounced, asymptotically reaching a non-glacierized basin state.

To constrain model simulations, we used 15 scenarios that account for the uncertainties in the glacier area delineation and in glacierized area–volume scaling (Table 3.3). The PW analysis does not apply to nonaccelerating glacier retreat (Baraer et al., 2012), so scenarios based on stable or decelerating retreats between 1989 and 2017 are not assigned any phase number and are labelled as "NA."

3.3.5.5 Additional simulations

As the last step, additional simulations were carried out to answer two questions arising from the PW analysis: (1) how reversible trend projections are for watersheds identified as having passed the PW should the retreat acceleration rate change and (2) whether the possible precipitation increase is responsible for some of the positive trends identified in time series.

Trend reversibility was assessed by conducting a hypothetical rapid-retreat simulation for each watershed for the three volume–area scaling factor alternatives. The rapid retreat corresponds to the use of an exaggerated glacier area loss acceleration factor Γ_{follow}, which should be well above those calculated based on the glacier inventory. The rapid-retreat scenario was anticipated to induce an increase in discharge for at least the first simulation year, regardless

of the initial conditions. The magnitude and duration of this increase reflect the potential of glaciers to further increase the watershed outflows in case of retreat acceleration (Baraer et al., 2012). The rapid-retreat simulation results were synthesized by calculating the glaciers' capacity to further increase the stream discharge $\int Q^+$:

$$\int Q^+ = \sum_{i=1}^{k} \frac{(Q_{yr\,i} - Q_{yr\,0})}{Q_{yr\,0}} \text{ for years } i \text{ where } Q_{yr\,i} > Q_{yr\,0}, \tag{3.15}$$

where $Q_{yr\,0}$ represents the first simulation year for annual discharge.

The influence of a possible increase in precipitation on measured hydrological trends was evaluated by conducting precipitation increase simulations. The model calculated the precipitation increase rate P_{req} [mm/year] that would be required to reverse a negative trend in yearly discharge (or a positive trend in the coefficient of variation) arising from the PW analysis. These simulations were conducted for all scenarios that did not lead to a P1 or P2 phase. To be considered as realistic, P_{req} values must be comparable to the magnitude of increase in precipitation observed at six different meteorological stations in the Adjusted and Homogenized Canadian Climate Data (Mekis & Vincent, 2011; Vincent et al., 2012).

3.4 Results

3.4.1 Glacier inventory

A ubiquitous decrease in glacier cover is observed across the studied region (Figure 3.2). The calculated regional area error for the glacier delineation for 1998 is 1.25% and for 2017 1.22%. The rates of retreat, however, differ among watersheds (Figure 3.2). The White and Alsek* River watersheds have the highest percentage of glacierized area, possess the largest glaciers, and are characterized by a large range of glacier elevation. They underwent the smallest decrease in % of glacierized area between 1989 and 2017: 7.9% and 7.6%, respectively. The Duke River watershed as well as the Tatshenshini and Takhini River watersheds show a comparable (to each other) decrease in % of glacierized area: 21.9%, 23.8%, and 21.7%,

respectively. The Wheaton River watershed lost 42.4% of its glacierized area over the 28-year period. This watershed is characterized by an abundance of small glaciers (<1 km^2) and has the smallest glacierized area but exhibits similar median glacier elevation in comparison with the other watersheds.

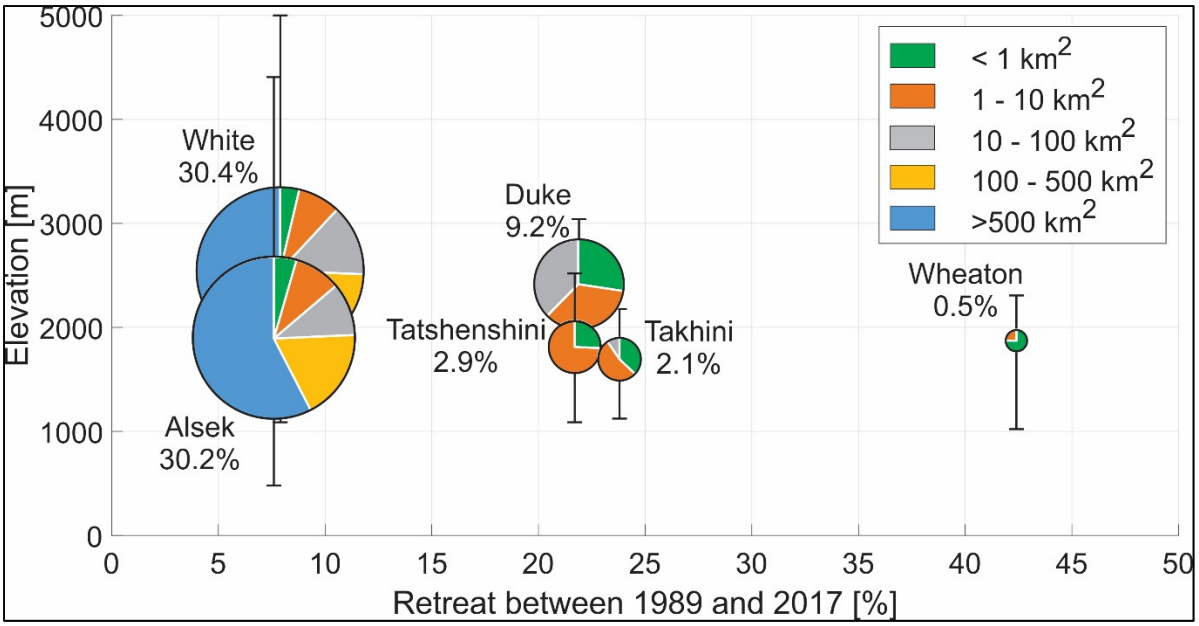

Figure 3.2 Changes in glacierized area in % for each watershed for the period 1989–2017. The size of each circle is proportional to the % of glacierized area of the watershed. The center of each circle corresponds to the mean elevation of glaciers, and the bars show their elevation range. The area of each circle is divided into segments that correspond to the % of glacierized area taken by glaciers of different sizes (see the legend) for 2017

Overall, Figure 3.2 shows an apparent correlation among the size, the total area, and the rate of retreat of glaciers for the different watersheds, except for the Duke River watershed, which plots with two watersheds of much lower glacierized area and smaller size cover (Tatshenshini and Takhini). The results from the glacier inventory confirm findings related to the fast rate of glacier area losses from other studies (Arendt et al., 2009; Barrand & Sharp, 2010; Derksen et al., 2012).

3.4.2 Hydrological regimes

Normalized hydrographs for the studied watersheds cluster into three groups, depending on the time of peak discharge and the monthly proportion of annual water production (Figure 3.3). We can observe that they are consistent with hydrological regimes previously identified for the Yukon River watershed (e.g., Brabets et al., 2000), namely, snowmelt runoff, glacier runoff, and lake runoff. The Takhini, Tatshenshini, and Wheaton River watersheds form the first group and are characterized by peak discharge in June, which corresponds to the time of freshet at low and mid-elevations. The White, Alsek*, and Duke River watersheds have glacierized areas between approximately 10% and more than 30% and form the glacier runoff group. In a watershed that is not hydrologically influenced by major lakes, the glaciers' impact on discharge is expected to be characterized by a delay in peak runoff compared with a snowmelt regime (Fountain & Tangborn, 1985). This characteristic is reflected by the normalized hydrograph of this group. The peak runoff occurs in July and persists in August, when the snowmelt runoff group exhibits a marked decline in discharge. Interestingly, watersheds with an almost 3% glacierized area (Tatshenshini) exhibit a snowmelt runoff pattern, whereas a watershed with a 10% glacierized area (Duke) clusters with highly glacierized catchments. This situates measurable glacier influence on the hydrological regime between 3% and 10% of the glacierized area. These values are consistent with previously reported values. Beamer et al. (2017) observed 4% for the Gulf of Alaska, and Birsan et al. (2005) and then Pellicciotti et al. (2010) observed 10% for the Alps.

The lake runoff group is formed by two watersheds that host large lakes: Lake Sekulmun (50.2 km^2 within the Sekulmun watershed) and Lake Kusawa (137.4 km^2 within the Takhini watershed). This group shows a more balanced distribution of the yearly discharge among the late spring to late fall months compared with the two other groups—a characteristic that arises from the flow regulation capacity of lakes (Gibson, Prowse, & Peters, 2006).

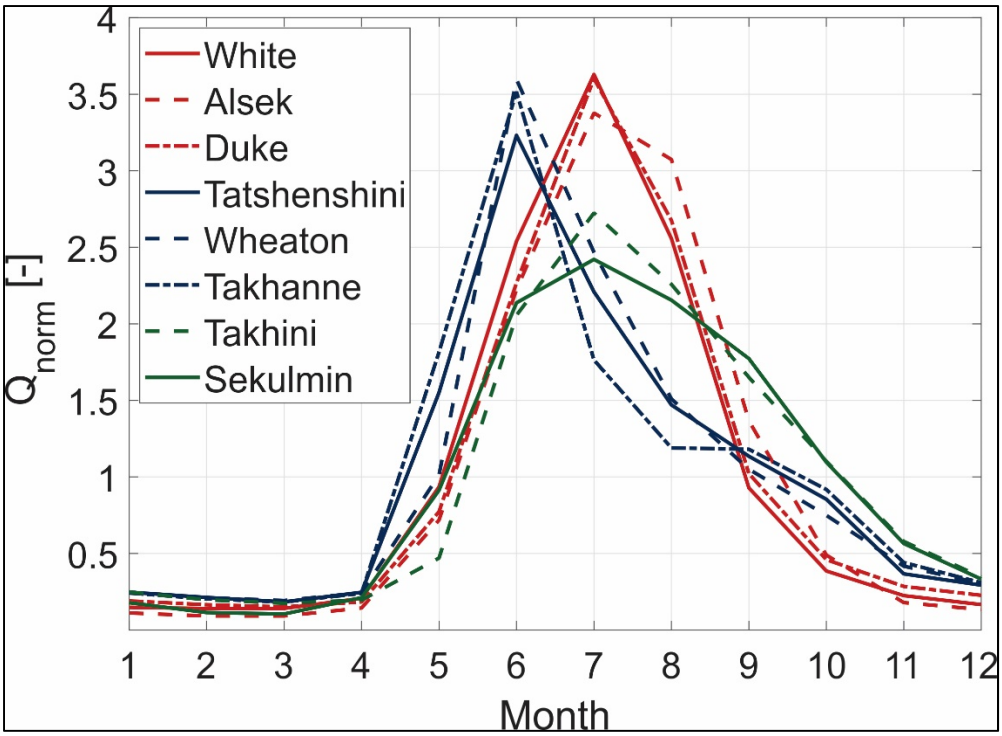

Figure 3.3 Normalized monthly discharge (Q_{norm}) of the analyzed watersheds. Different colors represent different hydrological regimes, namely, watersheds with glacier runoff (red), snowmelt runoff (blue), and lake runoff (green)

3.4.3 Trend detection

3.4.3.1 Trend detection in river discharge data

The results of the trend analysis show that all watersheds, not only those with significant glacier cover, underwent changes during the last decades (Table 3.4). For most of the explored variables, these results for three of the methods used—namely, MK, modified MK, and SR—are consistent with one another (Table 3.4). However, for the Alsek* River watershed, trends in CV_{abl1} and Q_w are not detected by SR, and for the Wheaton, Takhini, and Sekulmun River watersheds, any detected trends in Q_{max5d}, Q_{min5d}, and CV_{abl1}, are only detected by modified MK.

Table 3.4 Results of trend detection in discharge variables (see Section 3.3.2.1). The "+" sign indicates a positive trend, while the "−" sign indicates a negative one. Three signs represent the cases where all tests show statistically significant (α = 0.05) results. Two signs, both the MK and modified MK tests, show significant results. One sign, only the modified MK test, shows significant results. Different colors correspond to different hydrological regimes, namely, watersheds with glacier runoff (red), those with snowmelt runoff (blue), and those with lake runoff (green). Shaded rows present peak water-related variables

Variable	**Watersheds**							
	Glacier runoff			**Snowmelt runoff**			**Lake runoff**	
	White	Alsek*	Duke	Tatshenshini	Wheaton	Takhanne	Takhini	Sekulmun
Q_{yr}		+++						
Q_{abl1}		+++						
CV_{yr}	−−−						−−−	
CV_{abl1}	−−−	−−						−
Q_{abl2}	+++	+++					+++	
Q_{max5d}	−−−				+			
Q_{min5d}	+++		+++			+	+++	
D_{max5d}	−−−						−−−	
D_{min5d}						+++		
Q_w	+++	++			+++		+++	
D_{abl}	+++				−−−			

Among watersheds with glacier runoff (and among all the watersheds), the White and Alsek* watersheds noticeably stand out given the amount of change in different aspects of the hydrograph, namely, flow magnitude, timing, and variability (Table 3.4). They both exhibit an increase in Q_{abl2}, a decrease in CV_{abl1}, a shift of peak discharge toward earlier in the season, and an increase in Q_w. In addition, the Alsek* watershed exhibits an increase in Q_{yr}. For the

White watershed, we also observe a decrease in CV_{yr}, a decrease in Q_{max5d}, and shift in D_{abl} toward later in time. The third watershed from this group, the Duke watershed, shows a different pattern. It also shows an increase in winter discharge (Q_{min5d}) but does not show other changes.

In comparison with the first group, watersheds with snowmelt runoff underwent less significant hydrological changes during the last decades. They show changes in runoff magnitudes and timing only and not in variability. Among them, the Tatshenshini watershed does not show any statistically significant trends, and the Takhanne watershed only shows changes in winter discharge timing and magnitude. The shift in D_{abl} toward earlier in time is detected for the Wheaton watershed.

Watersheds with lake runoff, similar to those with glacier runoff, underwent changes in all three studied aspects: flow magnitudes, timing, and variability. The Takhini watershed shows numerous trends that are similar to the highly glacierized White and Alsek* watersheds; it manifests an increase in Q_{abl2} and Q_w, a shift of peak discharge toward earlier in the season, and a decrease in Cv_{yr}. For the second watershed of this group, the Sekulmun watershed, we observe a decrease in ablation season variability and a change in D_{abl}.

Overall, Table 3.4 shows that all metrics associated with the PW analysis in highly glacierized catchments (more than 30% of glacierized area) indicate a pre-PW phase (P1 or P2). Increases in winter and minimum discharge are encountered in all three hydrological regimes. Changes in the timing of peak or low discharge and changes in the start of the ablation season are also spread over the different hydrological regimes but in a less coherent direction.

3.4.3.2 Trend detection in air temperature and precipitation

A ubiquitous increase in temperature is observed in both annual and seasonal time series, and only a few stations exhibit changes in precipitation (Table 3.5). Trends in temperature were detected by both the MK and SR tests in almost all cases apart from the mean annual

temperature trend (T_{yr}) for station T and the mean ablation season temperature (T_{abl}) trend for station C. Trends in precipitation were only detected by the SR test, except for the mean annual precipitation (P_{yr}) for station C, where the MK test also detected an increase. A maximum increase rate in precipitation of 2.1563 mm/year is detected for station HJ for P_{yr}; stations T and C experience an increase in P_{yr} with the rates 0.7360 mm/year and 0.8353 mm/year, respectively. Station HJ also exhibits an increase in both ablation season (P_{abl}) and winter precipitation (P_w), and stations T and C experience changes in P_w with an increase for T and a decrease for C.

Table 3.5 Results of trend detection in meteorological time series. $P_{yr/abl/w}$ represents the mean annual, ablation season, and winter rate of precipitation change (mm/year), and $T_{yr/abl/w}$ represents the mean annual, ablation season, and winter rate of temperature change (°c/year). Results are reported as Sen's slope value, which is shown only if a statistical significance has been detected by SR and (**) /or (*) MK (significance level of 0.05)

	BL	**HJ**	**A**	**T**	**C**
P_{yr}	-	2.1563*	-	0.7360*	0.8353**
P_{abl}	-	0.3152*	-	-	-
P_w	-	0.7425*	-	-0.0397*	0.2474*
T_{yr}	0.0405**	0.0313**	0.0444**	0.0149*	0.0211**
T_{abl}	0.0300**	0.0174**	0.0390**	0.0100**	0.0085*
T_w	0.1100**	0.0658**	0.1118**	-	0.0667**

3.4.4 Hydrological modeling

3.4.4.1 Model parametrization and verification

Table 3.6 presents watershed-specific parameters. Important differences are observed among the watersheds in terms of the initial rate of glacier area loss Γ_0 and glacier area loss acceleration Γ_{follow}. The rate of glacier retreat increases for all the watersheds apart from (a) some scenarios for the Alsek* watershed and (b) all scenarios for the Wheaton watershed,

which show glacier area loss deceleration. Both highly glacierized watersheds (White and Alsek*) have comparable Γ_0 and Γ_{follow} and are characterized with the lowest Γ_0. The Duke and Takhini watersheds have higher Γ_0 but comparable Γ_{follow} with the first group. The Tatshenshini and Wheaton watersheds stand out because of their high retreat rates: the Tatshenshini watershed has both Γ_0 and Γ_{follow}, almost two times higher than the Duke and Takhini watersheds. Finally, the Takhini watershed, with the smallest A_{gl}, is characterized by the highest Γ_0 and the highest rate of deceleration.

Glacier volume–area scaling factor B varies between 0.011 and 0.122 and is the highest for two highly glacierized watersheds, which can mean that not only glacier area but also glacier volumes are the highest in these watersheds (Table 3.6).

Table 3.6 shows that all the watersheds in the region receive about 30% of yearly precipitation P_y during the ablation season. However, the proportion of yearly losses for evapotranspiration and deep infiltration from non-glacierized parts ($ETI_{ngl\,y}$) varies among the watersheds from 1% to 7% of P_y (Alsek*) to 35%–79% (White). We see that the Sekulmun watershed, followed by the Wheaton watershed, has the lowest values for P_y and P_{ab} and a relatively high value of $ETI_{ngl\,y}$, approximately 40% of P_y, whereas the Tatshenshini watershed has the highest P_y and P_{ab} and among the lowest values for $ETI_{ngl\,y}$, comprising only 1%–7% of P_y.

The comparison between the measured and simulated discharge values shows a good overall agreement (NSE of 0.97 and R^2 of 0.99), with a tendency to overestimate discharge values (the slope of the regression line is 1.1). This bias is confirmed with an NRMSE of 25%. These results are considered satisfactory for the purpose of this study because only trends and relative discharges are used for the PW analysis.

Table 3.6 Individual watershed parameters used in SWBM
(see Table 3.2 for parameter definitions)

Para-meter	$A_{gl(0)}$ %	A_l km^2	A_t km^2	Γ_0 x10^{-3}	Γ_{follow} x10^{-4}	B m$^{3-2\beta}$	P_y mm/y	P_{ab} mm/y	$ETI_{ngl\ y}$ mm/y
White	30.35	-	6,234	1.8–3.2	0.36–1	0.052–0.122	595	184	210–475
Alsek*	30.15	-	6,911	2.2–3.7	-0.75–0.57	0.045–0.104	523	162	5–40
Duke	9.23	-	658	7.6–8.8	0–0.8	0.018–0.043	462	143	85–125
Tatshen-shini	2.90	-	1,647	16.2–37.8	1.6-3	0.016–0.038	628	195	15–35
Takhini	2.05	137.4	7,690	6.8–8.3	0.18–1	0.011–0.026	406	126	140–150
Takhanne	0	-	372	-	-	-	556	172	175
Wheaton	0.53	0.66	1,619	44.8–46	-17.3–18.5	0.013–0.030	356	110	140–145
Sekulmun	0	50.2	1,240	-	-	-	269	83	80

3.4.4.2 Peak water analysis

The results of the PW analysis, summarized in Figure 3.4b, show contrasted situations among the watersheds and, in some cases, among the scenarios for a given watershed. Among the 15 tested scenarios, the most glacierized watershed (White) is assigned a pre-PW phase P1 nine times (60%) and a post-PW phase P3 three times (20%). A total of three scenarios (20%) do not meet the PW analysis conditions. A comparable situation is observed with the second-most glacierized watershed (Alsek*), with 40% of the scenarios not applicable and 40% indicating a phase P1 and 20% a phase P3. Despite the fact that the scenarios do not lead to a unanimous diagnostic, it can be noted that the majority of them lead to a pre-PW diagnostic for both watersheds. All the scenarios for the glacierized Duke watershed converge to P3, which characterizes a post-PW situation. Likewise, Figure 3.4b indicates that despite having a comparable A_{gl}, the Tatshenshini and Takhini watersheds present different positions in terms of PW. All the scenarios for the Tatshenshini watershed result in a pre-PW phases P1 and P2,

while 60% of the scenarios for the Takhini watershed lead to a post-PW phase P3. Finally, none of the scenarios for the Wheaton watershed are compatible with the PW phase attribution.

Interestingly, the position of the watersheds in terms of the PW phase does not seem to depend on either A_{gl} or hydrological regime. By contrast, the projected magnitude of the ablation season discharge increase at PW (Figure 3.4c), described by the variable Q_{peak}/Q_0, appears to be related to A_{gl}. The watersheds with A_{gl} just over 30% (White and Alsek*) are predicted to exhibit strong increases in Q_{abl1} as glaciers keep retreating. For the White watershed, the PW discharge is predicted to exceed the initial ablation season discharge by 1.52 times (median value) and for the Alsek* watershed by 1.19 times. However, these values should be taken with caution because the prediction range is quite large for these watersheds (100% and 50%). Therefore, even if such watersheds as Tatshenshini and Takhini are assigned similar PW phases, the potential for subsequent increases in Q_{abl1} situates under 3% in both cases, with a low prediction range.

The estimations of the relative amplitude of drop in the ablation season discharge at the time when glaciers will have lost their hydrological influence, represented by Q_{end}/Q_0, show small potential for changes in the watersheds where hydrological regime is not dominated by glaciers: the Tatshenshini, Takhini, and Wheaton watersheds all have scenarios indicating Q_{end}/Q_0 values above 0.8 (Figure 3.4d). By contrast, the White, Alsek*, and Duke watersheds should be affected by substantial decreases in Q_{abl1} once PW will have passed. A median reduction to 66% of the Q_{abl1} levels at the end of the last century is anticipated for the Duke watershed, to 53% for the Alsek* watershed, and to 18% for the White watershed once glaciers will have retreated to a point where they lose their hydrological influence. The scenarios for each watershed are relatively consistent with one another, with a maximum range of 40% in Q_{end}/Q_0 predictions.

3.4.4.3 Additional simulation results

Based on the obtained values of Γ_{follow}, we chose a rapid-retreat exaggerated glacier area loss acceleration factor of 0.001 to simulate a hypothetical rapid-retreat because this value is much higher than those calculated for each watershed (Table 3.6). The results of these simulations suggest that the two highly glacierized watersheds (White and Alsek*) are sensitive to possible changes in melt rates. For those watersheds, the glaciers' capacity to further increase the stream discharge $\int Q^{+}$ indicates that a drastic increase in the glacier retreat rate would result in a strong response in Q_{abl1} (Figure 3.4e). The Duke watershed, which still has more than 9% glacierized area, shows limited reactivity to the acceleration of the glacier retreat rate. This suggests that the watershed has lost the possibility of reversing the ablation season discharge decay induced by glacier retreat. Furthermore, the change in the acceleration rate for other watersheds does not induce any sensitive increase in Q_{abl1}. For the Takhini and Wheaton watersheds, which seem to have passed PW, the results suggest that the glaciers' contribution to Q_{abl1} will most likely keep decreasing.

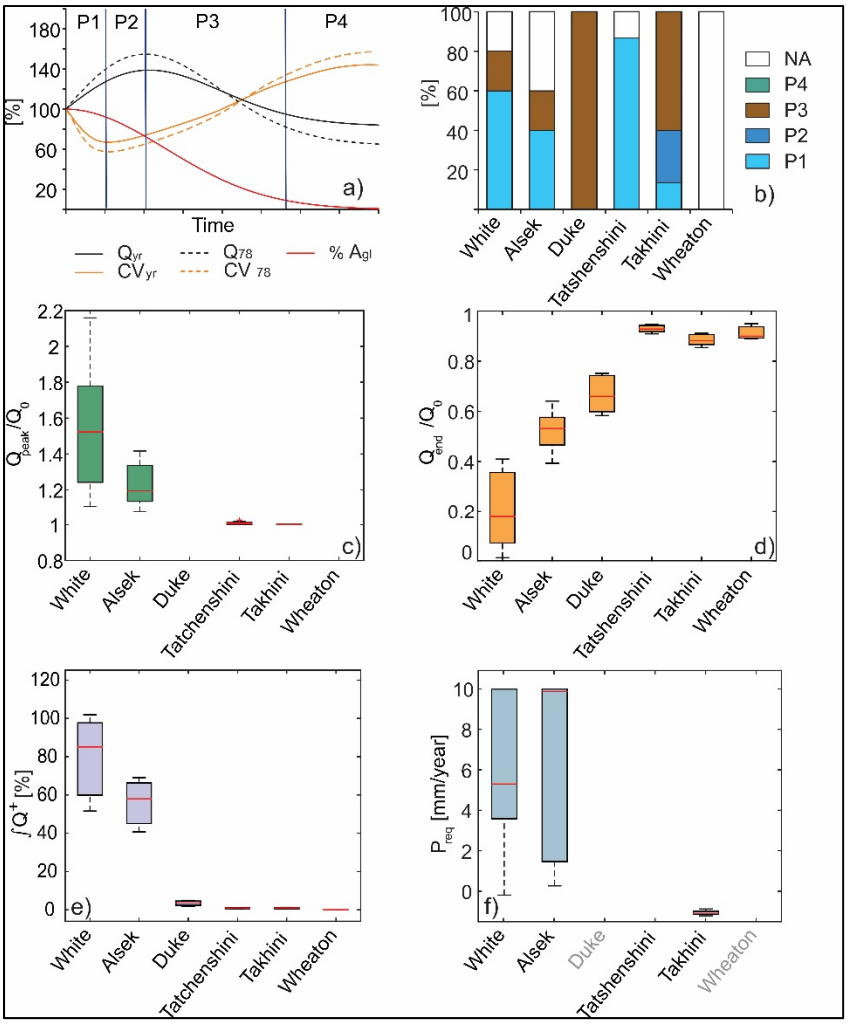

Figure 3.4 Peak water modeling results for glacierized catchments: (a) delineation of conceptual glacier retreat hydrological impact phases; discharge characteristics are normalized to their initial value; (b) PW phases (P1, P2, P3, or P4) corresponding to model outputs for the 15 scenarios considered for each watershed; "NA" is assigned to the scenarios with no glacier retreat acceleration between 1989 and 2017; (c) simulated ablation season discharge maximum value Q_{peak} divided by its initial value Q_0 for all the scenarios leading to P1 or P2 (pre-PW); (d) simulated final ablation season discharge Q_{end} divided by its initial value Q_0 for all the scenarios; (e) glaciers' capacity to further increase the ablation season discharge $\int Q^+$; (f) precipitation increase P_{req} required to reverse glacier retreat driven negative trends in the ablation season discharge

The P_{req} values indicate whether a positive trend in the measured Q_{abl1} (or a negative trend in the coefficient of variation) can be caused by an eventual increase in precipitation instead of glacier retreat. The P_{req} median value varies from 0.3 mm/year (Takhini) to 10 mm/year (Alsek*) (Figure 3.4f). Those values are, in general, much higher than the trends detected in precipitation at the nearby meteorological station(s) (Table 3.5). However, for the White and Duke watersheds, station BL (Figure 3.1) did not show any statistically significant change in precipitation. For the Alsek* watershed, the median value of P_{req} is 9.90 mm/year, with an interquartile range of 2.40 to 10.00 mm/year, whereas the observed trend at station HJ is 2.16 mm/year. This suggests that a measured increase in precipitation was insufficient to affect the phase allocation for these three glacierized watersheds. For the Takhini watershed, the P_{req} median value is 0.25 mm/year, with an interquartile range of 0.25–0.40 mm/year. Those values are slightly smaller than the detected rate of annual precipitation increase of 0.835 mm/year at station C. Therefore, we cannot assume that the pre-PW diagnostic for this particular watershed is not biased by a precipitation increase, which means that observed trends in discharge could be driven by changes in precipitation.

3.5 Discussion

3.5.1 Current hydrological changes and trend attribution

Trend detection shows that 7 of the 8 studied watersheds exhibit significant trends in at least one hydrological variable among the 11 that were used in the study. The most glacierized watershed (White) exhibits significant trends in 8 out of the 11 variables. Among all the watersheds, trends go in the same direction for 6 out of the 8 variables that show significant trends at more than one watershed.

Comparison of trend detection results to watershed classification based on hydrological regime allows for trend attribution. We observe that trends in winter discharge and in the timing of hydrological events are not specific to a unique cluster and affect glacierized, snow, and lake runoff regimes. This is compatible with recent studies that suggest that an increase in winter discharge is related to the thaw of permafrost (Smith, Pavelsky, MacDonald, Shiklomanov, &

Lammers, 2007; Toohey, Herman-Mercer, Schuster, Mutter, & Koch, 2016; Yang et al., 2002) and that the change in times of the freshet or ablation season start is associated with an earlier start of the seasonal snow-cover melt (Brown & Braaten, 1998; Williamson et al., 2018). Highly glacierized catchments (White and Alsek*) show trends in variables associated with the discharge in the ablation season or with the discharge variability corresponding to a pre-PW status. This is also the case, to a lesser extent, for a 2.1% glacierized catchment that clusters with the lake runoff watersheds (Takhini). By contrast, a 9.2% glacierized watershed (Duke) does not exhibit any significant tendency related to the PW situation when trend attribution is performed. On one hand, trend detection in discharge records for highly glacierized catchments shows glacier-specific signatures in hydrological changes because those changes are missing in non- to slightly glacierized catchments. On the other hand, it neither allows for an understanding of trends detected in the watersheds that are moderately glacierized nor guarantees that observed trends are not the consequence of changes in precipitation. The use of SWBM allows us to compensate, at least partially, for those limits.

Model simulations do not contradict significant trends in measured discharge time series in glacierized catchments. Most of the compatible scenarios lead to a pre-PW diagnostic for the highly glacierized White and Alsek* watersheds and suggest that the Takhini watershed may not have passed PW either. However, the fact that the hydrological regime of the latter shows a lake influence, the hydrological effect of which is not entirely represented in the SWBM, makes the diagnostic more hazardous for this watershed than for the highly glacierized watersheds.

Additionally, model simulations provide indications for the watersheds that did not show significant trends in PW-related discharge variables, namely, Q_{yr}, CV_{yr}, Q_{abl1}, and CV_{abl1}. For the Tatshenshini watershed, which is 2.9% glacierized, all the scenarios lead to a pre-PW diagnostic, and for the Duke watershed, which is 9% glacierized, all the scenarios indicate a post-PW situation. Interestingly, the Duke watershed showed an increase in the total discharge volume in 2003 (Fleming & Clarke, 2003) and, 1.5 decades later, does not exhibit many significant changes. According to the PW model, it has reached the turning point. However,

this is consistent with previous observations to the effect that even though such rivers as the Yukon are projected to reach PW by the end of the century, some glacierized headwaters may already be switching to the post-PW regime (Huss & Hock, 2018).

No PW phase was assigned by the model for the Wheaton watershed because no scenario provided an acceleration of the retreat, and the trend analysis for this watershed showed no trend in PW-related variables. Among the two non-glacierized catchments, only the Sekulmun watershed showed a trend in a PW-related variable. However, the presence of a lake influencing the hydrological regime for this watershed makes this unexplained trend not conclusive.

From the previous research in the region, we know that the streamflow of some watersheds in the SW Yukon potentially reacts to such modes of low-frequency climate variability as Pacific Decadal Oscillation, El Niño–Southern Oscillation, and Arctic Oscillation (Burn, Cunderlik, & Pietroniro, 2004; Fleming, Moore, & Clarke, 2006; Hodgkins, 2009). These climate modes affect both summer and winter temperatures (Bonsal, Shabbar, & Higuchi, 2001; Fleming & Whitfield, 2010; Vincent et al., 2015; Shabbar & Khandekar, 1996; Whitfield, Moore, Fleming, & Zawadzki, 2010) and do not seem to have a significant influence on precipitation (Fleming & Whitfield, 2010). We argue that, even if caused by changes in the phases of climate modes, the observed trends still reflect the difference between the hydrological response for glacier melt- and snowmelt-driven watersheds (Fleming et al., 2006). Unlike maritime glaciers where mass balance is observed to be strongly influenced by wintertime anomalies, continental glaciers react mostly to temperature changes during the ablation season caused by low-frequency climate variability, and as a result, glacierized watersheds will respond to warm/cold phases by increased/decreased glacier melt rates (Bitz & Battisti, 1999). By contrast, snowmelt-driven watersheds runoff will only react to temperature shifts in summer months because of changes in evapotranspiration losses caused by earlier/later snowmelt (Fleming et al., 2006). Thus, the different response to the low-frequency climate modes between glacier and snowmelt runoff will only be governed by the fact that the former exhibits an increased glacier melt. Moreover, the results from Arendt et al. (2009) indicate that climate mode phase

shifts are not the primary climate signals driving the glacier change in the region and that glaciers in this region respond to a climate forcing such as global climate changes rather than regional low-frequency climate modes. This suggests that not addressing potential teleconnections does not significantly affect the results of trend attribution and the general conclusions of this study.

3.5.2 Implications for regional water resources

Identifying a PW phase for different watersheds provides indications about the past and present evolution of their discharge characteristics. Watersheds identified as in a pre-PW phase should experience increases in glacier meltwater contribution that will lead to a further increase in Q_{yr} and Q_{abl1} in cases where precipitation remains stable over time. Estimating the magnitude of glaciers' influence on stream discharge requires supplemental indications. For that purpose, three indicators, namely, Q_{peak}/Q_0, Q_{end}/Q_0, and $\int Q^+$, were calculated for each tested scenario.

The results for Q_{peak}/Q_0 and $\int Q^+$ suggest that only the two highly glacierized catchments (White and Alsek*) can expect a perceivable strong increase in Q_{abl1} if glacier retreat keeps accelerating at the same pace as between 1989 and 2017. Similarly, it is at those watersheds only that the PW-related hydrological variables show a high sensitivity to the glacier retreat pace change. At the two other watersheds that have not passed PW yet (Tatshenshini and Takhini), a further increase in Q_{abl} or inversion of trends in PW-related variables should be of low magnitude, if perceivable. By the time glaciers will have lost their hydrological influence, all the watersheds with a presence of glaciers should experience a decline in Q_{abl} compared with 1989. Q_{end}/Q_0 seems to be correlated with A_{gl}. As a consequence of glacier retreat, the most glacierized watershed, for example, is predicted to have a decline in Q_{abl} with final values between 20% and 50% of its 1989 discharge level, whereas for the three watersheds with glacier cover less than 3%, Q_{abl} is not predicted to drop below 80% of the 1989 level. The relatively low magnitude of hydrological changes for the watersheds other than the two highly glacierized ones can explain why a limited number of significant trends have been detected in their discharge time series.

At a regional level, non-glacier-related hydrological changes, namely, an increase in minimum discharge and change in the timing of hydrological events, seem to be characteristic of all hydrological regimes. Therefore, such changes may be present at a large number of watersheds in the region, if not all. In glacierized catchments, the loss of glacier cover generates effects of diverse tendencies and amplitudes. Highly glacierized catchments (more than 30%) should be affected by pronounced changes in Q_{yr}, Q_{abl}, CV_{yr}, and CV_{abl}. The situation is less straightforward for the less-glacierized watersheds, where the amplitude and the direction of the hydrological changes are driven by different factors.

3.5.3 Driver of glacier retreat influence on watershed discharge

In this study, the retreat of glaciers is characterized by two factors: the initial rate of glacier area loss Γ_0 and the glacier area loss acceleration Γ_{follow}. In Table 3.6, we observe that the most glacierized watersheds (White and Alsek*) show comparable values of Γ_{follow}. Those two watersheds also show comparable PW phase profiles, with more scenarios indicating a pre-PW phase for the White watershed. Despite a relatively high glacierized area, the Duke watershed is much closer to the Takhini watershed than it is to White and Alsek* in terms of values for retreat factors. The Tatshenshini watershed is characterized by the second-highest Γ_0 and the highest Γ_{follow}. Furthermore, it is the only watershed with all the scenarios leading to a pre-PW diagnostic.

Even if a direct correlation cannot be quantified because of the limited number of studied watersheds, these observations suggest that the PW phase cannot be explained by A_{gl} only and that glacier retreat characteristics (i.e., Γ_0 and Γ_{follow}) are influencing trends in PW-related variables. On the other hand, as seen in Figure 3.4, A_{gl} seems to influence the amplitudes of PW and post-PW drop. This suggests that changes in A_{gl} may be a good marker to estimate long-term hydrological changes in the watershed, whereas glacier retreat factors may represent good markers of shorter-term changes, such as current trends and the PW phase.

3.5.4 Limitations of the method

The use of an enhanced dual approach for trend attribution in glacierized catchments of the SW Yukon made it possible to isolate and quantify the role of shrinking glaciers in recent hydrological changes in this region. The clustering of the watersheds based on their hydrological regimes resulted in expected outputs by providing a frame for associating particular trends with glacierized watersheds and identifying non-glacier-related trends. The clustering stage also helped identify lake-dominated regimes, the characteristics of which do not allow for a direct link between glacierized conditions and detected trends using the current methods.

Comparison of simulated and measured trends provides good confidence in PW phase allocation and in the depiction of the current situation with respect to glacier influence on discharge characteristics. However, the method used here presents obvious limits, including the absence of time perspective in projections, which reduces direct applicability of the research conclusion to water resource management. The assumption that glacier retreat will keep accelerating at the same pace as over the past 30 years also restricts the use of SWBM projections. We addressed this issue by conducting a hypothetical rapid-retreat simulation for each watershed for the three volume-area scaling factor alternatives. These simulations indicate that the two most glacierized watersheds are the most sensitive to the potential change in the glacier retreat acceleration rate.

Despite the precipitation increase simulation that provides a good confidence level in the overall conclusions of the research, it has not been possible to prove for all the watersheds that potential precipitation increases for a specific watershed have not influenced detected trend. Moreover, the observed increase in temperature and earlier freshet will both increase losses by evapotranspiration (Hamlet et al., 2007) and infiltration through a thickening of the active layer and will enhance permafrost thaw (Walvoord & Kurylyk, 2016). Thus, since losses for evapotranspiration and infiltration were kept constant during simulations, the model most likely underestimated the total discharge decrease from the non-glacierized portions of the

watersheds. Similarly, the fraction of glacier ablation by sublimation was kept constant throughout the simulation period since there are no projections about the change of sublimation rate in the region. Furthermore, its importance for the modeled discharge will decrease and probably become insignificant toward the end of the simulation period as glacier cover keeps decreasing.

Finally, it is important to highlight that such events as river piracy in the region (Barnett, 1974; Bryan, 1972; Shugar et al., 2017) as well as potential errors in delineating the drainage areas because of the unknown meltwater evacuation pathways within the icefields (Braithwaite & Olesen, 1988; Bryan, 1972) and the presence of debris-covered glaciers are not accounted for by the model.

Therefore, this study can be seen as a first step in characterizing glacier retreat impact on water resources in SW Yukon and as an encouragement to conduct studies on an individual basis.

3.6 Conclusions

In a context where hydrological changes are predicted to have numerous adverse impacts in the SW Yukon, the objective of this study was to isolate and quantify the role of shrinking glaciers in hydrological changes. The objective was met by performing trend attribution using an enhanced dual approach. Trend detection and glacier inventory confirmed large-scale transformations in glacierized areas and in discharge variables over the last three to four decades. Glacierized areas declined rapidly at all the studied watersheds, with retreat rates ranging from 0.28% to 1.51% per year between 1989 and 2017. Simultaneously, discharge in the studied watersheds showed a significant evolution in various aspects, such as those associated with PW, the timing of particular events (minimum discharge, ablation season start, maximum discharge), and winter discharge.

Results show that there is the link between shrinking glaciers and hydrological changes in the SW Yukon; however, this link is complex, and glacier retreat does not explain all the observed

changes in regional discharges. Increases in winter (minimum) discharge and changes in the timing of particular events do not seem to be related to the presence of glaciers.

In glacierized catchments, both trend detection and model outputs converge toward similar diagnostics. The two most glacierized watersheds have probably not passed PW. The situation is more complex for the watersheds with lower glacier cover. For example, even with a glacier cover of 9%, the Duke watershed seems to have passed PW, whereas the 2.9% glacierized Tatshenshini watershed has not. Once glaciers will have retreated to a point close to their extinction, major declines in discharge are expected at the watersheds that are currently more than 9% glacierized.

The results show that both the glacierized area and the rate of glacier retreat are necessary to characterize the impact of deglaciation on water resources.

The complex relation between glacier retreat and hydrological changes, and the fact that hydrological regimes dominated by major lakes share common characteristics with glacierized ones, suggests watershed-specific studies should be privileged where a precise characterization of glacier retreat impact on water resources is required.

The results of this study show that in regions with data scarcity, using a trend analysis of commonly measured meteorological and hydrological variables at valley bottoms, coupled with an SWBM and a PW analysis, can give a valuable estimation of future changes in water resources without relying upon climate projections and thus can provide important information for adaptation strategies and further research

3.7 Acknowledgements

This research is supported by the Geochemistry and Geodynamics Research Centre (GEOTOP) of Quebec, the Natural Science and Engineering Research Council (NSERC) of Canada, and *École de technologie supèrieure*, a constituent of the *Université de Quebec* network. We are also grateful for the thorough and constructive comments of three anonymous reviewers and

WRR Associate Editor, Erkan Istanbulluoglu, who helped considerably improve the manuscript. The glacier inventory data as well as the SWBM are openly available on the Open Science Framework (OSF) platform (at http://doi.org/10.17605/OSF.IO/TSCYX).

CHAPTER 4

HOW SIGNIFICANT ARE WATER SOURCES OTHER THAN GLACIERS IN AN ARID HIGHLY GLACIERIZED SUBARCTIC WATERSHED?

A. Chesnokova,[1] M. Baraër,[1] E. Bouchard,[1] and P. Lamontagne-Hallé[2]

[1]Department of Construction Engineering, École de technologie supérieure,
1100 Notre-Dame West, Montreal, Quebec, Canada H3C 1K3
[2]Department of Earth and Planetary Sciences, McGill University,
3450 University, Montreal, Quebec, Canada H3A 0E8

Paper submitted to the *Journal of Hydrology*, February 2020

Abstract

Subarctic glacierized catchments are hydrological systems of paramount importance for water resources management and for various ecosystem services. To accurately project the impacts of climate change on those systems, it is necessary to understand better the role of hydrological components other than glacier meltwater in runoff production. This study aims to quantify the contribution of different end-members to the total ablation season runoff from a highly (36.6%) glacierized watershed in St. Elias Mountains, Canada, under different meteorological conditions. Among others, studied conditions included abnormally warm temperatures due to the influence of the marine heat wave, and conditions when glacier surfaces are covered with snow. During three field campaigns in 2015, 2016 and 2017, all end-members potentially contributing to the total runoff were sampled and their contribution was quantified with a multi-component distributed hydrochemical mixing model. The results suggest that glaciers are still the dominant contributors to runoff in the studied watershed. Their contribution varied between 50±19.5% when their surface was snow covered, and 94.5±1.5% during the season 2015 influenced by "Blob" weather system. Areas hosting buried ice, hillslope tributaries and alpine meadow groundwater taken together represented between 5.4±0.1% for the 2015 season and 49.6±12% during the 2016 season, when glacier outflow was noticeably decreased due to the presence of a snow cover over the ice. Overall, results show that while glaciers remain the

most important contributor to runoff, under certain meteorological and environmental conditions, water sources other than glaciers can represent almost 50% of the total discharge.

Key Points

1. Even with glacier retreat, glacier meltwater remains the most important contributor to the runoff in a subarctic highly glacierized (36.6%) watershed.
2. Hydrological features such as buried ice formations, talus slopes and alpine meadow groundwater contribute significantly to the total runoff.
3. Under certain metrological conditions water sources other than glaciers can represent half of watershed runoff.

Keywords: glacierized watershed, climate change, St. Elias Mountains, subarctic, Blob, buried ice, mixing model, natural tracers, groundwater

4.1 Introduction

Subarctic glacierized mountain catchments are complex hydrological systems of paramount importance for water resources management (Barnett et al., 2005; Immerzeel et al., 2019; Viviroli et al., 2007) and for various ecosystem services (Fleming, 2005; Milner et al., 2017). Those catchments often host numerous hydrological components such as rock glaciers, buried ice formations, moraines, talus and alpine meadows, all of which are found in mountain settings of both arctic and temperate regions. In glacierized headwater catchments from different climatic regions, these hydrological components are known to have high storage capacities and complex groundwater distribution systems (Cochand et al., 2019; Jones, Harrison, Anderson, & Whalley, 2019; Hayashi, 2019; Rogger et al., 2017). For instance, in Argentinian Andes rock glaciers have been observed to store significant amounts of water and to contribute around 13% of summer runoff generated from a 57 km^2 watershed, which is 3.11% glacierized (Croce & Milana, 2002; Schrott, 1991). In a 0.4 km^2 watershed in the Canadian Rockies, Harrington, Mozil, Hayashi, and Bentley (2018) estimated the runoff from a rock glacier, which occupies 30% of the watershed area, to contribute up to 50% of the

summer baseflow. Other studies have shown the importance of runoff from talus slope in sustaining both summer (Canadian Rockies; Muir et al., 2011) and winter baseflow (Colorado Rockies; Clow et al., 2003). The outflow from a proglacial moraine complex in the Canadian Rockies proved to be an important component of the Lake O'Hara mass balance (Roy & Hayashi, 2008; 2009). Along with storing water and contributing to surface runoff, hillslopes and moraines in glacierized watersheds are known to contribute to the proglacial aquifers recharge (Dochartaigh et al., 2019). Similarly, buried ice formations participate in active layer recharge either directly (Cooper et al., 2002), or indirectly by acting as an impermeable layer preventing water percolation to deeper aquifers (Langston et al., 2011; McClymont et al., 2011). Finally, groundwater aquifers within alpine meadows are able to contribute significantly to stream recharge (Gordon et al., 2015; Somers et al., 2016) and maintain shallow groundwater table throughout the ablation season (Hayashi, 2019).

These components are different in terms of their characteristics such as their ice content, constitution, distribution and hydrological roles. Thus, their hydrological responses to climate forcing are diverse. This statement is particularly valid for rock glaciers, ice-cored moraines and buried ice formations which, similar to glaciers, show a particularly high sensitivity to changing climate (e.g., Johnson, 1986), thus adding to the vulnerability and hydrological instability of subarctic glacierized catchments. To accurately project climate change driven hydrological transformations, which will impact subarctic populations and ecosystems (Hinzman et al., 2005; Jacobsen et al., 2012; Larsen et al., 2014), it is therefore of primary importance to make progress in understanding surface water generation at glacierized headwaters by taking into account the role played by hydrological components other than glaciers.

In glacierized catchments, watershed-scale hydrological studies traditionally address runoff generation from different sources by grouping them in three categories: glacier meltwater, snowmelt and groundwater (e.g., Brown et al., 2006; Racoviteanu et al, 2013). This practice has allowed substantial improvements in understanding of hydrological processes, showing, for example, the importance and variability in groundwater contribution to glacierized

watersheds runoff (e.g., Baraer et al., 2015; Hood et al., 2006; Kong & Pang, 2012). As there are no direct methods to quantify groundwater contribution, indirect methods have been applied. Those methods include hydrograph separation using natural tracers to derive groundwater signatures based on water sampled from springs (e.g., Engel et al., 2016; Nolin et al., 2010; Racoviteanu et al., 2013), shallow wells (e.g, Baraer et al., 2015; Hu et al., 2019; Kong & Pang, 2012), or moraine seepage (e.g., Brown et al., 2006), or numerical approaches (e.g., Somers et al., 2019). A reference non-glacierized catchment of comparable geomorphologic attributes has also been used to estimate the glacierized catchment groundwater component (Baraer et al., 2009). Another technique used to assess groundwater component contribution to total runoff is calculating the residual of the catchment water mass balance (e.g., Hood et al., 2006). Despite the advances those studies represent, they associate groundwater to a unique or limited number of hydrological components, at the expense of capturing the complexity of such hydrological systems (Mimeau et al., 2019; Salzmann et al., 2014; Vincent et al., 2019) and their spatial variability (Zuecco et al., 2019; Penna & van Meerveld, 2019). Generally, separating runoff into snowmelt, glacier-melt and groundwater, does not allow differentiating the role of every hydrological component that exists in subarctic glacierized catchments.

In light of the above, the objective of the present study is to disentangle the importance of all identifiable hydrological components (e.g., glacier meltwater, buried ice formations, talus and alpine meadow) to the total runoff of a small (8.75 km^2) subarctic glacierized watershed in the Upper Duke River valley in Yukon, Canada, under different meteorological conditions. The Duke (Shar Ndu Chu) watershed has passed peak water (Chesnokova, Baraër, Robillard, & Huh, 2020) and thus hydrological components other than glacier meltwater will have more influence on runoff generation as glaciers continue to retreat. In addition to colluvial landforms, the studied watershed is characterized by the presence of large quantities of buried glacier ice in terminal and lateral moraines as a legacy of the Neoglacial maximum (Johnson, 1986; 1992). This diversity makes it possible to study the role water sources that are present in the region in the watershed's outflow. The study period covers the 2015, 2016 and 2017 ablation seasons. During summer 2015, the continental Pacific Northwest was under the

influence of the marine heat wave nicknamed “Blob” (Aaron-Morrison et al., 2017; Blunden et al., 2016; Bond et al., 2015). The “Blob” influence was characterized by above-average summer temperatures in Yukon (Blunden et al., 2016). Those high temperatures were suspected to be reflected in the water sources contribution to the runoff since bare ice was observed within both ablation and accumulation zones of all three glaciers in the watershed early in the ablation season. Comparison of the 2015 results with the subsequent two studied years provides one of the first estimations of “Blob” effects on different water sources in glacierized catchments. The 2016 season was characterized by glacier surfaces entirely covered with snow whereas snow from the ground had melted away. Finally, meteorological and field conditions during the 2017 season did not exhibit any abnormal characteristics. During this season the highest number of contributing water sources was observed and thus 2017 represented reference conditions.

Our overall objective is detailed into the following specific research questions: 1) is there any significant contribution from sources other than glaciers in the studied watershed? 2) Is it possible to identify specific contributing sources and to quantify their contributions to watershed runoff? 3) How does the runoff contribution from the different components change under different meteorological conditions? To address these research questions, the hydrochemical basin characterization method (HBCM) (Baraer et al., 2009, 2015) is used. HBCM is based on a multi-component distributed hydrochemical mixing model that allows quantifying the contribution of different end-members to glacierized watershed runoff (Saberi et al., 2019).

4.2 Methods

4.2.1 Method overview

The study is based on three field campaigns, which took place in July 2015, in June 2016 and in August 2017, and targeted different hydrological conditions. During those field campaigns, we used synoptic sampling (i.e. many water samples from different origins taken in a very short time period) of all water sources which we identified as possible contributors to

watershed runoff (Mark & Seltzer, 2003). Preliminary assignation of water sources origins was made based on field observations. Then, the water samples were analyzed for stable water isotopes and major ions, and the assumed origins were tested. Tracers that allowed differentiating samples based on their origins in a consistent way were then used to calculate the contribution of each water source to the watershed runoff using HBCM (Baraer et al., 2009, 2015). Finally, resulting contributions of different water sources were contextualized by analyzing air temperature and precipitation for the 2015, 2016 and 2017 ablation seasons.

The most complete picture of the hydrological system of the studied watershed was obtained in 2017, as the number of water sources identified during that year was the highest among the three sampling seasons. In contrary, the 2015 season has the smallest number of sources sampled. Therefore, results interpretation is first presented for the year 2017. Results for 2015 and 2016 are then explored in comparison to 2017's ones.

4.2.2 Study site

The study watershed, called watershed B throughout the paper, is situated in St. Elias Mountains, Yukon, Canada, and is a tributary of Duke River. Its area is 8.75 km^2 and it is 36.6% glacierized. There are three glaciers and in absence of known names they were arbitrary referred to as B1 (1.841 km^2), B2 (0.959 km^2) and B3 (0.419 km^2) (Figure 4.1). The elevation of the entire watershed ranges from 1674 to 2906 m above sea level (a. s. l.). It ranges from 1949 to 2827 m a. s. l. for glacier B1, 2165 to 2806 m a. s. l. for glacier B2 and 2285-2798 m a. s. l. for glacier B3. The main components of the drainage network originate from the outlets of these three glaciers. Other minor hydrologic components, while still meaningful, originate from hillslopes. The activity of those components varies between the seasons/years, some being dry during field season. The typical hydrograph for a glacierized watershed in the region rises in June primarily due to snowmelt and is sustained by glacier melt throughout the summer (Brabets et al., 2000; Chesnokova et al., 2020). Duke River watershed has high discharge during June-August with maximum runoff in July. The ablation season starts in mid-May and lasts till end of October (Chesnokova et al., 2020).

Climate in this region is continental with mean annual air temperature ranging between −2 and −6°C and a mean annual total precipitation varying between 250 and 400 mm/y (Wahl et al., 1987). Glaciers in the region are not in equilibrium with current climatic settings and experience almost continuous negative mass balances (Arendt et al., 2002; Barrand & Sharp, 2010; Chesnokova et al., 2020). Moraine formations containing buried ice are extensive in St. Elias region. They are most often formed as a result of glacier dynamics and thus consist mainly of glacier ice (Johnson, 1992). Another possible mechanism of formation for ice-cored moraines in the area is the accumulation of permanent snowbanks which get buried under debris (Johnson, 1978). Ice-cored moraines and buried ice formations were observed next to the B1 glacier tongue on both sides of the proglacial field, next to B3 glacier and next to the river downstream from the B2 glacier (marked in orange on Figure 4.1).

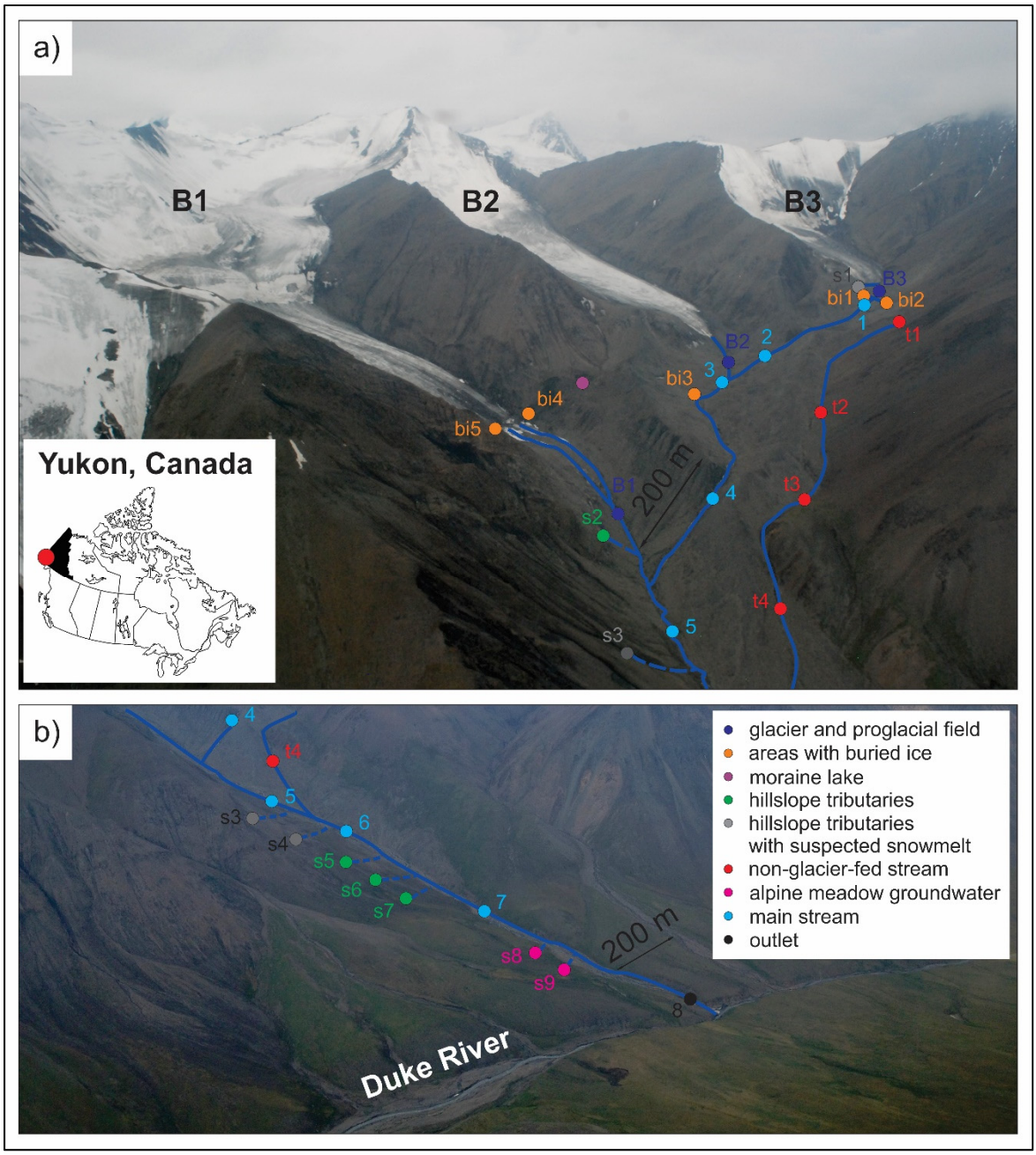

Figure 4.1 Bird view on the B watershed in June 2015. Top panel shows glaciers B1, B2 and B3 and drainage network of the upper part of the watershed. Bottom panel shows the lower part of the watershed. Approximate positions of 2017 season sampling points are marked for reference with circles color-coded depending on their genesis (see explanations in the section 4.2.4.1). Note that, in June 2015, glaciers showed abnormally limited snow cover for the beginning of the ablation season

4.2.3 Air temperature and precipitation measurement

To characterize meteorological condition during studied ablation season, in addition to our field observations, an automatic weather station (AWS) was installed at the watershed B outlet. It measured hourly air temperature from 30th of June 2015 till 31st of August 2017 at 1.5 m above the ground, and recorded liquid precipitation for the period of 30 June 2015 to 24 June 2016 (up to an equipment breakdown).

4.2.4 Hydrochemical basin characterization method

Waters originating from different sources can have unique hydrochemical and isotopic signatures as a result of the specific hydrological, geological, and biological processes to which they have been exposed (Drever, 1997; Drever, 2005). Using these signatures, the HBCM (Baraer et al., 2009, 2015) developed and applied a multi-component hydrochemical mixing model to nested interconnected sub-basins, called cells. As a result, it is possible to disentangle the contribution of different sources to the outflow from each cell and eventually to the entire watershed outflow. This approach helps to avoid making assumptions about spatial variability of sources signatures within the watershed (Penna & van Meerveld, 2019).

4.2.4.1 Water sample collection

The first step of HBCM is sampling of all sources, called end-members, which potentially contribute to the main stream, as well as the main stream at each cell inlet and outlet, called mixing points. The synoptic sampling was performed on the 7th of July 2015, the 22nd of June 2016 and on the 3rd of August 2017. For each year, samples were taken from all observed tributaries as well as other water bodies within the watershed in order to make its entire characterization. Based on our field observations, samples were divided into following genetic categories:

Glacier and proglacial field. Samples that follow into this category were taken from the immediate proglacial field outlet (Figure 4.1). Runoff at this outlet includes both glacier meltwater as well as runoff from side moraines.

Areas with buried ice. Samples from this category were most frequently taken from streamlets forming from ice remnants overlaid with debris layer, either at the point of formation of these streamlets (bi1, bi4) or further downstream (bi2). Water in these streamlets is hypothesized to originate from buried ice ablation. Sample bi3 was taken from the small pond formed next to buried ice formation. This pond was connected to the main stream with a small streamlet. Sample bi5 was taken from the streamlet generated at the base of the ice-cored moraine on the right side of B1 proglacial field. For this sample it was not possible to verify if other sources were contributing to these streamlets since the top of the streamlet was not seen.

Moraine lake. This category is represented by a sample from a lake (ml) on the top of the left-side ice-cored moraine of the B1 glacier (Figure 4.1), which was observed during all three field seasons. The origin of the lake water is hypothesized to be related to buried ice ablation.

Hillslope tributaries. Samples from this category were taken from streamlets forming from the talus slope on the right side of the B1 subwatershed. Headwaters of these streamlets were not visible. An exception is a tributary input within the B3 proglacial field, s1. Field observation suggested this tributary being at least partly fed by snow patch meltwater (Figure 4.1).

Non-glacier-fed stream. This group of samples was taken from the large non-glacier-fed stream which was only observed during the 2017 ablation season. This tributary coincides with the position of ice marginal channel: it emerges from the B3 lateral moraine and continues to flow along it (Figure 4.1). Within this lateral moraine, ice remnants were observed on the side of B3 proglacial field, where the sample bi2 was taken. Between samples t2 and t3 this non-glacier-fed stream disappears into the ground.

Alpine meadow groundwater. During seasons 2015 and 2016, samples from this category were taken from groundwater wells within alpine meadow. During the season 2017, small streamlets within alpine meadow were sampled to represent runoff from alpine meadow because groundwater wells were frozen (Figure 4.1).

Main stream samples. This group of samples was collected from the main stream upstream from tributaries and ca 100 m downstream from them to ensure that waters had mixed.

Sample names are given based on the 2017 field season, and for 2015 and 2016 we use the same names where possible.

All samples were collected into high density polyethylene bottles. 30 mL were taken for stable water isotopes analysis and 50 mL for major ions analysis. Samples for ionic analysis were filtered on site using 0.45-micron filters and were acidified with three drops of nitric acid 0.5M. All bottles were filled to the brim, sealed, and stored in dark conditions at 4°C. At each sampling location, conductivity, temperature, and pH were measured using a HI 9829 multimeter. Conductivity was calibrated using 0 µS/cm, 84 µS/cm, and 1413 µS/cm standards, and pH with 4.01, 7.01 and 10.01 buffer solutions.

4.2.4.2 Stable water isotopes analysis and interpretation

Water samples were analyzed for stable isotope ratios of oxygen, $\delta^{18}O$, and hydrogen, $\delta^{2}H$, using cavity ring down spectrometry (Picarro Analyzer L2130-I; guaranteed instrumental precision is 0.03‰ for $\delta^{18}O$ and 0.2 ‰ for $\delta^{2}H$). Both $\delta^{18}O$ and $\delta^{2}H$ were expressed in per mil (‰) relative to Vienna Standard Mean Ocean Water standard (Coplen, 1996). For each sample, six injections were performed and the last two or three, depending on the observed memory effect, were taken for averaging. Calibration was done after each 100 samples using 6 laboratory standards. In addition, a standard was analyzed every three samples to verify the stability of measurements and perform post analysis correction where needed. The results of

δ^2H were then plotted as a function of $\delta^{18}O$, and the Global Meteoric Water Line (GMWL) was shown for the reference.

Isotopic signature of water does not directly depend on the water path and, in the absence of phase changes or non-equilibrium fractionation along the flow path, reflects isotopic composition of parent meteoric waters (Sidle, 1998). Isotopic signal in parent precipitation depends on the atmospheric temperatures during cloud formation, which in turn depends on the season and elevation (Gat, 2010; Mook, 2001). In mountain environments, samples, which are enriched in δ^2H and $\delta^{18}O$ compared to the average, usually originate from precipitation reaching the ground at the lower elevations and warmer air temperatures. Samples depleted in in δ^2H and $\delta^{18}O$ most often originate from higher elevation and lower temperatures than the enriched ones (Rozanski, Araguás-Araguás, & Gonfiantini, 1993; Gat, 2010; Mook, 2001; Sidle, 1998). Being formed from solid precipitation at the watershed highest elevations, glacier ice is thus expected to be depleted in stable water isotopes compared to samples taken from non-glacierized parts of the watershed (Cable, Ogle, & Williams, 2011; Engel et al., 2019; Nolin et al., 2010). However, processes such as phase change or fractionation can alter this general pattern. For instance, isotopic signatures of snow, glacier ice and buried ice can be enriched due to removal of lighter isotopes as melt water percolates during freeze-melt cycles (Grabcsak, Niewodniczanski, & Rozanski, 1983; Taylor et al., 2001; Williams et al., 2006) or due to sublimation (Dietermann & Weiler, 2013; Nolin et al., 2010). Isotopic signature of groundwater will depend on the signatures of waters that recharge the aquifer as well as on potential mixing within the aquifer (Penna & Van Meerveld, 2019). It can also be altered by evaporation, in particular in shallow groundwater systems, leading to an increase in heavier isotopes (Hu et al., 2019). Finally, samples from the main stream, where water from different sources mix, should plot between the related end-members on the δ^2H-$\delta^{18}O$ diagram.

4.2.4.3 Major ions analysis and interpretation

Anionic concentrations in samples (F^-, Cl^- and SO_4^{2-}) were measured with an ionic chromatographer (Dionex ED50, Thermo Fisher Scientific). The equipment was calibrated

every 30 samples using seven standards ranging from 0.005 to 3.2 ppm for F^-, from 0.1 to 50 for Cl^- and from 0.2 to 75 for SO_4^{2-}. Every three samples a standard was inserted (0.2 ppm for F^-, 0.9 for Cl^- and 1.8 for SO_4^{2-}) followed by a blank sample to check the stability of measurements and to eventually correct results for drift in measurements. Cationic concentrations (Li^+, Na^+, K^+, Ca^{2+}, Mg^{2+}) were measured by inductively coupled plasma optical emission spectrometry (ICP-OES, 5110 Agilent). The instrument was calibrated each 23 samples using 9 standards ranging from 1 to 40 ppm for Ca^{2+} and for highly concentrated samples in Mg^{2+} and from 0 to 10 ppm for other ions. Two standards (10 ppm of Ca^{2+} and 5 ppm of other ions) followed by a blank sample were inserted every three samples to eventually correct the results for drift in measurements.

Unlike isotopic signature, the hydrochemical signature of water is a result mainly of the path and the composition of solid particles, which water is in contact with. The rate and mechanisms of weathering processes as well as the time of contact with those solids are the main factors controlling the total solute concentration in the water (Drever, 1997; Drever, 2005). Precipitation, snowmelt and ice melt samples are therefore expected to be poor in solutes (Engel et al., 2016; Penna, et al., 2017), whereas samples from buried ice areas are anticipated to exhibit higher concentration due to longer contact of ice meltwater with debris and fine particles (Penna et al., 2014). Similarly, due to longer contact with rocks, groundwater tends to have increased solute concentrations compared to other sources (Drever, 1997). Finally, the hydrochemical signature of samples taken from the main stream will depend on solute concentrations in contributing end-members.

The expected differences in hydrochemical signatures between sample categories were explored using principal component analysis (PCA) on scaled variables. Together with δ^2H-$\delta^{18}O$ diagrams, PCA allows studying similarities and dissimilarities between the samples, and therefore challenging the preliminary assignment of samples categories based on field observations. Samples for which the preliminary category assignment is not verified by the isotopic and/or the hydrochemical signatures are recategorized as “other”.

4.2.4.4 Identification of tracers to be used in HBCM

Among conservative tracers (La Frenierre & Mark, 2014), only those that fulfill the three following conditions are selected for use in HBCM: 1) tracer measured in a cell outflow cannot have a value outside of the range defined by the possible contributors; 2) tracer values at the cell outflow and at least one contributor must be greater than the detection limit of the analytical methods; and 3) there should be a minimum 5% difference between the extreme contributors tracer values (Baraer et al., 2015). As a result, the combinations of tracers possibly vary between cells due to tracer rejection when the above mentioned rules are not met. In addition, selected tracers values should be sensitive to end-members type or their spatial origin (Baraer et al., 2015).

4.2.4.5 Quantifying end-member contribution to the watershed outflow

HBCM spatial coverage requires defining cells where contributors, end members and/or other cells outlets, mix to form the cell outlet. Each cell outlet is therefore a contributor to the subsequent downstream cell. These cell-overlaps are used to accumulate end-member contributions for the entire watershed. There are two types of cells: the first type has tributary inputs as well as upstream mixing point as their contributors. The second type is characterized by two main stream samples located relatively far from each other with no substantial surface water contribution in between those two points. For this type of cells HBCM is used to identify potential subsurface inputs. This is done by testing several possible sources as potential contributor such as alpine meadow, streamlets and other sources even though geographically their contribution is of low probability. For each cell, HBCM calculates the relative contribution of end-members by using an over-parameterized set of mass balance equations. Mixing is assumed to be instantaneous and thus mass balance equations can be defined for each cell as follows:

$$C_{tot_j} = \frac{\sum_{i=1}^{n}(C_{ij}Q_i) + \varepsilon_j}{Q_{tot}}, \quad (4.1)$$

where i is a given end-member, n - the total number of end-members, j - a given tracer, C_{totj} - the relative concentration of tracer j at a mixing point, C_{ij} - the relative concentration of tracer j in end-member i, Q_{tot} - total discharge at a cell outlet, Q_i - the proportion of end-member in a total discharge and ε_j represents the accumulated error. In order to obtain the most accurate estimate of end-member contribution, m should be greater than n. Based on a quasi-Monte Carlo approach (James, 1980), HBCM is run for each cell for all possible combinations of m tracers. It solves Equation 4.1 for the unknown Q_i/Q_{tot} by minimizing the cumulative residual error term $\sum_{j=1}^{n} \varepsilon_j$, while filtering for Q_i values that respect the water balance equation $\sum_{i=1}^{n} Q_i = Q_{tot}$ within a 0.5% tolerance (Baraer et al., 2015).

In HBCM, uncertainty is accounted for by considering the 8 best solutions within three-fold of the lowest cumulative error as equiprobable. If less than 8 solutions fall within three-fold of the lowest cumulative error, then all those solutions are considered as equiprobable. HBCM results are then expressed using the average relative contribution of each end-member associated with their standard deviations. The latest is considered as representative of the method uncertainty for each cell (Baraer, McKenzie, & Mark, 2017).

At a final step, cumulative contribution of each end-member at the watershed outlet is calculated for each cell by multiplying cell outlet mean contribution to mean contribution of its inlets. Error associated to those cumulative contributions is calculated as being the square root of the sum of the square of the individual relative errors (Taylor, 1998). Cumulative contributions are then compiled per origin types to provide an overview of the different kind of water that contribute to the watershed outflows.

4.2.4.6 HBCM results verification

The ability of HBCM to estimate relative contributions of end-members was assessed using the inversed mass balance equation technique (Christophersen et al., 1990). To perform the verification, tracers which have concentrations above the detection limit and which are used for the majority of cells were chosen. Tracer concentrations were back-calculated using

HBCM-derived relative discharge results and then compared with measured concentrations. Ideally, back-calculated concentrations for these individual tracers should match their measured concentrations. Back-calculated concentrations were plotted against measured values and R^2 and p-value were calculated. Outliers were identified by means of 95% confidence intervals.

4.3 Results

4.3.1 Meteorological and field conditions at sampling

In 2017, sampling took place during the second half of the ablation season, on the 3rd of August (Figure 4.2a). At this time, snow from ablation zone has melted, and only persisted in accumulation zone. There was no snow on the ground apart from small snow patches at higher elevations and mountain tops. On the day of sampling, hourly air temperature at the AWS location reached 15.7°C (Table 4.1). For three days prior to sampling, air temperature stayed above 5°C during nights and above 12.5°C during days. Due to equipment failure, there were no measurements of precipitation for the 2017 sampling season. However, field observations confirm that all the snow had melted, and that there was not a precipitation event for at least 1 week prior to sampling.

During the 2016 sampling, air temperature was the lowest among the 3 campaigns, and the day of sampling had been preceded by a short cold period (Figure 4.2b). On the day of sampling, the 22nd of July, air temperature reached 14.5°C (Table 4.1), but on the previous day, the 21st of July, maximum daily air temperature was only 6°C. The 2016 season sampling conditions were also different from the other two seasons due to late season snowfall which took place one week before sampling. As a result, glaciers were entirely covered by snow. Snow from the ground, however, had melted by the time of the sampling and only high-elevation snow patches persisted.

The 2015 field campaign took place at the end of the “Blob” event (Blunden et al., 2016; Bond et al., 2015). The conditions during the 2015 season sampling differed from others’ due to

higher maximum and minimum daily temperatures (Figure 4.2c, Table 4.1). Glaciers exhibited bare and dark ice surfaces almost up to the top of their accumulation areas (Figure 4.1a) Also, observed river discharges were visibly higher than in two other seasons. Sampling for the 2015 season was performed on the 7th of July, with air temperature reaching 17.5°C (Table 4.1). Three days prior to sampling, nocturnal temperatures dropped to almost 0°C and maximum daily temperature reached only 4°C (Figure 4.2c). Even though sampling during this season was performed at the beginning of the ablation season, maximum daily air temperatures were higher than those in 2017.

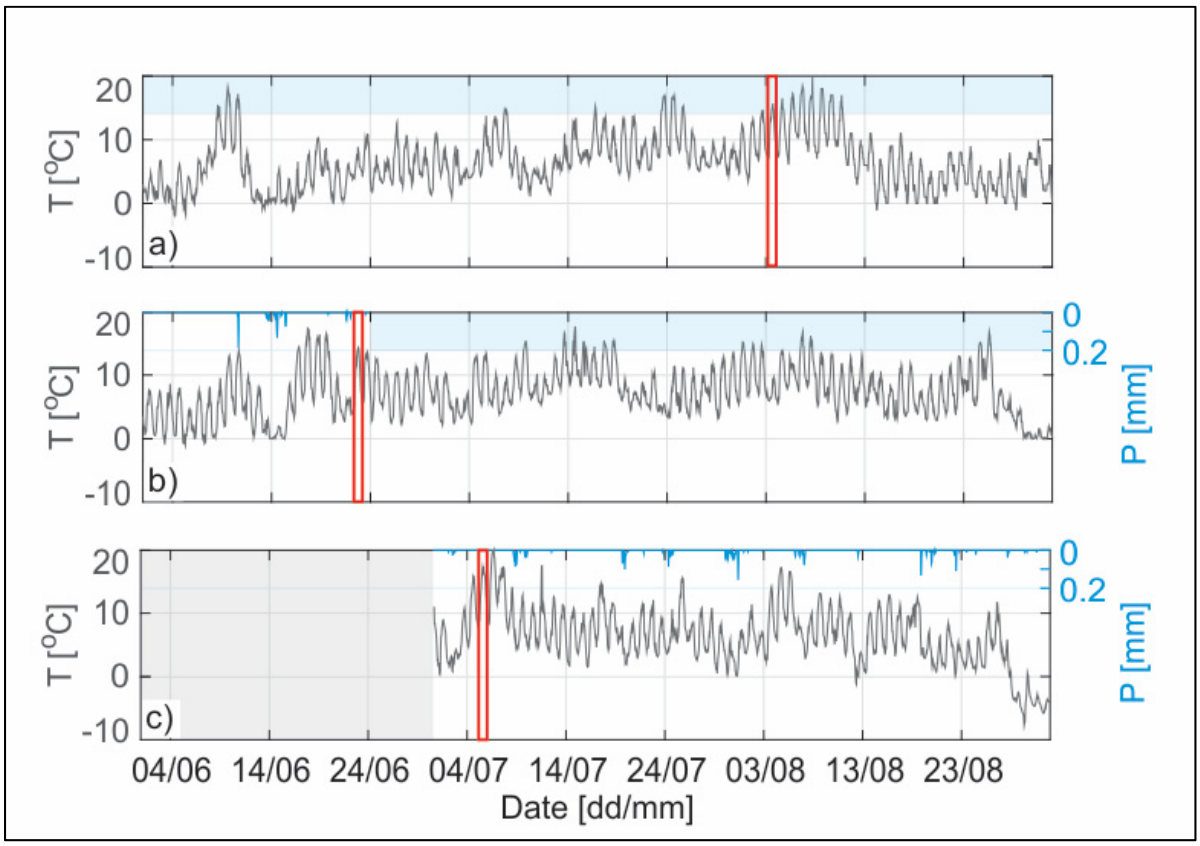

Figure 4.2 Hourly air temperature (T) and precipitation (P) during the ablation seasons a) 2017, b) 2016 and c) 2015; red rectangles highlight sampling days positions; grey shaded rectangle represent period with missing data for T and P; blue shaded rectangles represent period with missing data for P

The results illustrate the main differences between the meteorological and field conditions among three sampling campaigns. In particular, the 2015 season is characterized by abnormally warm temperatures due to the influence of "Blob" and by potentially enhanced glacier meltwater production due to the reduced snow cover on glaciers. The 2016 season is characterized by colder air temperatures in comparison with 2015 and 2017 and potentially reduced glacier melt due to presence of snow cover. Finally, the 2017 season does not manifest any abnormal characteristics, and its observed average daily temperatures are between the values obtained for other two seasons. Snow conditions on the glacier also correspond to an in-between case in comparison with the 2015 and 2016 seasons. Thus, this season can be considered as a reference in terms of meteorological and field conditions.

Table 4.1 Meteorological and field conditions for each sampling campaign

	2017	**2016**	**2015**
Max daily air temperature, °C	15.7	14.5	17.5
Min daily air temperature, °C	7.1	4.3	8.2
Mean daily air temperature and standard deviation, °C	11.2±2.9	9.5±3.6	13.2±3.2
Precipitation	no	3-days-long snowfall a week prior to sampling	no
Snow on glacier	Only in accumulation zone	Almost 100% coverage	Only in upper part of accumulation zone
Snow on ground	Only small patches on the mountain tops	Only small patches on the mountain tops	Only small patches on the mountain tops

4.3.2 Back calculations for individual tracers

Back calculations to assess reliability of HBCM results were performed for Mg^{2+} as this is the tracer which was used by HBCM for the majority of cells and its concentrations were above the detection limit. Figure 4.3 shows measured concentrations for Mg^{2+} plotted against back-calculated ones for each year together with fitted linear regression and its 95% confidence intervals. Calculated R^2 is equal to 0.95. Thus, overall back-calculated concentrations using Mg^{2+} seem to produce good results. Only one cell for the 2015 season, cell 8, gives negative concentrations and plots slightly outside of the 95% confidence interval (Figure 4.3). When interpreting HBCM results, particular attention is given to the identified problematic cell.

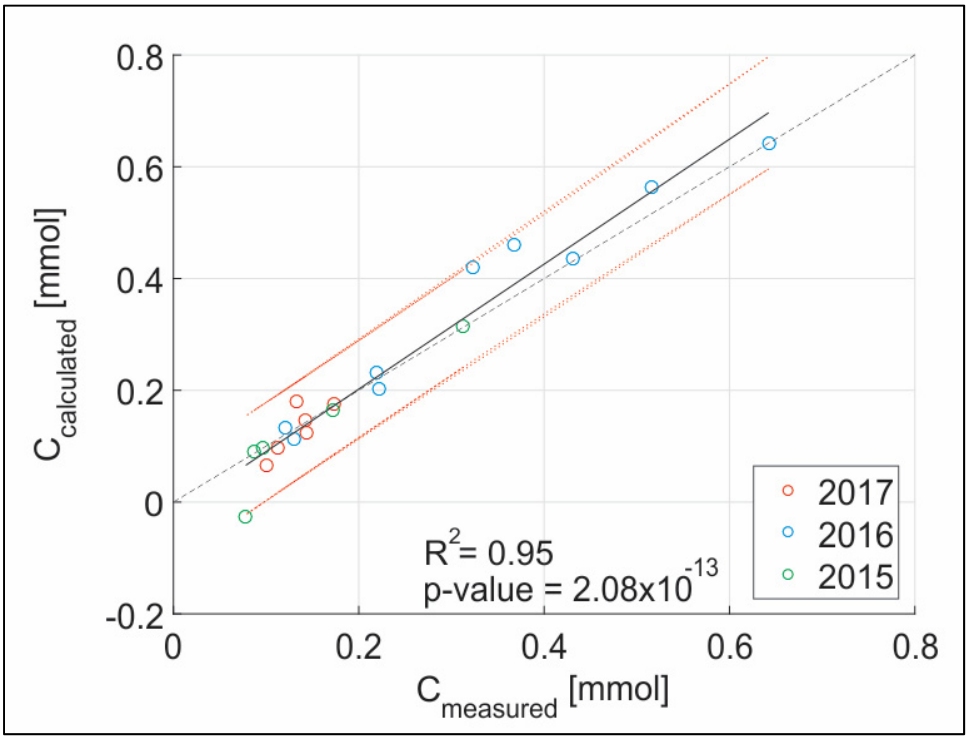

Figure 4.3 Comparison between measured ($C_{measured}$) and back-calculated concentrations ($C_{calculated}$) of Mg^{2+} for all mixing points for three sampling seasons. Black solid line presents fitted linear regression and red dashed lines mark its 95% confidence intervals; along grey dashed line $C_{measured}$ equals $C_{calculated}$;

4.3.3 Season 2017 results

4.3.3.1 Stable water isotopes analysis

The results of stable water isotopes analysis for the 2017 season are presented on Figure 4.4a. As anticipated, the three samples taken from glaciers outflows, namely B1, B2 and B3, are located on the lower right part of the $\delta^{18}O$ - $\delta^{2}H$ diagram (Figure 4.4a). Most of the samples taken from the main stream (shown in light blue) are situated in the same region of the graph as the samples that represent glaciers. The most upstream sample from the main stream, #1, plots next to samples from B3 glacier, and the sample from the outlet, #8, plots in between the three glaciers samples (Figure 4.4a, zoomed in). This confirms that glacier meltwater constitutes most of the outflow from the immediate proglacial area. However, two of stream samples, namely #5 and #7, do not follow that tendency. Sample #5 is taken from a mixing point for joint stream formed by glaciers B1 and B2 (samples B1 and 4, Figure 4.4c) and hillslope tributary s2. The fact that #5 does not plot in between those samples suggest that it was taken too close to the mixing point where water did not have time to mix. The sample #7 was taken after hillslope tributaries s5, s6 and s7 join the main stream (Figure 4.4c). Thus, this sample represents the mixture of isotopic signatures from #6 and aforementioned hillslope tributaries, and hence is supposed to plot between them on the $\delta^{18}O$ - $\delta^{2}H$ diagram. As this is not the case, we suspect that this sample was also taken where the stream water was not yet well mixed. Sample #5 was kept for the HBCM because it represents an important cell, but was treated with caution for the rest of the study. Sample #7 is not used for HBCM.

Samples from areas that were identified as containing buried ice (shown in orange) do not cluster together on the $\delta^{18}O$ - $\delta^{2}H$ diagram. Four of those five samples are enriched in heavy isotopes in comparison with samples that represent glaciers (Figure 4.4a). Only one sample, bi4, plots slightly below glacier samples. This position on the diagram is compatible with the bi4 primary origin assignation, namely buried ice ablation. Two samples in the B3 subwatershed, bi1 and bi2, originate from higher elevations than the three others. On the $\delta^{18}O$ - $\delta^{2}H$ diagram they show enrichment in $\delta^{18}O$ and $\delta^{2}H$ in comparison with bi4 and are located

slightly above the position of glacier samples. These positions support the hypothesis of buried ice ablation origin for samples bi1 and bi2. The sample from the pond next to a buried ice formation, bi3, is the most enriched in heavy isotopes. This result challenges either the buried ice ablation origin of the sample, or the genetic relation between the observed ice and glacier ice. Finally, sample from the right-side moraine in the B1 subwatershed, bi5, plots together with bi1 and is close to the moraine lake sample ml (shown in purple, Figure 4.4a), a characteristic that make the buried ice origin for the lake water possible.

Hillslope tributaries, which can potentially be, at least partly, fed by high elevation snow/ice meltwater, are shown in grey and in green on Figure 4.4a. Their positions on the $\delta^{18}O$ - $\delta^{2}H$ diagram vary a lot between samples. Sample s2 is the most enriched in heavy isotopes and plots far from the grouping made by the glacier and main stream samples. Snow/ice meltwater origin for that sample is thus considered as highly improbable. Samples s3 and s4 are the most depleted in heavy isotopes and plot lower than that cloud. These two samples are marked in grey also for the other two seasons to facilitate tracing those samples throughout the study. Sample s1 next to the B3 glacier was observed to be, at least partly, fed by a meltwater from a snow patch. As it plots together with the glacier samples it is also marked in grey. Finally, sample s5-7 plot close together and are located above glacier samples. Thus, contribution from snow/glacier meltwater is not suspected for these three hillslope tributaries.

Sources s8 and s9 are geomorphologically disconnected from all the other sources samples and are marked in pink for distinction from the other tributaries. These samples were taken from the lowest part of the B watershed close to the confluence of the B stream with the Duke River, an area that belongs to the alpine meadow of the larger Duke watershed (Figure 4.1b). Samples s8 and s9 are the most enriched in heavy isotopes among hillslope tributaries (Figure 4.4a). These two streamlets are fed by precipitations reaching the ground at the lowest elevations of the study site. Their high position on the $\delta^{18}O$ - $\delta^{2}H$ diagram, therefore, confirms the relation that was anticipated between isotopic signatures and elevation.

Finally, samples from the non-glacier-fed stream (shown in red) are relatively enriched in heavy isotopes and plot together with some of the samples from areas with buried ice as well as with samples from hillslope tributaries (Figure 4.4a). The upstream sample from this significant tributary, t1, plots relatively close to the sample bi2 which is geographically close and originates from the same lateral moraine (Figure 4.1). Thus, buried ice ablation contribution cannot be ruled out for this stream.

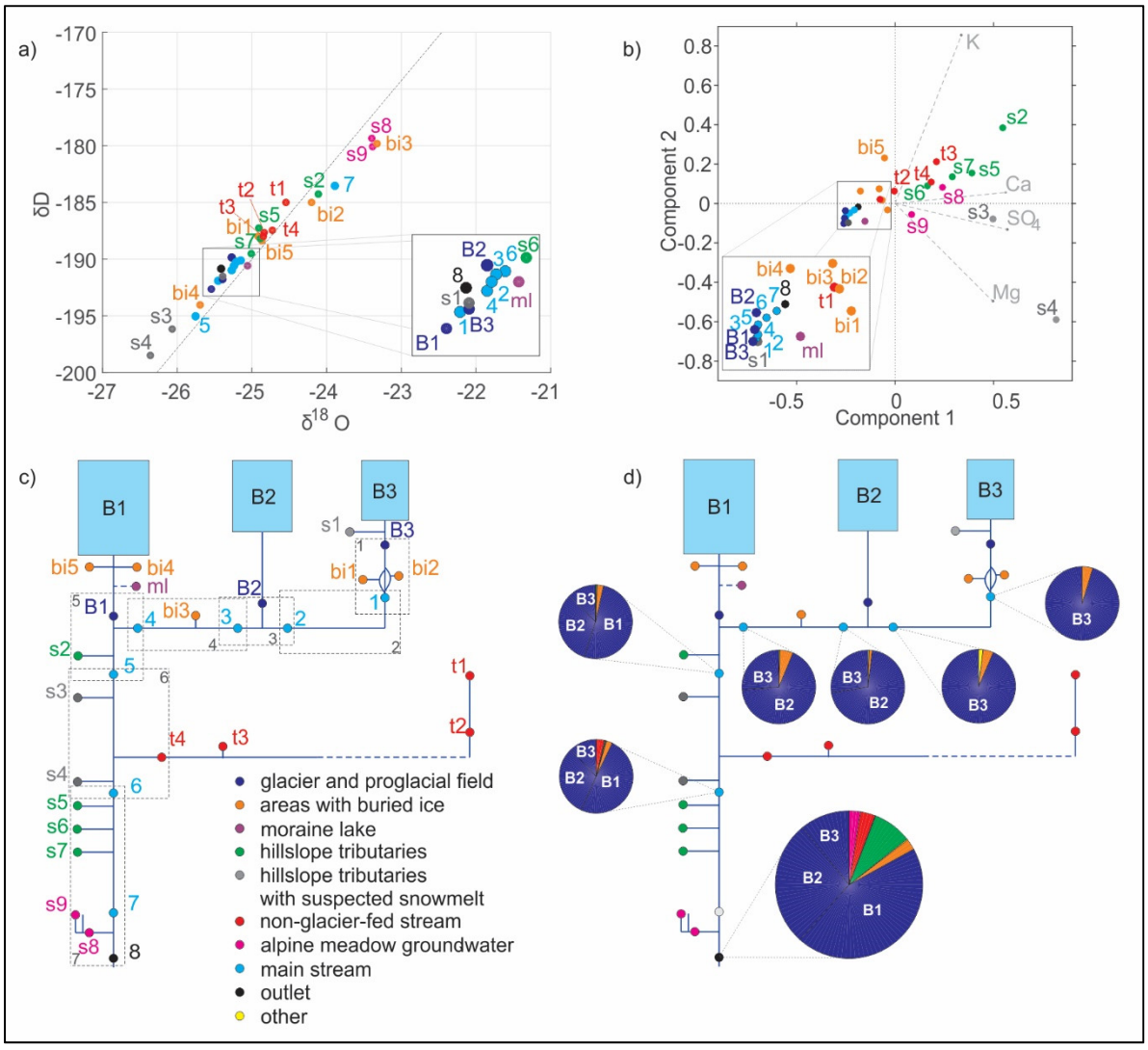

Figure 4.4 Results from the 2017 season: a) results of the stable water isotopes analysis where Global Meteoric Water Line is shown with dashed line; b) Principal Components Analysis diagram showing the results of analysis of major ions; c) HBCM representation of the B watershed where HBCM cells are shown with dashed lines; and d) results of HBCM where each pie chart presents cumulative relative contribution of end-members for each mixing point (blue circles)

4.3.3.2 Major ions analysis

Figure 4.4b shows the projection of water sample data taken during the 2017 season on the reduced space determined by PCA using K^+, Ca^{2+}, Mg^{2+} and SO_4^{2-}. Those tracers were chosen based on bivariate plots where they allowed differentiating samples based on their origins in a consistent way. PC1 is dominated by tracers Ca^{2+} and SO_4^{2-} and accounts for 0.74 of variance present in a data set; PC2 is dominated by K^+ and Mg^{2+} and accounts for 0.22 of variance; together those first two principal components account for 0.96 of variance. On the PCA diagram samples from similar assigned origins, excluding few exceptions, plot in groups (Figure 4.4b) suggesting that used tracers are selective enough for the PCA.

Samples from the main stream cluster together and plot closer to samples which represent glaciers, as opposed to with other end-members (Figure 4.4b). This pattern confirms findings based on analysis of isotopes, that glaciers are the main contributors to the stream. It can be observed that, in general, upstream samples from the main stream have hydrochemical signatures close to the one of glacier B1, and that, when moving downstream, samples gradually shift towards the hydrochemical signature of the main stream outlet (sample #8).

Samples that represent areas with buried ice plot relatively close to each other and are situated between glacier samples and samples from hillslope tributaries on the PCA diagram in most of the cases (Figure 4.4b). The proximity to samples from other categories, namely hillslope tributaries and non-glacier-fed stream, makes interpretation of bi1, bi2 and bi3 positions ambiguous. Being observed in the field to be connected to buried ice formation, bi1 and bi2 might originate from multiple sources including buried ice ablation. Similar to the results of stable water isotopes, sample bi3 is still considered as of minor buried ice constitution. Interestingly, both samples bi4 and bi5 plot in the upper left side of that group, visually further away from hillslope tributaries, as was also observed for the water isotope results. The moraine lake water sample situates in between glaciers and some buried ice samples on the PCA graph.

This supports the hypothesis of an ice melt origin of its water, which was formulated based on field observations and isotopic analyses.

Among samples from hillslope tributaries, those from the upstream hillslope tributaries (s2-4) plot closer to glacier and main stream samples than those taken from downstream hillslope tributaries (s5-7). The two sources that show the lowest heavy isotopes ratios on the $\delta^{18}O$ - $\delta^{2}H$ diagram, namely s3 and s4 (Figure 4.4a), also plot away from samples on the PCA diagram (marked in grey) confirming their difference. As a consequence, they are recategorized as being of meltwater origin for 2017, confirming the influence of the observed snow patches at their headwaters. Other hillslope tributary inputs (marked in green) occupy the upper left quarter on Figure 4.4b. Similarly to s3 and s4, sample s2, as it was the case with stable isotopes, plots away from other hillslope tributary inputs. The results of major ions analysis thus tend to confirm that those samples make a separate category.

The upstream sample from the large non-glacier fed tributary, t1, almost overlap with bi2 - a sample which is considered to be of mixed origin with buried ice ablation making one of its constituents (see Section 4.3.3.1). The proximity of those two samples was also observed on the δ18O - δ2H diagram (Figure 4.4a), suggesting common origins with possible contribution of buried ice ablation to t1. Downstream from t1, the stream hydrochemical signature (t2, t3 and t4) is closer to that of hillslope tributaries, a sign of an increased contribution from other sources (Figure 4.4b).

Samples that were taken from the alpine meadow area, s8 and s9, are not well separated from the hillslope tributaries s5, s6 and s7 but differentiate well from tributaries s3 and s4 which were identified as being fed by snow/ice meltwater.

4.3.3.3 Results of HBCM

During the 2017 season, the observed hydrological network is the most complex. Figure 4.4c shows the 2017 season configuration of cells for HBCM. After removing from the analysis the

main stream sample #7 based on the results of water stable isotopes (Section 4.3.3.1), 7 cells were distinguished. Most cells have tributary inputs as their contributors, except cell 2 that does not contain any tributaries and only has upstream and downstream mixing points.

Table 4.2 presents, for each HBCM cell taken independently (Figure 4.4c), the relative contributions of cell inflows to the cell outflow together with the standard deviation from all solution considered as equiprobable (two first columns), and the relative contribution of each cell inflow to the total watershed outflow with associated estimated error (two last columns). Table 4.2 shows that, except for cell 5, the standard deviation remains under four percent. These relatively low values suggest a good agreement among the solutions considered as equiprobable. This means that all major contributions (over 70%) are estimated with less than 4% of uncertainty, a result that can be considered as very satisfactory (Baraer, McKenzie, & Mark, 2017). Cell 5 shows much higher differences (27%) between solutions, highlighting HBCM difficulties to differentiate between B1 sample and main stream #4 sample. Consequently, other than glacier water sources upstream of #4, are associated with a higher than normal uncertainty. Table 4.2 also indicates that, while standard deviations associated with B1 and #4 relative contributions are high, the cumulative error for the total glacier outflow (i.e. combined contribution for glacier B1, B2 and B3) is relatively small. Based on field observations for the cell 5, input from hillslope tributaries is significantly smaller in comparison with the stream generated by glacier B1 or that at sampling point #4. Thus, while HBCM has troubles distinguishing between the outflows of different glaciers, results for glacier contribution as a separate category is associated with a smaller error.

Table 4.2 and Figure 4.4d present the cumulative contribution of each water source as we move downstream along cells. Overall, the contribution of three glaciers taken together to the total runoff during the 2017 season sampling period is by far larger than that of other sources (Figure 4.4d). At the watershed outlet glaciers are responsible for 82.5±4.4% of discharge production. Because the error associated to each glacier taken separately is too high for individual estimation, glacier contribution estimation was calculated as the residue from the contribution of sources other than glaciers.

Table 4.2 Relative contribution (in %) of sampled end-members to cell outflow and to watershed outlet for the season 2017. For individual cells, the standard deviation of all equiprobable solution represents the error associated to contributions standard deviation (stdev, in %)

Cell #	Sample name	At the cell outlet		At the watershed outlet	
		Contribution (%)	stdev (%)	Contribution (%)	Error (%)
1	bi1	1.05	2.1	0.12	0.25
	bi2	3.59	1.61	0.42	0.27
	B3	95.36	0.68	11.25	6.43
2	1	98.1	1.8		
	other	1.9	1.8	0.23	0.25
3	2	29.37	3.37		
	B2	70.63	3.37	28.91	16.24
4	3	95.57	1.58		
	bi3	4.43	1.58	1.90	1.26
5	4	48.08	26.88		
	B1	51.47	26.66	45.86	23.76
	s2	0.45	0.42	0.40	0.37
6	5	96.2	0.78		
	s3	0.16	0.11	0.15	0.10
	s4	0	0		
	t4	3.64	0.87	3.37	0.81
7	6	92.61	1.02		
	s8	2.52	3.74	2.52	3.74
	s7	0.78	1.69	0.78	1.69
	s6	7.58	0.22	7.58	0.22

It was possible to identify and quantify the contribution from other hydrological components to the total runoff. At the watershed outlet, sources related to areas with buried ice contribute 2.5±0.4%. However, before the main stream enters the alpine meadow, cell 7 (Figure 4.4c), contribution of areas with buried ice exceeds that of hillslope tributary inputs (Figure 4.4d). Moreover, samples that represent glaciers were taken at the downstream end of their immediate

proglacial field (Figure 4.1) and thus contributions of moraines, areas with buried ice and other hydrological components of these systems are also potentially included in glacier contribution to an unknown level. At the watershed outlet, hillslope tributaries are the second major source of water after glaciers and contribute 8.8±1.7% (Figure 4.4d). Among them, sources with potential contribution of snow meltwater, namely s3 and s4, contribute less than 0.5 %. The non-glacier-fed large tributary contributes 3.4±0.8% to the total runoff. The uncertainty associated with the alpine meadow streamlet s8 is high, and thus it cannot be stated that it is significant contributor the watershed outflow.

To account for possible subsurface contribution in cell 2, such sources as alpine meadow streamlets s8 and s9, t1, bi2, and bi3 were evaluated. Results indicate that it is possible that some other sources are contributing to the main stream since no iteration allocated 100% contribution to the upstream sample #1. However, the standard deviation is very large, and it has not been possible to determine with enough confidence which end-member is acting at that reach. The subsurface component is therefore classified as “other” in the Table 4.2.

4.3.4 Season 2016 results

4.3.4.1 Stable water isotopes analysis

End-member samples names for the 2016 season match those of the 2017 season. However, between the tributary formed by B3 and B2 glaciers and the next downstream mixing point (cell 6, Figure 4.5c) there are two hillslope tributary inputs, unlike the 2017 season where only one was identified (Figure 4.4c). As a result, for the 2016 these two inputs are called s2a and s2b.

The results of stable water isotopes analysis for the 2016 season are presented on Figure 4.5a. Samples that represent glacier runoff are more enriched in heavy water isotopes in comparison with 2017 sampling (Figure 4.4a). Similar to the 2017 season, samples taken from the main stream are located together with glacier samples in the central part of the $\delta^{18}O$ - $\delta^{2}H$ diagram

(Figure 4.5a). Samples #1 and #2 plot close to the B3 glacier sample, thus illustrating its influence on their isotopic signature. Sample #3, taken from the stream after the contribution of the B2 glacier (Figure 4.5c), seems to be influenced more by this glacier meltwater as it plots closer to B2 sample. When moving downstream, main stream samples plot closer to the sample from the B1 glacier. Unlike for the 2017, no stream samples plot outside of the field created by glacier samples and the outlet sample for this season.

Similar to the 2017 season, samples taken from areas containing buried ice do not cluster together on the $\delta^{18}O$ - $\delta^{2}H$ diagram. Two samples, bi4 and bi5, are depleted in heavy water isotopes and plot below glacier samples (Figure 4.5a). Two other samples, bi1 and bi3, plot within the cloud formed by samples from main stream and glaciers. Contrary to the 2017 season, the position of bi3 for the 2016 season suggests buried ice ablation contribution. Moraine lake sample plots close to samples bi1, bi3 and glacier samples. Positions of samples from both categories are thus compatible with primary origin assignation and imply buried ice ablation contribution.

Samples from hillslope tributaries plot together and above glacier samples on the $\delta^{18}O$ - $\delta^{2}H$ diagram. One exception is sample s1 which, similarly to 2017, is depleted in heavy water isotopes and plots below samples from glaciers and the main stream. This position can be explained by the contribution of snow meltwater observed in the field. Tributaries s3 and s4, which for the 2017 season were depleted in heavy water isotopes (Figure 4.4a), plot above glacier samples together with other hillslope tributaries for the 2016 season (Figure 4.5a). This suggests that potential contribution of snow/ice meltwater did not take place during this season sampling.

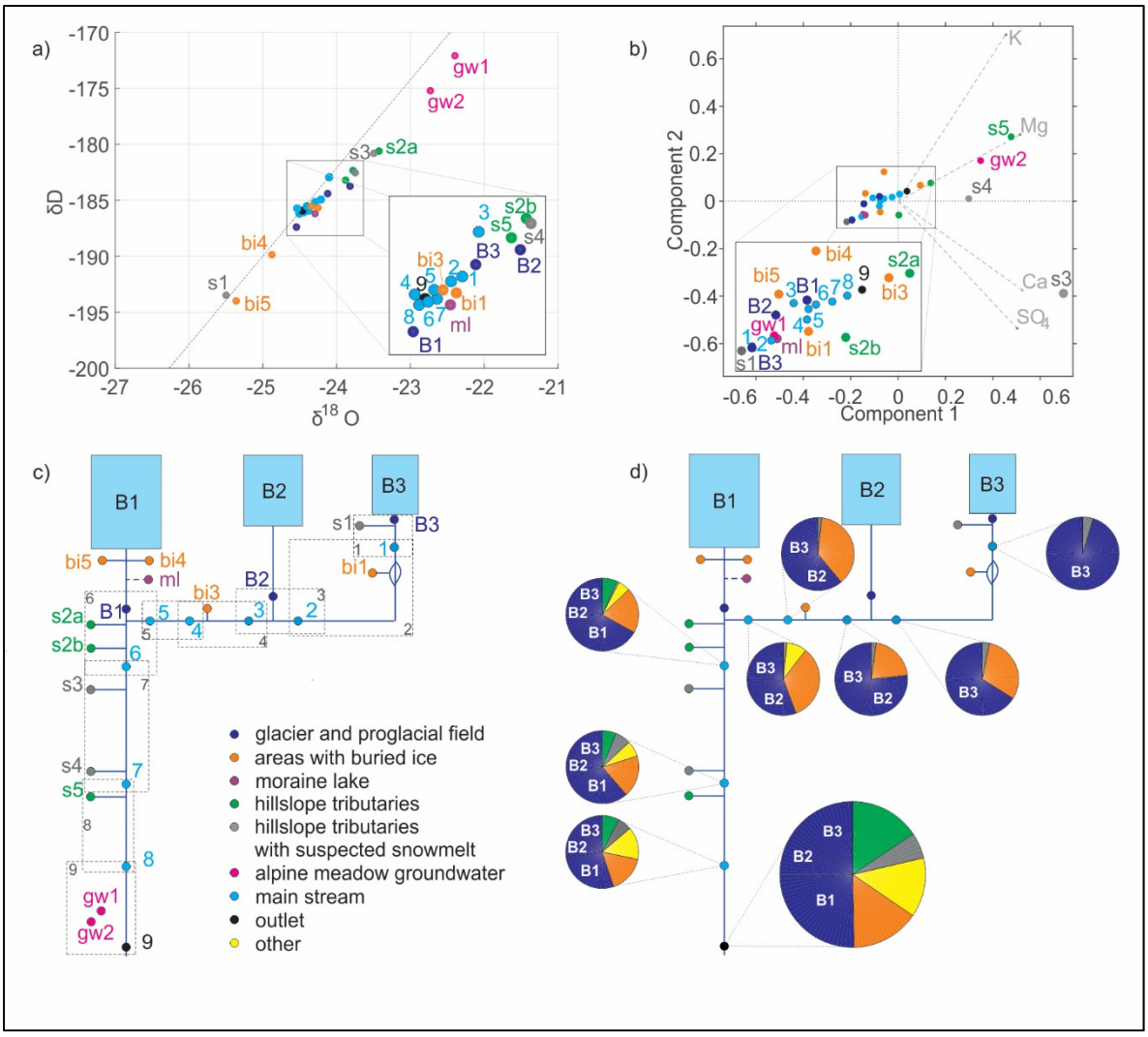

Figure 4.5 Results from the 2016 season: a) results of the stable water isotopes analysis where Global Meteoric Water Line is shown with dashed line; b) Principal Components Analysis diagram showing the results of analysis of major ions; c) HBCM representation of the B watershed where HBCM cells are shown with dashed lines and numbered; and d) results of HBCM where each pie chart presents cumulative relative contribution of end-members for each mixing point (blue circles)

Finally, two samples taken from alpine meadow groundwater wells (gw1 and gw2) are enriched in heavy isotopes and plot at the high part of the $\delta^{18}O$ - $\delta^{2}H$ diagram. This confirms groundwater recharge by lower elevation precipitation and supports the attribution of tributaries s8 and s9, observed during 2017, to the alpine meadow groundwater system.

4.3.4.2 Major ions analysis

Figure 4.5b shows the results of PCA. For the 2016 season PC1 is dominated by tracers Ca^{2+} and Mg^{2+} and accounts for 0.81 of variance present in a data set, and PC2 is dominated by K^{+} and SO_4^{2-} and accounts for 0.12 of variance; and, thus, together first two principal components account for 0.93 of variance. Unlike for the 2017 season, sources of different identified origins are not well separated on the diagram (Figure 4.5b).

Similarly to the 2017 season, samples taken from the main stream are situated together, where upstream samples tend to plot closer to samples from glaciers, and downstream samples plot closer to the sample from the main stream outlet (Figure 4.5b)

For this season most of the samples that represent areas with buried ice group together with samples that represent glaciers and main stream, and do not really form a distinct group. This confirms their origins due to buried ice ablation, assigned based on field observations. The only exception is bi3 sample which plots closer to hillslope tributary s2a.

Contrary to the 2017 results, sample from hillslope tributary of the lower part of the watershed (s3-5) plot further away from glacier and main stream samples than hillslope tributaries from the upper part (s2a and s2b). Samples s3 and s4 (shown in grey) plot away from the main cluster of samples (Figure 4.5b) as was also observed for the 2017, and thus their difference from other tributaries is confirmed.

Finally, two samples from alpine meadow groundwater wells do not group together on the PCA diagram (Figure 4.5b). One sample, gw1, clusters together with samples from the main stream and glaciers, and another sample, gw2, plots further away, closer to the hillslope tributary s5.

4.3.4.3 Results of HBCM

Configuration of the hydrological network during the 2016 season is comparable to that of 2017, although with less contributing tributaries. Large non-glacier-fed stream was not observed during this season. Moreover, there was no visible surface connection between alpine meadow groundwater system and the main stream. Figure 4.5c shows the configuration of cells for the 2016 season. Overall 9 cells were identified based on the location of surface tributaries to the main stream. Among them two cells, 5 and 9, have no tributary inputs as contributors.

Table 4.3 presents HBCM results for each cell taken individually (Figure 4.5c). First two columns show the relative contributions of cell inflows to the cell outflow together with the standard deviation based on all solution considered as equiprobable. For some cells only one HBCM solution fitted within three-fold of the lowest cumulative error and as a result no standard deviation is provided. Similar to the 2017 season results, cell where the runoff from glacier B1 joins that of glaciers B2 and B3, namely cell 6, shows much larger standard deviation in comparison with other cells - 47%. Thus, the uncertainty associated with sources upstream of the sample #5 for this season is also high at the watershed outlet. Two last columns of Table 4.3 show relative contribution of each water source to the total runoff form the watershed and associated error. Cell 8 also has relatively high uncertainty for "other" sources highlighting HBCM difficulties identifying their contribution.

Table 4.3 and Figure 4.5d present the cumulative contribution of each water source. During the 2016 season, glaciers together contribute 50±19.5% of total runoff, which is less than in the 2017. Despite higher associated uncertainty, categories such as areas with buried ice and hillslope tributaries contribute larger proportion of runoff in comparison with the 2017 sampling. Despite high uncertainty, areas with buried ice contribute 15.7±11.8%. It is worth highlighting that for the part of watershed before the B1 stream (cell 5, Figure 4.5c), areas with buried ice contribute almost one third of the runoff. Hillslope tributaries, in turn, contribute to the total watershed outflow 13.3±1.6%. Among them, sources s1, s3 and s4 contribute 5.6±1.4%.

Table 4.3 Relative contribution (in %) of sampled end-members to cell outflow and to watershed outlet for the season 2016. For individual cells, the standard deviation of all equiprobable solution represents the error associated to contributions standard deviation (stdev, in %)

Cell #	Sample name	At the cell outlet		At the watershed outlet	
		Contribution (%)	stdev (%)	Contribution (%)	Error (%)
1	s1	4.65	-*	0.7	1.28
	B3	95.35	-*	14.35	26.27
2	1	67.17	2.87		
	bi1	29.96	2.87	6.71	10.03
3	2	64.60	6.21		
	B2	29.19	6.21	10.12	10.70
4	3	80.97	-*		
	bi3	19.03	-*	8.15	6.08
5	4	91.65	-*		
	other	8.35	-*	3.90	2.06
6	5	60.38	46.73		
	B1	32.03	24.79	24.79	7.50
	s2a	6.32	4.89	4.89	0.88
	s2b	1.26	0.98	0.98	0.17
7	6	92.76	1.31		
	s3	0.73	0.43	0.61	0.01
	s4	5.16	1.35	4.31	0.53
	other	2.03	0.41	1.69	0.21
8	7	91.27	12.23		
	s5	2	4.61	1.83	0.08
	other	7.96	11.58	7.28	0.84
9	8	91.42	-*		
	other	8.58	-*	8.58	

***-** no stdev as only solution presented a residual within three-fold of the lowest cumulative error

HBCM was used to identify potential subsurface input for cells 5 and 9 where main stream samples are located relatively far from each other with no observed surface water contribution. Sources which were checked as potential subsurface components are marked in yellow on Figure 4.5d, and are referred to as “other” sources in Table 4.3. The possibility of contribution from buried ice-related source bi3, hillslope tributaries s2a, s2b, s3 and s4 was checked for cell

5. Among them, HBCM solution with the minimum error correspond to bi3 being the subsurface component. For cell 9 both s4 and s5 were checked as potential subsurface inputs, as well as water from alpine meadow groundwater wells. The results suggest that about 9% of this cell runoff is generated by subsurface components similar to s5 (referred to as "other" in Table 4.3). Alpine meadow groundwater was not detected as a subsurface input to the cell 9.

The HBCM results show that alpine meadow groundwater contributes 2±0.4% for cell 7 and 8±11.6% for cell 8. Thus, for the entire watershed groundwater potential contribution from alpine meadow is associated with high uncertainty and is included in the category "other" end-members.

4.3.5 Season 2015 results

4.3.5.1 Stable water isotopes analysis

The results of stable water isotopes analysis for the 2015 season are presented on Figure 4.6a. Similar to both 2016 and 2017 seasons, samples from the main stream plot together with the samples that represent glaciers (Figure 4.6a). Only one stream sample, #6, plots slightly lower than the cloud created by glacier and stream samples. During the 2015 season only one input from areas with buried ice was observed from right-side ice-cored moraine, bi4. Unlike seasons 2017 and 2016, it is more enriched in heavy isotopes and plots together with samples from glaciers (Figure 4.6a), which confirms its origins related to buried ice ablation. During this season the sample from the moraine lake has different isotopic signature in comparison with other two seasons. It is enriched in heavy water isotopes and plots away from the GMWL. This can be caused by fractionation due to evaporation since abnormally warm air temperatures were observed during sampling. Sample from hillslope tributary s5 is enriched in heavy water isotopes and plot at the top of $\delta^{18}O$ - $\delta^{2}H$ diagram (Figure 4.6a). No other hillslope tributary inputs were observed during this season. Finally, like the other seasons, sample taken from the alpine meadow groundwater is enriched in heavy water isotopes.

4.3.5.2 Major ions analysis

Figure 4.6b presents the results of PCA for the 2015 season. First two principal components for the 2015 season account for 0.95 of variance. PC1 is dominated by tracers Ca^{2+} and SO_4^{2-} and accounts for 0.80 of variance present in a data set; PC2 is dominated by K^+ and Mg^{2+} and accounts for 0.15 of variance.

Similar to the other two seasons, samples from the main stream cluster together with samples that represent glaciers (Figure 4.6b). Upstream samples plot closer to glaciers B2 and B3, and downstream samples shift towards B1 glacier and the sample from the main stream outlet.

Based on the PCA diagram it is not possible to confirm the primary origin assignation to sample bi4 since it plots away from glacier samples (Figure 4.6). Moraine lake sample, however, plots relatively close. Thus, buried ice ablation contribution to lake water is possible. Observed difference between the signature of bi4 and that of glaciers can be potentially explained by evaporation-driven increase in solute concentrations in lake water.

The only observed hillslope tributary, s5, plots away from other samples, similarly to the 2016 season, and so does the sample from alpine meadow groundwater (Figure 4.6). Thus, these two samples are well separated from samples from other categories.

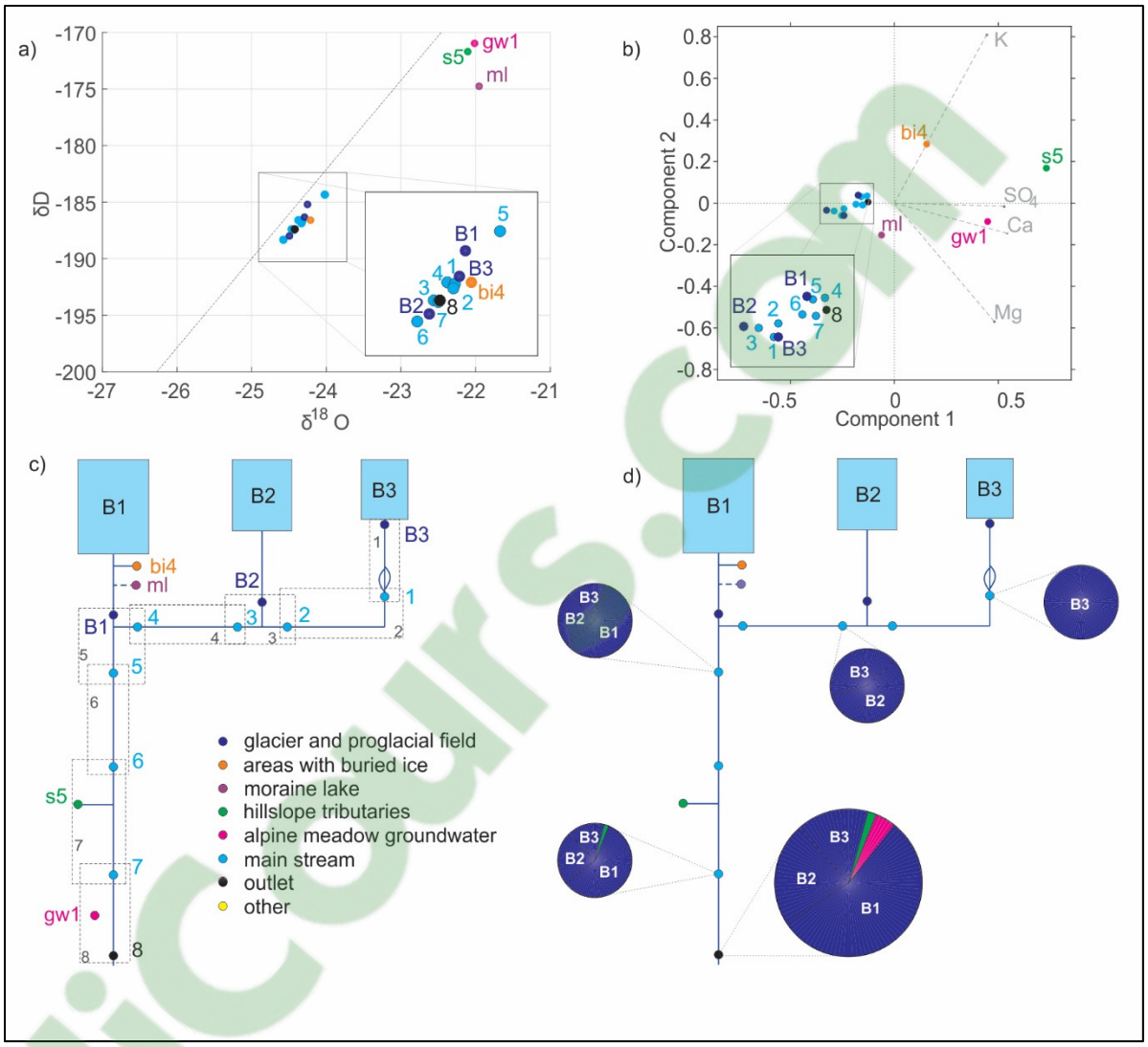

Figure 4.6 Results from the 2015 season: a) results of the stable water isotopes analysis where Global Meteoric Water Line is shown with dashed line; b) Principal Components Analysis diagram showing the results of analysis of major ions; c) HBCM representation of the B watershed where HBCM cells are shown with dashed lines and numbered; and d) results of HBCM where each pie chart presents cumulative relative contribution of end-members for each mixing point (blue circles)

4.3.5.3 Results of HBCM

Field observations report very few surface inputs to the main stream during the 2015 season. For this season, 8 cells were defined in the watershed (Figure 4.6c). Due to the very limited

number of tributaries, 5 cells among them had no other surface inflows apart from the upstream mixing points.

Table 4.4 Relative contribution (in %) of sampled end-members to cell outflow and to watershed outlet for the season 2015. For individual cells, the standard deviation of all equiprobable solution represents the error associated to contributions standard deviation (stdev, in %)

Cell #	Sample name	At the cell outlet		At the watershed outlet	
		Contribution (%)	stdev (%)	Contribution (%)	Error (%)
1	B3	100	-*	16.77	1.08
	other	0	-*		
2	1	100	-*	16.77	0.76
	other	0	-*		
3	2	42.55	2.96	16.77	0.87
	B2	57.45	2.96	22.65	0.87
4	3	100	-*		
	other	0	-*		
5	4	41.64	1.51	39.43	
	B1	58.36	1.51	55.25	0.89
6	5	100	-*	94.67	
	other	0	-*		
7	6	99.53	0.41		
	s5	0.47	0.41	0.45	0.00
8	8	95.12	-*		
	Gw1	4.88	-*	4.88	0.00

***-** no stdev as only solution presented a residual within three-fold of the lowest cumulative error

Table 4.4 presents the relative contributions of cell inflows to the each cell outflow. Similar to the 2016 season sampling, for the 2015 season some cells had only one HBCM solution that fitted within three-fold of the lowest cumulative error, therefore no standard deviation is provided for these cells (Table 4.4). Problematic cell 8, identified when performing back-calculation using Mg^{2+} (Figure 4.3), has only one solution when multiple tracers are used and thus its results have low uncertainty. Overall, as a result of low number of equiprobable solutions, standard deviations for all water sources are below three percent, and, unlike other

two seasons, cell where flow from glaciers B2 and B3 join the B1 glacier outflow has very low standard deviation. Thus, HBCM results are considered as very satisfactory.

During this sampling period most of the discharge at the outlet, 94.7±1.7%, is produced by the three glaciers (Figure 4.6d and Table 4.4). Other groups of sources contributing to the runoff generation from this watershed are alpine meadow groundwater (4.9±0.2%) and hillslope tributary (<1%). For this season no subsurface input was detected by HBCM.

4.4 Discussion

4.4.1 Is there any significant contribution from sources other than glaciers in the study watershed?

Results presented in this study provide a relatively clear answer to the first specific research question. Even for the 2015 sampling, the particularly dry and warm year under the influence of "Blob", HBCM results show sources not associated with glaciers contributing at least 5.3% (5.4-0.1%) to the watershed outflow. In 2016, this minimum level of non-glacier-related sources reached its maximum for the study at 37.6% (49.6-12%). In 2017, this minimal contribution was of 13.1% (17.5-4.4%). Considering that the study captures contributions in diverse meteorological and environmental conditions, it can be stated that the result show that sources other than glacier-related cannot be considered as negligible in such highly glacierized subarctic catchment.

4.4.2 Identified hydrological components and their contribution to watershed outflow

4.4.2.1 Glacier melt

In highly glacierized watersheds, where glacierized area is approximately 40% or more, contribution of glacier to runoff is sometimes assumed (e.g., Huss, 2011; Kaser et al., 2010) or measured (e.g., Brown et al., 2006; Racoviteanu et al., 2013) to be the dominant component of

runoff during the ablation season. The results of this study for the 2017 sampling period are consistent with those observations and show that 82.5±4.4% of watershed discharge is generated by the runoff from three glaciers. Importantly, this number includes water generated within the immediate proglacial field of studied glaciers with unknown input from ice-cored side moraines for the B1 sample and snowmelt-fed tributary for the sample B3. This means that the contribution by the glacier reported in the study is probably slightly overestimated. As seen above, the relative contribution of the glaciers shows high variability depending on the field conditions. When sampled during abnormally hot temperatures, as under the influence of the 2015 "Blob", proportion of glacier melt in total runoff increases and reaches 94.7±1.7%. Lower albedo due to darker bare glacier surface, observed during that sampling season, probably enhanced glacier meltwater production. During the 2016 sampling, in conditions when glacier runoff is partly shut down due to high quantities of snow on glacier surfaces, contribution from glaciers decreases to 50±19.5%.

4.4.2.2 Areas with buried ice

Buried ice end-members corresponds to areas with buried ice as identified based on field observations. Even though some samples showed consistencies on the PCA diagram, isotopic and hydrochemical signatures for this category are characterized by variability between the samples and between the years. In particular, on the $\delta^{18}O$ - $\delta^{2}H$ diagram samples from areas with buried ice do not cluster together and their signature varies between the sampling seasons (Figure 4.4a, 4.5a and 4.6a). Those variations can be caused by different reasons. Isotopic signature of areas containing buried ice depends on the elevation at which parent precipitation accumulated and at which the ice was formed as well as on ice genesis (i.e. buried glacier ice or buried permanents snowbanks; Johnson, 1978). Due to isotopic fractionation, ice in contact with water infiltrating through debris cover may lose lighter isotopes first and become enriched in heavy $\delta^{18}O$ isotopes (Williams et al., 2006). Even if those samples were hypothesized to be fed by buried ice ablation based on field observations, the meltwater flowed to the main stream through the debris cover most of the time. Thus, mixing with water from other origin most probably occurred before the meltwater from buried ice reaches the main stream, causing

isotopic and hydrochemical signature variability. The above-mentioned phenomena suggest that the presence of buried ice in the area of sampling does not guarantee that sampled water is fed by buried ice ablation. Therefore, when interpreting relative contribution calculated by HBCM for this category, the exact share of the buried ice ablation cannot be determined, and instead this category represents both buried ice ablation as well as storage in debris cover. Despite those limits, meltwater origin of streamlets flowing from buried ice areas have been supported, on different occasions, by their isotopic and hydrochemical signatures. This was the case, for example, for samples bi1, bi4 and bi5 of the 2017 campaign. Those samples by themselves establish a link between the buried ice and the stream flow and therefore suggest that buried ice contribution should require more attention in future studies.

4.4.2.3 Hillslope tributaries

During the three field campaigns several hillslope tributaries were observed to contribute to the main stream in the B watershed. The amount of hillslope tributary inputs was almost similar in 2017 and 2016 at around 8% but was barely detectable in 2015. Those tributaries are characterized by the absence of glacier and of visible buried ice in their drainage area. Some hillslope tributary samples from the 2017 sampling season (samples s3 and s4, Figure 4.4a) were depleted in heavy isotopes and plotted separately from the other members of this group. This can be explained by the fact that a snow patch is located at the head of the streamlet, producing meltwater from snow that reached the ground at an elevation higher than the catchment average. The contribution of these two potentially snowmelt-fed tributaries was minor according to the HBCM results (less than 0.5% of the total runoff during the 2017 sampling). In the 2016 two hillslope tributaries sampled in the same area cluster together with other hillslope tributaries suggesting that snowpack remains at the headwater of those hillslope tributaries that year were not supplying significant amount of water.

The large non-glacier-fed stream, which was only observed in the 2017, contributed 3.4±0.8% of the runoff. The stream starts from a talus slope and disappears under debris between samples t2 and t3. Both this tributary and the small stream sampled as bi2 originate from the same

moraine complex (Figure 4.1), although bi2 emerges at lower elevation. For the bi2 sample, some buried ice was detected just above the source, whereas on the other side of the moraine there were no signs of buried ice. Although two upstream samples from this large tributary, namely t1 and t2, cluster together with samples that represent buried ice on the PCA diagram (Figure 4.4b), they do plot together with bi2 on the $\delta^{18}O$ - $\delta^{2}H$ diagram (Figure 4.4a). This suggests that the hydrochemical signature of those samples does not depend on the presence of buried ice but on the nature of the debris that compose the talus slope instead.

4.4.2.4 Alpine meadow groundwater

Samples from groundwater wells within alpine meadow were enriched in heavy water isotopes in 2015 and 2016 (Figure 4.5a and 4.6a) confirming the low elevation origin of the precipitation that fed them. Streamlets s8 and s9 sampled in 2017 in the same area showed similar characteristics, suggesting they were also fed by the alpine meadow groundwater system. Water sources from the alpine meadow have been shown to contribute to the main stream in a significant way both in 2015 and 2017. In 2016, the difficulties met by HBCM in differentiating between water sources lead to contribution from the alpine meadow groundwater system remaining undetermined.

4.4.3 Variation of runoff components contribution under different meteorological conditions

The three periods of time when sampling took place represent a wide array of meteorological and environmental variability between ablation seasons. The 2015 sampling season was abnormally warm and dry due to the influence of the “Blob” (Blunden et al., 2016). A three-day snowfall took place a week prior to the 2016 sampling, and although at the moment of sampling the snow cover on the ground had been gone, it still remained on the glacier surfaces. Field observations suggested that this fresh snow strongly reduced glacier runoff as compared with the other sampling years. Finally, the 2017 sampling season illustrates conditions where the number of tributary inputs to the main stream is high.

Even if none of those conditions included surface runoff related to intense liquid precipitation, they produced strongly contrasting hydrological responses at the B watershed. For instance, the glaciers' relative contribution varied from 94.5±1.5% to 50±19.5% over the study period. Those results depict this highly glacierized catchment as hydrologically dynamic and responsive to variation in meteorological and environmental conditions. This underlines the necessity to further study the processes driving the contribution variations from different end-members as those have been shown to be non-negligible.

4.4.4 Method limitations

The synoptic sampling approach, necessary for HBCM, only provides a snapshot of the hydrological system at the sampling time. Therefore, this study does not allow making general conclusions about the behavior of the system over the entire ablation seasons.

The lack of a gauging station at the outlet of the studied watershed has not allowed transforming relative discharge in the absolute discharge values for all contributing end-members. The specific contribution calculation that would have resulted from those discharge measurements would have provided valuable insight for further understanding of hydrological dynamics at the scale of the watershed.

Another limitation of the applied method is the uncertainty associated with HBCM. The method showed to be vulnerable to high uncertainty at 3 cells out of a total of 24 cells for the complete study. The high uncertainties at these cells most likely stem from sampling the mixing points too close to the point where tributaries join and thus not giving enough time for waters to be well mixed. This was confirmed by back-calculation of Mg^{2+} concentrations that showed a slight deviation from expected 1:1 line for several cells. However, for a problematic cell indicated based on back-calculations results, HBCM solutions converged when multiple tracers were applied.

Finally, the method presents difficulties in identifying the origins of subsurface inputs. Even though potential subsurface inflow using isotopic and hydrochemical signatures of sampled end-members were used, it is probable that some subsurface inputs were missed in the present study.

4.5 Conclusions

This study aimed to disentangle the importance of all identifiable hydrological components to the total runoff of a small highly glacierized watershed in the subarctic Yukon under various meteorological and environmental conditions. These conditions included abnormally warm and dry weather under the influence of the "Blob" - the marine heat wave that endured between 2013 and 2016 in the Northeastern Pacific. The drainage network in this watershed arises from three glaciers and is connected to numerous hydrological components. During three field campaigns in beginning of July 2015, end of June 2016 and beginning of August 2017, all end-members contributing to the total runoff were sampled and their contribution was quantified by means of hydrochemical basin characterization method (Baraer et al., 2009, 2015).

The results of this study show that meltwater from three glaciers is the main contributor to the watershed outlet. However, this contribution varies depending on meteorological and environmental conditions. Over the three sampling campaigns the glacier contribution ranged between 94.5±1.5% under the influence of "Blob" to 50±19.5% when glacier runoff is reduced due to the effect of snow cover. The remaining fraction of runoff consists of outflow from areas with buried ice, hillslope tributary inputs, discharge from non-glacier fed stream and input from alpine meadow groundwater.

This study shows that, despite the important glacier cover (36.6%) the watershed mainstream is fed by other sources that, taken together can represent between 5.4±0.1% and 49.6±12% of the outflows. Even if the method had difficulties differentiating between contributing sources, alpine meadow groundwater, hillslope tributaries and buried ice areas have been shown to be among those contributors. Overall, this study illustrates how complex and dynamic the

hydrology of such subarctic glacierized system is and invites for further study on the topic. Considering high vulnerability of subarctic glacierized watersheds to climate change, focusing on other than glacier hydrological components should help to account in a future for the complexity of those watersheds, which has been so far underestimated in climate impact studies.

4.6 Acknowledgments

This research is supported by the Geochemistry and Geodynamics Research Centre (GEOTOP) of Quebec, the Natural Science and Engineering Research Council (NSERC) of Canada, *École de technologie supèrieure*, a constituent of the *Université de Quebec* network, and Polar Continental Shelf Program. We want to acknowledge that this research was conducted on the traditional territory of Kluane First Nation, and we are thankful for their support. We are also grateful for help to Parks Canada. Finally, we acknowledge help from Katherine Rodriguez and Michael Dubois in samples processing.

CHAPTER 5

PROGLACIAL ICINGS AS RECORDS OF WINTER HYDROLOGICAL PROCESSES

A. Chesnokova, M. Baraër, and E. Bouchard

Department of Construction Engineering, École de technologie supérieure,
1100 Notre-Dame West, Montreal, Quebec, Canada H3C 1K3

Paper submitted to the *Cryosphere*, February 2020

Abstract

The ongoing warming of the arctic-subarctic region is affecting hydrological processes, causing deep changes such as a ubiquitous increase in river winter discharges. However, the exact mechanisms leading to that increase remain poorly understood, mainly due to the lack of observations and field measurements in those cold and remote environments. This is the case for glacierized catchments that host many climate-sensitive water sources, including icings. Icings form from hydrological sources that remain active during the winter and thus can be seen as chroniclers of winter hydrological processes in remote subarctic watersheds. At the end of the cold season, they contain valuable information that can be used to better understand cold season hydrological processes. The present study focuses on extracting this information in order to provide insights into sources related to icing formation and winter runoff generation in two subarctic glacierized catchments in the Upper Duke, St. Elias Mountains, Yukon. To extract information from icings, we apply a multi-technique approach that includes (a) time lapse imagery analysis in conjunction with air temperature time series, (b) stable water isotope analysis, (c) water hydrochemical analysis, and (d) analysis of solid particles. For icings within both the proglacial field and the alpine meadow, it was possible to identify several groups of hydrological sources that remain active during the winter. The results confirm that glaciers of all sizes most likely contribute to proglacial icing formation as well as winter runoff. Other detected sources include hillslope tributaries and water stored in the suprapermafrost layer within the alpine meadow. A literature-based analysis of the possible contribution mechanisms

from the icings' parent waters allows us to propose that glaciers, directly or through the ground, the suprapermafrost layer, and non-glacier-related groundwater (via tributaries) could contribute to the observed regional increase in winter discharge.

Key Points

1. It is possible to identify sources that remain active during the winter season by studying icings in the early stage of the melt season.
2. In the headwaters of subarctic glacierized catchments, sources of different kinds stay active during the winter.
3. Icings within subarctic proglacial field are not only fed by discharge from poly-thermal glaciers.

Keywords: icings, aufeis; winter baseflow; subarctic; glacierized catchment; Yukon

5.1 Introduction

Increases in winter baseflow in response to climatic changes have been observed in many arctic and subarctic rivers in Eurasia (Danilovich, Zhuravlev, Kurochkina, & Groisman, 2019; Lammers, Shiklomanov, Vörösmarty, Fekete, & Peterson, 2001; Rennermalm, Wood, & Troy, 2010; Smith et al., 2007; Qin, Ding, & Han, 2020; Yang et al., 2002) and North America (Brabets & Walvoord, 2009; Chesnokova, Baraër, Robillard, & Huh, 2020; Jacques et al., 2009; Rennermalm et al., 2010; Walvoord & Striegl, 2007; Wang, 2019; Woo & Thorne, 2014). The hypotheses that have been proposed to explain this positive trend can be separated into two groups: (a) increased water storage capacity of aquifers and (b) an increase in water input to aquifers (Liljedahl et al., 2016). An increase in aquifer storage capacity can result from delayed soil freeze-up (e.g., Yang et al., 2002) and/or from increased suprapermafrost layer thickness (e.g., Ge et al., 2011; Toohey et al., 2016). Those phenomena lead to an increased amount of water, which is accumulated in the aquifer during summer, which can be released during the freezing season. The term "suprapermafrost layer," as suggested by Connon, Devoie, Hayashi, Veness, and Quinton, (2018), describes here the layer on top of permafrost

that includes both the active layer and suprapermafrost taliks, if any. Increases in the hydrological components such as precipitation (e.g., Neal, Todd Walter, & Coffeen, 2002), permafrost thaw (e.g., St. Jacques et al., 2009), and glacier melt (e.g., Liljedahl et al., 2016) can lead to an increase of water input into the aquifer and hence to increased winter discharge.

Although the aforementioned hypotheses have been accepted as the potential drivers of winter discharge increases the exact hydrological components responsible for this trend remain difficult to identify. For example, the role of the permafrost thaw in those changes is ambiguous. When recalculating the discharge increase into equivalent ground ice thaw from permafrost, McClelland, Holmes, Peterson, and Stieglitz (2004) obtained meltwater volumes from permafrost thaw that exceeded observed discharge changes. Moreover, decreases in winter flows were observed in areas where increasing permafrost thaw has been observed (Lyon et al., 2009). Finally, an upward trend in winter discharge is observed in both permafrost- and non-permafrost-underlined areas (McClelland et al., 2004; Smith et al., 2007), as well as in both glacierized and non-glacierized watersheds (Chesnokova, Baraër, Robillard, et al., 2020), making it impossible to attribute the trend to a single phenomenon. Those difficulties in identifying the features that originated the increase in winter discharge are not limited to storage change hypotheses. Indeed, due to data scarcity in arctic-subarctic regions, verifying the influence of precipitation changes on winter runoff also represents a major challenge (Smith et al., 2007; Woo & Thorne, 2014).

In the present study, we propose compensating for the scarcity of direct observations of winter hydrological processes in arctic-subarctic glacierized catchments by extracting information recorded in proglacial icings. Icing (“aufeis” in German, or “naled” in Russian) is a mass of ice formed during the winter when surface water or groundwater floods onto existing ice surfaces or snow cover and freezes to form an additional ice layer (Carey, 1973; Kane, 1981). Icings can redistribute runoff in the course of a year by releasing, during the ablation season, the water stored during the winter (Pavelsky & Zarnetske, 2017). Their contribution to summer runoff can be important for unglaciated watersheds in northern regions and account for a significant (up to 30%) portion of annual baseflow (Kane & Slaughter, 1973; Reedyk, Woo, &

Prowse, 1995; Yoshikawa et al., 2007). In glacierized watersheds, icings are known to be fed by both polythermal (Bukowska-jania & Szafraniec, 2005; Hambrey, 1984; Sobota, 2016; Stachnik et al., 2016; Wadham et al., 2000; Yde et al., 2012) and cold-based glacier meltwater (Bælum & Benn, 2011; Hodgkins et al., 2004; Hodgkins et al., 1998; Naegeli et al., 2014). In addition, such features as glacier-dammed lakes (Moorman, 2003; Wainstein et al., 2014; Yde & Knudsen, 2005) as well as buried ice formations within proglacial fields (Gokhman, 1987) can contribute to icing growth. In permafrost-underlined regions, there are different pathways that water can take to eventually flow to the surface to form an icing. Both supra- (French & Heginbottom, 1983; Pollard, 2005) and subpermafrost water (Hu & Pollard, 1997; Kane & Slaughter, 1973; Kane, 1981; Pollard, 2005; Yoshikawa et al., 2007) has been shown to contribute to icing formation. Also, as in glacierized watersheds, discharge from lakes via taliks can participate in icing growth (Veiette & Thomas, 1979). Even if their thickness can be increased by winter precipitation (Hodgkins et al., 2004; Wadham et al., 2000), icings are formed by water sources that are mainly active during the winter and thus cumulate water released within the watershed during that season. Hence, icings contain information related to the hydrological sources that contribute to winter baseflow.

Water sources that produce proglacial icings at least partly make winter runoff as well. Learning from the hydrological records kept in icings can therefore provide new insights for delving deeper into the phenomenon of arctic-subarctic winter runoff increase. In light of the above, the main objective of this study is to identify water sources that remain active during the winter by tracing back those that contribute to the formation of icings in the headwaters of arctic-subarctic glacierized watersheds. The Upper Duke River valley, Yukon, Canada, is used as the study site. Numerous icings are observed almost every year in the Upper Duke watershed. In addition, the watershed hosts complex hydrological systems made of numerous hydrological components such as glaciers, buried ice, talus slope and hillslope tributaries, snow cover, and permafrost which represent potential water sources. The objective is achieved by answering the three following research questions: (1) Is glacier runoff the most important water contributor to winter baseflow and icing formation? (2) Does water from the suprapermafrost layer contribute to icing formation and hence to winter baseflow? And (3) are there other

hydrological sources that contribute substantially to icing formation? Due to the hydrological complexity of the subarctic glacierized watershed, a multi-technique approach was chosen to study the genesis of icings. This approach consisted of (a) analyzing images from time lapse cameras (TLC) that were collected during the two winter seasons of 2015-2016 and 2016-2017, (b) comparing icings' hydrochemical and isotopic signatures to those of potential hydrological sources, and (c) analyzing solid samples taken on icing remains. This multi-technique approach was applied in two sub-catchments of the watershed to explore the complexity of hydrological systems of different sizes.

5.2 Methods

5.2.1 Study site

The two studied catchments are located in the headwaters of the Duke River (Shar Ndu Chu) in the St. Elias Mountains, Yukon. The climate in this region is continental, with a mean annual air temperature varying between −2 and −6°C and a mean annual total precipitation between 250 and 400 mm (Wahl et al., 1987). The glaciers in the region are not in equilibrium with current climatic settings and experience highly negative mass balance (Arendt et al., 2002; Barrand & Sharp, 2010). Large glaciers in the neighboring area are polythermal (Flowers et al., 2014), whereas smaller glaciers are potentially cold-based (Wilson et al., 2013). Many glaciers in the area are surging (Clarke, Schmok, Simon, Ommanney, & Collins, 1986). As a result of glacier retreat and surging events, such hydrological features as buried ice and ice-cored moraines are present within proglacial fields of glaciers in the region (Johnson, 1971; 1978; 1986; 1992). The study region is located within a zone of discontinuous permafrost (Brown et al., 2002). However, at elevations above 1500 m above sea level (a.s.l.), local permafrost coverage can be extensive or even continuous (Harris, 1987). Most of the permafrost monitoring sites in Northern America exhibit air temperature increase-driven transformations. Indeed, permafrost warming and active layer deepening are reported in the arctic (Hinzman et al., 2005) and subarctic (Smith et al., 2010; Smith et al., 2005; Tarnocai et al., 2004).

In the headwaters of the Duke River watershed we consider two catchments. The first one is the Upper Duke watershed (Figure 5.1a). The elevation within this first watershed ranges from 1598 to 3042 m a.s.l. Its area is 69.1 km^2, and it is 39.7%. The main glacier, Duke glacier, is known to be surging (Clarke et al., 1986). The second watershed was unnamed and will be referred to as watershed B (Figure 5.1a). Its area is 8.7 km^2, 36.6% of its area is glacierized, and its elevation ranges from 1674 to 2906 m a.s.l. The main glacier in this watershed will be also called B.

Within the Upper Duke River watershed, two different bedrock group formations are observed (Colpron, Israel, Murphy, Pigage, & Moynihan, 2016). The valley's bottom and its northern and northeastern slopes are made of sedimentary and volcanic rock formations from the Cambrian-Ordovician. They are characterized by greywacke, conglomerates, and volcanic breccia rich in sandstone, amphibolite, and greenstone, with traces of argillite and phyllite. The areas underlying the Duke glacier and glaciers in the watershed B (south and southwestern side of the valley) are sedimentary rock formations dating from the Devonian-Triassic and are characterized by quartz-rich, micaceous, calcareous siltstone to sandstone with traces of argillite, phyllite, limestone, gypsum, and anhydrite (Colpron et al., 2016). Moreover, fieldwork observations have shown that both bedrock and moraine sediments are rich in iron, as indicated by the frequent rust color on the rocks and by the presence of pyrite in the debris.

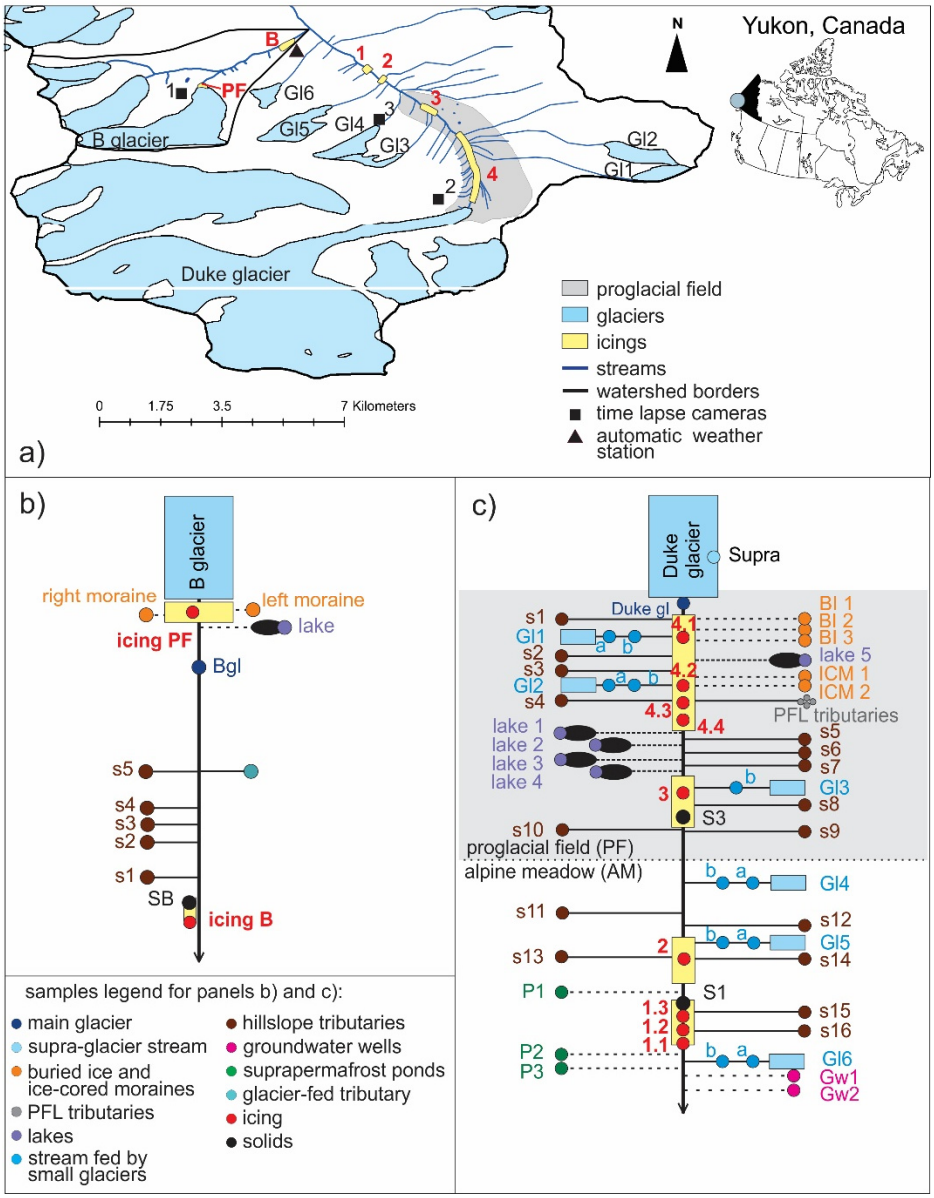

Figure 5.1 Study watersheds and sampling plans. Panel (a) shows Upper Duke River watershed and watershed B borders and the locations of time lapse cameras and the automatic weather station. Panels (b) and (c) present schematic maps of B and Duke watersheds, respectively, with relative locations of sampling points. Dashed lines show sources that are not directly connected above the surface with the main stream. In panel (c), for streams fed by small glaciers, "a" identifies samples taken close to the glacier tongue, and "b," sample taken close to the confluence with the Duke River

5.2.2 Analysis of time lapse images

The goal of using TLC images was to capture icing formation events and to visually locate sources that are contributing to icings' growth throughout the winter season. Three TLCs were installed at the study site during summer 2015 (Figure 5.1a). TLC1 was installed above the Glacier B's tongue and pointed toward the Glacier B's proglacial field, proglacial icing (Icing PF), and the right-side moraines of the Glacier B. TLC2 was installed in the Duke watershed just above the Duke Glacier's margin and pointed toward the Duke Glacier's proglacial field and the Duke River, where Icing 4 had formed. TLC3 was placed just above the proglacial field – alpine meadow border, and it pointed toward the Duke glacier's tongue and the upper part of its proglacial field, thus featuring Icings 3 and 4. All cameras were set to capture four visible color images per day at 8h, 11h, 13h, and 16h with a 72 dpi.

TLC analysis was performed visually and consisted of spotting the timing and the extent of two different types of hydrological activity: flooding events and snowfalls. Flooding events are associated with surface water or groundwater flow over the existing ice/snow surfaces. They can be detected by observing either a darkening/bluing of the white ice/snow pixels due to increased water content (e.g., Figure 5.2 b-d) or a sudden appearance of bright pixels due to the formation of a reflecting layer on top of a previously low-reflecting one (e.g., Figures 5.3b and f). Major snowfall events erase traces of flooding on images by whitening the scene, which facilitates detection of subsequent floods. On the other hand, snowfalls occasionally cover the lenses of the cameras, making observation impossible for several days. For each flooding event detected in images, possible water sources were listed based on the flooding location. The timeline of the detected flooding events was then superimposed on the air temperature time series. Temperature time series were obtained from an automatic weather station installed on the right shore of the Duke River upstream from the confluence with the Stream B (Figure 5.1a). It measured mean hourly air temperatures for the period 11 of July 2015 – 24 of June 2017 at a height of 1.5 m above the ground in a shielded case.

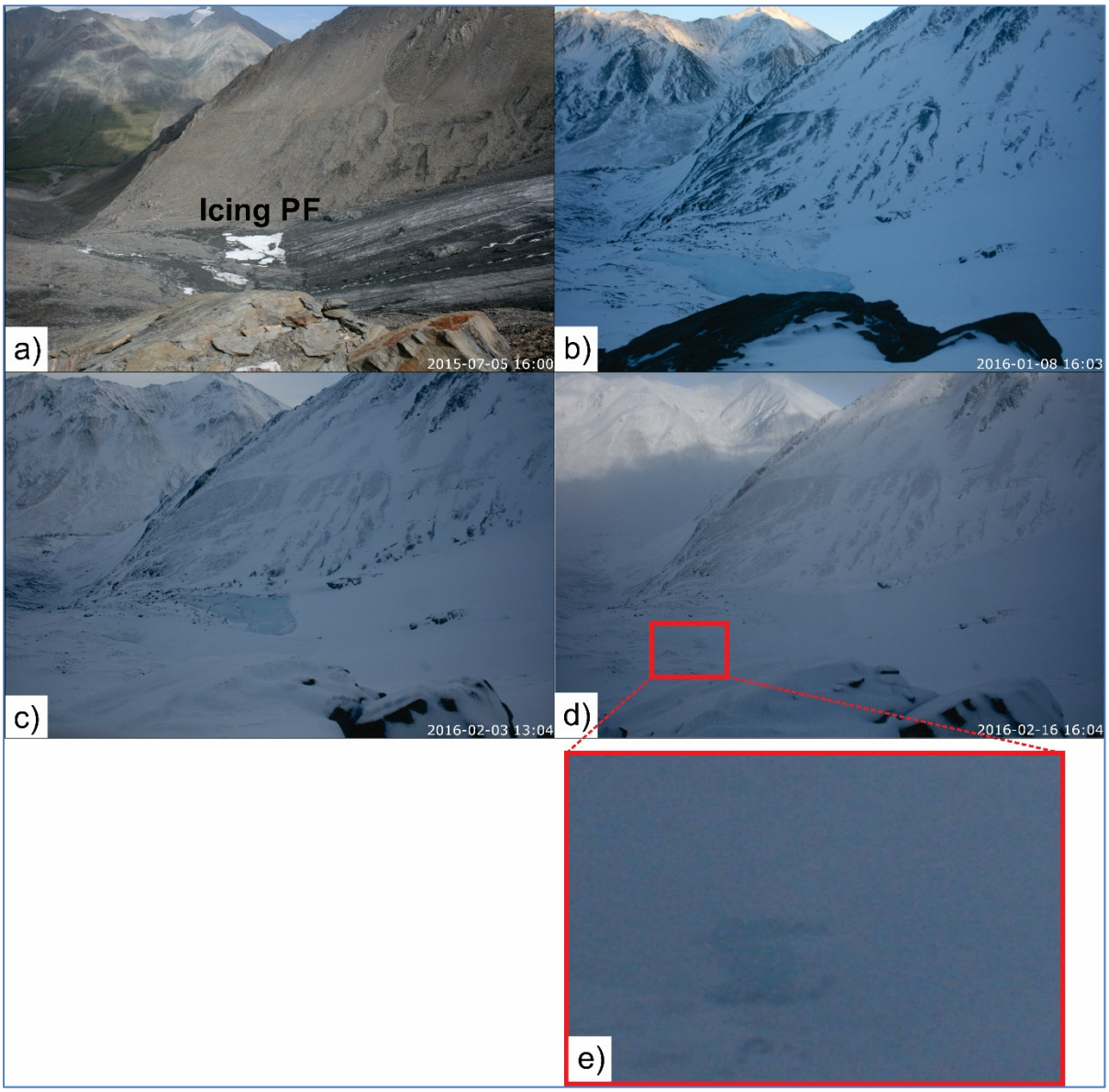

Figure 5.2 Glacier B tongue and hydrological activities visible in the TLC1 images. Panel (a) shows Glacier B's tongue, proglacial field, proglacial icing and the right side of the valley at the camera installation. Panels (b) and c) illustrate flooding events on the left (b) and the right (c) side of the proglacial field; panels (d) and (e) show flooding occurring on the left bottom side of the proglacial field

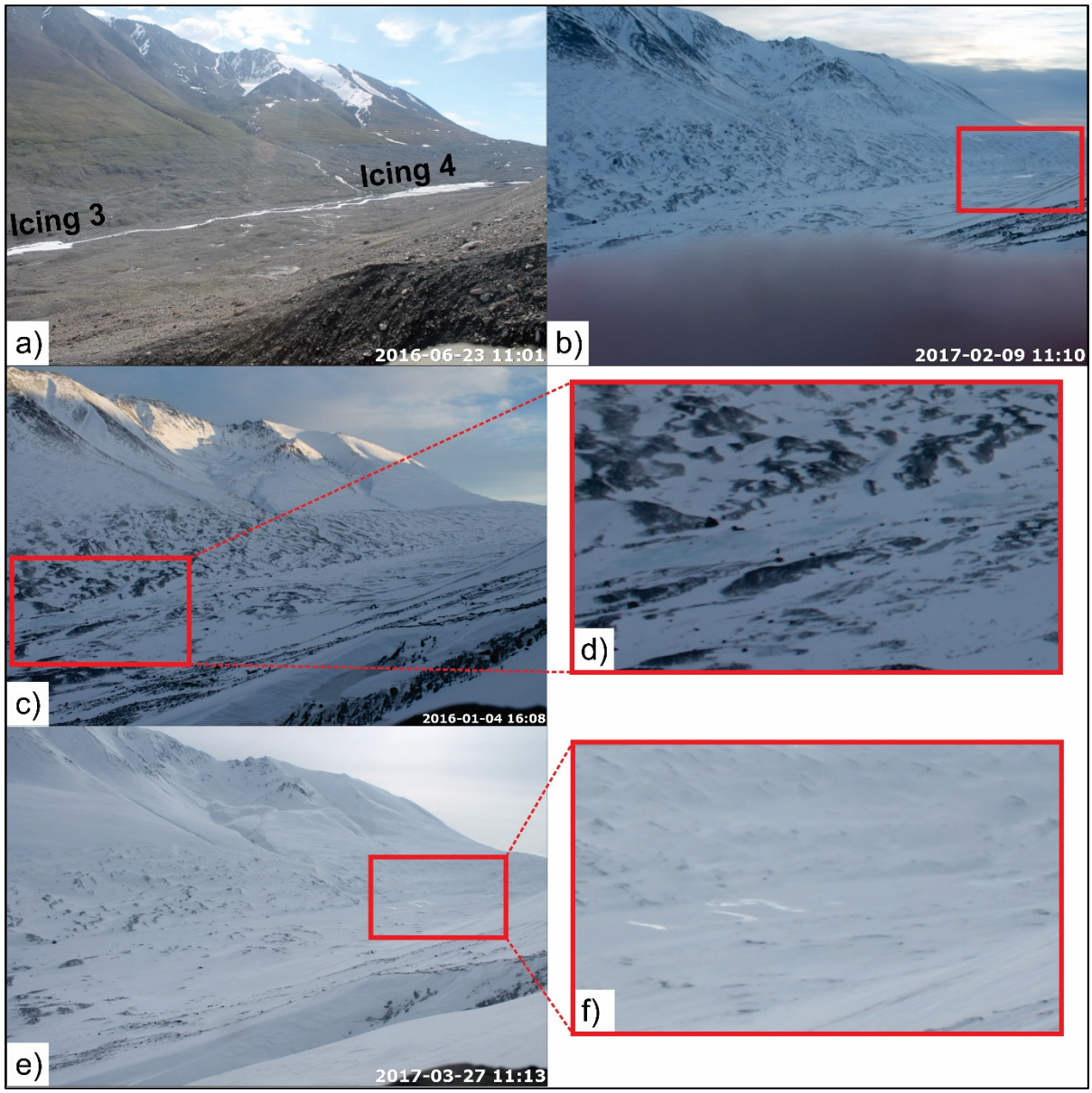

Figure 5.3 The Duke proglacial field visible in the TLC3 images. Panel (a) shows icings 3 (right side of the image) and 4 (left side of the image) at the camera installation; panel (b) shows an example of flooding originating from the Duke glacier; panels (c) and (d) show an example of the darkening/bluing of pixels as a results of flooding; panels (e) and (f) show an example of flooding being detectable from reflective (brightening) pixels

5.2.3 Sample collection

Waters originating from different sources (end-members) can have unique hydrochemical and isotopic signatures as a result of the specific hydrological, geological, and biological processes to which they have been exposed (Drever, 1997). Based on this principle, comparing the hydrochemical signatures of icings with those of other hydrological components should provide insights about the sources that contributed to icing formation.

During the field campaign of June 2016 in the Upper Duke River watershed, we observed and sampled four icings remnants within the Duke riverbed (Figures 5.1a and c) and two in the watershed B (Figures 5.1a and b). The icings in the Duke River were stretching along and, on several occasions, above the stream. Two of them (Icings 3 and 4) were situated within the proglacial field, and two others (Icings 1 and 2) within the alpine meadow (Figures 5.1a and c). Icing lengths varied between 70 and 1980 m, and widths ranged between several meters and several hundreds of meters. Where visible, ice thicknesses ranged from 0.5 m to 1.5 m. The icings in the watershed B were smaller than in the Duke watershed. Icing B stretched along the river and was 60 m long and 10 m wide. The second icing (Icing PF) was situated within the proglacial field next to the glacier B's tongue and was almost circular, ca 40 m in diameter (Figures 5.1a and b). All icings were characterized by an alternating sequence of layers of blue bubble-free and white bubble-reach ice, which result from slow and quick freezing of water, respectively (Moorman & Michel, 2000). Icings 1 and 2 had layers of candle ice closer to their tops, suggesting that melt events had already altered the ice (Stachnik et al., 2016). An ice mound, feature that forms when the top surface layer bulges as a result of freezing of water lenses trapped underneath (Carey, 1973), was still intact on Icing 4. Overall, 13 icing samples were taken in June 2016 (Figures 5.1b and c, Table 5.1) either from supra-icing ponds/channels (samples 1.1, 1.3, 2, 3, 4.2, 4.4, Icing B and Icing PF) or from water dripping from the icing surface (samples 1.2, 4.1, 4.3).

Table 5.1 Summary of samples collected in (a) watershed B and (b) Duke watershed. PF stands for proglacial field and AM stands for alpine meadow

Sample type	Sample location		samples
a) Watershed B			
Glacier B	PF	At the outlet of the immediate proglacial field where the whole drainage system of the glacier merges into one stream	1
Icing PF	PF	From supra-icing pond	1
Ice-cored moraine	PF	From purged ice wells made by steam-drill	2
Lake	PF	From lake situated on the left-side ice-cored moraine	1
Hillslope tributaries	PF	Close to the outlet of small streamlets	5
Glacier-fed tributary	PF	Large tributary formed by water from other glaciers in the watershed B	1
Icing B	AM	From supra-icing pond	1
Solids	AM	At Icing B surface	1
b) Upper Duke River watershed			
Duke glacier	PF	At glacier snout	1
		From supraglacial stream	1
Icing 4	PF	From supra-icing pond	2
		From water dripping from the icing	2
Icing 3	PF	From supra-icing pond	1
Buried ice and ice – cored moraines	PF	From purged ice wells made by steam-drill	3
		From meltwater flowing on buried ice- debris cover interface	2
Lakes	PF	From kettle moraine lakes	5
Streams fed by small glaciers	PF/AM	At the outlet stream close to glacier snout	6
		At the outlet stream close to the confluence with Duke river	5
Hillslope tributaries	PF/AM	From small streamlets	13
Icing 2	AM	From supra-icing pond	2
Icing1	AM	From supra-icing pond	2
		From water dripping from the icing	1
Suprapermafrost layer water	AM	From small ponds underlined by permafrost within the alpine meadow	3
Groundwater wells	AM	From purged shallow (0.5 m) wells	2
Solids	PF/AM	On Icing 1 and icing 3's surfaces	2
Snow	AM	Taken from snow on the ground	2
Rain	AM	Liquid precipitation	2

Over the same period of time, potential contributors to icing formation were systematically sampled as well (Table 5.1). In watershed B, the main glacier was sampled farther from the

glacier snout at the edge of its immediate proglacial field. Both left and right lateral ice-cored moraines were sampled from purged ice wells made by steam-drill. Within the left moraine complex, we also sampled a lake situated above the main stream but not visibly connected to it. In the downstream part of the watershed, hillslope tributaries originating from taluses were observed and sampled close to their confluence with the main stream. Finally, a large glacier-fed tributary was sampled as well, which represented the outflow from other two glaciers within the same watershed (Figure 5.1a).

In the Duke watershed, Duke glacier samples were taken at the glacier snout as well as from its supraglacial stream. Within the proglacial field, samples from ice-cored moraines and buried ice formations were taken either from meltwater streamlets on buried ice (samples BI3, ICM 2 and ICM 3) or from purged ice wells made by steam-drill (samples BI1, BI2 and ICM1). Other potential sources within the proglacial field included moraine kettle lakes and hillslope tributaries. The latter were also present within the alpine meadow part of the Duke watershed (Figure 5.1a). To identify the role of the proglacial field in icing formation, we created proglacial field (PFL) hillslope tributaries as a sample subgroup for the Duke watershed (13 samples). Streams fed by small glaciers in the Upper Duke watershed are also located within both proglacial field and the alpine meadow (Figure 5.1a). They were sampled upstream close to the glacier snout and downstream close to the confluence with the Duke River. Three water samples were taken from small ponds within the right side of the permafrost-underlined alpine meadow. Because of their positions, those samples are considered to represent the suprapermafrost layer water. Groundwater at the left side of the alpine meadow was sampled via purged shallow wells. Finally, rain-water and fresh snow samples were also collected over the field campaign.

Water samples were taken from different hydrological sources in a very short period of time following a synoptic sampling strategy (Mark & Seltzer, 2003). Samples were collected into high-density polyethylene plastic bottles. Volumes of 30 mL were collected for stable water isotope analysis and of 50 mL for solutes and dissolved organic carbon (DOC) analyses. Samples for solutes and DOC were filtered using 0.45-micron filters and acidified with three

drops of nitric acid 0.5M at the field. All bottles were filled to the brim, sealed, and kept in the dark at 4°C prior analysis whenever possible (at least 90% of time). Water samples were successively analyzed for isotopes, selected ions, as well as DOC.

During the field campaign of 2016, solid state samples were collected on Icings 1 and 3 in the Duke watershed, and on Icing B in sub-watershed B (Figure 5.1b and c; Table 5.1). The aim was to analyze cryogenic precipitates and, based on their composition, to learn about the characteristics of the parent waters. Samples were collected where clear association between the precipitate and the icing was possible. Around 5 g of samples were taken and stored into celled 50 mL plastic centrifuge tubes.

5.2.4 Analysis of isotopes

Samples were analyzed for relative concentrations of stable isotopes of oxygen, $\delta^{18}O$, and hydrogen, $\delta^{2}H$, using cavity ring down spectrometry (Picarro Analyzer L2130-I; guaranteed instrumental precision is 0.03‰ for $\delta^{18}O$ and 0.2 ‰ for $\delta^{2}H$). Both $\delta^{18}O$ and $\delta^{2}H$ were expressed in per mil relative to Vienna Standard Mean Ocean Water standard (‰) (Coplen, 1996). For each sample six injections were performed but only the last three were averaged to minimize the memory effect impact. The spectrometer was calibrated every 100 samples using six laboratory standards. In addition, one standard was analyzed after every third sample to verify the stability of measurements and eventually perform corrections. The results of $\delta^{2}H$ were then plotted as a function of $\delta^{18}O$. The local meteoric water line (LMWL) was built thanks to precipitation samples.

5.2.5 Analysis of selected ions

The anionic concentrations in the samples (F^-, Cl^- and SO_4^{2-}) were measured using an ionic chromatographer (Dionex ED50, Thermo Fisher Scientific). The equipment was calibrated every 30 samples using seven standards ranging from 0.005 to 3.2 ppm for F^-, from 0.1 to 50 for Cl^- and from 0.2 to 75 for SO_4^{2-}. After every third sample, we inserted a standard (0.2 ppm

for F^-, 0.9 for Cl^- and 1.8 for SO_4^{2-}) followed by a blank sample to guarantee analytical stability and to correct results from an eventual drift in measurements.

Cationic concentrations (Li^+, Na^+, K^+, Ca^{2+}, Mg^{2+}, Al^{3+}, Ag^+, Ba^{2+}, Cr^{3+}, Cu^{2+}, Fe^{3+}, Mn^{3+}, Si^{4+}, Sr^{2+}, Ti^{3+}, Zn^{2+}) were measured using an inductively coupled plasma optical emission spectrometer (ICP-OES, 5110 Agilent). Calibration was performed every 23 samples using nine standards ranging from 1 to 40 ppm for Ca^{2+}, Si^{4+}, and Mg^{2+} for some samples (those with high concentrations), and from 0 to 10 ppm for other ions. Two standards (10 ppm for Ca^{2+} and 5 ppm for all other ions) followed by a blank sample were inserted after every third sample to guarantee analytical stability and to correct results resulting from drift in measurements.

Connections between samples were investigated by conducting a principal component analysis (PCA) on selected tracers. Tracers were selected based on their ability to segregate different sample origins/types in bivariate plots (Baraer et al., 2015). The hydrochemical signature of the icing samples depends not only on the hydrochemical composition of the sources contributing to its formation, but also on cryochemical fractionation, such as solute rejections or salt precipitation associated with the freezing of water (Wadham et al., 2000). For that reason, based on the hypothesis that the proportions of ions remain constant through those processes, the relative concentrations of solutes (ion concentrations divided by the sum of anions/cations) were used instead of absolute concentrations in PCA (Baraer et al., 2015). Alongside PCA, conceptual maps of dominant ions relative concentrations were created to identify areas with particularly high concentrations of a given solutes. The upper quartile calculated for each selected ion based on its relative concentrations was chosen as a threshold value.

5.2.6 Analysis of dissolved organic carbon

Water sources originating from permafrost-underlined vegetated terrains are usually characterized by higher concentrations of DOC than the nearby permafrost-free areas due to extended exposure to the organic-reach suprapermafrost layer (Carey, 2003; Ma et al., 2019;

MacLean et al., 1999). DOC represents therefore a good tracer for permafrost-related water sources (e.g., Petrone et al., 2006; Toohey et al., 2016; Yoshikawa et al., 2007). In the present study, DOC concentrations in sample were measured using an Apollo 9000 Combustion Analyzer. Three injections were made for each sample, and calibration was performed every 20 samples by means of four standards ranging from 0 to 10 ppm. A standard was analyzed every five samples to assess the stability of measurements. The detection limit for the analysis was 1 ppm. Due to the low level of DOC in the majority of the samples, DOC results were interpreted separately from the ions.

5.2.7 Analysis of solid samples

Cryogenic precipitate is commonly encountered on the icing surface (Lacelle, Lauriol, & Clark, 2009). It is formed when sufficient concentrations of precipitating elements exist in the freezing water (Žák, Onac, & Perşoiu, 2008). Where such conditions are met, production of mineral precipitates occurs by solute expulsion during freezing (Bukowska-jania, 2007; Lacelle et al., 2009; Lauriol et al., 1991; Vogt, 1991). The most common mineral found at the surface of the icings in the melt season are carbonates ($CaCO_3$) and gypsum ($CaSO_4$) (Lacelle et al., 2009). In glacierized catchments, those cryogenic minerals have been shown to represent a unique archive of the hydrologic conditions that prevailed at their formation (Thomazo et al., 2017).

Two methods were applied to determine the chemical composition of solid samples: X-ray fluorescence (XRF) (ThermoScientific, Niton XL3T Gold) and acid digestion followed by anion and cation analysis. All samples were first dried at 110°C for 24h. For XRF, a smooth and plain pellet was produced out of 2 g of sample using a pellet press. For acid digestion, 1 g of dried sample was mixed with 4 mL of nitric acid (50%) and 10 mL of hydrochloric acid (20%) and heated for 2 hours at 90°C. The resulting solutions were then analyzed by means of ICP-OES (see above for the characteristics) for cationic concentrations. Both methods were used to determine the relative abundance of ions. Parent sources were then tentatively identified by comparing the XRF results and acid digestion products hydrochemical

compositions with the ionic concentrations of water samples from different sources by means of conceptual maps of selected ionic relative concentrations (Section 5.2.5).

5.3 Results of the watershed B

5.3.1 Time lapse images analysis

In general, the time lapse images showed that, in watershed B, the proglacial icing remnants from the previous winters persisted late into the melting season (till the end of September 2016 and July 2017). For Icing PF, it was possible to detect episodes if hydrological activity throughout the winters, whereas Icing B was not visible in TLC images.

Winter season 2015-2016 was characterized by consistent negative air temperatures between late September and late March, except two warm events: 25-27 November and 30 December. The first flooding event on the snowpack within the proglacial field occurred in mid-October (Figure 5.4, top panel), and by the beginning of November, icing formation had been observed on TLC images on the left side of the proglacial field. In general, flooding events over the icing surface were observed mainly in two locations: until January, they occurred on the left side (e.g., Figure 5.2b), where the main glacier outlet stream is observed in the summer; and after January, they occurred on the right side (e.g., Figure 5.2c). On two occasions during this season, namely 16 February and 6 March, flooding was observed next to the left-side lateral moraine, which shows exposed buried ice in the summer. On 16 February, a stream forming at the slope of this ice-cored moraine was observed (e.g., Figure 5.2d and 5.2e). As a moraine lake was observed at the top of this moraine in the summer, differentiating between the lake and buried ice origins based on the images was not possible.

In winter 2016-2017, air temperature stayed below zero between mid-October and mid-April, with warm episodes occurring on 30 December and 2 January (Figure 5.4, bottom panel). The icing's extent increased in late fall, when air temperature dropped below zero. By the end of October 2016, an icing had formed on the right side of the proglacial field (Figure 5.4, bottom panel). Unlike the 2015-2016 season, flooding events mostly happened on the right side of the

proglacial field before January, and afterwards - on its left side. During the 2016-2017 season, signs of contribution of either the left ice-cored moraine or the moraine lake to icing formation, were observed on 26 November and 28 March.

5.3.2 Analysis of stable water isotopes and ionic signatures

The results of stable water isotopes and ionic concentrations analyses are presented in Figure 5.5. For better readability, results are presented in four sub-figures: Figures 5.5a and 5.5b summarize the results for icings together with water sources identified as potential icing contributors based on time lapse images; Figures 5.5c and 5.5d allow comparison to other potential water sources. Figure 5.5a and 5.5c show the results for stable water isotopes together with the Local Meteoric Water Line (LMWL), which was built based on fresh snow samples taken during the field campaign. Figures 5.5b and 5.5d show the projection of water sample data on the reduced space determined by PCA using Ca^{2+}/SC^{+}, Mg^{2+}/SC^{+}, $Li^{+}+Na^{+}+K^{+}/SC^{+}$, SO_4^{2-}/SA^{-}, Sr^{2+}/SC^{+} and d-excess. These tracers were chosen based on bivariate plots since they best separate icings and different water sources. For the watershed B, PC1 accounts for 0.47 of variance present in the dataset, and PC2 accounts for 0.36 of variance. Thus, together, the first two principal components account for 0.83 of the total variance.

The sources identified based on TLC images are the main glacier, left ice-cored moraine, and moraine lake (Figures 5.5a and 5.5b). In the $\delta^{18}O$ - $\delta^{2}H$ diagram, the sample that represents the glacier runoff, Bgl, plots relatively close to the Icing PF sample. This means that potential contribution of this glacier to Icing PF formation cannot be ruled out by means of isotopes analysis. The sample from the left ice-cored moraine has a lighter isotopic than the sample from the proglacial field icing, and plots a bit farther from the Icing PF sample. The sample from the moraine lake, however, plots relatively close to the Icing PF sample and can be considered as potential contributor to its formation. We thus hypothesize that lake water is released during the winter from the moraine and supplies water for at least part of the icing formation. In the PCA diagram, however, the sample from the Icing PF plots away from all the other samples (Figure 5.5b), making it impossible to confirm the contribution from the

main glacier, left ice-cored moraine, and moraine lake to Icing PF formation via hydrochemical signatures.

Other potential water sources contributing to Icing PF's formation have been evaluated from Figure 5.5d. The sample from the right ice-cored side moraine, geographically close to Icing PF, shows an isotopic signature depleted in light isotopes and plots at the lower left corner of the $\delta^{18}O$ - $\delta^{2}H$ diagram (Figure 5.5c), far from the Icing PF sample. Similarly, that sample plots far from the Icing PF (Figure 5.5d) on the PCA diagram. Thus, the contribution from this source is not supported by those results.

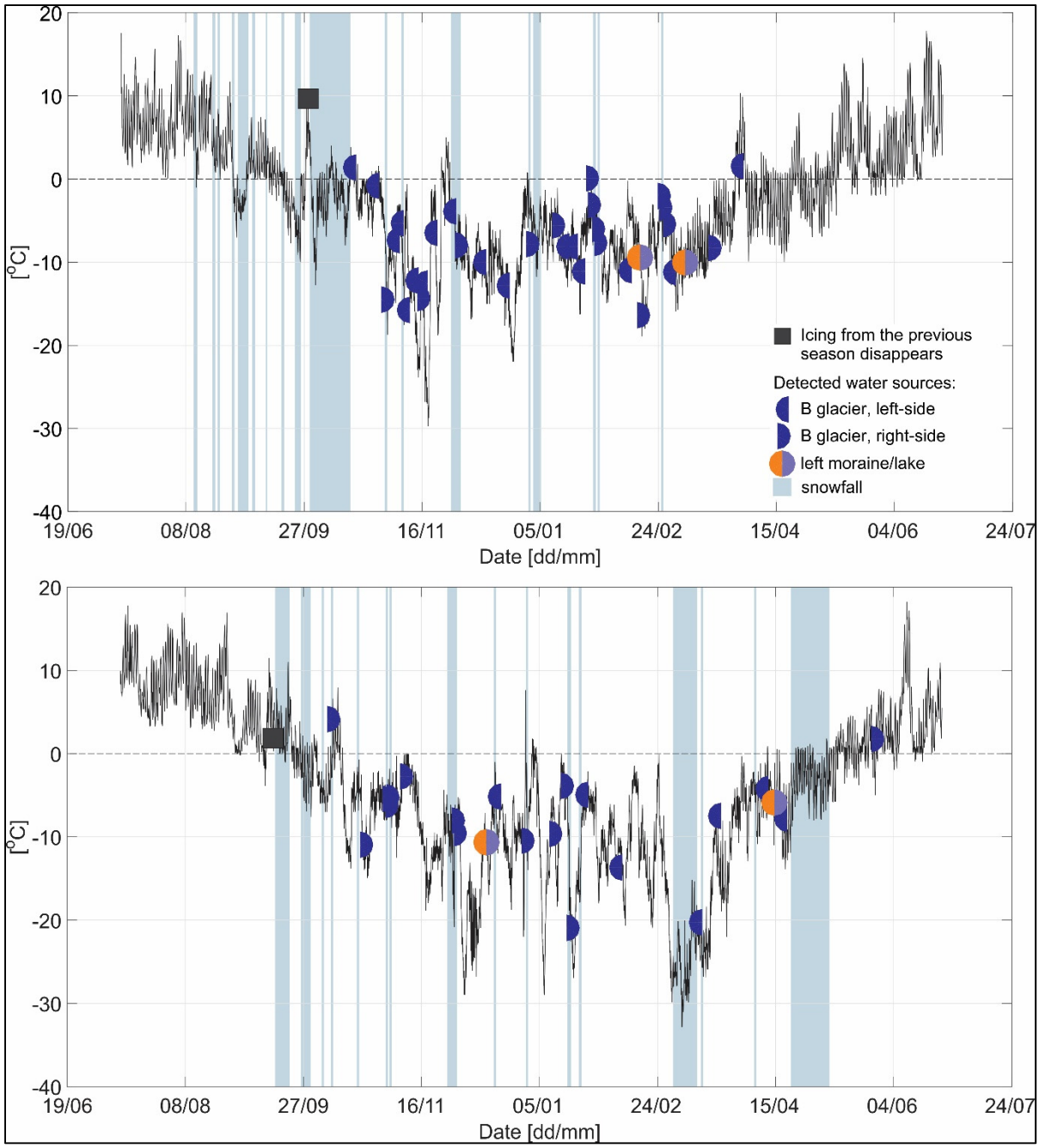

Figure 5.4 Hydrological activities observed in watershed B by the use of time lapse cameras for the 2015-2016 season (top panel) and the 2016-2017 season (bottom panel). Black solid lines show air temperature measured at the automatic weather station; half-circles mark the timing of hydrological activity on the left/right side of the proglacial field, and full circles represent the timing of hydrological activity related to either an ice-cored moraine or a moraine lake

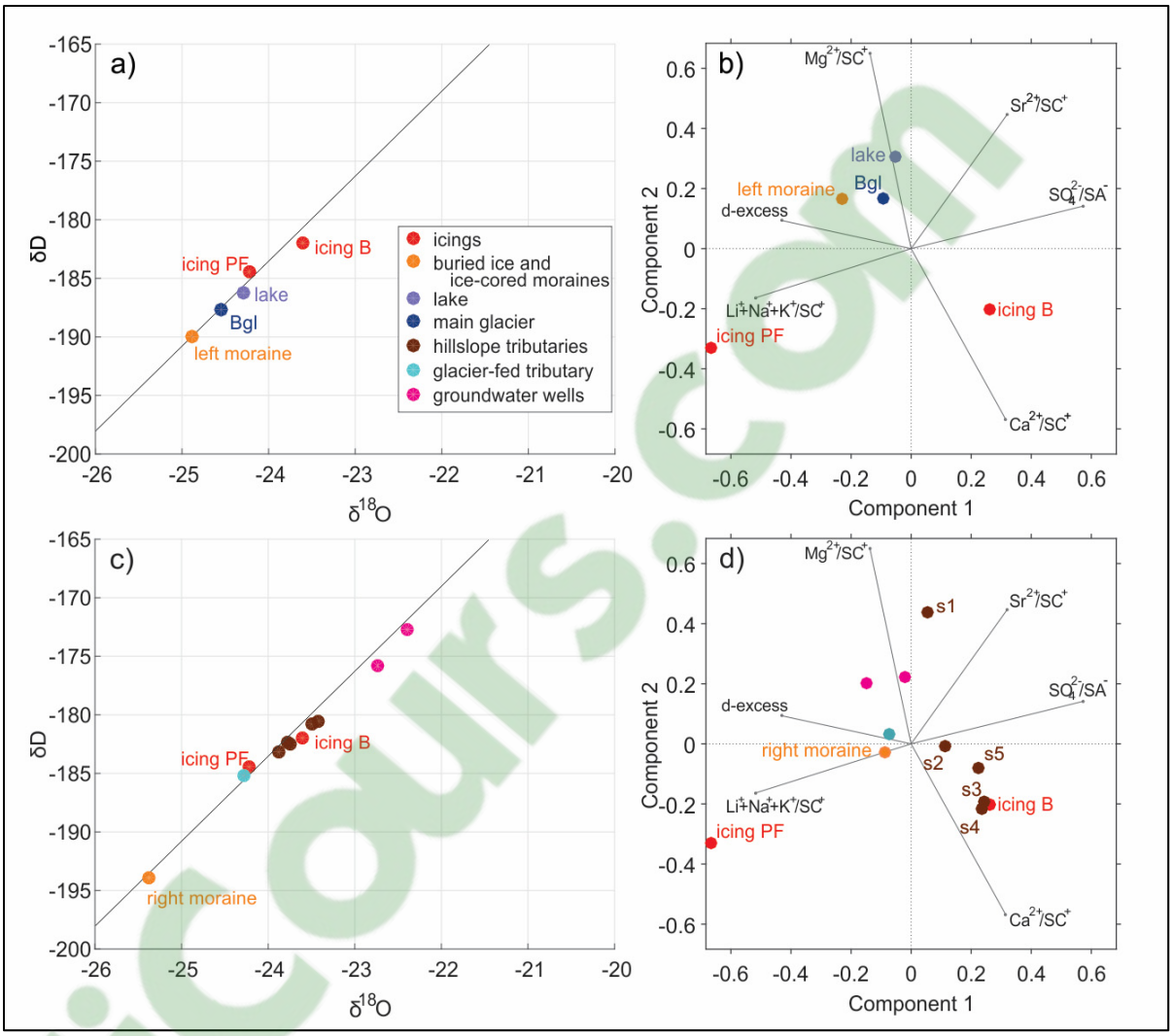

Figure 5.5 Results for the watershed B. Panels (a) and (c) show results from stable water isotope analysis. The straight line represents the Local Meteoric Water Line. Panels (b) and (d) show results of hydrochemical analysis. Panels (a) and (b) show the locations of sources identified by TLC; panels (c) and (d) show other potential sources for Icing PF and Icing B formation

In subwatershed B, close to its conjunction with the Duke River, another icing, called Icing B, was observed and sampled (Figure 5.1). This icing cannot be seen from TLC and thus can only be studied by means of isotopic analysis and hydrochemical analysis of both water and solid samples. In the $\delta^{18}O$ - $\delta^{2}H$ diagram, the sample from this icing (Icing B) is enriched in $\delta^{18}O$ and $\delta^{2}H$ in comparison with Icing PF, and plots close to samples from hillslope tributaries s1-5 (Figure 5.5c). Geographically, source s1 is the closest and is situated just upstream of the

icing (Figure 5.1). In the PCA diagram the sample from the icing B plots together with samples from hillslope tributaries s3 and s4, and s1 has a quite different hydrochemical signature and plots away from other sources. Samples from alpine meadow groundwater wells, as well as from glacier-fed tributary, plot away from Icing B sample in both the $\delta^{18}O$ - $\delta^{2}H$ and the PCA diagram (Figures 5.5c and 5.5d), and thus their contribution is not supported by those results.

5.3.3 Distribution of relative ionic concentrations

The conceptual map of relative ionic concentrations in water samples shows areas with high concentrations of Ca^{2+}, SO_4^{2-}, CO_3^{2-}, Fe^{3+}, and Al^{3+} (Figure 5.6). The calculated thresholds for relative concentrations of solutes (ion concentrations divided by the sum of anions/cations, [-]) are 0.37 for Ca^{2+}, 0.43 for SO_4^{2-}, 0.42 for CO_3^{2-}, 0.18 for Fe^{3+}, and 0.05 for Al^{3+}. In watershed B, hillslope tributaries, namely samples s1-5, are characterized by high relative concentrations of SO_4^{2-} (Figure 5.6a), while high relative concentrations of Ca^{2+} are only observed in tributaries s3-5. Sample s2 differs from the rest of the streams, as it presents above-threshold amounts of Fe^{3+}. Finally, the sample from the moraine lake close to Glacier B has noticeable concentrations of both Fe^{3+} and Al^{3+}.

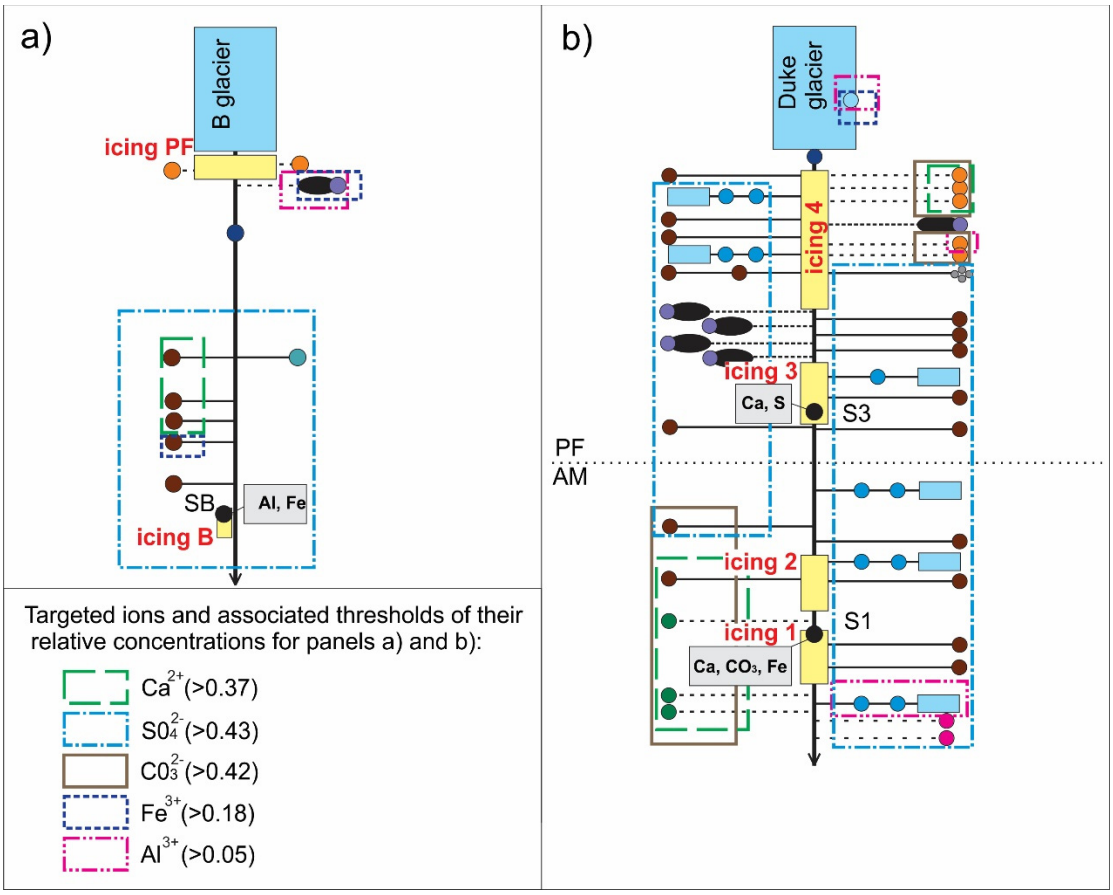

Figure 5.6 Conceptual maps of ionic content of water samples. Colored boxes delineate sampled areas with targeted ion relative concentration above the threshold. The names of sampling points can be found in Figure 5.1

5.3.4 Analysis of solid samples

The solid sample taken on Icing B was brown-grey and, according to both methods, namely XRF and acid digestion, presented high concentrations of Al^{3+} and Fe^{3+} (Table 5.2). High amounts of silicates were also measured by XRF. Those elements do not correspond to reported compositions of cryogenic precipitates occurring naturally on the earth (Lacelle et al., 2009). Thus, sampled solids were most probably made by sediments from the parent water. Unlike for cryogenic precipitates, the relation of this sediment to icing formation cannot be guaranteed. However, higher relative concentrations of both Al^{3+} and Fe^{3+} in the watershed B are observed in the water sample from the moraine lake, and higher relative concentrations of

Fe^{3+} are observed in water sample s2 (Figure 5.6). Thus, these sources could potentially be contributors to the formation of Icing B.

Table 5.2 Results of the analysis of solid samples performed by X-ray fluorescence (Method 1) and acid digestion (Method 2)

Icing	**Color**	**Most abundant ions**	
		Method 1	**Method 2**
B	brown-grey	Al^{3+}, Al_2O_3, Fe^{3+}, Fe_2O_3, Si^{4+}, SiO_2	Al^{3+}, Fe^{3+}
3	white	Ca^{2+}, CaO, S^{2-}, SO_3^{2-}	Ca^{2+}, SO_4^{2-}
1	brown-grey	Ca^{2+}, CaO	Ca^{2+}, Fe^{3+}

5.4 Results for the Duke watershed

5.4.1 Time lapse images analysis

Only Icings 3 and 4 were visible in TLC images for the Duke watershed. In comparison with watershed B, a larger number of water sources were identified as potential contributors to those icings' formation. These sources included the Duke glacier, two small glaciers (glaciers Gl1 and Gl2) and two hillslope tributaries (s3 and s4) on the right side of the valley, and three hillslope tributaries on the left side of the valley (s5, s6, and s7). In general, hydrological activities detected by TLC images occurred when the air temperature was below zero. On some occasions, several sources showed activity at the same time (on 29 November or 10 December, Figure 5.7 top panel). It was also observed that all sources detected as active during the season 2015-2016 were also active during the season 2016-2017.

For the 2015-2016 season, both Icings 3 and 4 melted away by the end of July. The next cold season, icings were detected by the end of November. The Duke glacier's hydrological activity was observed in the form of flooding of the upstream portion of Icing 4 (Figure 5.7, top panel). For the same season, hydrological activity of the small glacier Gl1 was detected on three occasions in December-January. The small glacier Gl2 appeared to be less active than Gl1, as only one flooding event was detected that winter (in November). Hillslope tributaries s4 and s3 were observed being active before January only, and tributaries s5-7 demonstrate some hydrological activity few times before January during the 2015-2016 season. As distinguishing between sources s5, s6, and s7 based on TLC images in winter conditions was almost impossible, they are represented by the same color in Figure 5.7. Those tributaries showed some hydrological activity a few times before January during the 2015-2016 season.

The 2016-2017 icings formed at the beginning of November. Icing 3 had melted away by the end of July, and Icing 4 persisted until the end of August (Figure 5.7, bottom panel). It seems also that, in November 2016, Icings 3 and 4 made one larger icing. As was the case during 2015-2016, the Duke glacier's hydrological activity was observed under negative temperatures most of the time. Flooding at positive temperatures occurred only once, on 2 January 2017 (Figure 5.7, bottom panel). Hydrological activity of the small glacier Gl1 was observed on five occasions during the 2016-2017 season: once in October, once in December, and three times at the end of March. The small glacier Gl2 exhibited hydrological activity twice that winter: at the beginning of January, and in April, before the temperature rose above zero. Finally, sources s5, s6, and s7 showed activity as from January only (Figure 5.7, bottom panel).

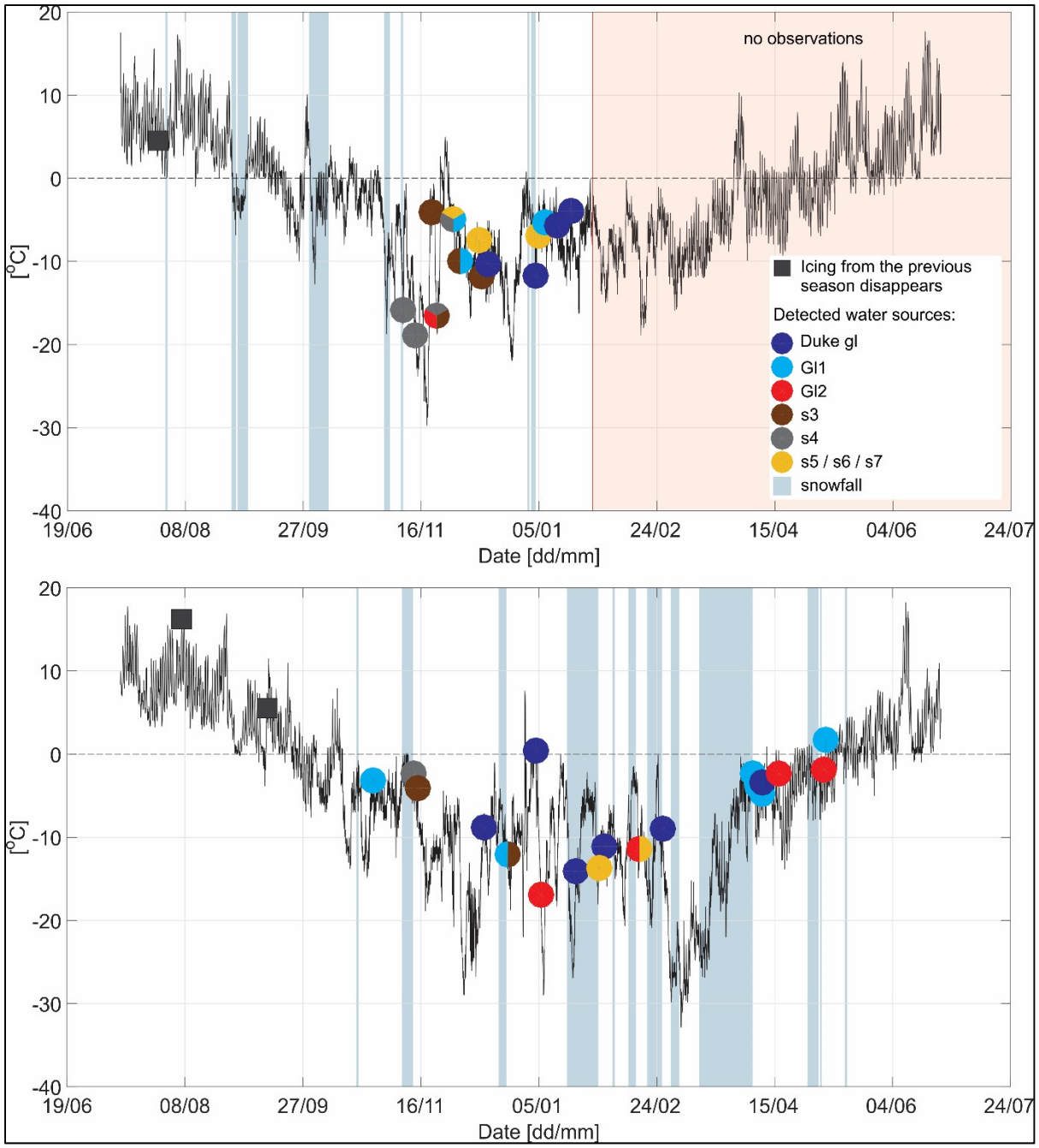

Figure 5.7 Hydrological activities observed in the Upper Duke watershed by the use of time lapse cameras for the 2015-2016 season (top panel) and the 2016-2017 season (bottom panel). Black solid lines show air temperature measured at the automatic weather station. Circles represent the timing of hydrological activity related to different water sources. Circle color identifies a specific sources type. In cases where different sources were observed to be active, the circles has in multiple colors

5.4.2 Analysis of stable water isotopes and ionic signature

The results from stable water isotope and ionic concentration analyses are presented in Figure 5.8. For readability, results' presentation is split into six sub-figures. Figures 5.8a and 5.8b show results for sources detected using TLC image analysis; Figures 5.8c and 5.8d show results for potential sources within the proglacial field; Figures 5.8e and 5.8f show results for potential sources within the alpine meadow. Figures 5.8a, 5.8c, and 5.8e show stable water isotope analysis for the Duke watershed. The PCA results are shown on Figures 5.8b, 5.8d, and 5.8f. PC1 accounts for 0.48 of the dataset variance, and PC2 accounts for 0.22 of variance. Thus, together, the first two PCs account for 0.7 of variance.

First, the contribution of sources detected in TLC images to Icings 3 and 4's formation are confirmed as possible and even probable in some cases - by the $\delta^{18}O$ - $\delta^{2}H$ and PCA diagrams (Figure 5.8a and b). For Icing 4, those include the Duke glacier, small glaciers Gl1 and Gl2, and hillslope tributaries s3 and s4, and for Icing 3 those include hillslope tributaries s5-7. Indeed, on Figure 5.8a, samples taken from the Icing 4 plot together in the lower part of the $\delta^{18}O$ - $\delta^{2}H$ diagram, and are situated close to samples taken at the Duke glacier outlet. This is particularly true for the most upstream icing sample 4.1. In the PCA diagram, samples from Duke glacier plot in the vicinity of Icing 4 and Icing 3 samples. Thus, contribution of the main glacier to Icing 3 and 4 formation remains a valid hypothesis. In both $\delta^{18}O$ - $\delta^{2}H$ and PCA diagrams, samples that represent the stream fed by small glacier Gl2, namely Gl2a and Gl2b, as well as samples s3 and s4 plot slightly closer to the sample from the icing 3 than to those taken from Icing 4 (Figures 5.8a and 5.8b). Thus, while geographically and based on TLC images, those sources were attributed to Icing 4, they should be considered as possible contributors to Icing 3 as well. In the $\delta^{18}O$ - $\delta^{2}H$ diagram, the upstream sample from the stream fed by glacier Gl1, namely Gl1a, plots away from both icings. Its downstream sample, Gl1b, plots closer to the sample from Icing 3 but still has a different isotopic signature. In the PCA diagram, samples from GL1 plot closer to Icing 3 sample. Thus, the flooding observed in TLC images on Icing 4, which initially was attributed to the small glacier Gl1, is most likely related to another hydrological source activity. Similarly, samples taken from the hillslope tributaries

s5-7 plot together with the icing 3 sample in the $\delta^{18}O$ - $\delta^{2}H$ diagram (Figure 5.8a) but not in the PCA diagram.

Other sources within the proglacial field that potentially contribute to the formation of Icings 3 and 4 can be hypothesized based on Figure 5.8c and d. Two samples taken from buried ice formations plot close to the Icings 3 and 4 samples both in the $\delta^{18}O$ - $\delta^{2}H$ diagram and the PCA diagram. These results suggest the potential contribution of areas with buried ice those icings. In both $\delta^{18}O$ - $\delta^{2}H$ and PCA diagrams, samples from one of the PFL tributaries, identified as PFL1, plot relatively close to the Icing 4 samples (Figures 5.8c and 5.8d). Finally, in the PCA diagram, the sample from kettle moraine lake 5 plots close to Icing 4 samples. As for Icing 3, on the $\delta^{18}O$ - $\delta^{2}H$ diagram, its sample plots close to hillslope tributary s2. In the PCA diagram, however, s2 plots relatively far from Icing 3.

In Figure 5.8e and f, samples taken from Icings 1 and 2, which were not observed by the TLC, do not appear as a homogeneous group, suggesting they might be of different parent waters. Potential contributors to those alpine meadow icings can be proposed based on the $\delta^{18}O$ - $\delta^{2}H$ and PCA diagrams. Sample 1.2 exhibit a very similar isotopic signature to one of the groundwater well sample, namely Gw2. In the PCA diagram, however, the samples from groundwater wells plot far from Icing 1 samples. Sample 1.3 has a similar isotopic signature to the samples from Icings 2 and 3, and to samples from the stream fed by small glacier Gl4 and hillslope tributary s14 (Figure 5.8e). The PCA results, however, do not confirm the contribution of these sources (Figure 5.8f). Finally, sample 1.1 plots in the diagram close to samples from streams formed by small glaciers Gl5 (samples Gl5a and Gl5b) and Gl6 (Gl6b) (Figure 5.8f). Small glacier Gl6 is located downstream from Icing 1 and thus cannot be the source of its formation (Figure 5.1).

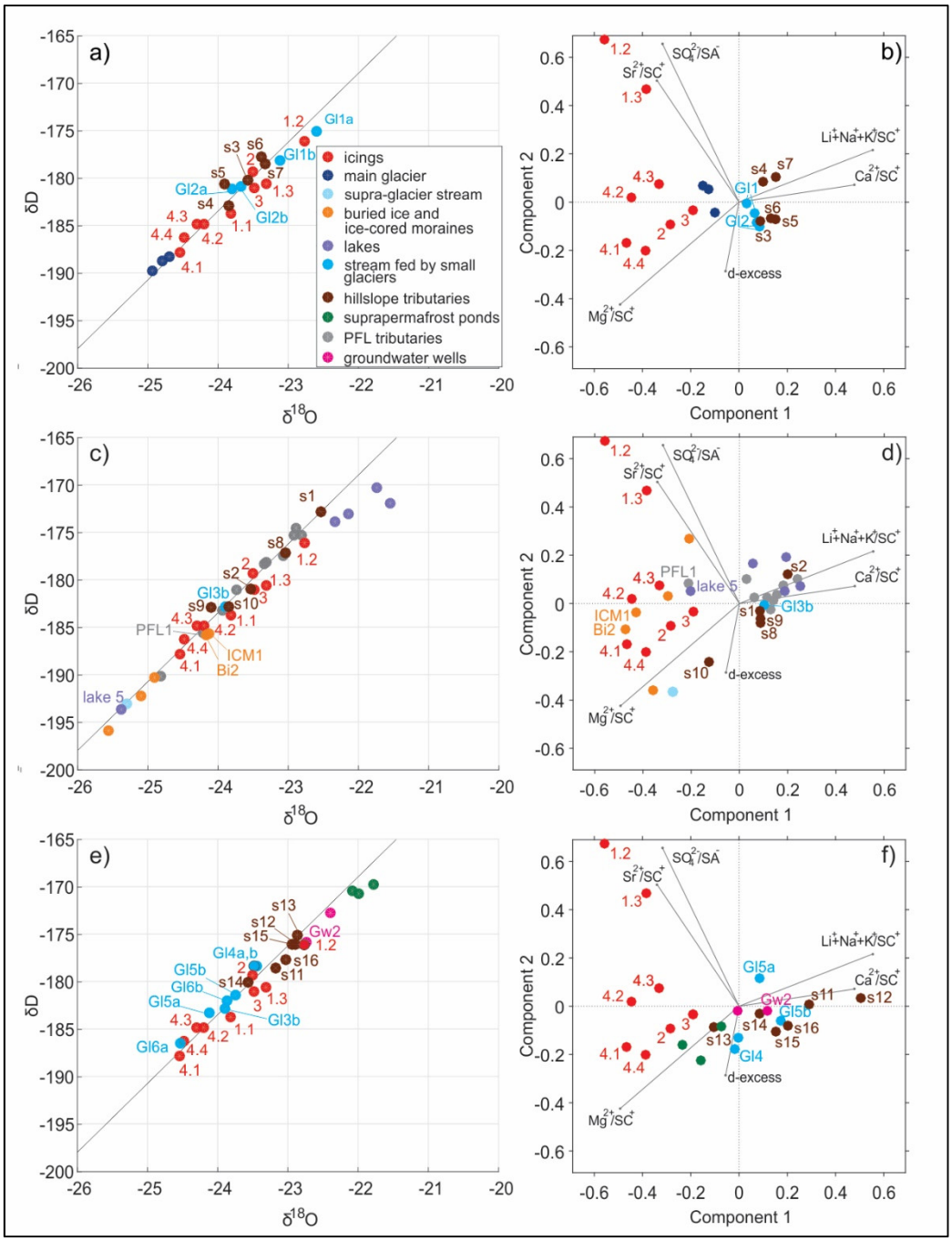

Figure 5.8 Results for the Duke watershed. Panels (a), (c), and (e) show results from stable water isotope analysis. The straight line represents the Local Meteoric Water Line. Panels (b), (d), and (f) show results of hydrochemical analysis. Panels (a) and (b) show the locations of sources identified in TLC images; panels (c) and (d) show sources within the proglacial field; panels (e) and (f) show sources within the alpine meadow

The sample taken from Icing 2 plots in the $\delta^{18}O$ - $\delta^{2}H$ diagram together with samples from Icing 3, samples from small glaciers and proglacial field tributaries (Figure 5.8d). Based on Icing 2 geographic location, one of the possible sources contributing to its formation can be small glacier Gl5. Both samples from this glacier, however, plot lower than sample 2 on the LMWL (Figure 5.8e) and relatively away in the PCA diagram (Figure 5.8f). Samples from another small glacier, Gl4, which is 890 m farther upstream, plot very close to the sample 2 in both $\delta^{18}O$ - $\delta^{2}H$ and PCA diagrams, and thus, this glacier potentially contributes to Icing 2 formation. Based on the geographical locations four other sources, namely s11-14, should be verified as possible contributors to Icing 2. Among them, s11 and s14 plot very close to the Icing 2 sample in the $\delta^{18}O$ - $\delta^{2}H$ diagram and therefore might be considered as its feeding sources (Figure 5.8e). The PCA diagram suggests that tributaries s11 and s13 can potentially contribute to Icing 2, whereas s12 and s11 plot farther away. Thus, only s11 is confirmed by both analyses.

In the PCA diagram, samples from both Icings 2 and 3 plot close to samples that are assumed to be of suprapermafrost layer origin, namely P1-3. Geographically, these three samples cannot be responsible for Icing 2 and 3 formation, and they plot away from icing samples in the $\delta^{18}O$ - $\delta^{2}H$ diagram. However, they can be seen as the representatives of the group of hydrological sources. This suggests that there might be some hydrological activity related to suprapermafrost layer waters and that these waters might contribute to winter icing formation. This suggestion will be verified by other methods.

5.4.3 Distribution of relative ionic concentrations

In the Duke watershed, the entire left part, except from samples from buried ice and from kettle lakes, is characterized by high concentrations of SO_4^{2-} (Figure 5.6b). As for the right side of the watershed, relative concentrations of SO_4^{2-} are high within the proglacial field as well, apart from s1, and in sample s11 from the alpine meadow. All samples from buried ice, as well as all samples from the suprapermafrost layer and sample s13, have high concentrations of Ca^{2+}. As for carbonates, the entire right side of the alpine meadow (namely suprapermafrost layer

water samples P1-3 and samples s11 and s13) and buried ice samples have high concentrations of CO_3^{2-}. Finally, the sample from the supraglacial stream has high Fe^{3+} and Al^{3+}, concentrations. One of the ice-cored moraine samples, together with samples from small glacier Gl6, is also characterized by higher Al^{3+} concentrations.

5.4.4 Dissolved organic carbon

Most of the samples taken from icings have DOC concentrations below the detection limit (1 ppm), with two exceptions. Sample 1.2 presents DOC concentrations at 5.9 ppm, and sample 2 at 2.3 ppm. Among the samples of potential parent water, high DOC concentrations are observed in the samples from the alpine meadow ponds and those taken from groundwater wells: P1 (8.6 ppm), P2 (5.4 ppm), P3 (5.4 ppm), GW1 (4.0 ppm), and GW2 (4.3 ppm). High values of DOC suggest that those samples represent suprapermafrost layer water. Thus, those results support the hypothesis that the suprapermafrost layer contributes to Icing 1 and, possibly, Icing 2's formation.

5.4.5 Analysis of cryogenic precipitate

The solid sample S3 from Icing 3 was white and presented high amounts of Ca^{2+} and S^{2-} when analyzed with XRF and of Ca^{2+} and SO_4^{2-} upon acid digestion (Table 5.2). Such composition is characteristic of cryogenic gypsum, the second most common cryogenic mineral found on icings (Lacelle et al., 2009). Figure 5.6b shows high relative concentrations of Ca^{2+} in buried ice samples (BI 2 and 3) and in samples from the suprapermafrost layer (P1-3) on the right side of the alpine meadow. Samples with high relative concentrations of SO_4^{2-} are observed throughout the proglacial field, apart from samples of hydrological components that are related to the Duke glacier (i.e. samples from buried ice and ice-cored moraines, Duke glacier sub- and supra-glacial discharge). High SO_4^{2-}concentrations were also found on the left side of the alpine meadow. All the above mentioned sources can potentially reach gypsum saturation during freezing and solute expulsion, except the samples that show high concentrations of carbonates: buried ice samples and samples from suprapermafrost layer. The solubility constant of calcite being more than 1000 times lower than that of gypsum (Zarga, Ben

Boubaker, Ghaffour, & Elfil, 2013), cryogenic precipitate from those sources should be made mainly of calcium carbonate. The results, therefore, rule out buried ice and the Duke glacier, since buried ice is likely made of remains of the Duke glacier. In addition, water from the suprapermafrost layer is not supported as the parent water of at least part of Icing 3since samples P1-3 show high concentration of carbonates.

The solid sample collected on Icing 1 was brownish-grey and presented high concentrations of Ca^{2+}, with some traces of iron (Table 5.2). Figure 5.6 shows high relative concentrations of carbonates and calcium in the upper part of the proglacial field in water samples from ice-cored moraine and buried ice (BI2, BI3, ICM1, and ICM2) and on the right side of the alpine meadow in samples of suprapermafrost layer water (P1-3) and sources s13 and s11. The distance from buried ices makes their contribution to Icing 1 formation highly improbable. Thus, these results suggest that either suprapermafrost layer water or tributaries s11 and s13 were at the origin of the cryogenic precipitates' formation on Icing 1.

5.5 Discussion

5.5.1 Summary of water sources detected for each icing

Table 5.3 provides a summary of the icing formation contributing sources suggested by each method presented above. This summary is given for each studied icing. Overall, we observe that all methods agree with each other's in only 22% of the cases. On four occasions, the methods unanimously support a potential source as a contributor to the icing formation: hillslope tributaries for Icing B, glacier-fed tributaries and hillslope tributaries for Icing 3 and the main glacier for Icing 4. On two occasions, no method supports the possibility of a given potential source contribution: glacier-fed tributaries and groundwater wells for Icing B. Having 78% of the potential contribution evaluation with no consensus among the methods confirms that the use of a multimethod approach is required for such study. Each method taken individually presents a noticeable level of uncertainty, and thus the evaluation they produce requires confirmation. Moreover, icings' remnants which are observed in spring might not be formed through a unique source/process but rather represent aggregated features formed as a

result of multiple sources and processes. Where such a multi-origin situation occurs, non-agreement between methods is legitimate. Taking into account those limits/difficulties, the results summarized in Table 5.3 are interpreted as follows: where all applicable methods agree, contribution to formation is considered as "most likely," and where a majority of the applicable methods support the contribution of a source, that contribution is considered to be "possible."

As a consequence, Table 5.3 suggests that proglacial Icing PF in watershed B is possibly fed by Glacier B and by the moraine lake water that seeps through the moraine during the winter (Table 5.3). Icing B, observed downstream in watershed B, is most likely fed by hillslope tributaries situated upstream from the icing (Table 5.3). In the Duke watershed, the most upstream icing, namely Icing 4, is most likely fed by the Duke glacier possibly by buried ice and ice-cored moraines, small glaciers (Gl1 and 2), and tributaries within the proglacial field (Table 5.3). Icing 3 is situated downstream from Icing 4, and based on TLC images, together they formed a unique icing at least once over the study period. This is probably the reason that the sources responsible for Icing 3's formation partly overlap with those contributing to Icing 4. Small glaciers (Gl1 and 2) and hillslope tributaries most likely contributed to the formation of Icing 3, while the contribution of the main glacier is possible. There is no consensus among methods about the parent water for Icing 2. However, tributaries fed by small glaciers (Gl 4 and 5), hillslope tributaries within the alpine meadow, and potentially suprapermafrost layer water are possible contributors. Finally, the results for the most downstream icing, Icing 1, indicate the possibility of contribution of water from groundwater wells. Contribution from the suprapermafrost layer and tributaries fed by small glaciers cannot be rejected based on Table 5.3.

Table 5.3 Summary of sources identified as potential contributors to icings formation. For each method (columns), the main potential sources identified for each icing are listed (rows). "+" indicates sources that are supported by the method, and "-" indicates sources that are not supported by the method. Potential sources supported by all applicable methods are highlighted in green; those supported by no method are highlighted in red. Grey cells indicate cases where particular method is not applicable

Potential sources contributing to icing formation	Time lapse images	Water stable isotopes	Ionic signatures	Solid samples	Dissolved organic carbon
Sources for Icing PF					
Main glacier	+	+	-		
Ice-cored moraine	+	-	-		
Moraine lake	+	+	-		
Sources for Icing B					
Hillslope tributaries		+	+	+	
Groundwater wells		-	-	-	
Moraine lake		-	-	+	
Sources for Icing 1					
Glacier-fed tributaries		+	-	+	-
Hillslope tributaries		+	-	+	-
Groundwater wells		+	-	+	+
Suprapermafrost layer water		-	-	+	+
Sources for Icing 2					
Glacier-fed tributaries		+	+		-
Hillslope tributaries		+	+		-
PFL tributaries		+	-		-
Groundwater wells		-	-		+
Suprapermafrost layer water		-	+		+
Sources for Icing 3					
Main glacier	+	-	+	-	
PFL tributaries	-	+	-	+	
Glacier-fed tributaries	+	+	+	+	
Hillslope tributaries	+	+	+	+	
Suprapermafrost layer water	-	-	+	-	
Sources for Icing 4					
Main glacier	+	+	+		
Buried ice	-	+	+		
moraine lake	-	-	+		
PFL tributaries	-	+	+		
Glacier-fed tributaries	+	+	-		
Hillslope tributaries	+	+	-		

5.5.2 Is glacier runoff the most important water contributor to icing formation and winter baseflow?

Even if the results in Table 5.3 analysis lead only to a “possible” contribution of Glacier B to Icing PF growth, the analysis of the TLC images in watershed B over the two study seasons leaves no room for doubt about its contribution. Because of the proximity of the TLC to Icing PF, TLC images represent a particularly solid method for that location. Those images show

reoccurring flooding events at the proglacial field next to Glacier B outlet throughout the winter season (Figure 5.4). Moreover, the resulting ice volume cannot be produced solely by minor active sources, and according to the site's geomorphology no water source other than the glacier could produce such water volumes. This contribution is confirmed by the stable water isotope analysis in the same watershed (Figure 5.5a). The fact that the ionic signatures interpretation is not conclusive on that contribution has to be seen as a limit in the ionic method detection ability.

In the Duke valley, all applied methods support the Duke glacier's generation of Icing 4 parent water. The Duke glacier is a polythermal glacier (Flowers et al., 2014; Wilson et al., 2013). The formation of icings has been commonly associated with polythermal glaciers in the Canadian Arctic (Moorman & Michel, 2000; Wainstein et al., 2008), Greenland (Yde & Knudsen, 2005) and Svalbard (Bukowska-jania & Szafraniec, 2005; Hambrey, 1984; Sobota, 2016; Stachnik et al., 2016; Wadham et al., 200; Yde et al., 2012). Regarding the contribution of the main glacier to Icing 3 formation, it can be considered as possible according to Table 5.3. For this icing, glacier-fed tributaries are one of the two categories that all four methods identify as parent water. This can be seen as of particular interest, as unlike the Duke glacier position versus Icing 4, Icing 3 forms at a distance of more than 1 kilometer from the tributary glaciers. By forming so far from its contributing sources, Icing 3 shows a contrast with what was observed with Icing PF and Icing B which formed right at the point where the parent water was released from its source.

Liljedahl et al. (2016) suggested for Tanana River, Alaska, that ubiquitous glacier mass loss leads to a continuous supply of meltwater, which is partly used for aquifer recharge. This recharge can enhance permafrost thaw by heat advection, thus simultaneously increasing aquifer storage capacity (Lamontagne-Hallé et al., 2018; McKenzie & Voss, 2013). As a result, actual glacier retreat should lead to an increase in groundwater discharge during the winter season. While detecting the contribution to icing formation from small glaciers located at a distance from the icing, the present study does not identify if the contribution occurs via surface

or underground pathways. The mechanism described here above could, however, explain why icings did not form at the glacier snout but far downstream.

5.5.3 Role of suprapermafrost layer water in icing formation and winter baseflow

In Alaska and the Canadian Arctic, most of the studied icings have been shown to be fed by subpermafrost water (Hu & Pollard, 1997; Kane & Slaughter, 1973; Kane, 1981; Pollard, 2005; Yoshikawa et al., 2007). Several studies that addressed water provenance for icing formation in regions with continuous and discontinuous permafrost explicitly concluded that suprapermafrost water does not participate in icing formation (Kane, 1981, in central Alaska, USA; Veiette & Thomas, 1979, in NWT, Canada; and Yoshikawa et al., 2007, in Brooks Range, Alaska, USA). In this study, the results of DOC analysis confirmed the hypothesis that the samples taken from alpine meadow ponds represent water from the suprapermafrost layer. In addition, the contribution of suprapermafrost layer water to the formation of the alpine meadow icing is shown to be possible based on the major ions analysis (Figure 5.8) and is confirmed by the analysis of cryogenic precipitate for Icing 1 (Table 5.3) and DOC analysis. While we detect the suprapermafrost layer's contribution to Icing 1 formation, it is not possible to say if suprapermafrost layer water contributes throughout the winter or only at the beginning of winter season. As previously observed, icings fed by suprapermafrost water typically stop growing before the end of the winter when the water stored in the suprapermafrost layer is exhausted (Pollard, 2005).

An increase in suprapermafrost layer thickness in response to the changing climate leads to aquifer's increased storage capacity, which in turn can lead to increased winter discharge (Ge et al., 2011; Toohey et al., 2016). In addition, talik formation activates the groundwater system, which is otherwise shut down during the winter season (Lamontagne-Hallé et al., 2018). Indeed, permafrost thaws in the study region (Smith, Lewkowicz, Ednie, Maxime, & Bevington, 2015). Since our results show that suprapermafrost layer water is a probable source of icing formation, it is reasonable to suggest that the observed permafrost thaw can contribute to the increased winter discharge in the region.

5.5.4 Are there other hydrological sources that contribute substantially to icing formation and winter baseflow?

Hillslope tributaries in both watersheds were shown to be most likely contributing to winter discharge (Table 3). As observed in ionic and isotopic signatures, most of these tributaries are not fed directly by ice melt and therefore are of groundwater origins. Similarly to the suprapermafrost layer water, their water storage capacity can potentially be increased by delayed freeze-up (Rennermalm et al., 2010; Yang et al., 2002). If confirmed, those contributions could increase with an increase in air temperature.

A similar mechanism will enhance winter runoff production from moraine debris in the proglacial field. In addition, buried ice ablation in response to increasing temperatures will increase the storage capacity of the debris layer. Several methods in both watersheds detected potential contribution from buried ice formations and ice-cored moraines, suggesting that these formations can contribute to an increase in winter discharge.

Finally, moraine lakes were suggested as water sources contributing to winter baseflow. Moorman (2003) and Wainstein et al. (2014) in Bylot Island, Canada, concluded that marginal glacier lakes did not freeze entirely, and due to pressure from the top and the presence of taliks, the water from the lake contributed to the winter runoff. Formation of new taliks, expected in response to changing climate, should thus enhance the contribution of moraine lakes to winter discharge. Therefore, based on our results and existing literature, we can hypothesize that hillslope tributaries, buried ice, ice-cored moraines, and moraine lakes can potentially contribute to an increase in winter baseflow.

5.5.5 Limitation of the method

This study provides valuable information about the genesis of icings in the headwaters of two subarctic glacierized watersheds of different size and complexity. Due to an extensive sampling campaign during the summer of 2016, it was possible to obtain the hydrochemical

and isotopic signatures of most of the water sources in watersheds as well as their DOC concentrations, and hence analyze their contribution to icing formation. While this helped to account for the spatial variability of hydrological components, it was only possible to account for temporal variability of hydrological activity in the watershed by means of analysis of TLC images. In addition, due to technical problems, one of the cameras in the Duke watershed stopped working at the end of the 2015-2016 season, thus eliminating the possibility to compare the number of events for each identified hydrological source between seasons (Figure 5.7, top panel). Moreover, several sources of uncertainty stem from the sampling procedure. First, samples of hydrological components that potentially contribute to icing formation were taken during the summer, whereas icings were formed during the winter. It is possible that due to such processes as cryochemical fractionation, resulting from freezing of water, the signatures of winter hydrological sources were altered. To address this issue, we accounted for cryochemical fractionation by using relative concentrations of ions. The icing sampling protocol can also represent a source of uncertainty. Indeed, icing remnants were sampled in a way that water from different layers was mixing. This could lead to the averaging of hydrochemical and isotopic signature of different layers of icing, and was not accounted for. We argue, however, that using a multi-technique approach helps to decrease the uncertainty.

Under the assumption that the sources of icing formation are similar to the sources of winter runoff, the results of this study helped to identify potential hydrological sources comprising winter baseflow. However, for some of the identified sources, such as suprapermafrost water and buried ice, it was not possible to confirm their activity throughout the winter. Finally, despite being able to detect potential sources contributing to icing formation, the methods used in this study cannot provide any quantitative estimate of their runoff. One potential way to account for temporal variability in hydrological sources' contribution to icing formation could consist of sampling each icing layer separately. Analysis of major ions and stable water isotope coupled with positioning the TLC closer to a particular icing could potentially provide a more detailed representation of icing formation throughout the winter.

5.6 Conclusions

Icings form from hydrological sources that remain active during the winter and thus can be seen as witnesses and chroniclers of winter hydrological processes in remote subarctic watersheds. At the end of the winter season, they contain valuable information that can be used to understand complex hydrological systems. In the present study, we applied a multi-technique approach to "read" this information and to understand which hydrological sources contribute to icing formation and thus potentially contribute to winter baseflow. Those techniques were (a) analysis of time lapse images in conjunction with air temperature time series, (b) water isotopes analysis, (c) water hydrochemical analysis, and (d) solid sample analysis. A multi-technique approach was used to analyze icing remnants in two watersheds of different scale and complexity in the headwaters of the Duke River watershed in the Canadian St. Elias Mountains.

This study showed that it is possible to identify sources that remain active during the winter by studying icings in the early stage of the melt season. The results suggest that proglacial field icings in both watersheds are most likely fed by glacier runoff and runoff from hillslope tributaries. Possible contribution from the suprapermafrost layer water was detected for icings within the alpine meadow. Finally, contribution from water sources such as buried ice, ice-cored moraines, and moraine lakes was supported by some of the methods that were used, but not by all.

Even though watershed B is a small, highly glacierized catchment, it seems that the sources contributing to icing formation, and thus winter hydrological processes occurring there, are comparable to those present in the longer and wider Upper Duke watershed. Indeed, the icing formations next to both the Duke glacier and Glacier B exhibit a strong influence of their respective glacier, the signal of which weakens in icings further downstream from the glaciers. The icings in those downstream sections of both studied watersheds have hillslope tributaries as important sources. However, the Duke watershed shows a larger variety of sources, where areas with buried ice and suprapermafrost layer water were also non-negligible component of

winter runoff. The comparison between the B and the Duke watersheds shows that the size of the watershed does not affect the spatial patterns of winter runoff generation, but a larger watershed is more complex, and its sources are therefore more diverse.

In a context of ubiquitous winter discharge increase in arctic and subarctic regions, our results show that icing remnants can help overcome the lack of direct observations in these remote environments and provide new insights on winter runoff generation. The multi-technique approach used in this study provided important information about the water sources active during the winter season in the headwaters of glacierized catchments. A literature-based analysis of the possible contribution mechanisms from the icings' parent waters allows us to propose that glaciers, directly or through the ground, the suprapermafrost layer and non-glacier-related groundwater (via tributaries) could contribute to the observed regional increase in winter discharge.

5.7 Acknowledgements

This research is supported by the Geochemistry and Geodynamics Research Centre (GEOTOP) of Quebec, the Natural Science and Engineering Research Council (NSERC) of Canada, *École de technologie supèrieure*, a constituent of the *Université de Quebec* network, and the Polar Continental Shelf Program. We want to acknowledge that this research was conducted on the traditional territory of Kluane First Nation, and we are thankful for their support. We are also grateful for help from Parks Canada.

CHAPTER 6

DISCUSSION

The aim of this project was to test the hypothesis that subarctic proglacial areas play an important role in the hydrology of glacierized valleys, and that glacier retreat is not the only driver of their hydrological response to climate change. The results of this project thus will complement current knowledge necessary to accurately project the impact of environmental changes on the hydrology of subarctic glacierized watersheds. By adopting a variety of methods such as numerical modelling, statistical analysis and fieldwork-based techniques, and by focusing on both regional and watershed scales, I was able to fulfill this aim. Following sections address three research questions identified in the introduction, overall project implications, its limitations and potential ways forward.

6.1 What is the role of shrinking glaciers in recent hydrological changes in the southwestern Yukon and what are future hydrological changes in the region?

When estimating climate changes impacts on hydrology of glacierized watersheds, it is often assumed that the evolution of glacier extent is the dominant factor for hydrological changes (Hood et al., 2006). The concept of peak water (PW, see Chapter 1) illustrates well the anticipated hydrological changes in response to a decrease in glacier cover. At the early stage of glacier retreat the discharge from the watershed is projected to increase following initial increase in glacier meltwater production triggered by temperature rise. Discharge then reaches a turning point - PW - and starts decreasing following the decrease in glacier volume. In British Columbia, Canada, most of the glacierized watersheds have already reached PW (Stahl & Moore, 2006), whereas in Yukon it was reported that PW has not been reached yet (Huss & Hock, 2018; Moore et al., 2009). For instance, the Yukon River Basin, headwaters of which are situated within the study region, is projected to reach the turning point by the end of this century (Huss & Hock, 2018). Chapter 3 addressed the PW analysis in a more precise way aiming putting hydrological changes in the southwestern Yukon in a context of glacier retreat. One specificity of the research described in Chapter 3 is that while there have been studies in

the area based on trend analyses of discharge time series (Fleming & Clarke, 2003) as well as numerical model applications (Huss & Hock, 2018) to obtain new insights into hydrological changes, no study gave a thorough treatment to both.

The results of chapter 3 showed that there is a ubiquitous glacier retreat in the study area and confirmed the fast rate of glacier area losses measured in other studies (Arendt et al., 2009; Barrand & Sharp, 2010; Barrand & Sharp, 2010; Derksen et al., 2012). Moreover, it was possible to show that some of the headwaters in the region, including the Duke (9.2% glacierized) and Takhini River (2.1% glacierized) watersheds, have already reached PW. For the Takhini watershed, however, it was not possible to determine if observed changes are due to glacier retreat or change in precipitation (Chapter 3). A decade and a half ago, the Duke watershed was still exhibiting an increase in annual discharge (Fleming & Clarke, 2003), which suggests it has reached the PW relatively recently. As a result, it is anticipated that the importance of glacier meltwater contribution to runoff has already started to decline at both watersheds. For instance, Duke watershed post-PW ablation season discharge is projected to decrease to 66% (IQR 60-74%) of its current levels.

Model outputs showed that the two watersheds with a glacierized area exceeding 30% and one watershed with 2.9% glacierized area have not reached PW yet. Thus, unlike to what has been previously proposed (e.g., Birsan et al., 2005; Fleming & Clarke, 2003; Hodgkins, 2009; Pellicciotti et al., 2010), the position of watersheds in terms of PW phase does not depend on glacierized area only, but rather on the rate of glacier retreat. Projected decline in post-PW discharge, however, does seem to depend on the actual glacier cover. Peak discharge of watersheds that are currently ca 30% glacierized is projected to drop even more: to 20-50% of its levels at the end of the last century.

The conclusions from the first research question confirmed that glacier retreat does not explain all the hydrological changes observed in the region. It showed, however, that increases in yearly and ablation season discharge, decreases in flow variability and changes in ablation season start are characteristics of watersheds where the hydrological response to climate changes is dominated by the presence of glaciers (Chapter 3).

The presence of watersheds characterized by lake regime, which shares common characteristics with those with glacier regime (Chapter 3), and the complexity of the relationships between glacier retreat and hydrological changes show that it is necessary to conduct watershed-focused studies to characterize glacier retreat impact on water resources at a specific site. Chapters 4 and 5 address this conclusion from Chapter 3. In particular, they address water production in the subarctic and are focused on the headwaters of the Duke River watershed.

Results from Chapter 4 for a small subwatershed of the Upper Duke River (watershed B) show that glaciers are the dominant hydrological components of the watershed outflow during the ablation season and provide 80-90% of the total runoff. However, when glaciers meltwater production is partly shut down by snow cover, which was illustrated by the 2016 field season sampling, half of the stream runoff is generated by other sources. Chapter 5 addresses winter runoff generation of two watersheds of different complexity (Duke River watershed and B watershed). The multi-technique approach used in this study helped to confirm that glaciers also contribute to baseflow runoff throughout winter in both watersheds.

6.2 Which hydrological components play an important role in summer runoff production in the headwaters of a subarctic watershed?

Results from Chapter 3 confirmed the second part of the hypothesis, namely that glacier retreat does not entirely define the hydrological response of subarctic glacierized watersheds to climate change. Based on the background research, I hypothesized that subarctic proglacial areas play an important role in the hydrology of glacierized valleys. In order to confirm or reject this hypothesis, I first looked at the summer hydrological components of the glacierized watershed runoff at different times of the ablation season under different meteorological and environmental conditions.

Results of both Chapter 4 and 5 confirmed presences of numerous hydrological components within the hydrological systems of the B and Upper Duke River watersheds. In particular, during the ablation season, such sources as areas with buried ice, hillslope tributary inputs,

non-glacier fed streams and alpine meadow have been observed to be active in these glacierized watersheds.

Chapter 4 focuses on B watershed - a small sub-watershed in Duke River headwaters that is 36.6% glacierized. Within this watershed, I aimed to obtain new insights into summer hydrological process by disentangling the importance of various hydrological components (e.g. glacier meltwater, areas with buried ice, talus slopes, and alpine meadow) to the total summer runoff under different meteorological and environmental conditions. Those conditions included the 2015 ablation season when the region was under the influence of the marine heat wave nicknamed “Blob” (Aaron-Morrison et al., 2017; Blunden et al., 2016; Bond et al., 2015; Alaska Ocean Observing System, 2016). The “Blob” led to the above-average summer temperature in Yukon (Blunden et al., 2016). During the 2016 season, on the contrary, glacier runoff was reduced due to the presence of snow cover on glaciers.

Chapter 4 showed that, despite the important glacier cover (36.6%) the watershed mainstream is fed by other sources that, taken together can represent between 5.4±0.1% and 49.6±12% of the outflows. Such water sources as alpine meadow groundwater, non-glacier-fed stream, hillslope tributaries and buried ice areas have been shown to be among those contributors.

Thus, there are numerous hydrological components acting in a small 36.6% glacierized subarctic watershed during the ablation season. Even though glacier meltwater is still the major component of discharge, those other sources contribute substantially to the ablation season runoff. Moreover, their hydrological roles will most likely increase while glaciers continue losing their volume, as is the case for the Duke watershed (Chapter 3).

6.3 Which hydrological components are responsible for the generation of winter baseflow in the headwaters of two subarctic watersheds of different complexity?

The regional study summarized in Chapter 3 showed that some hydrological changes in southwestern Yukon cannot be only explained by glacier retreat. An increase in winter discharge magnitude and shifts in its timing were observed in all the watersheds independently

on their hydrological regime (Chapter 3). Increases in winter discharges in response to climatic changes have been previously observed for arctic and subarctic rivers in Eurasia (Danilovich et al., 2019; Lammers et al., 2001; Rennermalm et al., 2010; Smith et al., 2007; Yang et al., 2002) and in North America (Brabets & Walvoord, 2009; Jacques et al., 2009; Rennermalm et al., 2010; Walvoord & Striegl, 2007; Wang, 2019; Woo & Thorne, 2014), but no consensus on its main drivers has been reached. Just like for the ablation season, I hypothesized that subarctic proglacial areas play an important role in the winter hydrology of glacierized valleys. In this context, answering the third research question helps to obtain new insights into the generation of winter baseflow and winter hydrological processes in the highly glacierized headwaters of two subarctic watersheds of different complexity, namely the Duke and B watersheds. During the 2016 summer field work, large icing remnants were observed in the study area. Icings are formed during winter and thus it was decided to analyze their composition and their formation in order to "read out" the contained information about the winter hydrological processes at their origins.

A multi-technique approach allowed detecting winter hydrological activity within the proglacial field and alpine meadow of both the Upper Duke River and B watersheds. This methodology showed that both Duke and B1 glaciers contribute to the formation of icings in their proglacial field. However, whereas Duke glacier seems to most likely contribute to the most upstream icing formation in the Duke watershed, its signal is decreasing while moving downstream from main glacier. Small side glaciers shall not be ignored, as they seem to also contribute to downstream icing formations. Chapter 3 showed increases in winter runoff for both glacierized and non-glacierized watersheds. Alongside with these results, the composition of icings presented in Chapter 5 confirms that glaciers are important sources of winter runoff, but not the only one. Other hydrological sources could therefore be at the origin of the observed increases in baseflow.

Based on the results of Chapter 5 in each watershed (Duke and B watersheds), it was possible to observe that, apart from the main glaciers and the snow cover, there are other sources contributing to the icing formations. As during the ablation season (Chapter 4), Hillslope tributary inputs within both the alpine meadow and the proglacial field most likely participate

in building icings mass in both studied watersheds and thus are potentially involved in the winter runoff generation (Chapter 5). While hillslope tributaries seem to contribute only to the icing formation at the lower part of the B watershed, their contribution is detected for all icings in the Duke watershed. In addition, ice-cored moraines, areas with buried ice and moraine lakes seem to contribute to icing volume and thus potentially produce winter runoff (Chapter 5).

The initial goal to address this research question was to select two watersheds of different scale and complexity. While the B watershed is a small highly glacierized catchment, it turned out that the important winter hydrological processes occurring there are similar to those present in the longer and wider Upper Duke watershed. Indeed, the icing formations next to both Duke and B1 glaciers exhibit a strong influence of their respective glacier which weakens as icings are further from the glaciers. Icings in the downstream sections of both studied watersheds have hillslope tributaries as importance sources. However, the larger Duke watershed shows a larger variety of sources, with groundwater also being a non-negligible component of winter runoff. The comparison between the B and the Duke watersheds shows that the size of the watershed does not affect the spatial patterns of winter runoff generation (i.e., icings close to main glacier are mostly fed by glacier runoff, whereas as we move downstream, the contribution from other sources becomes more detectable, and glacier signal is fading), but a larger watershed is usually more complex and sources are therefore more diverse.

These new insights on winter baseflow sources presented in Chapter 5, alongside with the second research question answered in Chapter 4, provide information about the sources contributing to stream runoff in the headwaters of subarctic glacierized watersheds throughout the year. It was found that contributing sources during the ablation season also seem to be active in winter, hence highlighting the importance of the proglacial field for the hydrology of headwaters independently of the season. However, some differences in the glacier contribution to runoff exist between the ablation and winter seasons.

6.4 Project implications

6.4.1 Theoretical implications

The findings regarding the glacier contribution of Chapter 4 and Chapter 5 seem to concord with the findings of Chapter 3. Even though the scale and the context of these studies vary, they all found that glaciers are not the unique components of subarctic glacierized watershed hydrology and that they cannot be the only cause of the hydrological changes currently occurring in these environments. While Chapter 3 proposed that other sources are at the origin of these changes, Chapter 4 and 5 presented that, even for highly glacierized catchments, the hydrological importance of a proglacial field should not be overlooked. To understand the hydrological changes taking place in subarctic mountainous environments, the combination of these three research questions proposes that more attention should be given to the headwaters of glacierized watersheds without focusing only on glaciers' contribution.

This project confirms that glacier retreat cannot explain all the hydrological changes in the study region and illustrates the hydrological role of subarctic proglacial field on a watershed scale by estimating the contribution of its hydrological components to the ablation season runoff, and by detecting their hydrological activity during the winter season. Previous studies that explored runoff production in the proglacial fields of other regions have either considered only a limited number of hydrological features (e.g., Langston et al., 2011; McClymont et al., 2011; Muir et al., 2011; Williams et al., 2006) or assumed that the non-glacierized portions of the watershed only produce groundwater thus ignoring surface water production and storage in other hydrological features (e.g., Brown et al., 2006; Engel et al., 2016; Hu et al., 2019; Racoviteanu et al, 2013). This project provides an integrated view of subarctic hydrology and shows that studies about runoff generation occurring in subarctic headwaters should consider more than a glacier-, snowmelt and groundwater runoff.

Understanding the relative contribution of each water source is an important first step towards projecting accurately the response of subarctic glacierized watersheds to climate. As shown in the first part of this project, some watersheds in the area have reached their PW, which means

that glacier melt will eventually lose its dominant role in watershed runoff generation. In current watershed models, however, hydrological processes related to the presence of such features as ice-cored moraines and buried ice, are not represented (Dochartaigh et al., 2019; Levy et al., 2015). Consequently, those are not used for projections of watershed response to changes in climatic forcing. By highlighting hydrological role of sources other than glaciers, this project demonstrates that the inability to reproduce adequately runoff generation from the subarctic glacierized watershed in a numerical model could lead to inaccuracies. Thus it is important that these features are included in conceptual and numerical hydrological models. Future research focus in mountainous hydrology should be put on identifying the role of those specific hydrological features and components on a watershed scale.

6.4.2 Practical implications

Projected discharge changes for PW and post-PW phases, addressed in Chapter 3, give a good indication of how future hydrological systems will evolve and thus can be used as guidelines to help water resources management corporations adapt to future hydrological changes and make informed decisions to ensure a sustainable development for subarctic communities. This information can be particularly valuable for highly glacierized watersheds where discharge is projected to increase by up to 50%, and then drop to 20% of its current (pre-PW) values. Therefore, this project is also demonstrating the value of undertaking a PW analysis, which can provide important information for adaptation strategies.

Moreover, the first part of the project provides an approach to perform PW analysis for subarctic region that can be used for other watersheds. Most of the SWBM parameters are from the literature, and, when losses to evapotranspiration and deep infiltration can be estimated, the SWBM model can be applied to ungauged watersheds and provide valuable estimations of future changes in water resources without relying upon climate projections.

The implications of these findings are not limited to the management of water resources for local consumption. Historically, the remoteness of many subarctic communities has compelled

them to rely on fossil fuels as their main source of energy (National Resources Canada, 2018). However, in an effort to become more independent and to decrease greenhouse gases emissions, local governments have started to develop hydroelectric plants and dams during the last decades (Government of Canada, 2017). While the local power demand is likely to increase in the future, knowing the location, the timing and the magnitude of future hydrological changes is essential prior to the development of any hydroelectric project. The findings provided in this project provide useful information not only to Yukon power companies, but also to companies developing a project in a glacierized catchment.

6.5 Project limitation and ways forward

My approach has several limitations which are mainly related to fieldwork-based data collection and transferability of the results to other watersheds. Regarding the data collection, one obstacle was the short duration of field campaigns. This restriction led to limitation in sampling. Namely, it was only possible to sample once per each ablation season. Even though field campaigns were strategically planned to be conducted at different times of the ablation season, resulted sampling coverage still underrepresents the variability of meteorological conditions. A second obstacle is related to the equipment. For instance, two gauging stations were installed in both B stream and Duke River in order to support the findings of the project with absolute values of discharge for both the ablation and winter seasons. However, due to high stream dynamics, it was not possible to use discharge measurements from neither of the stations. In this context, more frequent field campaigns during the summer will help addressing issues with monitoring equipment since equipment-related problems can be detected and solved during the same summer season without the need to wait for the next one. Other potential ways forward can include using ultrasonic measurements of water surface change, or using backpack drill to attach gauging stations to large stable boulders.

A second group of limitations is related to the complexity of the studied watersheds and thus the potential over-simplifications when making generalizations based on the results of this project about other subarctic glacierized watersheds. Even though the fieldwork-based part of

the project covered two watersheds of different size and complexity (Upper Duke River watershed and B watershed), it is hard to judge if other watersheds in the area behave similarly. In this context, a logical way forward would be conducting similar analysis in other glacierized watersheds of the region to detect potential similarities.

Furthermore, it was not possible to quantify the relative contribution of the different sources to winter baseflow and, for some of them, confirm their activity throughout the winter. However, the main goal of this study was to determine if icing formations are coming from one or many water sources. The results have shown that the water composing the icings have various origins, which explains the complexity behind the winter runoff increase observed in subarctic rivers.

In general, the results of this project suggest that, in the future, more research should be done on quantifying the role of different hydrological features (i.e., areas with buried ice and ice-cored moraines, hillslope tributaries from talus slopes) on a watersheds scale. In particular, this project illustrates the need to understand better the changes in water storage capacity and water path ways of the identified important hydrological features at different times during both winter and summer seasons. This will in turn help to understand how the water production of these features will be affected by climate change. In order to address the latter, it is necessary to develop continuous monitoring systems in subarctic glacierized watershed to analyse the evolution of the contribution for each hydrological feature throughout the year. Finally, the results of this project highlight the need to develop a numerical model plug-in which will represent a proglacial field in numerical hydrological models.

CONCLUSIONS

In this project I hypothesize that, to accurately project the response of subarctic glacierized catchments to environmental changes, it is necessary to better understand the role of hydrological components other than glacier meltwater in runoff production. I, thus, set out to explore the role of the subarctic proglacial areas in the hydrology of glacierized watersheds.

The results confirm that glacier retreat, even if shown being of primary importance, does not explain all the hydrological changes in the study region by itself. This project demonstrates that hydrological components of proglacial areas such as hillslope tributaries, and possibly buried ice areas, contribute significantly (up to 50%) to runoff production during the ablation season. It was also found that the same contributing sources are, at least at certain times, active during the winter, hence highlighting the importance of a proglacial field for the hydrology of headwaters during both seasons. In addition, the results of this project demonstrate the benefits of using a multi-technique approach to study complex and remote environments such as glacierized subarctic watersheds. There is an uncertainty associated with each method which can make their individual use potentially unconvincing. However, by applying several complementary methods that converge to agreeing results, we are more confident in the conclusions of this study. In the light of the above, this project shows that a multi-technique approach is potentially more reliable and should be privileged to study hydrological processes in the subarctic.

The findings of this project show that, in order to understand the hydrological changes taking place in subarctic mountainous environments, more attention should be given to the headwaters of glacierized watersheds, focusing on glaciers' contribution of course but without omitting the other water sources. Instead, future research should focus on identifying the role of specific hydrological features and components, such as areas with buried ice and talus slopes, on a watershed scale. Finally, the present thesis tends to demonstrate the importance of working towards incorporating the important and complex hydrological components, such as buried ice

formations, moraines and talus slopes, identified in this study in conceptual and numerical hydrological models.

LIST OF BIBLIOGRAPHICAL REFERENCES

Aaron-Morrison, A. P., Ackerman, S. A., Adams, N. G., Adler, R. F., Albanil, A., Alfaro, E. J., & Romanovsky, V. E. (2017). State of the climate in 2016. *Bulletin of the American Meteorological Society*, *98*(8), Si-S280. https://doi.org/10.1175/2017BAMSStateoftheClimate.1

Ajami, H., Troch, P. A., Maddock, T., Meixner, T., & Eastoe, C. (2011). Quantifying mountain block recharge by means of catchment-scale storage-discharge relationships. *Water Resources Research*, *47*(4), pp 1–14. https://doi.org/10.1029/2010WR009598

Anderson, L., Abbott, M. B., Finney, B. P., & Burns, S. J. (2005). Regional atmospheric circulation change in the North Pacific during the Holocene inferred from lacustrine carbonate oxygen isotopes, Yukon Territory, Canada. *Quaternary Research*, *64*(1), 21–35. https://doi.org/10.1016/j.yqres.2005.03.005

Arendt, A. A., Walsh, J., & Harrison, W. (2009). Changes of Glaciers and Climate in Northwestern North America during the Late Twentieth Century. *Journal of Climate*, *22*(15), 4117–4134. https://doi.org/10.1175/2009JCLI2784.1

Arendt, A., Echelmeyer, K., Harrison, W., Lingle, C., Zirnheld, S., Valentine, V., & Druckenmiller, M. (2006). Updated estimates of glacier volume changes in the western Chugach Mountains, Alaska, and a comparison of regional extrapolation methods. *Journal of Geophysical Research: Earth Surface*, *111*(3), pp 1–12. https://doi.org/10.1029/2005JF000436

Arendt, Anthony a, Echelmeyer, K. a, Harrison, W. D., Lingle, C. S., & Valentine, V. B. (2002). Rapid wastage of Alaska glaciers and their contribution to rising sea level. *Science (New York, N.Y.)*, *297*(5580), pp 382–386. https://doi.org/10.1126/science.1072497

Arndt, D. S., Baringer, M. O., Johnson, M. R., Alexander, L. V., Diamond, H. J., Fogt, R. L., & Willett, K. M. (2010). State of the climate in 2009. *Bulletin of the American Meteorological Society*, *91*(7). https://doi.org/10.1175/BAMS-91-7-StateoftheClimate

Bacon, F. (1960). *The New Organon and related writings*. (F. H. Anderson, Ed.). New York: Liberal Arts Press.

Bælum, K., & Benn, D. I. (2011). Thermal structure and drainage system of a small valley glacier (Tellbreen, Svalbard), investigated by ground penetrating radar. *Cryosphere*, *5*(1), pp 139–149. https://doi.org/10.5194/tc-5-139-2011

Bahr, B., Meier, F., & Peckham, S. D. (1997). The physical basis of glacier volume-area

scaling perturbations in the ice mass balance rate D (rate of ice accumulation area at relatively high elevations low elevations (D < 0 on a yearly average), Volume-Size. *Journal of Geophysical Research*, *102*(B9), pp 20355–20362. https://doi.org/doi:10.1029/97JB01696

Baraer, M., Mark, B. G., McKenzie, J. M., Condom, T., Bury, J., Huh, K.-I., & Rathay, S. (2012). Glacier recession and water resources in Peru's Cordillera Blanca. *Journal of Glaciology*, *58*(207), pp 134–150. https://doi.org/10.3189/2012JoG11J186

Baraer, M., McKenzie, J. M., Mark, B. G., Bury, J., & Knox, S. (2009). Characterizing contributions of glacier melt and groundwater during the dry season in a poorly gauged catchment of the Cordillera Blanca (Peru). *Advances in Geosciences*, *22*, pp 41–49. Retrieved from https://kb.osu.edu/dspace/handle/1811/49183

Baraer, M., McKenzie, J. M., Mark, B. G., Gordon, R. P., Bury, J., Condom, T., & Fortner, S. (2014). Contribution of groundwater to the outflow from ungauged glacierized catchments: a multi-site study in the tropical Cordillera Blanca, Peru. *Hydrological Processes*. https://doi.org/10.1002/hyp.10386

Baraer, M., McKenzie, J., & Mark, B. G. (2017). Applied Geochemical Methods for Mountain Hydrology Workshop. Montreal.

Baraer, Michel, Mckenzie, J., Mark, B. G., Gordon, R., Bury, J., Condom, T., & Fortner, S. K. (2015). Contribution of groundwater to the outflow from ungauged glacierized catchments: A multi-site study in the tropical Cordillera Blanca, Peru. *Hydrological Processes*, *29*(11), pp 2561–2581. https://doi.org/10.1002/hyp.10386

Barnett, A. P. (1974). Hydrological Studies of the Slims River, Yukon, June-August 1970. *Icefield Ranges Research Project, Scientific Results*, *4*.

Barnett, T. P., Adam, J. C., & Lettenmaier, D. P. (2005). Potential impacts of a warming climate on water availability in snow-dominated regions. *Nature*, *438*(7066), pp 303–309. https://doi.org/10.1038/nature04141

Barrand, N. E., & Sharp, M. J. (2010). Sustained rapid shrinkage of Yukon glaciers since the 1957-1958 International Geophysical Year. *Geophysical Research Letters*, *37*(7). https://doi.org/10.1029/2009GL042030

Beamer, J. P., Hill, D. F., McGrath, D., Arendt, A., & Kienholz, C. (2017). Hydrologic impacts of changes in climate and glacier extent in the Gulf of Alaska watershed. *Water Resources Research*, *53*(9), 7502–7520. https://doi.org/10.1002/2016WR020033

Beniston, M., Farinotti, D., Stoffel, M., Andreassen, L. M., Coppola, E., Eckert, N., & Vincent,

C. (2018). The European mountain cryosphere: a review of its current state, trends, and future challenges. *Cryosphere*, *12*(18), pp 759–794. https://doi.org/10.5194/tc-12-759-2018

Benn, D. I., Bolch, T., Hands, K., Gulley, J., Luckman, A., Nicholson, L. I., & Wiseman, S. (2012). Response of debris-covered glaciers in the Mount Everest region to recent warming, and implications for outburst flood hazards. *Earth-Science Reviews*, *114*(1–2), pp 156–174. https://doi.org/10.1016/j.earscirev.2012.03.008

Bense, V. F., Kooi, H., Ferguson, G., & Read, T. (2012). Permafrost degradation as a control on hydrogeological regime shifts in a warming climate. *Journal of Geophysical Research: Earth Surface*, *117*(3), pp 1–18. https://doi.org/10.1029/2011JF002143

Berthier, E., Schiefer, E., Clarke, G. K. C., Menounos, B., & Rémy, F. (2010). Contribution of Alaskan glaciers to sea-level rise derived from satellite imagery. *Nature Geoscience*, *3*(2), pp 92–95. https://doi.org/10.1038/ngeo737

Beven, K. (2006). A manifesto for the equifinality thesis. *Journal of Hydrology*, *320*(1–2), pp 18–36. https://doi.org/10.1016/j.jhydrol.2005.07.007

Birsan, M. V., Molnar, P., Burlando, P., & Pfaundler, M. (2005). Streamflow trends in Switzerland. *Journal of Hydrology*, *314*(1–4), pp 312–329. https://doi.org/10.1016/j.jhydrol.2005.06.008

Bitz, C., & Battisti, D. (1999). Interannual to decadal variability in climate and the glacier mass balance in Washington, Western Canada, and Alaska. *Journal of Climate*, *12*(11), pp 3181–3196. https://doi.org/10.1175/1520-0442(1999)012<3181:ITDVIC>2.0.CO;2

Bliss, A., Hock, R., & Radić, V. (2014). Global response of glacier runoff to twenty-first century climate change. *Journal of Geophysical Research*, *119*, pp 1–14. https://doi.org/10.1002/2013JF002931.Received

Blume, T., van Meerveld, I., & Weiler, M. (2017). The role of experimental work in hydrological sciences–insights from a community survey. *Hydrological Sciences Journal*, *62*(3), pp 334–337. https://doi.org/10.1080/02626667.2016.1230675

Blunden, J., Arndt, D., Berry, D., Hughes, C., Jevrejeva, S., & Naveria Garabato, A. (2016). State of the Climate in 2015. *Bulletin of the American Meteorological Society*, *97*(8) (Supplement), pp 1–275. https://doi.org/10.1175/2017BAMSStateoftheClimate.1

Bond, N. A., Cronin, M. F., Freeland, H., & Mantua, N. (2015). Causes and impacts of the 2014 warm anomaly in the NE Pacific. *Geophysical Research Letters*, *42*(9), pp 3414–3420. https://doi.org/10.1002/2015GL063306

Bonsal, B. R., Shabbar, Am., & Higuchi, K. (2001). Impacts of low frequency variability

modes on Canadian winter temperature. *International Journal of Climatology*, *21*(1), pp 95–108. https://doi.org/10.1002/joc.590

Box, J. E., & Steffen, K. (2001). Sublimation on the Greenland ice sheet from automated weather station observations. *Journal of Geophysical Research Atmospheres*, *106*(D24), pp 33965–33981. https://doi.org/10.1029/2001JD900219

Brabets, T. P., & Walvoord, M. A. (2009a). Trends in streamflow in the Yukon River Basin from 1944 to 2005 and the influence of the Pacific Decadal Oscillation. *Journal of Hydrology*, *371*(1–4), pp 108–119. https://doi.org/10.1016/j.jhydrol.2009.03.018

Brabets, T. P., & Walvoord, M. A. (2009b). Trends in streamflow in the Yukon River Basin from 1944 to 2005 and the influence of the Pacific Decadal Oscillation. *Journal of Hydrology*, *371*(1–4), pp 108–119. https://doi.org/10.1016/j.jhydrol.2009.03.018

Brabets, T. P., Wang, B., & Meade, R. H. (2000). Environmental and Hydrologic Overview of the Yukon River Basin, Alaska and Canada. *U.S. Geological Survey*, 106.

Braithwaite, R. J., & Olesen, O. B. (1988). Effect of glaciers on annual run-off, Johan Dahl, South Greenland. *Journal of Glaciology*, *34*(117).

Brown, J., Ferrians, O., Heginbottom, J., & Melnikov, E. (2002). Circum-Arctic Map of Permafrost and Gound-Ice Conditions, version 2. *National Snow & Ice Data Center*, *Boulder*, *C*, 2002.

Brown, L. E., Hannah, D. M., Milner, A. M., Soulsby, C., Hodson, A. J., & Brewer, M. J. (2006). Water source dynamics in a glacierized alpine river basin (Taillon-Gabiétous, French Pyrénées). *Water Resources Research*, *42*(8). https://doi.org/10.1029/2005WR004268

Brown, R. D., & Braaten, R. O. (1998). Spatial and Temporal Variability of Canadian Monthly Snow Depths, 1946-1995. *Atmosphere-Ocean*, *36*(1), pp 37–54. https://doi.org/10.1080/07055900.1998.9649605

Brun, F., Berthier, E., Wagnon, P., Kääb, A., & Treichler, D. (2017). A spatially resolved estimate of High Mountain Asia glacier mass balances from 2000 to 2016. *Nature Geoscience*, *10*(9), pp 668–673. https://doi.org/10.1038/ngeo2999

Bryan, M. (1972). Variations in Quality and Quantity of Slims River Water, Yukon Territory. *Canadian Journal of Earth Sciences*, *9*, pp 1469–1478.

Bukowska-jania, E. (2007). The role of glacier system in migration of calcium carbonate on Svalbard. *Polish Polar Research*, *28*(2), pp 137–155. Retrieved from http://polar.pan.pl/ppr28/ppr28-137EN.htm

Bukowska-jania, E., & Szafraniec, J. (2005). Distribution and morphometric characteristics of icing fields in Svalbard. *Polar Research*, *24*, pp 41–53.

Bunbury, J., & Gajewski, K. (2012). Temperatures of the past 2000 years inferred from lake sediments, southwest Yukon Territory, Canada. *Quaternary Research*, *77*(3), pp 355–367. https://doi.org/10.1016/j.yqres.2012.01.002

Burn, C. R. (1994). Permafrost, tectonics, and past and future regional climate change, Yukon and adjacent Northwest Territories. *Canadian Journal of Earth Sciences*, *31*, pp 182–191. https://doi.org/10.1139/e94-015

Burn, D. H., Cunderlik, J. M., & Pietroniro, A. (2004). Hydrological trends and variability in the Liard River basin. *Hydrological Sciences Journal*, *49*(1), pp 53–68. https://doi.org/10.1623/hysj.49.1.53.53994

Burn, D. H., & Hag Elnur, M. A. (2002). Detection of hydrologic trends and variability. *Journal of Hydrology*, *255*(1–4), pp 107–122. https://doi.org/10.1016/S0022-1694(01)00514-5

Burt, T. P., & McDonnell, J. J. (2015). Whither field hydrology? the need for discovery science and outrageous hydrological hypotheses. *Water Resources Research*, *51*(8), pp 5919–5928. https://doi.org/10.1002/2014WR016839

Cable, J., Ogle, K., & Williams, D. (2011). Contribution of glacier meltwater to streamflow in the Wind River Range, Wyoming, inferred via a Bayesian mixing model applied to isotopic measurements. *Hydrological Processes*, *25*(February), pp 2228–2236. https://doi.org/10.1002/hyp.7982

Canadian National Committee for the International Hydrological Decade. (1978). *Hydrological Atlas of Canada/Atlas Hydrologique du Canada.*

Carey, K. L. (1973). *Icings developed from surface water and ground water. US Army Cold Regions Research and Engineering Laboratory Monograph* (Vol. III).

Carey, M., Baraer, M., Mark, B. G., French, A., Bury, J., Young, K. R., & McKenzie, J. M. (2014). Toward hydro-social modeling: Merging human variables and the social sciences with climate-glacier runoff models (Santa River, Peru). *Journal of Hydrology*, *518*, pp 60–70. https://doi.org/10.1016/j.jhydrol.2013.11.006

Carey, S. K. (2003). Dissolved organic carbon fluxes in a discontinuous permafrost subarctic alpine catchment. *Permafrost and Periglacial Processes*, *14*(2), pp 161–171. https://doi.org/10.1002/ppp.444

Carey, S. K., & Quinton, W. L. (2004). Evaluating snowmelt runoff generation in a discontinuous permafrost catchment using stable isotope, hydrochemical and hydrometric data. *Nordic Hydrology*, *35*(4–5), pp 25–29. Retrieved from http://www.wlu.ca/documents/29071/Carey%26Quinton_2004.pdf

Carey, S. K., & Woo, M.-K. K. (1998). Snowmelt Hydrology of Two Subarctic Slopes, Southern Yukon, Canada. *Nordic Hydrology*, *29*, pp 331–346. Retrieved from http://cat.inist.fr/?aModele=afficheN&cpsidt=1652766

Carey, S. K., & Woo, M.-K. K. (2001a). Slope runoff processes and flow generation in a subarctic, subalpine catchment. *Journal of Hydrology*, *253*, pp 110–129. Retrieved from http://www.sciencedirect.com/science/article/pii/S0022169401004784

Carey, S. K., & Woo, M.-K. K. (2001b). Spatial variability of hillslope water balance, Wolf Creek basin, subarctic Yukon. *Hydrological Processes*, *15*(16), pp 3113–3132. https://doi.org/10.1002/hyp.319

Chen, J., & Ohmura, A. (1990). Estimation of Alpine glacier water resources and their change since the 1870s. *Hydrology in Mauntainous Regions*, *V*(193), pp 127–136.

Chesnokova, A., Baraër, M., Laperrière-Robillard, T., & Huh, K. (2020). Linking Mountain Glacier Retreat and Hydrological Changes in Southwestern Yukon. *Water Resources Management*, *56*. https://doi.org/10.1029/2019WR025706

Christophersen, N., Neal., C., Hooper, R. P., Vogt, R. D., & Andersen, S. (1990). Modeling streamwater chemistry as a mixture of soiwater end-members - a step towards 2nd generation acidification models. *Journal of Hydrology*, *116*, pp 307–320.

Clark, I. D., & Lauriol, B. (1997). Aufeis of the Firth River Basin, Northern Yukon, Canada: Insights into Permafrost Hydrogeology and Karst. *Arctic and Alpine Research*, *29*(2), pp 240–252.

Clarke, G. K. C., Jarosch, A. H., Anslow, F. S., Radić, V., & Menounos, B. (2015). Projected deglaciation of western Canada in the twenty-first century. *Nature Geoscience*, *8*(5), pp 372–377. https://doi.org/10.1038/ngeo2407

Clarke, G. K. C., Schmok, J. P., Simon, C., Ommanney, L., & Collins, S. G. (1986). Characteristics of Surge-Type Glaciers. *Journal of Geophysical Research*, *91*(5), pp 7165–7180.

Clarke, R. T. (2010). On the (mis)use of statistical methods in hydro-climatological research. *Hydrological Sciences Journal*, *55*(2), pp 139–144. https://doi.org/10.1080/02626661003616819

Clow, D. W., Schrott, L., Webb, R., Campbell, D. H., Torizzo, A., & Dornblaser, M. (2003). Ground Water Occurrence and Contributions to Streamflow in an Alpine Catchment, Colorado Front Range. *Ground Water*, *41*(7), pp 937–950.

Cochand, M., Christe, P., Ornstein, P., & Hunkeler, D. (2019). Groundwater Storage in High Alpine Catchments and Its Contribution to Streamflow. *Water Resources Research*, *55*(4), pp 2613–2630. https://doi.org/10.1029/2018WR022989

Colpron, M., Israel, S., Murphy, S., Pigage, D., & Moynihan, D. (2016). Yukon bedrock geology map, scale 1:1 000 000, map and legend. *Yukon Geological Survey*. https://doi.org/10.1109/ciced.2018.8592188

Condom, T., Escobar, M., Purkey, D., Pouget, J. C., Suarez, W., Ramos, C., & Gomez, J. (2012). Simulating the implications of glaciers' retreat for water management: A case study in the Rio Santa basin, Peru. *Water International*, *37*(4), pp 442–459. https://doi.org/10.1080/02508060.2012.706773

Connon, R., Devoie, É., Hayashi, M., Veness, T., & Quinton, W. L. (2018). The Influence of Shallow Taliks on Permafrost Thaw and Active Layer Dynamics in Subarctic Canada. *Journal of Geophysical Research: Earth Surface*, *123*(2), pp 281–297. https://doi.org/10.1002/2017JF004469

Cooper, R. ., Wadham, J., Tranter, M., Hodgkins, R., & Peters, N. . (2002). Groundwater hydrochemistry in the active layer of the proglacial zone, Finsterwalderbreen, Svalbard. *Journal of Hydrology*, *269*(3–4), pp 208–223. https://doi.org/10.1016/S0022-1694(02)00279-2

Coplen, T. B. (1996). Deciphering when Patients Feign Symptoms to Avoid Incarceration - Journal of Emergency Medical Services. *Geochimica et Cosmochimica Acta*, *60*(17), 3359–3360. Retrieved from https://www.jems.com/articles/print/volume-39/issue-8/departments-columns/berry-musing/deciphering-when-patients-feign-symptoms.html

Cox, A. D. R., & Stuart, A. (1955). Some Quick Sign Tests for Trend in Location and Dispersion. *Biometrika Trust*, *42*(1), pp 80–95.

Croce, F. A., & Milana, J. P. (2002). Internal structure and behaviour of a rock glacier in the arid Andes of Argentina. *Permafrost and Periglacial Processes*, *13*(4), pp 289–299. https://doi.org/10.1002/ppp.431

Crompton, J. W., & Flowers, G. E. (2015). Correlations of suspended sediment size with bedrock lithology and glacier dynamics, pp 1–19.

Crossman, J., Bradley, C., Boomer, I., & Milner, A. M. (2011). Water Flow Dynamics of Groundwater-Fed Streams and Their Ecological Significance in a Glacierized Catchment. *Arctic, Antarctic, and Alpine Research*, *43*(3), pp 364–379. https://doi.org/10.1657/1938-4246-43.3.364

Croux, C., & Dehon, C. (2010). Influence functions of the Spearman and Kendall correlation measures. *Statistical Methods and Applications*, *19*(4), pp 497–515 . https://doi.org/10.1007/s10260-010-0142-z

Dahlke, H. E., Lyon, S. W., Stedinger, J. R., Rosqvist, G., & Jansson, P. (2012). Contrasting trends in hydrologic extremes for two sub-arctic catchments in northern Sweden - does glacier melt matter? *Hydrology and Earth System Sciences Discussions*, *9*(1), pp 1041–1084. https://doi.org/10.5194/hessd-9-1041-2012

Dahmen, E. R., & Hall, M. J. (1990). *Screening of hydrological data: Tests for stationarity and relative consistency*. Wageningen, The Netherlands: International Institute for Land Reclamation and Improvement.

Danilovich, I., Zhuravlev, S., Kurochkina, L., & Groisman, P. (2019). The Past and Future Estimates of Climate and Streamflow Changes in the Western Dvina River Basin. *Frontiers in Earth Science*, *7*(August 2019), pp 1–16. https://doi.org/10.3389/feart.2019.00204

de Kok, R. J., Tuinenburg, O. A., Bonekamp, P. N. J., & Immerzeel, W. W. (2018). Irrigation as a Potential Driver for Anomalous Glacier Behavior in High Mountain Asia. *Geophysical Research Letters*, *45*(4), pp 2047–2054. https://doi.org/10.1002/2017GL076158

Derksen, C., Smith, S. L., Sharp, M. J., Brown, L. E., Howell, S., Copland, L., & Walker, A. (2012). Variability and change in the Canadian cryosphere. *Climatic Change*, *115*(1), pp 59–88. https://doi.org/10.1007/s10584-012-0470-0

Dery, S. J., Stahl, K., Moore, R. D., Whitfield, P. H., Menounos, B., & Burford, J. E. (2009). Detection of runoff timing changes in pluvial, nival, and glacial rivers of western Canada. *Water Resources Research*, *45*(4), pp 1–11. https://doi.org/10.1029/2008WR006975

Dietermann, N., & Weiler, M. (2013). Spatial distribution of stable water isotopes in alpine snow cover. *Hydrology and Earth System Sciences*, *17*(7), pp 2657–2668. https://doi.org/10.5194/hess-17-2657-2013

Dillard, A. (1988). *Teaching a Stone to Talk: Expeditions and Encounters*. New York, NY: Harper Perennial. Retrieved from http://books.google.com/books?id=ZlGXyYoJH2EC&pgis=1

Dochartaigh, B. É. Ó., Macdonald, A. M., Black, A. R., Everest, J., Wilson, P., & Darling, W. G. (2019). Groundwater – glacier meltwater interaction in proglacial aquifers. *Hydrological Earth Systems*, *23*, pp 4527–4539.

Dorava, J. M., & Milner, A. M. (2000). Role of lake regulation on glacier fed rivers in enhancing salmon productivity: The Cook Inlet watershed south central Alaska, USA. *Hydrological Processes*, *14*(16–17), pp 3149–3159. https://doi.org/10.1002/1099-1085(200011/12)14:16/17<3149::AID-HYP139>3.0.CO;2-Y

Drever, J. I. (1997). *The Geochemistry of Natural Waters: Surface and Groundwater*

Environments (third). New jersey, USA: Prentice Hall. https://doi.org/10.2134/jeq1998.00472425002700010037x

Drever, J. I. (2005). *Surface and Ground Water, Weathering, and Soils*. Oxford: Eslevier-Pergamon. https://doi.org/10.2134/jeq2006.0618br

Duethmann, D., Bolch, T., Farinotti, D., Kriegel, D., Vorogushyn, S., Merz, B., & Güntner, A. (2015). Attribution of streamflow trends in snow-and glacier melt dominated catchments of the Tarim River, Central Asia. *Water Resources Research*, *51*, pp 4727–4750. https://doi.org/10.1002/2014WR016716.Received

Eaton, B., & Moore, R. D. (2010). Chapter 4 - Regional Hydrology. In K. D. Pike, R.G., Redding, T.E., Moore, R.D., Winkler, R.D. and Bladon (Ed.), *Compendium of Forest Hydrology and Geomorphology in British Columbia* (B.C. Min., Vol. 2, p. 446). Kamloops, B.C.: B.C. Min. For. Range, For. Sci. Prog., Victoria, B.C. and FORREX Forum for Research and Extension in Natural Resources. Retrieved from https://www.for.gov.bc.ca/hfd/pubs/Docs/Lmh/Lmh66.htm

Engel, M., Penna, D., Bertoldi, G., Dell'Agnese, A., Soulsby, C., & Comiti, F. (2016). Identifying run-off contributions during melt-induced run-off events in a glacierized alpine catchment. *Hydrological Processes*, *30*(3), pp 343–364. https://doi.org/10.1002/hyp.10577

Engel, Michael, Penna, D., Bertoldi, G., Vignoli, G., Tirler, W., & Comiti, F. (2019). Controls on spatial and temporal variability in streamflow and hydrochemistry in a glacierized catchment. *Hydrology and Earth System Sciences*, *23*(4), pp 2041–2063. https://doi.org/10.5194/hess-23-2041-2019

Engelhardt, M., Schuler, T. V., & Andreassen, L. M. (2014). Contribution of snow and glacier melt to discharge for highly glacierised catchments in Norway. *Hydrology and Earth System Sciences*, *18*(2), pp 511–523. https://doi.org/10.5194/hess-18-511-2014

Evans, S. G., & Ge, S. (2017). Contrasting hydrogeologic responses to warming in permafrost and seasonally frozen ground hillslopes. *Geophysical Research Letters*, *44*(4), pp 1803–1813. https://doi.org/10.1002/2016GL072009

Evans, S. G., Ge, S., Voss, C. I., & Molotch, N. P. (2018). The Role of Frozen Soil in Groundwater Discharge Predictions for Warming Alpine Watersheds. *Water Resources Research*, *54*(3), pp 1599–1615. https://doi.org/10.1002/2017WR022098

Everest, J., & Bradwell, T. (2003). Buried glacier ice in southern Iceland and its wider significance. *Geomorphology*, *52*(3–4), pp 347–358. https://doi.org/10.1016/S0169-555X(02)00277-5

Farinotti, D., Immerzeel, W. W., Kok, R. J. De, Quincey, D. J., & Dehecq, A. (2020).

Manifestations and mechanisms of the Karakoram glacier Anomaly. *Nature Geoscience*, *13*(January). https://doi.org/10.1038/s41561-019-0513-5

Farinotti, D., Usselmann, S., Huss, M., Bauder, A., & Funk, M. (2012). Runoff evolution in the Swiss Alps: Projections for selected high-alpine catchments based on ENSEMBLES scenarios. *Hydrological Processes*, *26*(13), pp 1909–1924. https://doi.org/10.1002/hyp.8276

Farnsworth, R. K., & Thompson, E. S. (1982). Mean Monthly, Seasonal , and Annual Pan Evaporation for the United States. *NOAA Technical Reports*, (December), pp 1–82.

Finger, D., Heinrich, G., Gobiet, A., & Bauder, A. (2012). Projections of future water resources and their uncertainty in a glacierized catchment in the Swiss Alps and the subsequent effects on hydropower production during the 21st century. *Water Resources Research*, *48*(2), pp 1–20. https://doi.org/10.1029/2011WR010733

Fleming, S. W. (2004). *Comparative Statistical Hydroclimatology of Glacial and Nival Rivers in Southwest Yukon and Northwest British Columbia*. *The University of British Columbia*. Retrieved from http://biblioteca.usac.edu.gt/tesis/08/08_2469_C.pdf

Fleming, S. W. (2005). Comparative analysis of glacial and nival streamflow regimes with implications for lotic habitat quantity and fish species richness. *River Research and Applications*, *21*(4), pp 363–379. https://doi.org/10.1002/rra.810

Fleming, S. W. (2018). Machine learning, soft computing, and complex systems analysis: emerging approaches for discovering and predicting nonlinear phenomena in water resources and climate. In *Presentation to the Center for Nonlinear Studies*. Los Alamos National Laboratory, Los Alamos, NM.

Fleming, S. W., & Clarke, G. K. C. (2003). Glacial Control of Water Resource and Related Environmental Responses to Climatic Warming: Empirical Analysis Using Historical Streamflow Data from Northwestern Canada. *Canadian Water Resources Journal*, *28*(1), pp 69–86. https://doi.org/10.4296/cwrj2801069

Fleming, S. W., & Clarke, G. K. C. (2005a). Attenuation of high-frequency interannual streamflow variability by watershed glacial cover. *Journal of Hydraulic Engineering*, *131*(7), pp 615–618. https://doi.org/10.1061/(ASCE)0733-9429(2005)131:7(615)

Fleming, S. W., & Clarke, G. K. C. (2005b). Attenuation of High-Frequency Interannual Streamflow Variability by Watershed Glacial Cover. *Journal of Hydraulic Engineering*, *131*(2), pp 97–105. https://doi.org/10.1061/(ASCE)0733-9429(2005)131

Fleming, S. W., & Dahlke, H. E. (2014a). Erratum: Modulation of linear and nonlinear

hydroclimatic dynamics by mountain glaciers in Canada and Norway: Results from information-theoretic polynomial selection. *Canadian Water Resources Journal*, *39*(4), 472. https://doi.org/10.1080/07011784.2014.974308

Fleming, S. W., & Dahlke, H. E. (2014b). Modulation of linear and nonlinear hydroclimatic dynamics by mountain glaciers in Canada and Norway: Results from information-theoretic polynomial selection. *Canadian Water Resources Journal*, *39*(3), pp 324–341. https://doi.org/10.1080/07011784.2014.942164

Fleming, S. W., Moore, R. D., & Clarke, G. K. C. (2006). Glacier-mediated streamflow teleconnections to the Arctic Oscillation. *International Journal of Climatology*, *26*(5), pp 619–636. https://doi.org/10.1002/joc.1273

Fleming, S. W., & Whitfield, P. (2010). Spatediotemporal mapping of ENSO and PDO surface meteorological signals in British Columbia, Yukon, and southeast Alaska. *Atmosphere - Ocean*, *48*(2), pp 122–131. https://doi.org/10.3137/AO1107.2010

Flowers, G. E., Copland, L., & Schoof, C. G. (2014). Contemporary Glacier Processes and Global Change: Recent Observations from Kaskawulsh Glacier and the Donjek Range, St. Elias Mountains. *ARCTIC*, pp 1–13. Retrieved from http://arctic.synergiesprairies.ca/arctic/index.php/arctic/article/view/4356

Fountain, A. G., & Tangborn, W. V. (1985). The Effect of Glaciers on Streamflow Variations. *Water Resources Research*, *21*(4), pp 579–586.

Frans, C., Istanbulluoglu, E., Lettenmaier, D. P., Fountain, A. G., & Riedel, J. (2018). Glacier recession and the response of summer streamflow in the Pacific Northwest United States, 1960-2099. *Water Resources Research*, pp 1–24. https://doi.org/10.1029/2017WR021764

Franz, K. J., & Karsten, L. R. (2013). Calibration of a distributed snow model using MODIS snow covered area data. *Journal of Hydrology*, *494*, pp 160–175. https://doi.org/10.1016/j.jhydrol.2013.04.026

French, H. M., & Heginbottom, J. A. (1983). Guidebook to permafrost and related features of the Northern Yukon territory and Mackenzie Delta, Canada. *Fourth International Conference on Permafrost*, 194.

Gascoin, S., Kinnard, C., Ponce, R., Lhermitte, S., MacDonell, S., & Rabatel, A. (2011). Glacier contribution to streamflow in two headwaters of the Huasco River, Dry Andes of Chile. *Cryosphere*, *5*(4), pp 1099–1113. https://doi.org/10.5194/tc-5-1099-2011

Gat, J. (2010). *Isotope hydrology: a study of water cycle, series on environmental science and management* (Vol. 6). London: Imperial College Press.

Ge, S., McKenzie, J., Voss, C., & Wu, Q. (2011). Exchange of groundwater and surface-water mediated by permafrost response to seasonal and long term air temperature variation. *Geophysical Research Letters*, *38*(14), pp 1–6. https://doi.org/10.1029/2011GL047911

Gibson, J. J., Prowse, T. D., & Peters, D. L. (2006). Hydroclimatic controls on water balance and water level variability in Great Slave Lake. *Hydrological Processes*, *20*, pp 4155–4172. https://doi.org/10.1002/hyp

Gokhman, V. V. (1987). Distribution and conditions of formation of glacial icings on spitsbergen. *Polar Geography and Geology*, *11*(4), pp 249–260. https://doi.org/10.1080/10889378709377334

Gordon, R. P., Lautz, L. K., McKenzie, J. M., Mark, B. G., Chavez, D., & Baraer, M. (2015). Sources and pathways of stream generation in tropical proglacial valleys of the Cordillera Blanca, Peru. *Journal of Hydrology*, *522*, pp 628–644. https://doi.org/10.1016/j.jhydrol.2015.01.013

Government of Canada. (2017). *Pan-Canadian Framework on Clean Growth and Climate Change*. *Government of Canada Canada*. https://doi.org/https://www.canada.ca/content/dam/themes/environment/documents/weather1/20170113-1-en.pdf

Grabcsak, J., Niewodniczanski, J., & Rozanski, K. (1983). Isotope Stratification in High Mountain Glaciers: Examples from the Peruvian Andes and Himalaya. *Journal of Glaciology*, *29*(103), pp 417–424.

Grill, G., Lehner, B., Lumsdon, A. E., MacDonald, G, K., Zarfl, C., & Liermann, C. R. (2015). An index-based framework for assessing patterns and trends in river fragmentation and flow regulation by global dams at multiple scales. *Environmental Research Letters*, *10*. https://doi.org/10.1088/1748-9326/aa5dc6

Grinsted, A. (2013). An estimate of global glacier volume. *Cryosphere*, *7*(1), pp 141–151. https://doi.org/10.5194/tc-7-141-2013

Hall, D. K., Ormsby, J. P., Bindschadler, R. A., & Siddalingaiah, H. (1987). characterizazion of snow and ice reflectance zones on glaciers using LANDSAT Thematic Mapper data. *Annals of Glaciology*, *9*.

Hambrey, M. J. (1984). Sedimentary processes and buried ice phenomena in the pro-glacial areas of Spitsbergen glaciers. *Journal of Glaciology*, *30*(104), pp 116–119. https://doi.org/10.1017/S002214300000856X

Hamed, K. H. (2009). Exact distribution of the Mann-Kendall trend test statistic for persistent data. *Journal of Hydrology*, *365*(1–2), pp 86–94. https://doi.org/10.1016/j.jhydrol.2008.11.024

Hamed, Khaled H., & Rao, R. A. (1998). A modified Mann-Kendall trend test for

autocorrelated data. *Journal of Hydrology*, *204*(1–4), pp 182–196. https://doi.org/10.1016/S0022-1694(97)00125-X

Hamlet, A. F., Mote, P. W., Clark, M. P., & Lettenmaier, D. P. (2005). Effects of temperature and precipitation variability on snowpack trends in the Western United States. *Journal of Climate*, *18*(21), pp 4545–4561. https://doi.org/10.1175/JCLI3538.1

Hamlet, A. F., Mote, P. W., Clark, M. P., & Lettenmaier, D. P. (2007). Twentieth-century trends in runoff, evapotranspiration, and soil moisture in the western United States. *Journal of Climate*, *20*(8), pp 1468–1486. https://doi.org/10.1175/JCLI4051.1

Hanshaw, M. N., & Bookhagen, B. (2014). Glacial areas, lake areas, and snow lines from 1975 to 2012: Status of the cordillera vilcanota, including the Quelccaya Ice Cap, northern central Andes, Peru. *Cryosphere*, *8*(2), pp 359–376. https://doi.org/10.5194/tc-8-359-2014

Harrington, J. S., Mozil, A., Hayashi, M., & Bentley, L. R. (2018). Groundwater flow and storage processes in an inactive rock glacier. *Hydrological Processes*, *32*(20), pp 3070–3088. https://doi.org/10.1002/hyp.13248

Harris, S. A. (1987). Altitude Trends in Permafrost Active Layer Thickness, Kluane Lake, YT. *Arctic*, *40*(3), pp 179–183. Retrieved from http://arctic.synergiesprairies.ca/arctic/index.php/arctic/article/view/1764

Hayashi, M. (2013). The Cold Vadose Zone: Hydrological and Ecological Significance of Frozen-Soil Processes. *Vadose Zone Journal*, *13*(1) https://doi.org/10.2136/vzj2013.03.0064er

Hayashi, Masaki. (2019). Alpine Hydrogeology: The Critical Role of Groundwater in Sourcing the Headwaters of the World. *Groundwater*. https://doi.org/10.1111/gwat.12965

Heckmann, T., Mccoll, S., & Morche, D. (2016). Retreating ice: Research in pro-glacial areas matters. *Earth Surface Processes and Landforms*, *41*, pp 271–276. https://doi.org/10.1002/esp.3858

Herdes, É. (2014). Evolution of seasonal variations in motion of the Kaskawulsh Glacier, Yukon Territory.

Herreid, S., Pellicciotti, F., Ayala, A., Chesnokova, A., Kienholz, C., Shea, J., & Shrestha, A. (2015). Satellite observations show no net change in the percentage of supraglacial debris-covered area in northern Pakistan from 1977 to 2014. *Journal of Glaciology*, *61*(227), pp 524–536. https://doi.org/10.3189/2015JoG14J227

Hewitt, K. (2005). The Karakoram Anomaly ? Glacier Expansion and the 'Elevation Effect,' Karakoram Himalaya The Karakoram Anomaly ? Glacier Expansion and the ' Elevation

Effect ,' Karakoram Himalaya. *Mountain Research and Development*, *25*(4), pp 332–340.

Hidalgo, H. G., Das, T., Dettinger, M. D., Cayan, D. R., Pierce, D. W., Barnett, T. P., & Nozawa, T. (2009). Detection and attribution of streamflow timing changes to climate change in the Western United States. *Journal of Climate*, *22*(13), pp 3838–3855. https://doi.org/10.1175/2009JCLI2470.1

Hijmans, R. J., Cameron, S. E., Parra, J. L., Jones, P. G., & Jarvis, A. (2005). Very high resolution interpolated climate surfaces for global land areas. *International Journal of Climatology*, *25*(15), pp 1965–1978. https://doi.org/10.1002/joc.1276

Hinzman, L. D., Bettez, N. D., Bolton, W. R., Chapin, F. S., Dyurgerov, M. B., Fastie, C. L., & Winker, K. S. (2005). Evidence and Implications of Recent Climate Change in Northern Alaska and Other Arctic Regions. *Climatic Change*, *72*, pp 251–298. https://doi.org/10.1007/~10584-005-5352-2

Hirose, J. M. R., & Marshall, S. J. (2013). Glacier Meltwater contributions and Glaciometeorological regime of the Illecillewaet river basin, British Columbia, Canada. *Atmosphere - Ocean*, *51*(4), pp 416–435. https://doi.org/10.1080/07055900.2013.791614

Hock, R. (2005). Glacier melt : a review of processes and their modelling. *Progress in Physical Geography*, *29*(3), pp 362–391. https://doi.org/10.1191/0309133305pp453ra

Hock, R., Jansson, P., & Braun, L. N. (2005). Modelling the Response of Mountain Glacier Discharge to Climate Warming. *Global Change and Mountain Regions*, pp 243–252. Retrieved from http://link.springer.com/content/pdf/10.1007/1-4020-3508-X_25.pdf

Hodgkins, G. A. (2009). Streamflow changes in Alaska between the cool phase (1947-1976) and the warm phase (1977-2006) of the Pacific Decadal Oscillation: The influence of glaciers. *Water Resources Research*, *45*(6). https://doi.org/10.1029/2008WR007575

Hodgkins, R., Tranter, M., & Dowdeswell, J. A. (1998). The hydrochemistry of runoff from a "cold-based" glacier in the High Artic (Scott Turnerbreen, Svalbard). *Hydrological Processes*, *12*(1), pp 87–103. https://doi.org/10.1002/(SICI)1099-1085(199801)12:1<87::AID-HYP565>3.0.CO;2-C

Hodgkins, R., Tranter, M., & Dowdeswell, J. A. (1997). Solute provenance, transport and denudation in a high Arctic glacierised catchment. *Hydrological Processes*, *11*(November 1995), pp 1813–1832. https://doi.org/10.1002/(SICI)1099-1085(199711)11:14<1813::AID-HYP498>3.3.CO;2-3

Hodgkins, R., Tranter, M., & Dowdeswell, J. a. (2004). The characteristics and formation of a high-arctic proglacial icing. *Geografiska Annaler*, *86*(3), pp 265–275.

Hood, E., & Berner, L. (2009). Effects of changing glacial coverage on the physical and biogeochemical properties of coastal streams in southeastern Alaska. *Journal of Geophysical Research: Biogeosciences*, *114*(3), pp 1–10. https://doi.org/10.1029/2009JG000971

Hood, J. L., Roy, J. W., & Hayashi, M. (2006). Importance of groundwater in the water balance of an alpine headwater lake. *Geophysical Research Letters*, *33*(13), pp 1–5. https://doi.org/10.1029/2006GL026611

Horton, P., Schaefli, B., Mezghani, A., Hingray, B., & Musy, A. (2006). Assessment of climate-change impacts on alpine discharge regimes with climate model uncertainty. *Hydrological Processes*, *20*(10), pp 2091–2109. https://doi.org/10.1002/hyp.6197

Howarth, P. J., & Ommanney, C. S. L. (1986). The use of Landsat Digital Data for glacier inventories. *Annals of Glaciology*, *8*, pp 90–92. Retrieved from papers://bcab5980-e9b6-4eaf-b643-294662106260/Paper/p171

Hu, X., & Pollard, W. H. (1997). The hydrologic analysis and modelling of river icing growth, North Fork Pass, Yukon Territory, Canada. *Permafrost and Periglacial Processes*, *8*(July), pp 279–294. https://doi.org/10.1002/(SICI)1099-1530(199709)8:3<279::AID-PPP260>3.3.CO;2-Z

Hu, Y., Ma, R., Wang, Y., Chang, Q., Wang, S., Ge, M., & Sun, Z. (2019). Using hydrogeochemical data to trace groundwater flow paths in a cold alpine catchment. *Hydrological Processes*, (September 2018), pp 1942–1960. https://doi.org/10.1002/hyp.13440

Huss, M. (2011). Present and future contribution of glacier storage change to runoff from macroscale drainage basins in Europe. *Water Resources Research*, *47*(7). https://doi.org/10.1029/2010WR010299

Huss, M. (2013). Density assumptions for converting geodetic glacier volume change to mass change. *The Cryosphere*, *7*(3), pp 877–887. https://doi.org/10.5194/tc-7-877-2013

Huss, M., Bauder, A., & Funk, M. (2009). Homogenization of long-term mass-balance time series. *Annals of Glaciology*, *50*(50), pp 198–206. https://doi.org/10.3189/172756409787769627

Huss, M., Bookhagen, B., Huggel, C., Jacobsen, D., Bradley, R. S., Clague, J. J., & Winder, M. (2017). Toward mountains without permanent snow and ice Earth' s Future. *Earrth's Future*, *5*(May), pp 418–435. https://doi.org/10.1002/eft2.207

Huss, M., & Hock, R. (2018a). Global-scale hydrological response to future glacier mass loss. *Nature Climate Change*, *8*(2), pp 135–140. https://doi.org/10.1038/s41558-017-0049-x

Huss, M., & Hock, R. (2018b). Global-scale hydrological response to future glacier mass loss Supplementary Information. *Nature Climate Change*. https://doi.org/10.1038/s41558-017-0049-x

Immerzeel, W.W., Lutz, A. F., Andrade, M., Bahl, A., Biemans, H., Bolch, T., & Baillie, J. E. M. (2019). Importance and vulnerability of the world's water towers. *Nature*. https://doi.org/10.1038/s41586-019-1822-y

Immerzeel, Walter W., van Beek, L. P. H., Konz, M., Shrestha, A., & Bierkens, M. F. P. (2012). Hydrological response to climate change in a glacierized catchment in the Himalayas. *Climatic Change*, *110*(3–4), pp 721–736. https://doi.org/10.1007/s10584-011-0143-4

IPCC. (2014). Climate Change 2014: Synthesis Report. Contribution of Working Groups I, II and III to the Fifth Assessment Report of the Intergovernmental Panel on Climate Change [Core Writing Team, R.K. Pachauri and L.A. Meyer (eds.)].rmany), Ismail Elgizouli (Sudan), . *IPCC, Geneva, Switxerland: Kristin Seyboth (USA)*, 151. Retrieved from https://www.ipcc.ch/pdf/assessment-report/ar5/syr/AR5_SYR_FINAL_Front_matters.pdf

IPCC (Intergovernmental Panel on Climate Change). (2019). Special Report: The Ocean and Cryosphere in a Changing Climate (final draft). *IPCC Summary for Policymalers*. https://doi.org/https://www.ipcc.ch/report/srocc/

Irvine-Fynn, T., & Hodson, A. J. (2011). Polythermal glacier hydrology: A review. *Reviews of Geophysics*, *49*(2010), pp 1–37. https://doi.org/10.1029/2010RG000350.1.

Jacobsen, D., Milner, A. M., Brown, L. E., & Dangles, O. (2012). Biodiversity under threat in glacier-fed river systems. *Nature Climate Change*, *2*(5), pp 361–364. https://doi.org/10.1038/nclimate1435

Jacques, J. M. S., Sauchyn, D. J., St. Jacques, J.-M., Sauchyn, D. J., Jacques, J. M. S., & Sauchyn, D. J. (2009). Increasing winter baseflow and mean annual streamflow from possible permafrost thawing in the Northwest Territories, Canada. *Geophysical Research Letters*, *36*(1), L01401. https://doi.org/10.1029/2008GL035822

James, F. (1980). Monte Carlo theory and practice. *Reports on Progress in Physics*, *43*(9), pp 1145–1189. https://doi.org/10.1088/0034-4885/43/9/002

James, M., Lewkowicz, A. G., Smith, S. L., & Miceli, C. M. (2013). Multi-decadal degradation and persistence of permafrost in the Alaska Highway corridor, northwest Canada. *Environmental Research Letters*, *8*(4), 045013. https://doi.org/10.1088/1748-9326/8/4/045013

Janowicz, J. R. (2008). Apparent recent trends in hydrologic response in permafrost regions of northwest Canada. *Hydrology Research*, *39*(4), pp 267–275. https://doi.org/10.2166/nh.2008.103

Janowicz, J. R. (2010). Observed trends in river ice regimes of northwaest Canada. *Hydrology Research*, *41*, pp 462–470.

Janowicz, J. R. (2011). Streamflow responses and trends between permafrost and glacierized regimes in northwestern Canada. *IAHS-AISH Publication*, *346*, pp 9–14.

Jansson, P., Hock, R., & Schneider, T. (2003). The concept of glacier storage: a review. *Journal of Hydrology*, *282*(1–4), pp 116–129. https://doi.org/10.1016/S0022-1694(03)00258-0

Jeelani, G., Feddema, J. J., Van Der Veen, C. J., & Stearns, L. (2012). Role of snow and glacier melt in controlling river hydrology in Liddar watershed (western Himalaya) under current and future climate. *Water Resources Research*, *48*(12), pp 1–16. https://doi.org/10.1029/2011WR011590

Johnson, P. G. (1971). Ice Cored Moraine Formation and Degradation, Donjek Glacier, Yukon Territory, Canada. *Geografiska Annaler. Series A, Physical Geography*, *53*(3), 198. https://doi.org/10.2307/520789

Johnson, P. G. (1978). Rock glacier types and their drainage systems, Grizzly Creek, Yukon Territory. *Canadian Journal of Earth Sciences*, *15*(9), pp 1496–1507. https://doi.org/10.1139/e78-155

Johnson, P. G. (1986). Holocene paleohydrology of the St. Elias Mountains, British Columbia and Yukon. *Geographie Physique et Quaternaire*, *40*, pp 47–53. https://doi.org/10.7202/032622ar

Johnson, P. G. (1992). Stagnant glacier ice, St Elias Mountains, Yukon. *Geografiska Annaler: Series A: Physical Geography*, *74*(1), pp 13–19.

Jones, D. B., Harrison, S., Anderson, K., & Whalley, W. B. (2019). Rock glaciers and mountain hydrology: A review. *Earth-Science Reviews*, *193*(March), pp 66–90. https://doi.org/10.1016/j.earscirev.2019.04.001

Jost, G., Moore, R. D., Menounos, B., & Wheate, R. (2012). Quantifying the contribution of glacier runoff to streamflow in the upper Columbia River Basin, Canada. *Hydrology and Earth System Sciences*, *16*(3), pp 849–860. https://doi.org/10.5194/hess-16-849-2012

Kane, D. L. (1981). Physical mechanics of aufeis growth. *Canadian Journal of Civil Engineering*, *8*(2), pp 186–195. https://doi.org/10.1139/l81-026

Kane, D. L., & Slaughter, C. W. (1973). Seasonal regime and hydrological significance of stream icings in central Alaska. *The Role of Snow and Ice in Hydrology: Proceedings of*

the Banff Symposia, pp 528–540. Retrieved from http://hydrologie.org/redbooks/a107/107041.pdf

Kang, E., Liu, C., Xie, Z., Xin, L. I., & Shen, Y. (2009). Assessment of glacier water resources based on the glacier inventory of China. *Annals of Glaciology*, *50*(53), pp 104–110. https://doi.org/10.3189/172756410790595822

Kargel, J. S., Leonard, G. J., Bishop, M. P., Kaab, A., & Raup, B. H. (2014). *Global Land Ice Measurements from Space*. https://doi.org/10.1007/978-3-540-79818-7

Kaser, G., Grosshauser, M., & Marzeion, B. (2010). Contribution potential of glaciers to water availability in different climate regimes. *Proceedings of the National Academy of Sciences of the United States of America*, *107*(47), pp 20223–20227. https://doi.org/10.1073/pnas.1008162107

Kendall, M. G. (1975). *Rank Correlation Methods* (4th ed.). New York: Oxford Univ. Press. https://doi.org/10.2307/2986801

Kienholz, C., Herreid, S., Rich, J. L., Arendt, A. A., Hock, R., & Burgess, E. W. (2015). Derivation and analysis of a complete modern-date glacier inventory for Alaska and northwest Canada. *Journal of Glaciology*, *61*(227), pp 403–420 . https://doi.org/10.3189/2015JoG14J230

Kistin, E. J., Fogarty, J., Pokrasso, R. S., McCally, M., & McCornick, P. G. (2010). Climate change, water resources and child health. *Archives of Disease in Childhood*, *95*(7), pp 545–549. https://doi.org/10.1136/adc.2009.175307

Klok, E. J., Nolan, M., & Van den Broeke, M. R. (2005). Analysis of meteorological data and the surface energy balance of McCall Glacier, Alaska, USA. *Journal of Glaciology*, *51*(174), pp 451–461. https://doi.org/10.3189/172756505781829241

Kobierska, F., Jonas, T., Kirchner, J., & Bernasconi, S. M. (2014). Linking baseflow separation and groundwater storage dynamics in an alpine basin (Dammagletscher, Switzerland). *Hydrology and Earth System Sciences Discussions*, *11*(11), pp 12187–12221. https://doi.org/10.5194/hessd-11-12187-2014

Koboltschnig, G. R., & Schöner, W. (2011). The relevance of glacier melt in the water cycle of the Alps: The example of Austria. *Hydrology and Earth System Sciences*, *15*(2008), pp 2039–2048. https://doi.org/10.5194/hess-15-2039-2011

Koboltschnig, Gernot R., Schöner, W., Zappa, M., & Holzmann, H. (2007). Contribution of glacier melt to stream runoff: if the climatically extreme summer of 2003 had happened in 197. *Annals of Glaciology*, *46*, pp 303–308. https://doi.org/10.3189/172756407782871260

Kong, Y., & Pang, Z. (2012). Evaluating the sensitivity of glacier rivers to climate change based on hydrograph separation of discharge. *Journal of Hydrology*, pp *434–435*, 121–129. https://doi.org/10.1016/j.jhydrol.2012.02.029

Kormann, C., Bronstert, A., Francke, T., Recknagel, T., & Graeff, T. (2016). Model-Based Attribution of High-Resolution Streamflow Trends in Two Alpine Basins of Western Austria. *Hydrology*, *3*(1), 7. https://doi.org/10.3390/hydrology3010007

Kundzewicz, Z. W., & Robson, A. (2000). Detecting Trend and Other Changes in Hydrological Data. *World Climate Programme - Water*, (May), 158 . https://doi.org/WMO/TD-No. 1013

La Frenierre, J. L., & Mark, B. G. (2014). A review of methods for estimating the contribution of glacial meltwater to total watershed discharge. *Progress in Physical Geography*, *38*(2), pp 173–200. https://doi.org/10.1177/0309133313516161

Lacelle, D., Lauriol, B., & Clark, I. D. (2009). Formation of seasonal ice bodies and associated cryogenic carbonates in caverne de l'ours, Québec, Canada: Kinetic isotope effects and pseudo-biogenic crystal structures. *Journal of Cave and Karst Studies*, *71*(1), pp 48–62.

Lammers, R. B., Shiklomanov, A. I., Vörösmarty, C. J., Fekete, B. M., & Peterson, B. J. (2001). Assessment of contemporary Arctic river runoff based on observational discharge records. *Journal of Geophysical Research Atmospheres*, *106*(D4), pp 3321–3334. https://doi.org/10.1029/2000JD900444

Lamontagne-Hallé, P., McKenzie, J. M., Kurylyk, B. L., & Zipper, S. C. (2018). Changing groundwater discharge dynamics in permafrost regions. *Environmental Research Letters*, *13*(8), 084017. https://doi.org/10.1088/1748-9326/aad404

Langston, G., Bentley, L. R., Hayashi, M., Mcclymont, A. F., & Pidlisecky, A. (2011). Internal structure and hydrological functions of an alpine proglacial moraine. *Hydrological Processes*, *25*(19), pp 2967–2982. https://doi.org/10.1002/hyp.8144

Larsen, J. N., Anisimov, O. A., Constable, A., Hollowed, A. B., Maynard, N., Prestrud, P., & J. M. R. Stone. (2014). Polar regions. In V. R. Barros, C. B. Field, D. J. Dokken, M. D. Mastrandrea, K. J. Mach, T. E. Bilir, & L. L. White (Eds.), *Climate change 2014: impacts, adaptation, and vulnerability. Part B, regional aspects. Contribution of Working Group II to the Fifth Assessment Report of the Intergovernmental Panel on Climate Change* (pp. 1567-1612 in). Cambridge, UK: University Press. https://doi.org/10.2307/1881805

Lauriol, B., C, M. J., & Clark, J. (1991). Localisation, Genèse et Fonte de Quelques Naleds du Nord du Yukon (Canada). *Permafrost and Periglacial Processes*, *2*(3), pp 225–236. https://doi.org/10.1002/ppp.3430020306

Levy, A., Robinson, Z., Krause, S., Waller, R., & Weatherill, J. (2015). Long-term variability of proglacial groundwater-fed hydrological systems in an area of glacier retreat,

Skeidararsandur, Iceland. *Earth Surface Processes and Landforms*, *994*(January), pp 981–994. https://doi.org/10.1002/esp.3696

Li, Z., Wang, W., Zhang, M., Wang, F., & Li, H. (2010). Observed changes in streamflow at the headwaters of the Urumqi River, eastern Tianshan, central Asia. *Hydrological Processes*, *24*, pp 217–224. https://doi.org/10.1002/hyp

Liljedahl, A., Gaedeke, A., O'Neel, S., Gatesman., T., & Douglas, T. (2016). Glacierized headwater streams as aquifer recharge corridors, subarctic Alaska. *Geophysical Research Letters*, *44*, pp 6876–6885. https://doi.org/10.1002/2017GL073834

Loukas, A., Vasiliades, L., & Dalezios, N. R. (2002). Climatic impacts on the runoff generation processes in British Columbia, Canada. *Hydrology and Earth System Sciences*, *6*(2), pp 211–228. https://doi.org/10.5194/hess-6-211-2002

Loukas, A., Vasiliades, L., & Dalezios, N. R. (2002). Climatic impacts on the runoff generation processes in British Columbia, Canada. *Hydrology and Earth System Sciences*, *6*(2), pp 211–228. https://doi.org/10.5194/hess-6-211-2002

Luthcke, S. B., Arendt, A. A., Rowlands, D. D., McCarthy, J. J., & Larsen, C. F. (2008). Recent glacier mass changes in the Gulf of Alaska region from GRACE macon solutions. *Journal of Glaciology*, *54*(188), pp 767–777. https://doi.org/10.3189/002214308787779933

Lyon, S. W., Destouni, G., Giesler, R., Humborg, C., Mörth, M., Seibert, J., & Troch, P. a. (2009). Estimation of permafrost thawing rates in a sub-arctic catchment using recession flow analysis. *Hydrology and Earth System Sciences Discussions*, *6*(1), 63–83. https://doi.org/10.5194/hessd-6-63-2009

Ma, Q., Jin, H., Yu, C., & Bense, V. F. (2019). Dissolved organic carbon in permafrost regions: A review. *Science China Earth Sciences*, *62*(2), pp 349–364. https://doi.org/10.1007/s11430-018-9309-6

Ma, R., Sun, Z., Hu, Y., Chang, Q., Wang, S., Xing, W., & Ge, M. (2017). Hydrological connectivity from glaciers to rivers in the Qinghai-Tibet Plateau: Roles of suprapermafrost and subpermafrost groundwater. *Hydrology and Earth System Sciences*, *21*(9), pp 4803–4823. https://doi.org/10.5194/hess-21-4803-2017

MacLean, R., Oswood, M. W., Irons, J. G., & McDowell, W. H. (1999). The effect of permafrost on stream biogeochemistry: A case study of two streams in the Alaskan (U. S. A.) taiga. *Biogeochemistry*, *47*, pp 239–267. Retrieved from http://link.springer.com/article/10.1007/BF00992909

Magnusson, J. O., Kobierska, F., Huxol, S., Hayashi, M., Jonas, T., & Kirchner, J. W. (2014).

Melt water driven stream and groundwater stage fluctuations on a glacier forefield (Dammagletscher, Switzerland). *Hydrological Processes*, *28*(3), pp 823–836. https://doi.org/10.1002/hyp.9633

Mailhot, A., Talbot, G., Ricard, S., Turcotte, R., & Guinard, K. (2018). Assessing the potential impacts of dam operation on daily flow at ungauged river reaches. *Journal of Hydrology: Regional Studies*, *18*(June), pp 156–167. https://doi.org/10.1016/j.ejrh.2018.06.006

Mann, H. B. (1945). Nonparametric tests against trend. *Econometrica*, *13*, pp 245–259.

Mark, B. G., French, A., Baraer, M., Carey, M., Bury, J., Young, K. R., & Lautz, L. (2017). Glacier loss and hydro-social risks in the Peruvian Andes. *Global and Planetary Change*, *159*(October 2017), pp 61–76. https://doi.org/10.1016/j.gloplacha.2017.10.003

Mark, B. G., Mckenzie, J. M., & Gomez, J. (2005). Hydrochemical evaluation of changing glacier meltwater contribution to stream discharge: Callejon de Huaylas , Peru. *Hydrological Sciences*, *50*(6), pp 975–988. Retrieved from http://bprc.osu.edu/glacierchange/papers/2005 HSJ Marketal.pdf

Mark, B. G., & Seltzer, G. O. (2003). Tropical glacier meltwater contribution to stream discharge: A case study in the Cordillera Blanca, Peru. *Journal of Glaciology*. https://doi.org/10.3189/172756503781830746

Marzeion, B., Jarosch, A. H., & Hofer, M. (2012). Past and future sea-level change from the surface mass balance of glaciers. *The Cryosphere*, *6*(6), pp 1295–1322. https://doi.org/10.5194/tc-6-1295-2012

McClelland, J. W., Holmes, R. M., Peterson, B. J., & Stieglitz, M. (2004). Increasing river discharge in the Eurasian Arctic: Consideration of dams, permafrost thaw, and fires as potential agents of change. *Journal of Geophysical Research: Atmospheres*, *109*(18), pp 1–12. https://doi.org/10.1029/2004JD004583

McClymont, A. F., Roy, J. W., Hayashi, M., Bentley, L. R., Maurer, H., & Langston, G. (2011). Investigating groundwater flow paths within proglacial moraine using multiple geophysical methods. *Journal of Hydrology*, *399*(1–2), pp 57–69 . https://doi.org/10.1016/j.jhydrol.2010.12.036

McDonnell, J. J., Sivapalan, M., Vaché, K., Dunn, S., Grant, G., Haggerty, R., & Weiler, M. (2007). Moving beyond heterogeneity and process complexity: A new vision for watershed hydrology. *Water Resources Research*, *43*(7), pp 1–6 . https://doi.org/10.1029/2006WR005467

McKenzie, J. M., & Voss, C. I. (2013). Permafrost thaw in a nested groundwater-flow system. *Hydrogeology Journal*, *21*, pp 299–316. https://doi.org/10.1007/s10040-012-0942-3

Meehl, G. A., Stocker, T. F., Collins, W. D., Friedlingstein, P., Gaye, A. T., Gregory, J. M., & Zhao, Z. C. (2007). Global Climate Projections. In S. Solomon, D. Qin, M. Manning, Z. Chen, M. Marquis, K. B. Averyt, & H. L. Miller (Eds.), *Climate Change 2007: The Physical Science Basis. Contribution of Working Group I to the Fourth Assessment Report of the Intergovernmental Panel on Climate Change* (pp. 747–845). Cambridge, UK: Cambridge University Press. https://doi.org/10.1109/ICEPT.2010.5582830

Mekis, É., & Vincent, L. A. (2011). An overview of the second generation adjusted daily precipitation dataset for trend analysis in Canada. *Atmosphere - Ocean*, *49*(2), pp 163–177. https://doi.org/10.1080/07055900.2011.583910

Merz, B., Vorogushyn, S., Uhlemann, S., Delgado, J., & Hundecha, Y. (2012). HESS Opinions: “More efforts and scientific rigour are needed to attribute trends in flood time series.” *Hydrology and Earth System Sciences*, *16*(5), pp 1379–1387. https://doi.org/10.5194/hess-16-1379-2012

Michel, A. (1986). Isotope geochemistry of frost-blister ice , North Fork Pass , Yukon , Canada. *Canadian Journal of Earth Sciences*.

Milner, A. M., Brown, L. E., & Hannah, D. M. (2009). Hydroecological response of river systems to shrinking glaciers. *Hydrological Processes*, *23*, pp 62–77. https://doi.org/10.1002/hyp

Milner, A. M., Khamis, K., Battin, T. J., Brittain, J. E., Barrand, N. E., Füreder, L., & Brown, L. E. (2017). Glacier shrinkage driving global changes in downstream systems. *Proceedings of the National Academy of Sciences*, 201619807. https://doi.org/10.1073/pnas.1619807114

Mimeau, L., Esteves, M., Zin, I., Jacobi, H.-W., Brun, F., Wagnon, P., & Arnaud, Y. (2019). Quantification of different flow components in a high-altitude glacierized catchment (Dudh Koshi, Himalaya): some cryospheric-related issues. *Hydrology and Earth System Sciences*, *23*(9), pp 3969–3996. https://doi.org/10.5194/hess-23-3969-2019

Mook, W. G. (2001). Environmental isotopes in the hydrological cycle: Principles and applications, Volume I: Introduction: Theory, Methods, Review. *International Hydrological Programme IHP-V*, *1*, pp 1–165. Retrieved from http://www.hydrology.nl/ihppublications/149-environmental-isotopes-in-the-hydrological-cycle-principles-and-applications.html%5Cn

Moore, R., Allen, D., & Stahl, K. (2007). Climate Change and Low Flows: Influences of Groundwater and Glaciers. Final Report for Climate Change Action Fund Project A875, (August).

Moore, R. D., & Demuth, M. N. (2001). Mass balance and streamflow variability at Place Glacier , Canada , in relation to recent climate fluctuations. *Hydrological Processes*, *3486*(May), pp 3473–3486. https://doi.org/10.1002/hyp.1030

Moore, R. D., Fleming, S. W., Menounos, B., Wheate, R., Fountain, A. G., Stahl, K., & Jakob, M. (2009). Glacier change in western North America: influences on hydrology, geomorphic hazards and water quality. *Hydrological Processes*, *23*(1), pp 42–61. https://doi.org/10.1002/hyp.7162

Moorman, B. J. (2003). Glacier-permafrost hydrology interactions, Bylot Island, Canada. *Proceedings of the 8th International Conference on Permafrost*, pp 783–788.

Moorman, B. J., & Michel, F. (2000). Glacial hydrological system characterization using ground-penetrating radar. *Hydrological Processes*, *14*(15), pp 2645–2667. https://doi.org/10.1002/1099-1085(20001030)14:15<2645::AID-HYP84>3.0.CO;2-2

Morse, P. D., & Wolfe, S. A. (2016). Long-Term River Icing Dynamics in Discontinuous Permafrost, Subarctic Canadian Shield. *Permafrost and Periglacial Processes*, (June 2015). https://doi.org/10.1002/ppp.1907

Muir, D. L., Hayashi, M., & Mcclymont, A. F. (2011). Hydrological storage and transmission characteristics of an alpine talus. *Hydrological Processes*, *25*(March), pp 2954–2966. https://doi.org/10.1002/hyp.8060

Naegeli, K., Lovell, H., Zemp, M., & Benn, D. I. (2014). Dendritic subglacial drainage systems in cold glaciers formed by cut-and-closure processes. *Geografiska Annaler, Series A: Physical Geography*, *96*(4), pp 591–608. https://doi.org/10.1111/geoa.12059

National Resources Canada. (2018). Online Remote Community Energy Database. Retrieved from http://atlas.gc.ca/rcedbdece/en/index.html

Natural Resources Canada. (2016). Canvec dataset. Retrieved June 20, 2009, from http://ftp.maps.canada.ca/pub/nrcan_rncan/vector/canvec/shp/

Naz, B. S., Frans, C. D., Clarke, G. K. C., Burns, P., & Lettenmaier, D. P. (2014). Modeling the effect of glacier recession on streamflow response using a coupled glacio-hydrological model. *Hydrology and Earth System Sciences*, *18*(2), pp 787–802. https://doi.org/10.5194/hess-18-787-2014

Neal, E. G., Todd Walter, M., & Coffeen, C. (2002). Linking the pacific decadal oscillation to seasonal stream discharge patterns in Southeast Alaska. *Journal of Hydrology*, *263*(1–4), pp 188–197. https://doi.org/10.1016/S0022-1694(02)00058-6

Nienow, P. W., Sharp, M. J., & Willis, I. (1998). Seasonal changes in the morphology of the subglacial drainage system, Haut Glacier d'Arolla, Switzerland. *Earth Surface Processes and Landforms*, *23*(9), pp 825–843. https://doi.org/10.1002/(SICI)1096-9837(199809)23:9<825::AID-ESP893>3.0.CO;2-2

Nilsson, C., Polvi, L. E., & Lind, L. (2015). Extreme events in streams and rivers in arctic and subarctic regions in an uncertain future. *Freshwater Biology*. https://doi.org/10.1111/fwb.12477

Nolin, A. W., Phillippe, J., Jefferson, A., & Lewis, S. L. (2010). Present-day and future contributions of glacier runoff to summertime flows in a Pacific Northwest watershed: Implications for water resources. *Water Resources Research*, *46*, pp 1–14. https://doi.org/10.1029/2009WR008968

O'Donnell, J. A., Aiken, G. R., Walvoord, M. A., & Butler, K. D. (2012). Dissolved organic matter composition of winter flow in the Yukon River basin: Implications of permafrost thaw and increased groundwater discharge. *Global Biogeochemical Cycles*, *26*(4), pp 1–18. https://doi.org/10.1029/2012GB004341

O'Neel, S., Hood, E., Bidlack, A. L., Fleming, S. W., Arimitsu, M. L., Arendt, A., & Pyare, S. (2015). Icefield-to-ocean linkages across the northern pacific coastal temperate rainforest ecosystem. *BioScience*, *65*(5), pp 499–512 . https://doi.org/10.1093/biosci/biv027

Oerlemans, J. (2005). Atmospheric science: Extracting a climate signal from 169 glacier records. *Science*, *308*(5722), pp 675–677. https://doi.org/10.1126/science.1107046

Oltmanns, M., Straneo, F., & Tedesco, M. (2019). Increased Greenland melt triggered by large-scale, year-round cyclonic moisture intrusions. *Cryosphere*, *13*(3), pp 815–825. https://doi.org/10.5194/tc-13-815-2019

Paul, F. (2002a). Changes in glacier area in Tyrol, Austria, between 1969 and 1992 derived from Landsat 5 Thematic Mapper and Austrian Glacier Inventory data. *International Journal of Remote Sensing*, *23*(4), pp 787–799. https://doi.org/10.1080/01431160110070708

Paul, F. (2002b). Combined technologies allow rapid analysis of glacier changes. *EOS, Transactions American Geophysical Union*, *83*(2), pp 3–6. Retrieved from http://onlinelibrary.wiley.com/doi/10.1029/2002EO000177/abstract

Pavelsky, T. M., & Zarnetske, J. P. (2017). Rapid decline in river icings detected in Arctic Alaska: Implications for a changing hydrologic cycle and river ecosystems. *Geophysical*

Research Letters, *44*(7), pp 3228–3235. https://doi.org/10.1002/2016GL072397

Pellicciotti, F., Bauder, A., & Parola, M. (2010). Effect of glaciers on streamflow trends in the Swiss Alps. *Water Resources Research*, *46*(10), pp 1–16. https://doi.org/10.1029/2009WR009039

Penna, D., Engel, M., Bertoldi, G., & Comiti, F. (2017). Towards a tracer-based conceptualization of meltwater dynamics and streamflow response in a glacierized catchment. *Hydrology and Earth System Sciences*, *21*(1), pp 23–41. https://doi.org/10.5194/hess-21-23-2017

Penna, D., Engel, M., Mao, L., Dell'agnese, A., Bertoldi, G., & Comiti, F. (2014). Tracer-based analysis of spatial and temporal variations of water sources in a glacierized catchment. *Hydrology and Earth System Sciences*, *18*(12), pp 5271–5288. https://doi.org/10.5194/hess-18-5271-2014

Penna, D., & van Meerveld, H. J. Ilja. (2019). Spatial variability in the isotopic composition of rainfall in a small headwater catchment and its effect on hydrograph separation. *Journal of Hydrology*, *547*(January), pp 755–769. https://doi.org/10.1016/j.jhydrol.2017.01.045

Petrone, K. C., Jones, J. B., Hinzman, L. D., & Boone, R. D. (2006). Seasonal export of carbon, nitrogen, and major solutes from Alaskan catchments with discontinuous permafrost. *Journal of Geophysical Research*, *111*. https://doi.org/10.1029/2005JG000055

Pfeffer, W. T., Arendt, A. A., Bliss, A., Bolch, T., Cogley, J. G., Gardner, A. S., & Consortium, T. H. E. R. (2014). The Randolph Glacier Inventory: a globally complete inventory of glaciers. *Journal of Glaciology*, *60*(221), pp 537–552 . https://doi.org/10.3189/2014JoG13J176

Pollard, W. H. (2005). Icing processes associated with high Arctic perennial springs, Axel Heiberg Island, Nunavut, Canada. *Permafrost and Periglacial Processes*, *16*(1), pp 51–68. https://doi.org/10.1002/ppp.515

Pomeroy, J. W., Gray, D. M., Brown, T., Hedstrom, N. R., Quinton, W. L., Granger, R. J., & Carey, S. K. (2007). The cold regions hydrological model: a platform for basing process representation and model structure on physical evidence. *Hydrological Processes*, *21*(19), pp 2650–2667. https://doi.org/10.1002/hyp.6787

Prowse, T. D. (2009). Introduction: hydrologic effects of a shrinking cryosphere. *Hydrological Processes*, *23*. https://doi.org/10.1002/hyp

Qin, J., Ding, Y., & Han, T. (2020). Quantitative assessment of winter baseflow variations and their causes in Eurasia over the past 100 years. *Cold Regions Science and Technology*, 734427. https://doi.org/10.1016/j.aquaculture.2019.734427

Quinton, W. L., & Baltzer, J. L. (2013). The active-layer hydrology of a peat plateau with

thawing permafrost (Scotty Creek, Canada). *Hydrogeology Journal*, *21*(1), pp 201–220. https://doi.org/10.1007/s10040-012-0935-2

Quinton, William L., & Marsh, P. (1999). A Conceptual Framework for Runoff Generation in a Permafrost Environment. *Hydrological Processes*, *13*(July 1998), pp 2563–2581. Retrieved from http://www.wlu.ca/documents/29063/Quinton%26Marsh99.pdf

Racoviteanu, A. E., Armstrong, R., & Williams, M. W. (2013). Evaluation of an ice ablation model to estimate the contribution of melting glacier ice to annual discharge in the Nepal Himalaya. *Water Resources Research*, *49*(9), pp 5117–5133. https://doi.org/10.1002/wrcr.20370

Racoviteanu, A. E., Paul, F., Raup, B., Khalsa, S., & Armstrong, R. (2009). Challenges and recommendations in mapping of glacier parameters from space: results of the 2008 Global Land Ice Measurements from Space (GLIMS) workshop, Boulder, Colorado. *Annals of Glaciology*, *50*(53), 53–69. Retrieved from http://www.ingentaconnect.com/content/igsoc/agl/2010/00000050/00000053/art00008

Racoviteanu, A. E., Williams, M. W., & Barry, R. G. (2008). Optical Remote Sensing of Glacier Characteristics: A Review with Focus on the Himalaya. *Sensors*, *8*(5), pp 3355–3383. https://doi.org/10.3390/s8053355

Radić, V., & Hock, R. (2010). Regional and global volumes of glaciers derived from statistical upscaling of glacier inventory data. *Journal of Geophysical Research: Earth Surface*, *115*(1), pp 1–10. https://doi.org/10.1029/2009JF001373

Ragettli, S., Cortés, G., McPhee, J., & Pellicciotti, F. (2014). An evaluation of approaches for modelling hydrological processes in high-elevation, glacierized Andean watersheds. *Hydrological Processes*, *28*(23), pp 5674–5695. https://doi.org/10.1002/hyp.10055

Ragettli, S., Immerzeel, W. W., & Pellicciotti, F. (2016). Contrasting climate change impact on river flows from high-altitude catchments in the Himalayan and Andes Mountains. *Proceedings of the National Academy of Sciences*, *113*(33), pp 9222–9227. https://doi.org/10.1073/pnas.1606526113

Ragettli, S., Pellicciotti, F., Immerzeel, W. W., Miles, E. S., Petersen, L., Heynen, M., & Shrestha, A. (2015). Unraveling the hydrology of a Himalayan catchment through integration of high resolution in situ data and remote sensing with an advanced simulation model. *Advances in Water Resources*, *78*, pp 94–111. https://doi.org/10.1016/j.advwatres.2015.01.013

Rasouli, K., Pomeroy, J. W., Janowicz, J. R., Carey, S. K., & Williams, T. J. (2014). Hydrological sensitivity of a northern mountain basin to climate change. *Hydrological*

Processes, *28*(14), pp 4191–4208. https://doi.org/10.1002/hyp.10244

Reedyk, S., Woo, M.-K. K., & Prowse, T. D. (1995). Contribution of icing ablation to streamflow in a discontinuous permafrost area. *Canadian Journal of Earth Sciences*, *32*(1972), pp 13–20. https://doi.org/10.1139/e95-002

Rennermalm, A. K., Wood, E. F., & Troy, T. J. (2010). Observed changes in pan-arctic cold-season minimum monthly river discharge. *Climate Dynamics*, *35*, pp 923–939. https://doi.org/10.1007/s00382-009-0730-5

Robinson, Z. P., Fairchild, I. J., & Russell, A. J. (2008). Hydrogeological implications of glacial landscape evolution at Skeietharársandur, SE Iceland. *Geomorphology*, *97*(1–2), pp 218–236. https://doi.org/10.1016/j.geomorph.2007.02.044

Rogger, M., Chirico, G. B., Hausmann, H., Krainer, K., Bruckl, E., Stadler, P., & Bloschl, G. (2017). Impact of mountain permafrost on flow path and runoff response in a high alpine catchment. *Water Resources Research*, pp 1–21. https://doi.org/10.1002/2016WR019341.Received

Roy, J. W., & Hayashi, M. (2008). Groundwater exchange with two small alpine lakes in the Canadian Rockies. *Hydrological Processes*, *22*(April), pp 1–16. https://doi.org/10.1002/hyp

Roy, J. W., & Hayashi, M. (2009). Multiple, distinct groundwater flow systems of a single moraine-talus feature in an alpine watershed. *Journal of Hydrology*, *373*(1–2), pp 139–150. https://doi.org/10.1016/j.jhydrol.2009.04.018

Rozanski, K., Araguás-Araguás, L., & Gonfiantini, R. (1993). Isotopic Patterns in Modern Global Precipitation. In P. K. Swart (Ed.), *Geophysical Monograph 78* (pp. 1–36). American Geophysical Union. https://doi.org/10.1029/gm078p0001

Ruairuen, W., Fochesatto, G. J., Sparrow, E. B., Schnabel, W., Zhang, M., & Kim, Y. (2015). Evapotranspiration cycles in a high latitude agroecosystem: Potential warming role. *PLoS ONE*, *10*(9), pp 1–30. https://doi.org/10.1371/journal.pone.0137209

Saberi, L., McLaughlin, R. T., Ng, G.-H. C., La Frenierre, J., Wickert, A. D., Baraer, M., & Mark, B. G. (2019). Multi-scale temporal variability in meltwater contributions in a tropical glacierized watershed. *Hydrology and Earth System Sciences*, *23*(1), pp 405–425. https://doi.org/10.5194/hess-23-405-2019

Saelthun, N. R., Aittoniemi, P., Bergstrom, S., Einarsson, K., Johannesson, T., Lindstrom, G., & Aamodt, K. O. (1998). *Climate change impacts on runoff and hydropower in the Nordic countries. Final report from the project "Climate Change and Energy Production".*

TemaNord (Vol. 552). Copenhagen.

Salzmann, N., Huggel, C., Rohrer, M., & Stoffel, M. (2014). Data and knowledge gaps in glacier, snow and related runoff research - A climate change adaptation perspective. *Journal of Hydrology*, *518*(PB), 225–234. https://doi.org/10.1016/j.jhydrol.2014.05.058

Schomacker, A. (2008). What controls dead-ice melting under different climate conditions? A discussion. *Earth-Science Reviews*, *90*(3–4), pp 103–113. https://doi.org/10.1016/j.earscirev.2008.08.003

Schrott, L. (1991). Global solar radiation, soil temperature and permafrost in the Central Andes, Argentina: A progress report. *Permafrost and Periglacial Processes*, *2*(1), pp 59–66. https://doi.org/10.1002/ppp.3430020110

Sen, P. K. (1968). Estimates of the Regression Coefficient Based on Kendall's Tau. *Journal of the American Statistical Association*, *63*(324), pp 1379–1389. https://doi.org/10.1080/01621459.1968.10480934

Sevestre, H., & Benn, D. I. (2015). Climatic and geometric controls on the global distribution of surge-type glaciers: Implications for a unifying model of surging. *Journal of Glaciology*, *61*(228), pp 646–662. https://doi.org/10.3189/2015JoG14J136

Shabbar, A., & Khandekar, M. (1996). The impact of el Nino-Southern oscillation on the temperature field over Canada: Research note. *Atmosphere - Ocean*, *34*(2), pp 401–416. https://doi.org/10.1080/07055900.1996.9649570

Shahgedanova, M., Afzal, M., Severskiy, I., Usmanova, Z., Saidaliyeva, Z., Kapitsa, V., & Dolgikh, S. (2018). Changes in the mountain river discharge in the northern Tien Shan since the mid-20th Century: Results from the analysis of a homogeneous daily streamflow data set from seven catchments. *Journal of Hydrology*, *564*(July), pp 1133–1152. https://doi.org/10.1016/j.jhydrol.2018.08.001

Shugar, D. H., Clague, J. J., Best, J. L., Schoof, C., Willis, M. J., Copland, L., & Roe, G. H. (2017). River piracy and drainage basin reorganization led by climate-driven glacier retreat. *Nature Geoscience*, *10*(5), pp 370–375. https://doi.org/10.1038/ngeo2932

Sidle, W. C. (1998). Environmental isotopes for resolution of hydrology problems. *Environmental Monitoring and Assessment*, *52*(3), pp 389–410. https://doi.org/10.1023/A:1005922029958

Smith, L. C., Pavelsky, T. M., MacDonald, G. M., Shiklomanov, A. I., & Lammers, R. B. (2007). Rising minimum daily flows in northern Eurasian rivers: A growing influence of groundwater in the high-latitude hydrologic cycle. *Journal of Geophysical Research:*

Biogeosciences, *112*(4). https://doi.org/10.1029/2006JG000327

Smith, S. L., Romanovsky, V. E., Lewkowicz, A. G., Burn, C. R., Allard, M., Clow, G. D., & Throop, J. (2010). Thermal state of permafrost in North America: A contribution to the international polar year. *Permafrost and Periglacial Processes*, *21*(2), pp 117–135. https://doi.org/10.1002/ppp.690

Smith, S. L., Roy, L., Lewkowicz, A. G., & Chartrand, J. (2017). *Ground thermal data collection along the Alaska Highway corridor (KP1559-1895), Yukon, summer 2016*.

Smith, Sharon L., Burgess, M. M., Riseborough, D., & Nixon, F. M. (2005). Recent trends from Canadian permafrost thermal monitoring network sites. *Permafrost and Periglacial Processes*, *16*(1), pp 19–30. https://doi.org/10.1002/ppp.511

Smith, Sharon L, Lewkowicz, A. G., Ednie, M., Maxime, A., & Bevington, A. (2015). Characterization of Permafrost Thermal State in the Southern Yukon. *68e Conférence Canadienne de Géotechnique et 7e Conférence Canadienne Sur Le Pergélisol, 20 Au 23 Septembre 2015, Québec, Québec.*, (September 2015).

Smith, T., Bookhagen, B., & Cannon, F. (2015). Improving semi-automated glacier mapping with a multi-method approach: Applications in central Asia. *Cryosphere*, *9*(5), pp 1747–1759. https://doi.org/10.5194/tc-9-1747-2015

Sobota, I. (2016). Icings and their role as an important element of the cryosphere in High Arctic glacier forefields. *Bulletin of Geography, Physical Geography Series*, *10*(10), 81–93.

Somers, L. D., Gordon, R. P., McKenzie, J. M., Lautz, L. K., Wigmore, O., Glose, A. M., & Condom, T. (2016). Quantifying groundwater–surface water interactions in a proglacial valley, Cordillera Blanca, Peru. *Hydrological Processes*, *30*(17), pp 2915–2929. https://doi.org/10.1002/hyp.10912

Somers, L. D., McKenzie, J. M., Mark, B. G., Lagos, P., Ng, G. C., Wickert, A. D., & Silva, Y. (2019). Groundwater buffers decreasing glacier melt in an Andean watershed - but not forever. *Geophysical Research Letters*, 2019GL084730 . https://doi.org/10.1029/2019GL084730

Stachnik, Ł., Yde, J. C., Kondracka, M., Ignatiuk, D., & Grzesik, M. (2016). Glacier naled evolution and relation to the subglacial drainage system based on water chemistry and GPR surveys (Werenskioldbreen, SW Svalbard). *Annals of Glaciology*, pp 1–12. https://doi.org/10.1017/aog.2016.9

Stahl, K., Hisdal, H., Hannaford, J., Tallaksen, L. M., Van Lanen, H. A. J., Sauquet, E., & Jodar, J. (2010). Streamflow trends in Europe: Evidence from a dataset of near-natural

catchments. *Hydrology and Earth System Sciences*, *14*(12), pp 2367–2382. https://doi.org/10.5194/hess-14-2367-2010

Stahl, K., & Moore, R. D. (2006). Influence of watershed glacier coverage on summer streamflow in British Columbia, Canada. *Water Resources Research*, *42*(6), pp 2–6. https://doi.org/10.1029/2006WR005022

Stahl, K., Moore, R. D., Shea, J. M., Hutchinson, D., & Cannon, A. (2008). Coupled modelling of glacier and streamflow response to future climate scenarios. *Water Resources Research*, *44*(2). https://doi.org/10.1029/2007WR005956

Stewart, I. T., Cayan, D. R., & Dettinger, M. D. (2005). Changes toward earlier streamflow timing across western North America. *Journal of Climate*, *18*(8), pp 1136–1155. https://doi.org/10.1175/JCLI3321.1

Stoelzle, M., Schuetz, T., Weiler, M., Stahl, K., & Tallaksen, L. M. (2019). Beyond binary baseflow separation: delayed flow index as a fresh perspective on streamflow contributions. *Hydrology and Earth System Sciences Discussions*, (May), pp 1–30. https://doi.org/10.5194/hess-2019-236

Tarnocai, C., Nixon, M. F., & Kutny, L. (2004). Circumpolar-Active-Layer-Monitoring (CALM) sites in the Mackenzie Valley, northwestern Canada. *Permafrost and Periglacial Processes*, *15*(2), pp 141–153. https://doi.org/10.1002/ppp.490

Taylor, J. R. (1998). *An Introduction to Error Analysis: The Study of Uncertainties in Physical Measurements*. *Measurement Science and Technology* (2nd editio). Sausalito, California: University Science Books. https://doi.org/10.1088/0957-0233/9/6/022

Taylor, S., Feng, X., Kirchner, J. W., Osterhuber, R., Klaue, B., & Renshaw, C. E. (2001). Isotopic evolution of a seasonal snowpack and its melt. *Water Resources Research*, *37*(3), pp 759–769. https://doi.org/10.1029/2000WR900341

Thomazo, C., Buoncristiani, J. F., Vennin, E., Pellenard, P., Cocquerez, T., Mugnier, J. L., & Gérard, E. (2017). Geochemical processes leading to the precipitation of subglacial carbonate crusts at bossons glacier, mont blanc massif (French alps). *Frontiers in Earth Science*, *5*(September), pp 1–16. https://doi.org/10.3389/feart.2017.00070

Toohey, R. C., Herman-Mercer, N. M., Schuster, P. F., Mutter, E. A., & Koch, J. C. (2016). Multidecadal increases in the Yukon River Basin of chemical fluxes as indicators of changing flowpaths, groundwater, and permafrost. *Geophysical Research Letters*, *43*(23), pp 12120-12130. https://doi.org/10.1002/2016GL070817

Unger-Shayesteh, K., Vorogushyn, S., Farinotti, D., Gafurov, A., Duethmann, D., Mandychev,

A., & Merz, B. (2013). What do we know about past changes in the water cycle of Central Asian headwaters? A review. *Global and Planetary Change*, *110*, pp 4–25. https://doi.org/10.1016/j.gloplacha.2013.02.004

Valentin, M. M., Hogue, T. S., & Hay, L. E. (2018). Hydrologic regime changes in a high-latitude glacierizedwatershed under future climate conditions. *Water (Switzerland)*, *10*(2). https://doi.org/10.3390/w10020128

Van de Wal, R. S. W., & Wild, M. (2001). Modelling the response of glaciers to climate change by applying volume-area scaling in combination with a high resolution {GCM}. *Climate Dynamics*, *18*(3), pp 359–366. https://doi.org/10.1007/s003820100184

van Tiel, M., Kohn, I., Van Loon, A. F., & Stahl, K. (2019). The compensating effect of glaciers: characterising the relation between interannual streamflow variability and glacier cover. *Hydrological Processes*, (September), pp 1–16. https://doi.org/10.1002/hyp.13603

Van Tiel, M., Teuling, A. J., Wanders, N., Vis, M. J. P., Stahl, K., & Van Loon, A. F. (2018). The role of glacier changes and threshold definition in the characterisation of future streamflow droughts in glacierised catchments. *Hydrology and Earth System Sciences*, *22*(1), pp 463–485. https://doi.org/10.5194/hess-22-463-2018

Veiette, J. J., & Thomas, R. D. (1979). Icings and seepage in frozen glaciofluvial deposits, District of Keewatin, N.W.T. *Canadian Geotechnical*, *16*, pp 789–798.

Velicogna, I., Tong, J., Zhang, T., & Kimball, J. S. (2012). Increasing subsurface water storage in discontinuous permafrost areas of the Lena River basin, Eurasia, detected from GRACE. *Geophysical Research Letters*, *39*(9), pp 1–5. https://doi.org/10.1029/2012GL051623

Vincent, A., Violette, S., & Aðalgeirsdóttir, G. (2019). Groundwater in catchments headed by temperate glaciers: A review. *Earth-Science Reviews*, *188*(October 2018), pp 59–76. https://doi.org/10.1016/j.earscirev.2018.10.017

Vincent, L. A., Wang, X. L., Milewska, E. J., Wan, H., Yang, F., & Swail, V. (2012). A second generation of homogenized Canadian monthly surface air temperature for climate trend analysis. *Journal of Geophysical Research Atmospheres*, *117*(17), pp 1–13. https://doi.org/10.1029/2012JD017859

Vincent, L. A., Zhang, X., Brown, R. D., Feng, Y., Mekis, E., Milewska, E. J., & Wang, X. L. (2015). Observed trends in Canada's climate and influence of low-frequency variability modes. *Journal of Climate*, *28*(11), pp 4545–4560. https://doi.org/10.1175/JCLI-D-14-00697.1

Viviroli, D., Dürr, H. H., Messerli, B., Meybeck, M., & Weingartner, R. (2007). Mountains of

the world, water towers for humanity: Typology, mapping, and global significance. *Water Resources Research*, *43*(7). https://doi.org/10.1029/2006WR005653

Vogt, T. (1991). Cryogenic Physico-chemical Precipitations : Iron , Silica , Calcium Carbonate. *Permafrost and Periglacial Processes*, *1*, pp 283–293.

Vuille, M., Carey, M., Huggel, C., Buytaert, W., Rabatel, A., Jacobsen, D., & Sicart, J. E. (2018). Rapid decline of snow and ice in the tropical Andes – Impacts, uncertainties and challenges ahead. *Earth-Science Reviews*, *176* (May 2017), pp 195–213. https://doi.org/10.1016/j.earscirev.2017.09.019

Wadham, J. L., Tranter, M., & Dowdeswell, J. A. (2000). Hydrochemistry of meltwaters draining a polythermal-based, high-Arctic glacier, south Svalbard: II. Winter and early Spring. *Hydrological Processes*, *14*(10), pp 1767–1786. https://doi.org/10.1002/1099-1085(200007)14:10<1767::AID-HYP103>3.0.CO;2-Q

Wagener, T., Sivapalan, M., Troch, P. A., McGlynn, B. L., Harman, C. J., Gupta, H. V., & Wilson, J. S. (2010). The future of hydrology: An evolving science for a changing world. *Water Resources Research*, *46*(5), pp 1–10. https://doi.org/10.1029/2009WR008906

Wahl, H. E., Fraser, D. B., Harvey, R. C., & Maxwell, J. B. (1987). *Climate of Yukon*. *Climatological Studies* (Vol. 40). Atmospheric Environment Service, Environment Canada.

Wainstein, P., Moorman, B. J., & Whitehead, K. (2008). Importance of glacier-permafrost interactions in the preservation of a proglacial icing: Fountain Glacier, Bylot Island, Canada. *Ninth International Conference on Permafrost*, pp 1881–1886. Retrieved from http://scholar.google.com/scholar?hl=en&btnG=Search&q=intitle:Importance+of+GlacierPermafrost+Interactions+in+the+Preservation+of+a+Proglacial+Icing+:+Fountain+Glacier+,+Bylot+Island+,+Canada#0

Wainstein, P., Moorman, B. J., & Whitehead, K. (2014). Glacial conditions that contribute to the regeneration of Fountain Glacier proglacial icing, Bylot Island, Canada. *Hydrological Processes*, *28*(5), pp 2749–2760. https://doi.org/10.1002/hyp.9787

Walder, J. S., & Fountain, A. G. (1998). Water flow through temperate glaciers. *Reviews of Geophysics*, *36*(3), pp 299.

Walvoord, M. A., & Kurylyk, B. L. (2016). Hydrologic Impacts of Thawing Permafrost—A Review. *Vadose Zone Journal*, *15*(6). https://doi.org/10.2136/vzj2016.01.0010

Walvoord, M. a., & Striegl, R. G. (2007). Increased groundwater to stream discharge from permafrost thawing in the Yukon River basin: Potential impacts on lateral export of carbon and nitrogen. *Geophysical Research Letters*, *34*(12). https://doi.org/10.1029/2007GL030216

Walvoord, M. a., Voss, C. I., & Wellman, T. P. (2012). Influence of permafrost distribution on groundwater flow in the context of climate-driven permafrost thaw: Example from Yukon Flats Basin, Alaska, United States. *Water Resources Research*, *48*(7), pp 1–17. https://doi.org/10.1029/2011WR011595

Wang, S. (2019). Freezing Temperature Controls Winter Water Discharge for Cold Region Watershed. *Water Resources Research*, (2006), pp 1–15. https://doi.org/10.1029/2019WR026030

Wang, X., Liu, S. W., & Zhang, J. L. (2019). A new look at roles of the cryosphere in sustainable development. *Advances in Climate Change Research*, *10*(2), pp 124–131. https://doi.org/10.1016/j.accre.2019.06.005

Ward, J. V., Malard, F., Tockner, K., & Uehlinger, U. (1999). Influence of ground water on surface water conditions in a glacial flood plain of the Swiss Alps. *Hydrological Processes*, *13*(3), pp 277–293. https://doi.org/10.1002/(SICI)1099-1085(19990228)13:3<277::AID-HYP738>3.0.CO;2-N

Wheler, B. A., & Flowers, G. E. (2011). Glacier subsurface heat-flux characterizations for energy-balance modelling in the Donjek Range, southwest Yukon, Canada. *Journal of Glaciology*, *57*(201), pp 121–133. https://doi.org/10.3189/002214311795306709

Whitfield, P. H. (2001). Linked hydrologic and climate variations in British Columbia and Yukon. *Environmental Monitoring and Assessment*, *67*(1–2), pp 217–238. https://doi.org/10.1023/A:1006438723879

Whitfield, Paul H., & Cannon, A. J. (2000). Recent Variations in Climate and Hydrology in Canada. *Canadian Water Resources Journal*, *25*(1), pp 19–65. https://doi.org/10.4296/cwrj2501019

Whitfield, Paul H., Moore, R. D., Fleming, S. W., & Zawadzki, A. (2010). Pacific Decadal Oscillation and the Hydroclimatology of Western Canada—Review and Prospects. *Canadian Water Resources Journal*, *35*(1), pp 1–28. https://doi.org/10.4296/cwrj3501001

Williams, M. W., Knauf, M., Caine, N., Liu, F., & Verplanck, P. L. (2006). Geochemistry and source waters of rock glacier outflow, Colorado Front Range. *Permafrost and Periglacial Processes*, *17*(1), pp 13–33. https://doi.org/10.1002/ppp.535

Williamson, S. N., Anslow, F. S., Clarke, G. K. C., Gamon, J. A., Jarosch, A. H., & Hik, D. S. (2018). Spring warming in Yukon mountains is not amplified by the snow albedo feedback. *Scientific Reports*, *8*(1), pp 1–13. https://doi.org/10.1038/s41598-018-27348-7

Wilson, N. J., & Flowers, G. E. (2013). Environmental controls on the thermal structure of alpine glaciers. *The Cryosphere*, *7*(1), pp 167–182. https://doi.org/10.5194/tc-7-167-2013

Wilson, N. J., Flowers, G. E., & Mingo, L. (2013). Comparison of thermal structure and

evolution between neighboring subarctic glaciers. *Journal of Geophysical Research: Earth Surface*, *118*(3), pp 1443–1459. https://doi.org/10.1002/jgrf.20096

Wilson, Nicole .J., Walter, T. M., & Waterhouse, J. (2015). Indigenous Knowledge of Hydrologic Change in the Yukon River Basin. *Arctic*, *68*(1), pp 1–42. https://doi.org/10.14430/arctic4459

Woo, M.-K. K. (2012). *Permafrost Hydrology*. Springer. https://doi.org/10.1002/0470848944

Woo, M.-K. K., & Thorne, R. (2014). Winter flows in the Mackenzie drainage system. *Arctic*, *67*(2), pp 238–256. https://doi.org/10.14430/arctic4384

Woo, M. (1986). Permafrost hydrology in north america. *Atmosphere - Ocean*, *24*(3), pp 201–234. https://doi.org/10.1080/07055900.1986.9649248

Xiao, C. De, Wang, S. J., & Qin, D. H. (2015). A preliminary study of cryosphere service function and value evaluation. *Advances in Climate Change Research*, *6*(3–4), pp 181–187. https://doi.org/10.1016/j.accre.2015.11.004

Yang, D., Kane, D. L., Hinzman, L. D., Zhang, X., Zhang, T., & Ye, H. (2002). Siberian Lena River hydrologic regime and recent change. *Journal of Geophysical Research Atmospheres*, *107*(23). https://doi.org/10.1029/2002JD002542

Yde, J. C., Hodson, A. J., Solovjanova, I., Steffensen, J. P., Nørnberg, P., Heinemeier, J., & Olsen, J. (2012). Chemical and isotopic characteristics of a glacier-derived naled in front of Austre Grønfjordbreen, Svalbard. *Polar Research*, *31*(SUPPL.), pp 1–15. https://doi.org/10.3402/polar.v31i0.17628

Yde, J. C., & Knudsen, N. T. (2005). Observations of debris-rich naled associated with a major glacier surge event, Disko Island, West Greenland. *Permafrost and Periglacial Processes*, *16*(4), pp 319–325. https://doi.org/10.1002/ppp.533

Yoshikawa, K., Hinzman, L. D., & Kane, D. L. (2007). Spring and aufeis (icing) hydrology in Brooks Range, Alaska. *Journal of Geophysical Research: Biogeosciences*, *112*(4), pp 1–14. https://doi.org/10.1029/2006JG000294

Yuan, W., Liu, S., Liang, S., Tan, Z., Liu, H., & Young, C. (2012). Estimations of Evapotranspiration and Water Balance with Uncertainty over the Yukon River Basin. *Water Resources Management*, *26*(8), pp 2147–2157. https://doi.org/10.1007/s11269-012-0007-3

Yue, S., Pilon, P., & Phinney, B. (2003). Canadian streamflow trend detection: impacts of serial and cross-correlation. *Hydrological Sciences Journal*, *48*(1), pp 51–63. https://doi.org/10.1623/hysj.48.1.51.43478

Žák, K., Onac, B. P., & Perşoiu, A. (2008). Cryogenic carbonates in cave environments: A review. *Quaternary International*, *187*(1), pp 84–96.

https://doi.org/10.1016/j.quaint.2007.02.022

Zarga, Y., Ben Boubaker, H., Ghaffour, N., & Elfil, H. (2013). Study of calcium carbonate and sulfate co-precipitation. *Chemical Engineering Science*, *96*, pp 33–41. https://doi.org/10.1016/j.ces.2013.03.028

Zemp, M., Frey, H., Gärtner-Roer, I., Nussbaumer, S. U., Hoelzle, M., Paul, F., & Vincent, C. (2015). Historically unprecedented global glacier decline in the early 21st century. *Journal of Glaciology*, *61*(228), pp 745–762. https://doi.org/10.3189/2015JoG15J017

Zhang, X., Harvey, K. D., Hogg, W. D., & Yuzyk, T. R. (2001). Trends in Canadian streamflow. *Water Resources Research*, *37*(4), pp 987–998.

Zhang, Yanlin, Cheng, G., Li, X., Han, X., Wang, L., Li, H., & Flerchinger, G. N. (2013). Coupling of a simultaneous heat and water model with a distributed hydrological model and evaluation of the combined model in a cold region watershed. *Hydrological Processes*, *27*(25), 3762–3776. https://doi.org/10.1002/hyp.9514

Zhang, Yu, Chen, W., & Riseborough, D. W. (2008a). Disequilibrium response of permafrost thaw to climate warming in Canada over 1850-2100. *Geophysical Research Letters*, *35*(2), pp 2–5. https://doi.org/10.1029/2007GL032117

Zhang, Yu, Chen, W., & Riseborough, D. W. (2008b). Transient projections of permafrost distribution in Canada during the 21st century under scenarios of climate change. *Global and Planetary Change*, *60*(3–4), pp 443–456. https://doi.org/10.1016/j.gloplacha.2007.05.003

Zuecco, G., Carturan, L., De Blasi, F., Seppi, R., Zanoner, T., Penna, D., & Dalla Fontana, G. (2019). Understanding hydrological processes in glacierized catchments: Evidence and implications of highly variable isotopic and electrical conductivity data. *Hydrological Processes*, *33*(5), 816–832. https://doi.org/10.1002/hyp.13366